



# Test Systems for Voltage Stability Analysis and Security Assessment

PREPARED BY THE  
Power System Dynamic Performance Committee  
Power System Stability Subcommittee  
Test Systems for Voltage Stability and Security  
Assessment Task Force

THIS PAGE LEFT BLANK INTENTIONALLY

# **IEEE PES Task Force on Test Systems for Voltage Stability Analysis and Security Assessment**

## **Technical Report**

**Thierry Van Cutsem, Chair**

**Mevludin Glavic, Secretary**

**William Rosehart, Past Chair**

### **Contributors (*in alphabetical order*)**

<b>Jhonatan Andrade dos Santos</b>	<b>Lampros Papangelis</b>
<b>Claudio Cañizares</b>	<b>Rodrigo Andrade Ramos</b>
<b>Marios Kanatas</b>	<b>Behnam Tamimi</b>
<b>Leonardo Lima</b>	<b>Glauco Taranto</b>
<b>Federico Milano</b>	<b>Costas Vournas</b>

**August 25, 2015**

---

This report documents the work of the IEEE PES Task Force on Test Systems for Voltage Stability Analysis and Security Assessment. The report starts with a short introduction about the motivation and the scope of the work. Next, the models of respectively the Nordic and the RVS test systems are presented in detail, together with a sample of long-term dynamic simulations of their responses to large disturbances. Appendices are devoted to complementary analyses and simulation results obtained with other time-domain simulation software.

The system data and a sample of representative outputs will be available on a Web site maintained by the Dynamic Security Assessment Working Group of the Power System Dynamic Performance Committee (please refer to <http://ewh.ieee.org/soc/pes/psdpc/index.htm> for more information).

# Contents

<b>1</b>	<b>Introduction</b>	<b>6</b>
1.1	Motivation . . . . .	6
1.2	Basic definitions . . . . .	7
1.3	Purpose of dynamic models . . . . .	7
1.4	The test systems detailed in this report . . . . .	9
<b>I</b>	<b>The Nordic test system</b>	<b>10</b>
<b>2</b>	<b>Nordic test system: models and data</b>	<b>11</b>
2.1	System overview . . . . .	11
2.2	Network data . . . . .	14
2.3	Operating point data . . . . .	18
2.4	Synchronous machine data . . . . .	23
2.5	Exciter, automatic voltage regulator and power system stabilizer model and data . . . . .	25
2.6	Overexcitation limiter model and data . . . . .	26
2.7	Generator capability curves . . . . .	29
2.8	Turbine model and data . . . . .	33
2.9	Speed governor model and data . . . . .	33

2.10 Load data . . . . .	34
2.11 Load tap changer data . . . . .	34
<b>3 Nordic test system: dynamic responses to contingencies</b>	<b>36</b>
3.1 Operating point A . . . . .	36
3.2 Operating point B . . . . .	42
<b>4 Nordic test system: preventive voltage security assessment</b>	<b>46</b>
4.1 Determination of secure operation limits . . . . .	46
4.2 Determination of loadability limits . . . . .	52
<b>5 Nordic test system: corrective (post-disturbance) control</b>	<b>54</b>
5.1 Modified tap changer control . . . . .	54
5.2 Undervoltage load shedding . . . . .	56
5.3 Long-term voltage instability analysis through sensitivities . . . . .	57
<b>II The Reliability and Voltage Stability (RVS) test system</b>	<b>59</b>
<b>6 RVS test system: models and data</b>	<b>60</b>
6.1 System overview . . . . .	60
6.2 Operating point data . . . . .	62
6.3 Network data . . . . .	62
6.4 Shunts and SVC data . . . . .	71
6.5 Load tap changer model and data . . . . .	73
6.6 Load models and data . . . . .	74
6.7 Synchronous machine models and data . . . . .	76

6.8	Exciter and power system stabilizer model and data . . . . .	76
6.9	Overexcitation limiter model and data . . . . .	81
6.10	Generator capability curves . . . . .	84
6.11	Turbine and speed governor models and data . . . . .	84
6.12	Static VAR Compensator (SVC) model and data . . . . .	91
<b>7</b>	<b>RVS test system: simulation results</b>	<b>92</b>
7.1	Steady-state analysis . . . . .	92
7.2	Dynamic responses to contingencies . . . . .	93
<b>III</b>	<b>Appendices</b>	<b>114</b>
<b>8</b>	<b>Nordic test system: simulation results using DSATools</b>	<b>115</b>
8.1	General remarks on the use of DSATools . . . . .	115
8.2	Simulation conditions . . . . .	115
8.3	Dynamic simulations . . . . .	116
8.4	PV curves from power flow computations . . . . .	119
<b>9</b>	<b>RVS test system: simulation results using PSAT</b>	<b>125</b>
9.1	General remarks on the use of PSAT . . . . .	125
9.2	Steady-state analysis . . . . .	125
9.3	Dynamic simulations . . . . .	127
<b>10</b>	<b>RVS test system: simulation results using DSATools</b>	<b>135</b>
10.1	Steady-state analysis . . . . .	135
10.2	Dynamic simulations . . . . .	135

<b>11 Nordic test system: simulation results using QSS simulation tool WpSTAB</b>	<b>144</b>
<b>12 Nordic test system: simulation results using ANATEM</b>	<b>148</b>
12.1 General remarks on the use of ANATEM . . . . .	148
12.2 Dynamic simulations . . . . .	150
12.3 Determination of loadability limits . . . . .	154
<b>Bibliography</b>	<b>156</b>

# **Chapter 1**

## **Introduction**

### **1.1 Motivation**

This report completes the mandate of the IEEE Power and Energy Society (PES) Task Force on Test Systems for Voltage Stability Analysis and Security Assessment under the auspices of the Power System Stability Subcommittee of the Power System Dynamic Performance Committee.

The creation of the Task Force was motivated partly by the observation that a significant number of publications dealing with voltage stability were resorting to test systems not truly limited by voltage instability. As a result, those systems exhibit low critical (transmission) voltages<sup>1</sup> with the consequence that secure system operation would be limited by other phenomena (e.g. protection activation), well before such low voltages are reached.

Hence, this report presents detailed models and the corresponding data of two voltage-stability constrained test systems, together with a selection of time-domain simulation results, for well identified disturbances, allowing the user to validate their implementation in various dynamic simulation programs.

At the time of writing this report, there are plans to make the data available in electronic form on a Web site maintained by the Dynamic Security Assessment Working Group of the same subcommittee and committee. There are also plans to post a sample of time evolutions to facilitate the validation of the implementation in various power system simulation programs, as well as to host volunteered contributions involving these test systems.

The material detailed in this report will hopefully help researchers and developers to test new solutions for the assessment, the detection and the mitigation of voltage instability. It is also hoped that it will provide valuable case studies to students and lecturers.

---

<sup>1</sup>The latter may be defined as the voltages at the last stable operating point when applying to the power system a smooth load increase.

## 1.2 Basic definitions

This report is not aimed at explaining what is voltage (in)stability; there are well established publications for that purpose (e.g. [1, 2, 3, 4, 5, 6]). However, for the sake of completeness and to clarify the purpose of this report, some definitions are recalled below. The interested reader is invited to refer to [7] for more details.

*Voltage stability* refers to the ability of a power system to maintain steady voltages at all buses in the system after being subjected to a disturbance from a given initial operating condition.

*Large-disturbance voltage stability* refers to the system's ability to maintain steady voltages following large disturbances such as system faults, loss of generation, or circuit contingencies.

*Small-disturbance voltage stability* refers to the system's ability to maintain steady voltages when subjected to small perturbations such as incremental changes in system load.

*Voltage collapse* is the process by which the sequence of events accompanying voltage instability leads to a blackout or abnormally low voltages in a significant part of the power system.

The time frame of interest for voltage stability problems may vary from a few seconds to tens of minutes. In this respect, it is important to distinguish between short- and long-term instabilities:

- *short-term voltage stability* involves dynamics of fast acting load components such as induction motors, electronically controlled loads, and HVDC converters. This type of voltage instability evolves in time frame of several seconds;
- *long-term voltage stability* involves slower acting equipment such as tap-changing transformers, thermostatically controlled loads, and generator current limiters. This type of voltage instability evolves in time frame of several minutes.

In this report, the *focus is on long-term voltage instability*. Simply stated, the latter results from the inability of the combined generation and transmission systems to provide the power requested by loads. In such circumstances, some load power restoration mechanisms are responsible for a progressive, typically monotonic, fall of the transmission voltages.

## 1.3 Purpose of dynamic models

Conventional voltage stability analysis uses steady-state tools and static models, for instance to determine PV curves, from which a “distance to instability” is obtained in terms of load power margin. The static models usually takes on the form of power flow equations with appropriate generator reactive power limits and active power dispatch, together with constant power loads<sup>2</sup>.

---

<sup>2</sup>To anticipate the effect of load tap changers keeping distribution voltages near their set-point values.

This modelling may no longer be satisfactory when simulating large disturbances, especially if the system is equipped with post-disturbance controls reacting to its dynamic evolution, such as secondary voltage control or automatic shunt compensation switching, for instance [4]. Dynamic simulation of the system long-term evolution (over 5 to 10 minutes) is required in this case. This has led some transmission system operators to routinely use dynamic simulations to assess the voltage security of their systems. Such simulations may involve simplified models, such as the quasi steady-state approximation of long-term dynamics [4] (see Chapter 11 of this report). Alternatively, with the increase in computational power, it has become quite feasible to simulate models including both short- and long-term dynamics [8].

Furthermore, dynamic simulations are mandatory when devising emergency controls against voltage instability, such as tap changer blocking, load voltage reduction or, in the last resort, undervoltage load shedding. Devising such System Integrity Protection Schemes (SIPS) requires extensive dynamic simulations of models of the type shown in this report.

Last but not least, the deployment of the synchrophasor measurement technology will give rise to wide-area monitoring, protection and control systems dealing in particular with voltage instability. The proper tuning of those systems (to avoid both false alarms and late emergency detections [9]) relies on time responses such as those shown in this report.

Simply stated, the models involved in the simulation of long-term voltage stability are those already involved in short-term dynamic studies (focusing on rotor angle and frequency dynamics [7]) complemented with an appropriate representation of:

1. load power restoration, mainly under the effect of load tap changers and/or thermostatic load control;
2. limiters acting after some delay on the field or armature currents of synchronous generators to avoid thermal deterioration of the latter;
3. discrete controls responding to degraded voltage evolution, such as automatic switching of shunt compensation, secondary voltage control, modified tap changer control or undervoltage load shedding;
4. other controls not directly aimed at supporting voltages but taking place in the same time frame: automatic phase shifting transformers or secondary frequency control.

The models detailed in this report cover most aspects of items 1 to 3. Although relevant, some controls or components have not been considered, since they are comparatively less widely used: armature current limiters, automatic control of generator step-up transformer ratios, and secondary voltage control. Those items could be considered in future extensions of the models.

Of course, the models and data provided in this report can also be used in static analyses. Examples of the latter are provided in Chapters 8, 9 and 10.

## **1.4 The test systems detailed in this report**

Two test systems are considered in the remaining of this report.

The first system, with 50 Hz nominal frequency, is a variant of the former so-called Nordic32 test system [10]. Dynamic models and parameters were adjusted to make them more representative. This system has rather long transmission lines of 400-kV nominal voltage. Frequency is controlled by generators of hydro plants located in the exporting areas. The overall characteristics are: 74 buses, 102 branches, 20 generators (all with step-up transformers and overexcitation limiters modeled), 22 loads at distribution level (all controlled by load tap changers). This system has been used in various studies including contingency evaluation, voltage security assessment, instability detection and emergency control. These various results can be found in Refs. [11]-[23].

The second system, with 60 Hz nominal frequency, corresponds to a large extent to the 1979 IEEE Reliability Test System [24], more precisely the so-called “one area RTS-96” system [25]. The corresponding original models and data were used in a number of publications, see for instance Refs. [26]-[32]. This report deals with a variant of the above test system, in which the parameters were adjusted to make voltage instability more pronounced. Its overall characteristics are: 75 buses, 145 branches, 32 generators, 17 loads at distribution level, and two switched shunt capacitors.

## **Part I**

### **The Nordic test system**

# Chapter 2

## Nordic test system: models and data

### 2.1 System overview

This test system is a variant of the so-called Nordic32 test system, proposed by K. Walve<sup>1</sup> and detailed in [10]. As indicated in this reference, the system is fictitious but similar to the Swedish and Nordic system (at the time of setting up this test system).

The one-line diagram is shown in Fig. 2.1.

This system consists of four areas:

- “North” with hydro generation and some load
- “Central” with much load and thermal power generation
- “Equiv” connected to the “North”, which includes a very simple equivalent of an external system
- “South” with thermal generation, rather loosely connected to the rest of the system.

The system has rather long transmission lines of 400-kV nominal voltage. Figure 2.2 shows the structure of the 400-kV backbone, rendering the geographic locations of the stations. Five lines are equipped with series compensation; the percentage of compensation is shown in the same figure. The model also includes a representation of some regional systems operating at 220 and 130 kV, respectively (see Fig. 2.1).

Table 2.1 gives the active power load and generation in each area and for the whole system.

The nominal frequency is 50 Hz. Frequency is controlled through the speed governors of the hydro generators in the “North” and “Equiv” areas only (see Fig. 2.1). g20 is an equivalent generator, with a large

---

<sup>1</sup>At that time with Svenska Kraftn  t, Sweden.

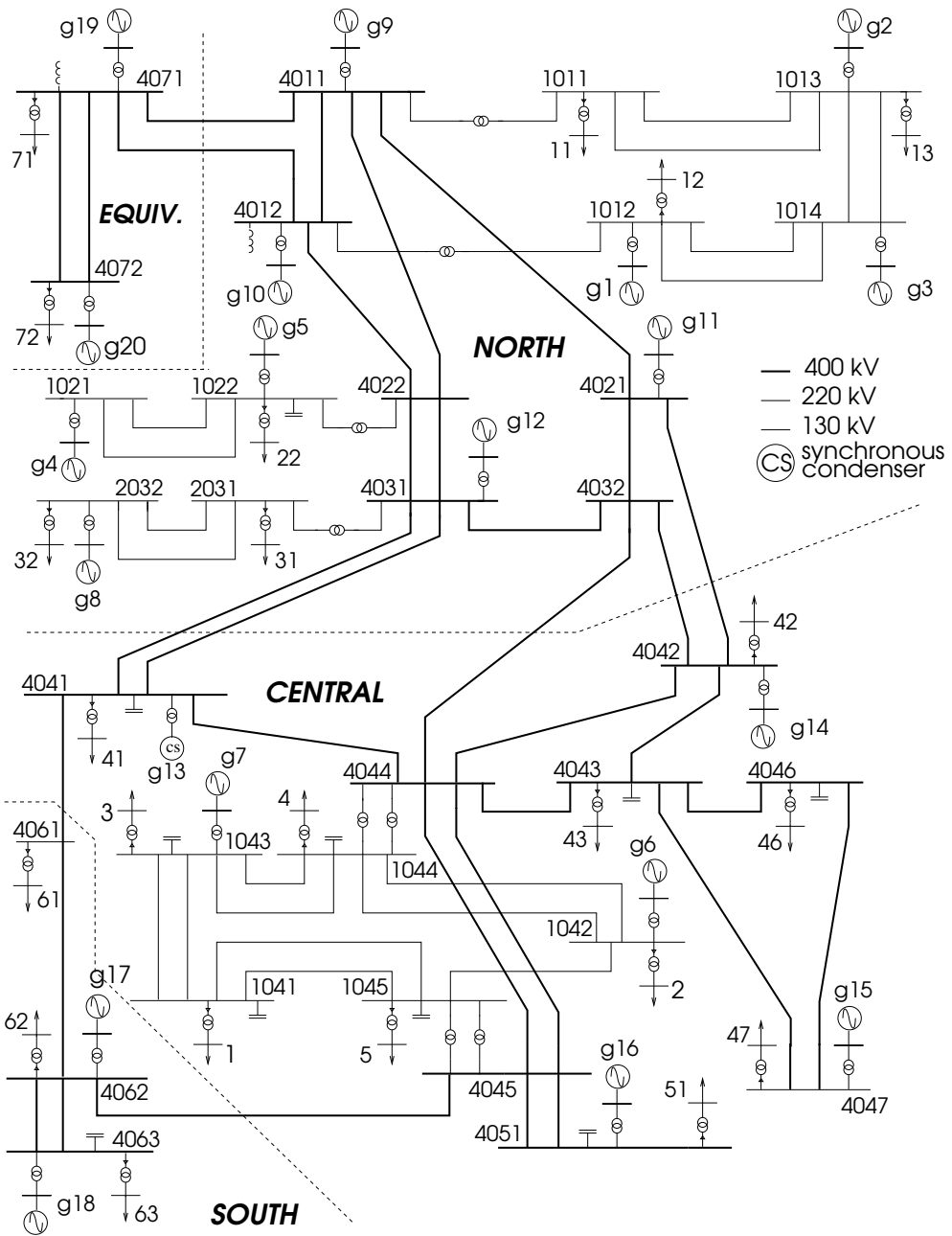


Figure 2.1: One-line diagram of the test system

Table 2.1: Active power load and generation

area	generated power (MW)	consumed power (MW)
North	4628.5	1180.0
Central	2850.0	6190.0
South	1590.0	1390.0
Equiv	2437.4	2300.0
total	11505.9	11060.0

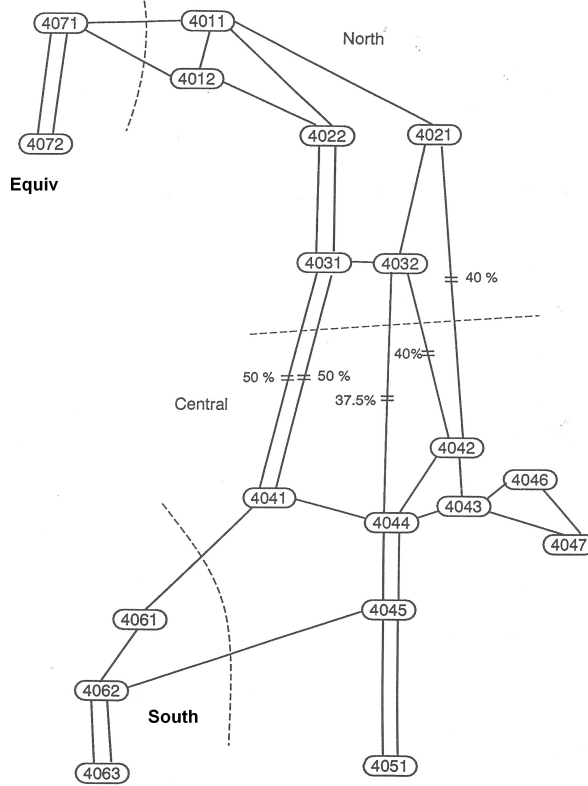


Figure 2.2: Structure of the 400-kV system

participation in primary frequency control. The thermal units of the Central and South areas do not participate in this control.

The system is heavily loaded with large transfers essentially from North to Central areas. Secure system operation is limited by transient angular and long-term voltage instability. The contingencies likely to yield voltage instability are:

- the tripping of a line in the North-Central corridor, forcing the North-Central power to flow over the remaining lines;
- the outage of a generator located in the Central area, compensated (through speed governors) by the Northern hydro generators, thereby causing an additional power transfer over the North-Central corridor.

The maximum power that can be delivered to the Central loads is strongly influenced by the reactive power capabilities of the Central and some of the Northern generators. Their reactive power limits are enforced by OverExcitation Limiters (OELs). On the other hand, Load Tap Changers (LTCs) aim at restoring distribution voltages and hence load powers. If, after a disturbance (such as a generator or a line outage), the maximum power that can be delivered by the combined generation and transmission system is smaller than what the LTCs attempt to restore, voltage instability results. It is driven by OELs and LTCs and takes place in one to two minutes after the initiating event. It is thus a case of long-term voltage instability. A similar mechanism

takes place in case of a demand increase.

The model involves 74 buses: 32 at transmission level, 22 at distribution level, and 20 generator terminal buses. It includes 102 branches, among which 22 distribution and 20 step-up transformers.

## 2.2 Network data

The line parameters are given in Table 2.2 and 2.3, respectively. The nominal apparent power  $S_{nom}$  is given for information. For series-compensated lines (see Fig. 2.2), the reactance  $X$  accounts for the series capacitor (i.e. the series reactance has been decreased accordingly).  $B/2$  is half the shunt susceptance of the line.

Table 2.2: Transmission line data

line name	from bus	to bus	$R$ ( $\Omega$ )	$X$ ( $\Omega$ )	$B/2$ ( $\mu S$ )	$S_{nom}$ (MVA)
1011-1013	1011	1013	1.69	11.83	40.841	350.
1011-1013b	1011	1013	1.69	11.83	40.841	350.
1012-1014	1012	1014	2.37	15.21	53.407	350.
1012-1014b	1012	1014	2.37	15.21	53.407	350.
1013-1014	1013	1014	1.18	8.450	29.845	350.
1013-1014b	1013	1014	1.18	8.450	29.845	350.
1021-1022	1021	1022	5.07	33.80	89.535	350.
1021-1022b	1021	1022	5.07	33.80	89.535	350.
1041-1043	1041	1043	1.69	10.14	36.128	350.
1041-1043b	1041	1043	1.69	10.14	36.128	350.
1041-1045	1041	1045	2.53	20.28	73.827	350.
1041-1045b	1041	1045	2.53	20.28	73.827	350.
1042-1044	1042	1044	6.42	47.32	177.50	350.
1042-1044b	1042	1044	6.42	47.32	177.50	350.
1042-1045	1042	1045	8.45	50.70	177.50	350.
1043-1044	1043	1044	1.69	13.52	47.124	350.
1043-1044b	1043	1044	1.69	13.52	47.124	350.
2031-2032	2031	2032	5.81	43.56	15.708	500.
2031-2032b	2031	2032	5.81	43.56	15.708	500.
4011-4012	4011	4012	1.60	12.80	62.832	1400.
4011-4021	4011	4021	9.60	96.00	562.34	1400.
4011-4022	4011	4022	6.40	64.00	375.42	1400.
4011-4071	4011	4071	8.00	72.00	438.25	1400.
4012-4022	4012	4022	6.40	56.00	328.30	1400.
4012-4071	4012	4071	8.00	80.00	468.10	1400.
4021-4032	4021	4032	6.40	64.00	375.42	1400.

Table 2.3: Transmission line data (cont'd)

line name	from bus	to bus	$R$ ( $\Omega$ )	$X$ ( $\Omega$ )	$B/2$ ( $\mu S$ )	$S_{nom}$ (MVA)
4021-4042	4021	4042	16.0	96.00	937.77	1400.
4022-4031	4022	4031	6.40	64.00	375.42	1400.
4022-4031b	4022	4031	6.40	64.00	375.42	1400.
4031-4032	4031	4032	1.60	16.00	94.248	1400.
4031-4041	4031	4041	9.60	64.00	749.27	1400.
4031-4041b	4031	4041	9.60	64.00	749.27	1400.
4032-4042	4032	4042	16.0	64.00	625.18	1400.
4032-4044	4032	4044	9.60	80.00	749.27	1400.
4041-4044	4041	4044	4.80	48.00	281.17	1400.
4041-4061	4041	4061	9.60	72.00	406.84	1400.
4042-4043	4042	4043	3.20	24.00	155.51	1400.
4042-4044	4042	4044	3.20	32.00	186.93	1400.
4043-4044	4043	4044	1.60	16.00	94.248	1400.
4043-4046	4043	4046	1.60	16.00	94.248	1400.
4043-4047	4043	4047	3.20	32.00	186.93	1400.
4044-4045	4044	4045	3.20	32.00	186.93	1400.
4044-4045b	4044	4045	3.20	32.00	186.93	1400.
4045-4051	4045	4051	6.40	64.00	375.42	1400.
4045-4051b	4045	4051	6.40	64.00	375.42	1400.
4045-4062	4045	4062	17.6	128.00	749.27	1400.
4046-4047	4046	4047	1.60	24.00	155.51	1400.
4061-4062	4061	4062	3.20	32.00	186.93	1400.
4062-4063	4062	4063	4.80	48.00	281.17	1400.
4062-4063b	4062	4063	4.80	48.00	281.17	1400.
4071-4072	4071	4072	4.80	48.00	937.77	1400.
4071-4072b	4071	4072	4.80	48.00	937.77	1400.

The transformer data are given in Tables 2.4 to 2.6. The resistance corresponding to copper losses and the magnetizing susceptance are neglected. For the orientation of the transformer, please refer to Fig. 2.3.  $X$  is in per unit on the base ( $V_{Bfrom}$ ,  $S_{nom}$ ) where  $V_{Bfrom}$  is the network base voltage of the “from” bus and  $S_{nom}$  the nominal apparent power of the transformer.  $n$  is in pu/pu on the base ( $V_{Bto}$ ,  $V_{Bfrom}$ ), where  $V_{Bto}$  is the network base voltage of the “to” bus.

The step-up transformers of all generators and the step-down transformers of all loads are represented explicitly.

The step-down transformers have their ratios adjusted in the initial power flow calculation so that the distribution bus voltage is 1.0 pu.

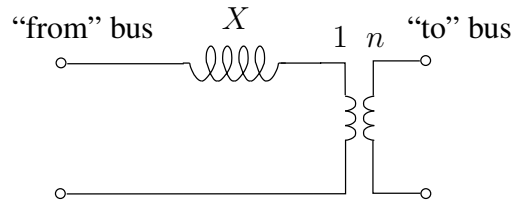


Figure 2.3: Transformer representation

Table 2.4: Data of the step-up transformers

generator name	from bus	to bus	$X$ (pu)	$n$ (pu/pu)	$S_{nom}$ (MVA)
g1	g1	1012	0.15	1.00	800.0
g2	g2	1013	0.15	1.00	600.0
g3	g3	1014	0.15	1.00	700.0
g4	g4	1021	0.15	1.00	600.0
g5	g5	1022	0.15	1.05	250.0
g6	g6	1042	0.15	1.05	400.0
g7	g7	1043	0.15	1.05	200.0
g8	g8	2032	0.15	1.05	850.0
g9	g9	4011	0.15	1.05	1000.0
g10	g10	4012	0.15	1.05	800.0
g11	g11	4021	0.15	1.05	300.0
g12	g12	4031	0.15	1.05	350.0
g13	g13	4041	0.10	1.05	300.0
g14	g14	4042	0.15	1.05	700.0
g15	g15	4047	0.15	1.05	1200.0
g16	g16	4051	0.15	1.05	700.0
g17	g17	4062	0.15	1.05	600.0
g18	g18	4063	0.15	1.05	1200.0
g19	g19	4071	0.15	1.05	500.0
g20	g20	4072	0.15	1.05	4500.0

Table 2.5: Data of the 400/220 and 400/130 transformers

transformer name	from bus	to bus	$X$ (pu)	$n$ (pu/pu)	$S_{nom}$ (MVA)
1011-4011	1011	4011	0.10	0.95	1250.0
1012-4012	1012	4012	0.10	0.95	1250.0
1022-4022	1022	4022	0.10	0.93	833.3
2031-4031	2031	4031	0.10	1.00	833.3
1044-4044	1044	4044	0.10	1.03	1000.0
1044-4044b	1044	4044	0.10	1.03	1000.0
1045-4045	1045	4045	0.10	1.04	1000.0
1045-4045b	1045	4045	0.10	1.04	1000.0

Table 2.6: Data of the step-down transformers

transformer name	from bus	to bus	$X$ (pu)	$n$ (pu/pu)	$S_{nom}$ (MVA)
11-1011	11	1011	0.10	1.04	400.0
12-1012	12	1012	0.10	1.05	600.0
13-1013	13	1013	0.10	1.04	200.0
22-1022	22	1022	0.10	1.04	560.0
1-1041	1	1041	0.10	1.00	1200.0
2-1042	2	1042	0.10	1.00	600.0
3-1043	3	1043	0.10	1.01	460.0
4-1044	4	1044	0.10	0.99	1600.0
5-1045	5	1045	0.10	1.00	1400.0
31-2031	31	2031	0.10	1.01	200.0
32-2032	32	2032	0.10	1.06	400.0
41-4041	41	4041	0.10	1.04	1080.0
42-4042	42	4042	0.10	1.03	800.0
43-4043	43	4043	0.10	1.02	1800.0
46-4046	46	4046	0.10	1.02	1400.0
47-4047	47	4047	0.10	1.04	200.0
51-4051	51	4051	0.10	1.05	1600.0
61-4061	61	4061	0.10	1.03	1000.0
62-4062	62	4062	0.10	1.04	600.0
63-4063	63	4063	0.10	1.03	1180.0
71-4071	71	4071	0.10	1.03	600.0
72-4072	72	4072	0.10	1.05	4000.0

The shunt capacitor/inductor data are given in Table 2.7.  $Q_{nom}$  is the reactive power produced by the shunt element under a 1 pu voltage. Negative values relate to inductors.

Table 2.7: Shunt compensation data

bus	$Q_{nom}$ (Mvar)
1022	50.
1041	250.
1043	200.
1044	200.
1045	200.
4012	-100.
4041	200.
4043	200.
4046	100.
4051	100.
4071	-400.

## 2.3 Operating point data

Two operating points are considered. The first one, denoted A, is insecure, i.e. the system cannot stand some N-1 contingencies.

The system is made secure by rather simple modifications; this leads to operating point B.

### Operating point A

The system operating point is specified in Tables 2.8 to 2.10, which provide, for each bus, the consumed active and reactive power, the generated active and reactive power and the initial voltage obtained from a power flow calculation. In this calculation, bus g20 has been taken as slack-bus.

Table 2.8: Operating point A: data of generator buses

bus	base voltage (kV)	generated power		initial voltage	
		active (MW)	reactive (Mvar)	magnitude (pu)	phase angle (deg)
g1	15.0	600.0	58.3	1.0684	2.59
g2	15.0	300.0	17.2	1.0565	5.12
g3	15.0	550.0	20.9	1.0595	10.27
g4	15.0	400.0	30.4	1.0339	8.03
g5	15.0	200.0	60.1	1.0294	-12.36
g6	15.0	360.0	138.6	1.0084	-59.42
g7	15.0	180.0	60.4	1.0141	-68.95
g8	15.0	750.0	232.6	1.0498	-16.81
g9	15.0	668.5	201.3	0.9988	-1.63
g10	15.0	600.0	255.7	1.0157	0.99
g11	15.0	250.0	60.7	1.0211	-29.04
g12	15.0	310.0	98.3	1.0200	-31.88
g13	15.0	0.0	50.1	1.0170	-54.30
g14	15.0	630.0	295.9	1.0454	-49.90
g15	15.0	1080.0	377.9	1.0455	-52.19
g16	15.0	600.0	222.6	1.0531	-64.10
g17	15.0	530.0	48.7	1.0092	-46.85
g18	15.0	1060.0	293.4	1.0307	-43.32
g19	15.0	300.0	121.2	1.0300	0.03
g20	15.0	2137.4	377.4	1.0185	0.00

Table 2.9: Operating point A: data of transmission buses

bus	base voltage (kV)	initial voltage	
		magnitude (pu)	phase angle (deg)
1011	130.0	1.0618	-6.65
1012	130.0	1.0634	-3.10
1013	130.0	1.0548	1.26
1014	130.0	1.0611	4.26
1021	130.0	1.0311	2.64
1022	130.0	1.0512	-19.05
1041	130.0	1.0124	-81.87
1042	130.0	1.0145	-67.38
1043	130.0	1.0274	-76.77
1044	130.0	1.0066	-67.71
1045	130.0	1.0111	-71.66
2031	220.0	1.0279	-36.66
2032	220.0	1.0695	-23.92
4011	400.0	1.0224	-7.55
4012	400.0	1.0235	-5.54
4021	400.0	1.0488	-36.08
4022	400.0	0.9947	-20.86
4031	400.0	1.0367	-39.46
4032	400.0	1.0487	-44.54
4041	400.0	1.0506	-54.30
4042	400.0	1.0428	-57.37
4043	400.0	1.0370	-63.51
4044	400.0	1.0395	-64.23
4045	400.0	1.0533	-68.88
4046	400.0	1.0357	-64.11
4047	400.0	1.0590	-59.55
4051	400.0	1.0659	-71.01
4061	400.0	1.0387	-57.93
4062	400.0	1.0560	-54.36
4063	400.0	1.0536	-50.68
4071	400.0	1.0484	-4.99
4072	400.0	1.0590	-3.98

Table 2.10: Operating point A: data of distribution buses

bus	base voltage (kV)	consumed power		initial voltage	
		active (MW)	reactive (Mvar)	magnitude (pu)	phase angle (deg)
1	20.	600.	148.2	0.9988	-84.71
2	20.	330.	71.0	1.0012	-70.49
3	20.	260.	83.8	0.9974	-79.97
4	20.	840.	252.0	0.9996	-70.67
5	20.	720.	190.4	0.9961	-74.59
11	20.	200.	68.8	1.0026	-9.45
12	20.	300.	83.8	0.9975	-5.93
13	20.	100.	34.4	0.9957	-1.58
22	20.	280.	79.9	0.9952	-21.89
31	20.	100.	24.7	1.0042	-39.47
32	20.	200.	39.6	0.9978	-26.77
41	20.	540.	131.4	0.9967	-57.14
42	20.	400.	127.4	0.9952	-60.22
43	20.	900.	254.6	1.0013	-66.33
46	20.	700.	211.8	0.9990	-66.93
47	20.	100.	44.0	0.9950	-62.38
51	20.	800.	258.2	0.9978	-73.84
61	20.	500.	122.5	0.9949	-60.78
62	20.	300.	83.8	1.0002	-57.18
63	20.	590.	264.6	0.9992	-53.49
71	20.	300.	83.8	1.0028	-7.80
72	20.	2000.	396.1	0.9974	-6.83

## Operating point B

Operating point B is obtained from operating point A by making the following changes.

- In parallel with g16 and its step-up transformer, an identical generator - named g16b - and an identical step-up transformer are connected. The additional generator produces the same active power under the same terminal voltage (respectively 600 MW and 1.0531 pu: see Table 2.8). The additional production of 600 MW is compensated by the slack-bus. The power flow in the North-Central corridor is decreased by almost the same power, which makes the system significantly more robust.
- Still, the system cannot stand the loss of either g15 or g18 (producing respectively 1080 and 1060 MW : see Table 2.8)<sup>2</sup>. Here, the choice is to make the contingencies less severe, by replacing each of these generators by two identical generators with half nominal apparent power (600 instead of 1200 MVA: see Table 2.11), half nominal turbine power (540 instead of 1080 MW: see same table), and half production (540 instead of 1080 MW for g15, 530 instead of 1060 MW for g18). Each generator is connected to the rest of the system by a step-up transformer with half nominal apparent power (600

<sup>2</sup>Indeed, the lost production is compensated by generators in the North and Equiv areas, which increases the flow in the North-Central corridor by the corresponding power.

instead of 1200 MVA: see table 2.4). Both generators have the same terminal voltage as the generator they replace.

Figure 2.4 compares the input data and some results of power flow calculations at points A and B, respectively.

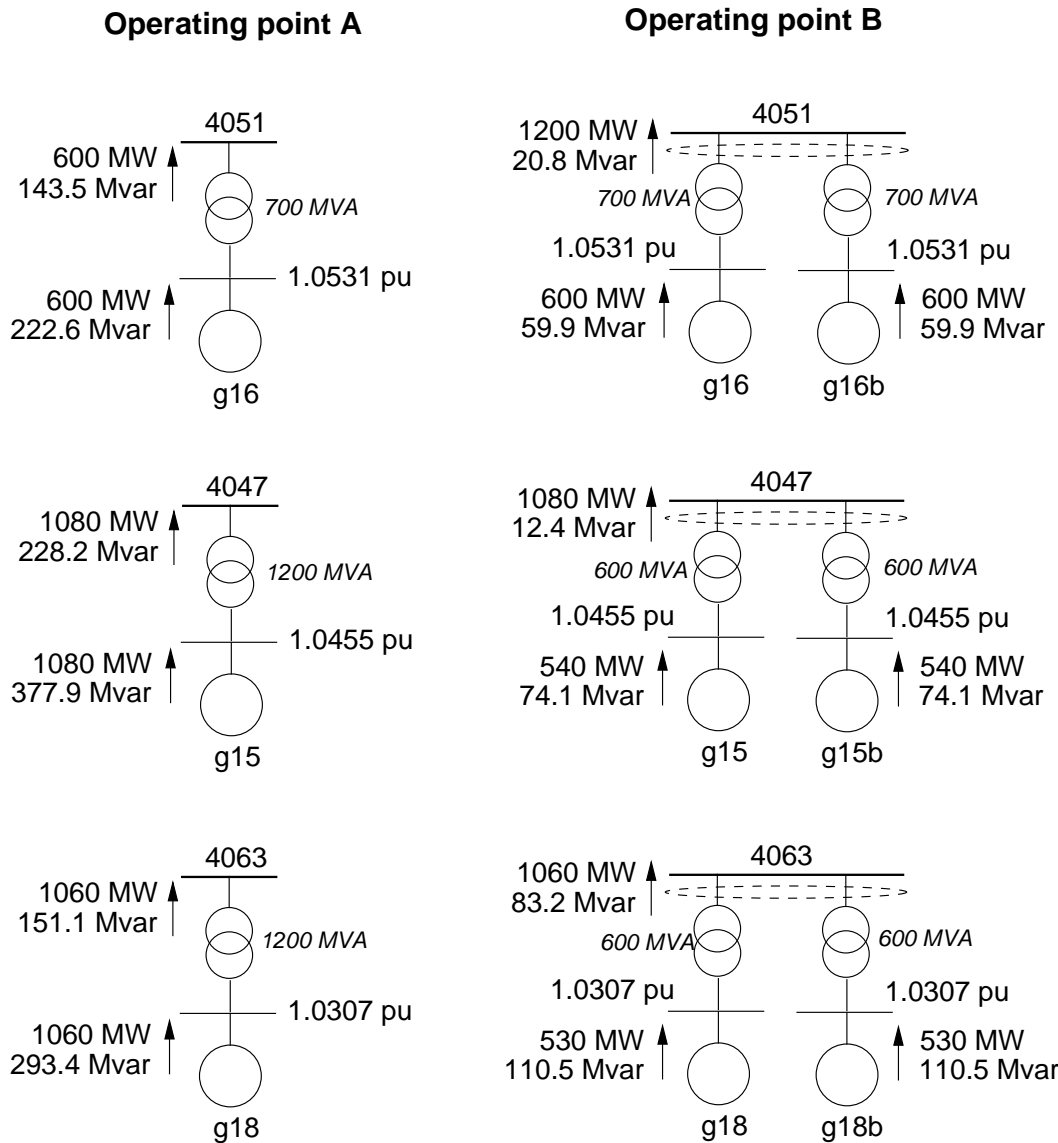


Figure 2.4: (Partial) comparison of operating points A and B

## 2.4 Synchronous machine data

Synchronous machines are represented by a standard model (e.g. [3]) with three rotor windings for the salient-pole machines of hydro power plants, and four rotor windings for the round-rotor machines of thermal plants. g13 is a synchronous condenser and, as such, is modeled as a salient pole machine.

The nominal apparent power  $S_{nom}$  of each generator together with the nominal active power  $P_{nom}$  of its turbine are given in Table 2.11. As can be seen, the generator power factor, computed as  $P_{nom}/S_{nom}$ , is 0.95 for the hydro plants (North and Equiv areas) and 0.90 for the thermal plants (Central and South areas, where most of the load is located).

Table 2.11: Nominal apparent powers of synchronous machines and nominal active powers of their turbines

gener.	$S_{nom}$ (MVA)	$P_{nom}$ (MW)
g1	800.	760.0
g2	600.	570.0
g3	700.	665.0
g4	600.	570.0
g5	250.	237.5
g6	400.	360.0
g7	200.	180.0
g8	850.	807.5
g9	1000.	950.0
g10	800.	760.0
g11	300.	285.0
g12	350.	332.5
g13	300.	-
g14	700.	630.0
g15	1200.	1080.0
g16	700.	630.0
g17	600.	540.0
g18	1200.	1080.0
g19	500.	475.0
g20	4500.	4275.0

The machine reactances, time constants and inertia coefficients are given in Table 2.12. The reactances are in pu on the base ( $V_B, S_{nom}$ ) where  $V_B$  is the network base voltage of the machine bus.

Saturation is modelled in all machines. The standard saturation curve relating the no-load armature voltage  $V_{nl}$  to the field current  $i_{fd}$  is given in Fig. 2.5. With reference to this figure, the saturation characteristics is given by:

$$k = \frac{|AC|}{|AB|} = 1 + m(V_{nl})^n$$

The following data apply to all machines:

- for  $V_{nl} = 1$  pu,  $k = 1.1$  which yields  $1.1 = 1 + m$  and hence  $m = 0.1$ ;

Table 2.12: Synchronous machine data

	round rotor	salient pole	salient-pole
	g6, g7, g14, g15, g16, g17, g18	g1, g2, g3, g4, g5, g8, g9, g10, g11, g12, g19, g20	g13
$X_d$ (pu)	2.20	1.10	1.55
$X_q$ (pu)	2.00	0.70	1.00
$X'_d$ (pu)	0.30	0.25	0.30
$X'_q$ (pu)	0.40		
$X''_d$ (pu)	0.20	0.20	0.20
$X''_q$ (pu)	0.20	0.20	0.20
$T'_{do}$ (s)	7.0	5.0	7.0
$T'_{qo}$ (s)	1.5		
$T''_{do}$ (s)	0.05	0.05	0.05
$T''_{qo}$ (s)	0.05	0.10	0.10
$H$ (s)	6.0	3.0	2.0
$i_{fd}^{rated}$ (pu)	2.9160	1.8087	2.8170

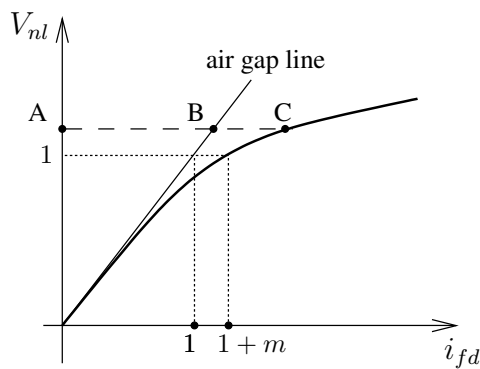


Figure 2.5: Saturation characteristics

- for  $V_{nl} = 1.2$  pu,  $k = 1.3$  which yields  $1.3 = 1 + 0.1 \times 1.2^n$  and hence  $n = 6.0257$ ;
- (unsaturated) leakage reactance  $X_\ell = 0.15$  pu in both axes.

The last row in Table 2.12 provides the generator field currents  $i_{fd}^{rated}$  under rated operating conditions, i.e. when the machine operates with:

$$\begin{aligned} V &= 1 \\ P &= P_{nom} \\ S &= S_{nom} \Leftrightarrow \sqrt{P_{nom}^2 + Q^2} = S_{nom} \Leftrightarrow Q = \sqrt{S_{nom}^2 - P_{nom}^2} \end{aligned}$$

where  $P$ ,  $V$  and  $S$  are in per unit. The  $i_{fd}^{rated}$  values are in per unit on a base such that  $i_{fd} = 1$  pu when the generator operates at no load with a 1 pu terminal voltage and without saturation (operation on the air gap line). This corresponds to the leftmost point on the abscissa axis in Fig. 2.5.

## 2.5 Exciter, automatic voltage regulator and power system stabilizer model and data

Figure 2.6 shows the simple model used to represent the exciter, the Automatic Voltage Regulator (AVR) and the Power System Stabilizer (PSS). The same model is used for all generators but with different parameters, as shown in Table 2.13.  $v_{fd}$  is the field voltage, in per unit on a base such that  $v_{fd} = 1$  pu when the generator operates at no load with a 1 pu terminal voltage and without saturation (operation on the air gap line).  $V$  is the magnitude of the generator terminal voltage, in pu.

Table 2.13: Parameters of exciter, AVR, PSS and OEL

generator	$i_{fd}^{lim}$ (pu)	$f$	$r$	$L_1$	$G$	$T_a$ (s)	$T_b$ (s)	$L_2$ (pu)	$K_p$	$T_w$ (s)	$T_1$ (s)	$T_2$ (s)	$C$ (pu)
g1, g2, g3	1.8991	0.	1.	-11.	70.	10.	20.0	4.	75.	15.	0.20	0.010	0.1
g4	1.8991	0.	1.	-11.	70.	10.	20.0	4.	150.	15.	0.20	0.010	0.1
g5	1.8991	0.	1.	-11.	70.	10.	20.0	4.	75.	15.	0.20	0.010	0.1
g6	3.0618	1.	0.	-20.	120.	5.	12.5	5.	75.	15.	0.22	0.012	0.1
g7	3.0618	1.	0.	-20.	120.	5.	12.5	5.	75.	15.	0.22	0.012	0.1
g8, g9, g10	1.8991	0.	1.	-11.	70.	10.	20.0	4.	75.	15.	0.20	0.010	0.1
g11	1.8991	1.	0.	-20.	70.	10.	20.0	4.	75.	15.	0.20	0.010	0.1
g12	1.8991	1.	0.	-20.	70.	10.	20.0	4.	75.	15.	0.20	0.010	0.1
g13	2.9579	0.	1.	-17.	50.	4.	20.0	4.	0.				
g14	3.0618	0.	1.	-18.	120.	5.	12.5	5.	75.	15.	0.22	0.012	0.1
g15, g16	3.0618	0.	1.	-18.	120.	5.	12.5	5.	75.	15.	0.22	0.012	0.1
g17, g18	3.0618	0.	1.	-18.	120.	5.	12.5	5.	150.	15.	0.22	0.012	0.1
g19, g20	1.8991	0.	1.	-11.	70.	10.	20.0	4.	0.				

The exciter is represented by a first-order system with a time constant of 0.1 s and non-windup limits on  $v_{fd}$ . The AVR includes a transient gain reduction. The latter has been chosen to limit the overshoot in terminal voltage following a step change in voltage reference when the generator operates in open circuit.

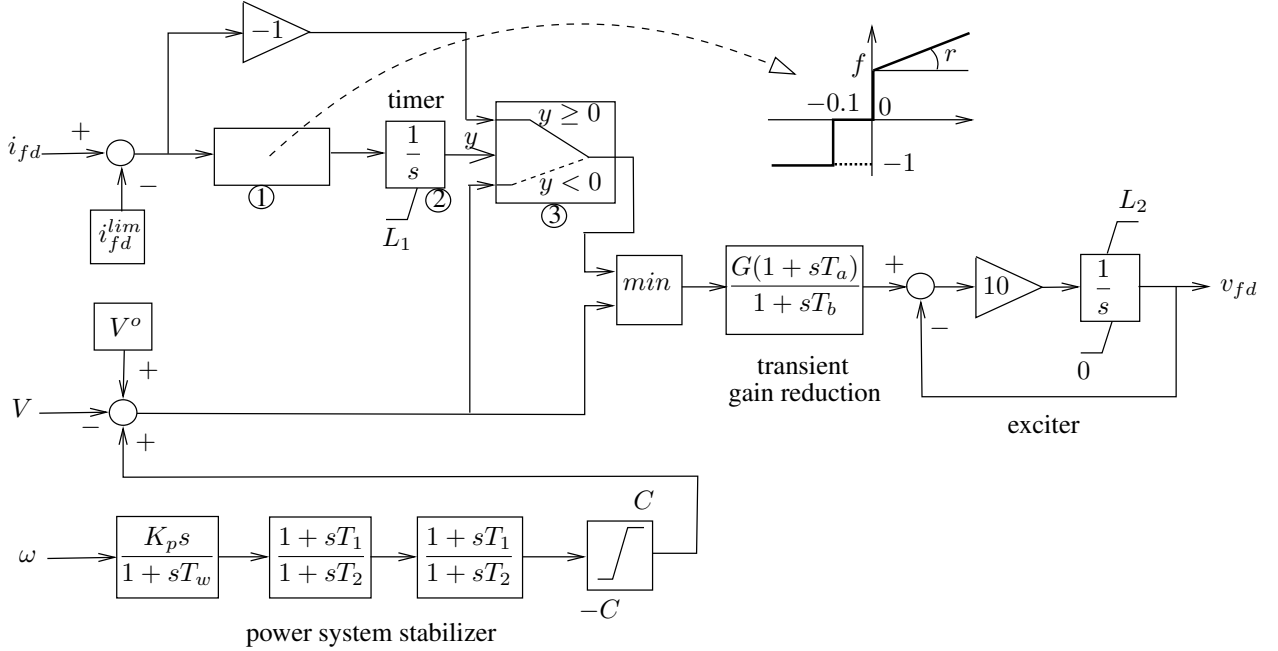


Figure 2.6: Model of exciter, AVR, PSS and OEL

All generators except g13, g19 and g20 are equipped with PSS using the rotor speed  $\omega$  as input (a zero value for  $K_p$  in Table 2.13 indicates the absence of PSS).  $\omega$  is in per unit. Each PSS includes a washout filter<sup>3</sup> and two identical lead filters in cascade. The PSS phase compensation was chosen considering the maximum and minimum equivalent Thevenin impedances seen by the machines of each group (units 7 and 18 for the round-rotor, units 4 and 12 for the salient-pole machines). The PSS transfer functions provide damping for oscillation frequencies from 0.2 Hz to more than 1 Hz.

$K_p$  has been set to a higher value for generators g17 and g18, in order these generators to have enough damping after the tripping of line 4061-4062, which leaves them radially connected to the rest of the system. It was also set to a higher value for generator g4, in order to provide enough damping for it after the tripping of line 1021-1022.

No attempt was made to further “optimize” the PSS settings, which is appropriate for a test system.

## 2.6 Overexcitation limiter model and data

Each machine is equipped with an OverExcitation Limiter (OEL) keeping its field current within limits. Since the focus is on scenarios with sagging voltages and overexcited generators, the model does not include UnderExcitation Limiter (UEL). Armature current and V/Hz limiters are not considered either.

<sup>3</sup>Note that the numerator of this transfer function can be also defined as  $K_p T_w s$ , which leads to much smaller values of  $K_p$  since  $T_w = 15$  s

The field current limit enforced by the OEL, denoted by  $i_{fd}^{lim}$ , is set to 105 % of  $i_{fd}^{rated}$ . Thus, if  $i_{fd}$  settles to any value below  $i_{fd}^{lim} = 1.05 i_{fd}^{rated}$ , the field current is not limited.

The four smallest generators, namely g6, g7, g11 and g12 have a fixed-time OEL that operates after 20 seconds.

All other machines have an OEL with inverse time characteristics, i.e. the higher the field current, the faster the limitation takes place. This takes advantage of the overload capability of the rotor. For the three types of generators quoted in Table 2.12, Figs. 2.7 to 2.9 show respectively : the variation of the overload delay with the field current  $i_{fd}$  (solid line), four points of the ANSI curve, and the  $i_{fd}^{lim}$  value (dashed vertical line). As can be seen, the OEL has been set to react faster than what the ANSI curve allows.

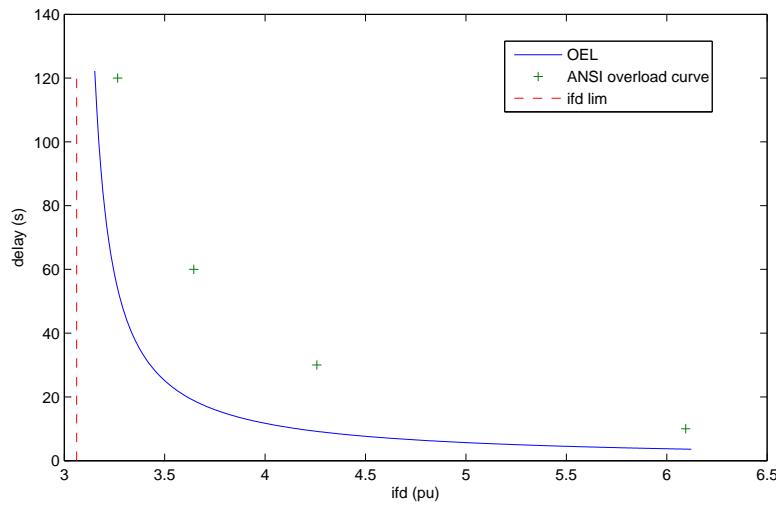


Figure 2.7: Overexcitation delay: generators g14 - g18

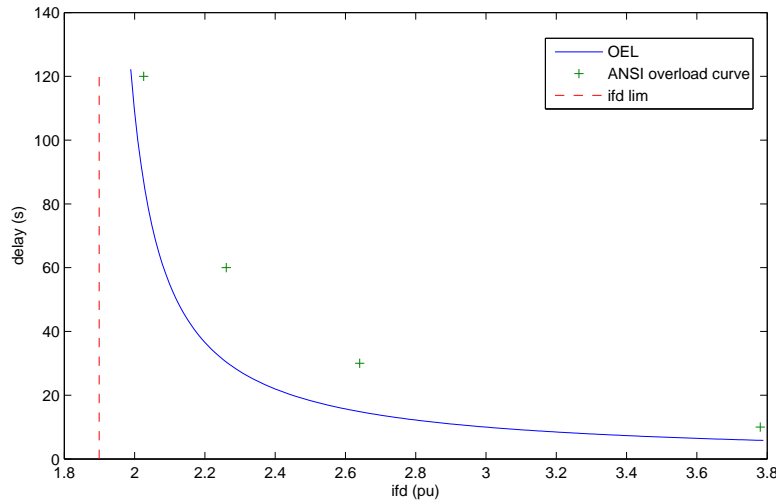


Figure 2.8: Overexcitation delay: generators g1 - g5, g8 - g10, g19, g20

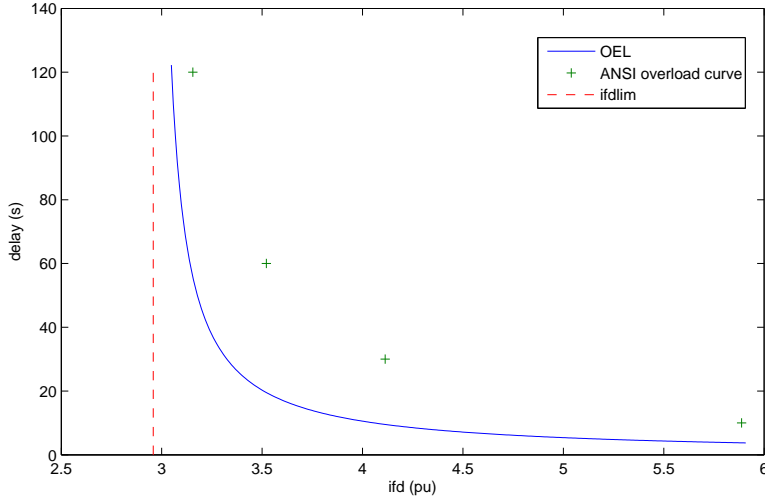


Figure 2.9: Overexcitation delay: generator g13

There is a wide variety of OELs and relatively few standard models [2, 4]. Other models than the one described hereafter can be used provided the correct value  $i_{fd}^{lim}$  is enforced after the correct delay.

The OEL model is shown in Fig. 2.6. It is of the takeover type [4] and applies the so-called “error signal substitution” (the alternative would be the “control signal substitution”). Operation is as follows.

In normal operating conditions  $i_{fd}$  is lower than  $i_{fd}^{lim}$  and the output of block 1 is -1. This keeps the integrator of block 2 at its lower limit  $L_1$ , which is negative. It results that the switch in block 3 remains in the lower position. The minimum gate passes on the  $V^o - V$  signal to the AVR.

If  $i_{fd}$  becomes larger than  $i_{fd}^{lim}$ , the output of block 1 becomes positive, causing the output of block 2 to rise. When it becomes positive, it makes the switch change position, and the negative signal  $i_{fd}^{lim} - i_{fd}$  is sent to the minimum gate. The latter selects the signal coming from the OEL, which is thus passed on to the AVR, and the generator changes from voltage to field current control. In steady state, the gain  $G$  forces  $i_{fd}$  to a value a bit smaller than  $i_{fd}^{lim}$ . The difference  $i_{fd} - i_{fd}^{lim}$  is expected to lie in the interval  $[-0.1, 0]$ . Hence, the output of block 1 is zero (see Fig. 2.6), which avoids switching back under voltage control.

Block 2 operates as a timer, adding an intentional delay corresponding to the thermal overload capability of the field winding. For generators g6, g7, g11 and g12,  $f = 1$  and  $r = 0$  (see Table 2.13). Thus, the switching takes place after a delay that does not depend on the overload  $i_{fd} - i_{fd}^{lim}$ . The other generators have  $f = 0$  and  $r = 1$ ; hence, the larger the overload, the shorter the delay before limiting the field current. This yields the above mentioned inverse-time characteristics.

If the field current has been limited but operating conditions require less excitation, the model automatically resets under voltage control. This is done by the minimum gate choosing the terminal voltage signal.

## 2.7 Generator capability curves

All the data regarding generator limitations have been given in the previous sections. The steady-state characteristics can be derived in the form of generator capability curves, which are convenient for power flow calculations.

Figures 2.10 and 2.11 show the capability curves of respectively the round-rotor and the salient-pole generators, identified in Columns 2 and 3 of Table 2.12<sup>4</sup>. In these figures, the powers are in per unit on the MVA machine base; all machines of the same group have the same per unit capability curves. The UEL curves are shown for information only, since the correspond limiters are not present in the model.

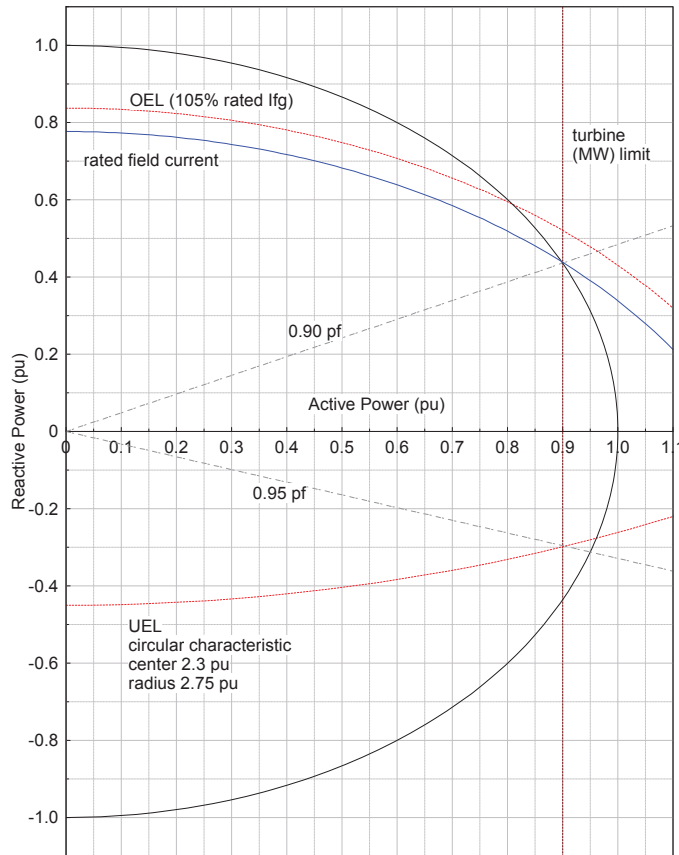


Figure 2.10: capability curves of round-rotor generators (identified in Table 2.12)

Note that the curves have been obtained for a 1 pu voltage at the generator bus. They must be adjusted with the generator voltage (base case generator voltages are available in Table 2.8). Figures 2.12 and 2.13 precisely show the field and stator current limits for a terminal voltage equal to 0.95, 1.00 and 1.05 pu, respectively.

<sup>4</sup>the synchronous condenser at bus g13 is not considered

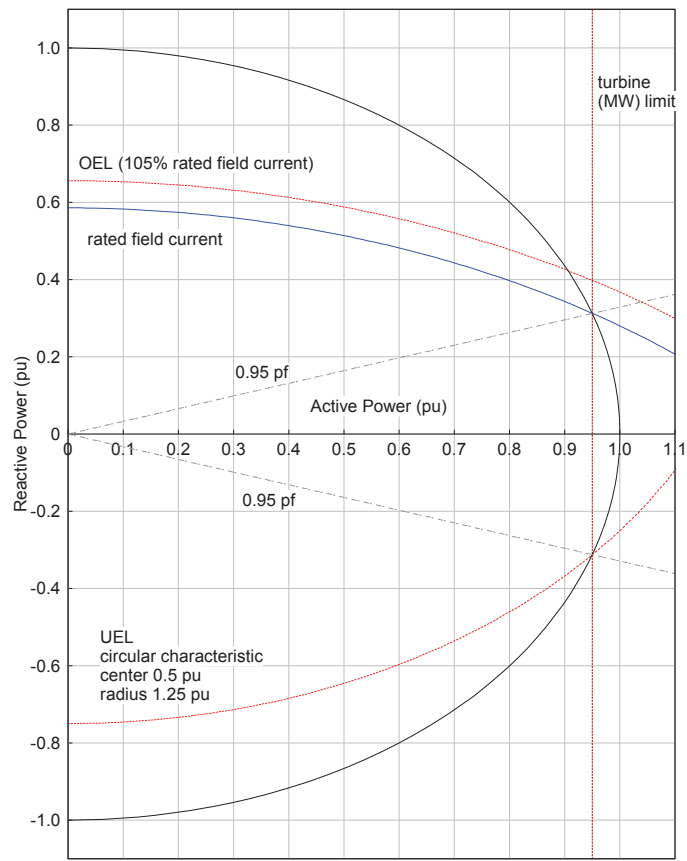


Figure 2.11: capability curves of salient-pole generators (identified in Table 2.12)

From those curves, one can easily obtain the reactive power upper limit  $Q_{max}$  of a generator to consider in a power flow calculation. To match the dynamic simulations shown in the next section, only the field current limit is to be considered, since the stator current limit is not enforced.

**Example.** Consider generator g12 which operates at 1.02 pu voltage and  $310/350 = 0.886$  pu of active power. From Figure 2.13, one obtains  $Q_{max} = 0.4$  pu  $= 0.4 \times 350 = 140$  Mvar.

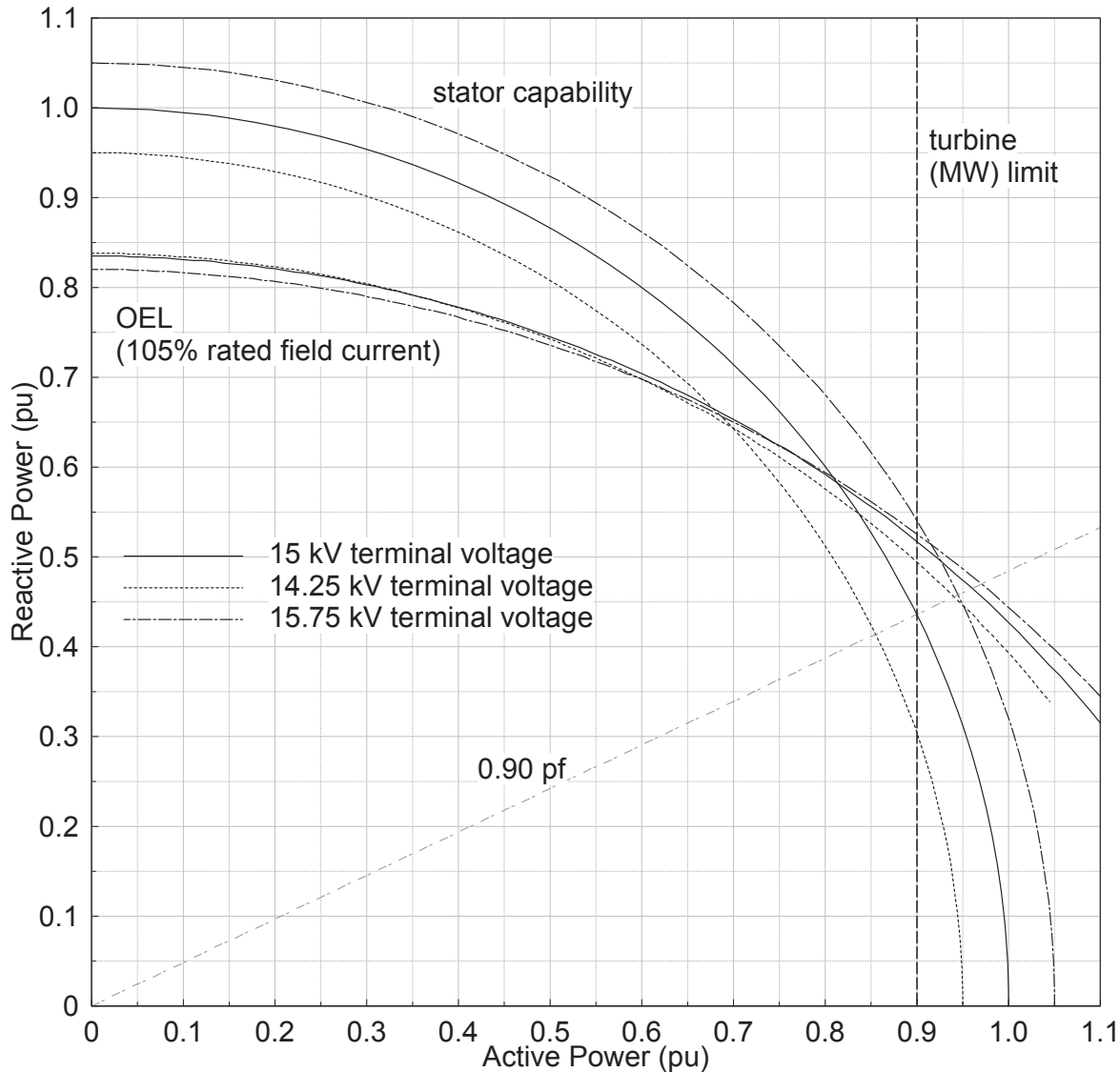


Figure 2.12: (partial) capability curves of round-rotor generators (identified in Table 2.12) for different terminal voltages

No capability curve is provided for g13, which is a synchronous condenser. For the latter, the maximum reactive power, corresponding to the rotor current limit is 1.0782 pu (= 323.4 Mvar) at 1 pu voltage, 1.0926 pu (= 327.8 Mvar) at 0.95 pu voltage, and 1.0488 pu (= 314.6 Mvar) at 1.05 pu voltage.

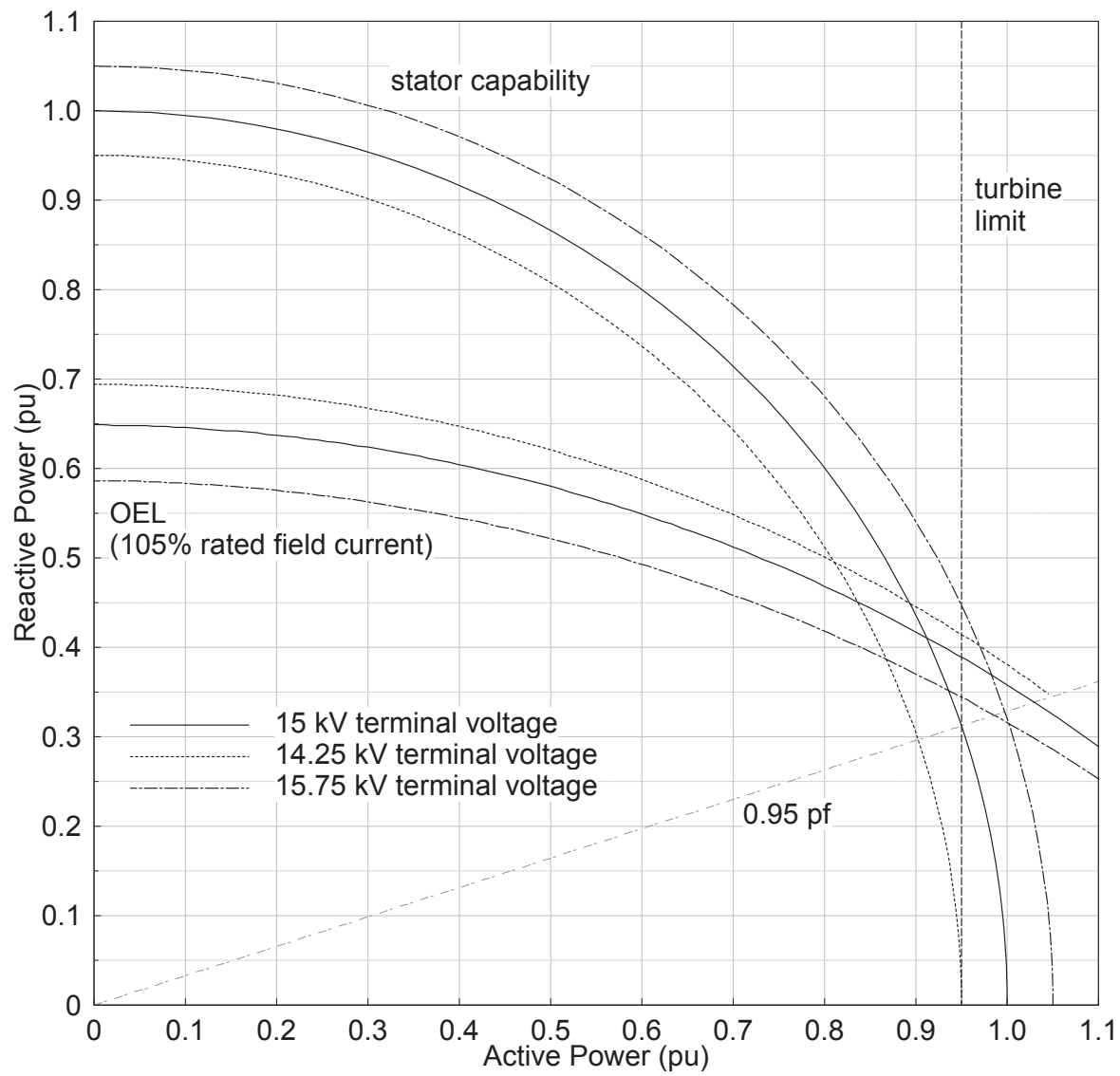


Figure 2.13: (partial) capability curves of salient-pole generators (identified in Table 2.12) for different terminal voltages

## 2.8 Turbine model and data

For already explained reasons, a constant mechanical torque is assumed for the machines of thermal plants. The hydraulic turbines have the nominal active power  $P_{nom}$  listed in Table 2.11. They are all represented by the simple, lossless model of Fig. 2.14 with a water time constant  $T_w$  of 1 second. In this model,  $z$  is the gate opening,  $q$  the water flow,  $H$  the head,  $P_m$  the mechanical power and  $T_m$  the mechanical torque, all in pu on the  $P_{nom}$  base.  $\omega$  is the rotor speed in pu. Thus  $T_m = P_m/\omega$ , as shown in the figure.

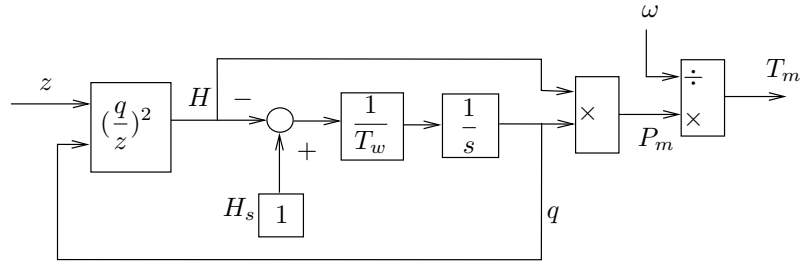


Figure 2.14: Model of hydro turbine

## 2.9 Speed governor model and data

The model of the speed governor used for all hydro turbines is shown in Fig. 2.15. The model includes a simple power measurement, a PI control and a servomotor.  $P$  is the active power produced by the generator,  $P^o$  is the power setpoint,  $z$  is the gate opening and  $\omega$  is the rotor speed. All four are in per unit; for  $P$  and  $P^o$  the base is the turbine nominal power. The active power enters a low-pass filter with a time constant of 2 s. The servomotor is represented by a first-order system with a time constant of 0.2 s, non-windup limits on  $z$ , and limits on the derivative of  $z$ . Only the value of the permanent speed droop  $\sigma$  varies from one machine to another, as indicated in Table 2.14.

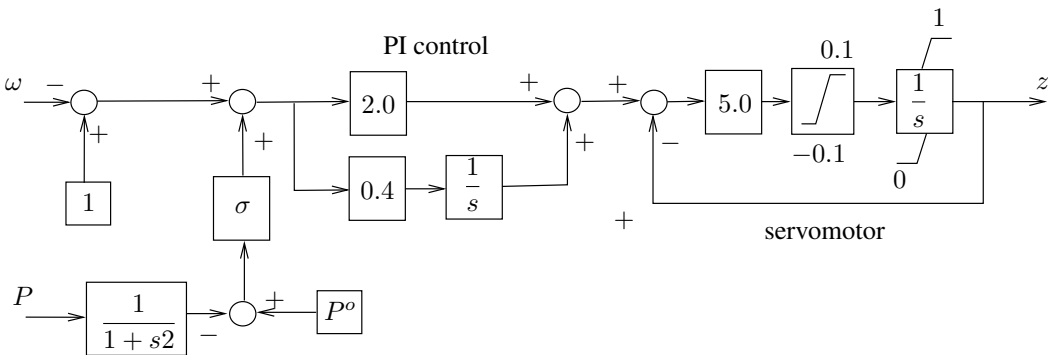


Figure 2.15: Model of speed governor

Table 2.14: Permanent speed droops of the speed governors

generators	$\sigma$
g19, g20	0.08
g1 - g5, g8 - g12	0.04

## 2.10 Load data

All loads are connected to the 20-kV buses. They have an exponential model:

$$P = P_o \left( \frac{V}{V_o} \right)^\alpha \quad Q = Q_o \left( \frac{V}{V_o} \right)^\beta \quad (2.1)$$

with  $\alpha = 1.0$  (constant current) and  $\beta = 2.0$  (constant impedance), respectively.  $V_o$  is set to the initial voltage at the bus of concern.

## 2.11 Load tap changer data

All distribution transformers are equipped with LTCs keeping the distribution voltage in the deadband [0.99 1.01] pu<sup>5</sup>. The LTCs adjust the transformer ratios in the range [0.88 1.20] over 33 positions (thus from one position to the next, the ratio varies by 0.01).

The LTCs have intentional delays. When the distribution voltage leaves the above deadband at time  $t_o$ , the first tap change takes place at time  $t_o + \tau_1$  and the subsequent changes at times  $t_o + \tau_1 + k\tau_2$  ( $k = 1, 2, \dots$ )<sup>6</sup>. The delay is reset to  $\tau_1$  after the controlled voltage has re-entered (or jumped from one side to the other of) the deadband. The values of  $\tau_1$  and  $\tau_2$  are given in Table 2.15; they differ from one transformer to another in order to avoid unrealistic tap synchronization.

---

<sup>5</sup>It can be checked in Table 2.10 that all initial bus voltages lie in this deadband.

<sup>6</sup>Therefore, the second tap change will take place at time  $t_o + \tau_1 + \tau_2$ , the third one at time  $t_o + \tau_1 + 2\tau_2$ , etc.

Table 2.15: Delays of load tap changers

transformer	delays	
	$\tau_1$ (s)	$\tau_2$ (s)
11-1011	30	8
12-1012	30	9
13-1013	30	10
22-1022	30	11
1-1041	29	12
2-1042	29	8
3-1043	29	9
4-1044	29	10
5-1045	29	11
31-2031	29	12
32-2032	31	8
41-4041	31	9
42-4042	31	10
43-4043	31	11
46-4046	31	12
47-4047	30	8
51-4051	30	9
61-4061	30	10
62-4062	30	11
63-4063	30	12
71-4071	31	9
72-4072	31	11

# **Chapter 3**

## **Nordic test system: dynamic responses to contingencies**

### **3.1 Operating point A**

The system response to a particular disturbance is considered. The system initially operates at point A, detailed in Section 2.3.

#### **Disturbance**

The disturbance of concern is a three-phase solid fault on line 4032-4044. It is assumed to take place very near bus 4032, so that it is applied to the bus itself. The fault lasts 5 cycles (0.1 s) and is cleared by opening the line, which remains opened.

The initiating fault is simulated to be more realistic but it is the resulting line outage that causes long-term voltage instability. Simulating the line outage without the fault would yield similar results, with some discrete events shifted in time.

#### **Voltages**

The evolution of transmission system voltages is shown in Fig. 3.1.

In response to the initial disturbance, the system undergoes electromechanical oscillations that die out in some 30 seconds. At that time the system settles at a short-term equilibrium, until the LTCs start acting at  $t = 35$  s. Subsequently, the voltages evolve under the effect of LTCs and OELs.

The system is long-term voltage unstable and eventually collapses less than 3 minutes after the initiating line outage.

As illustrated by the figure, essentially the Central area is affected; voltages at Northern or Southern buses are comparatively little influenced.

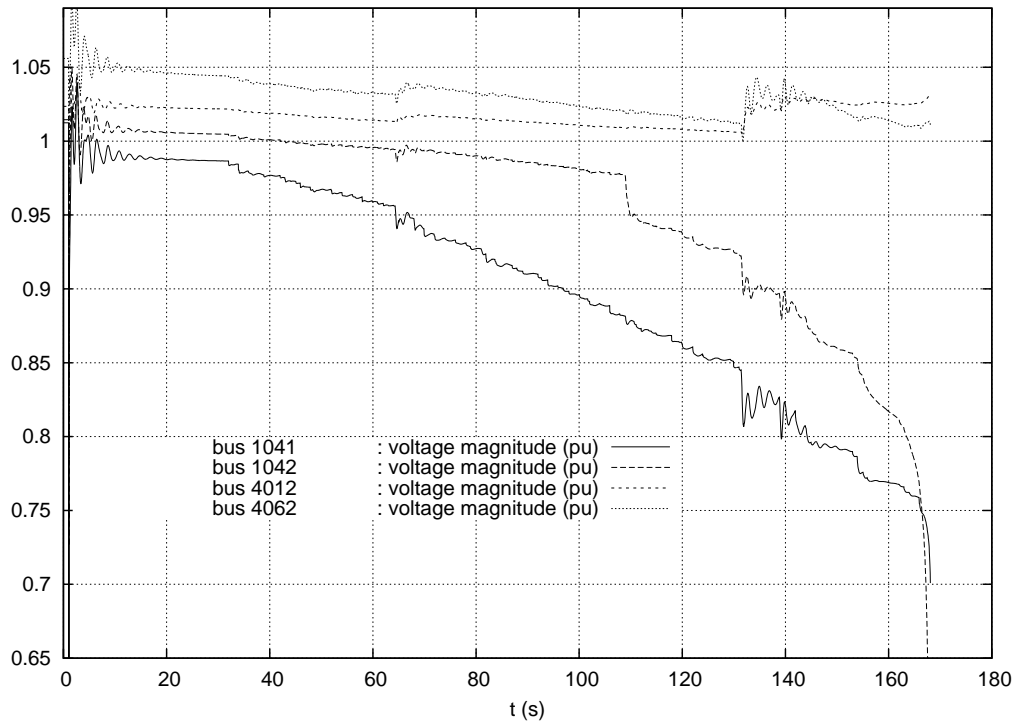


Figure 3.1: Operating point A, fault on line 4032-4044 cleared by opening line: transmission voltages

### Generator field currents and terminal voltages

Figures 3.2 and 3.3 show the evolution of field currents. After settling to post-disturbance values, they start increasing at  $t = 35$  s, when the LTCs start acting. Figure 3.2 refers to the seven generators that get limited: these are in order g12, g14, g7, g11, g6, g15 and g16. Figure 3.3 refers to three non limited generators.

Figure 3.4 shows the terminal voltages of two limited generators. It is easily seen that the voltage is kept fairly constant by the automatic voltage regulator, until the field current gets limited. After that, the voltage drops are pronounced. Note that the voltage of generator g7 eventually reaches a very low value. In a more realistic simulation, this generator should be tripped under the effect of an undervoltage protection, which would obviously aggravate the system degradation. For instance, assuming that this protection is set to act at a generator voltage of 0.85 pu, the tripping would take place near  $t = 140$  s. It is acceptable to ignore the presence of such an undervoltage protection since, at  $t = 140$  s, the system operating conditions are already unacceptable and other models, in particular that of loads, should be also adjusted.

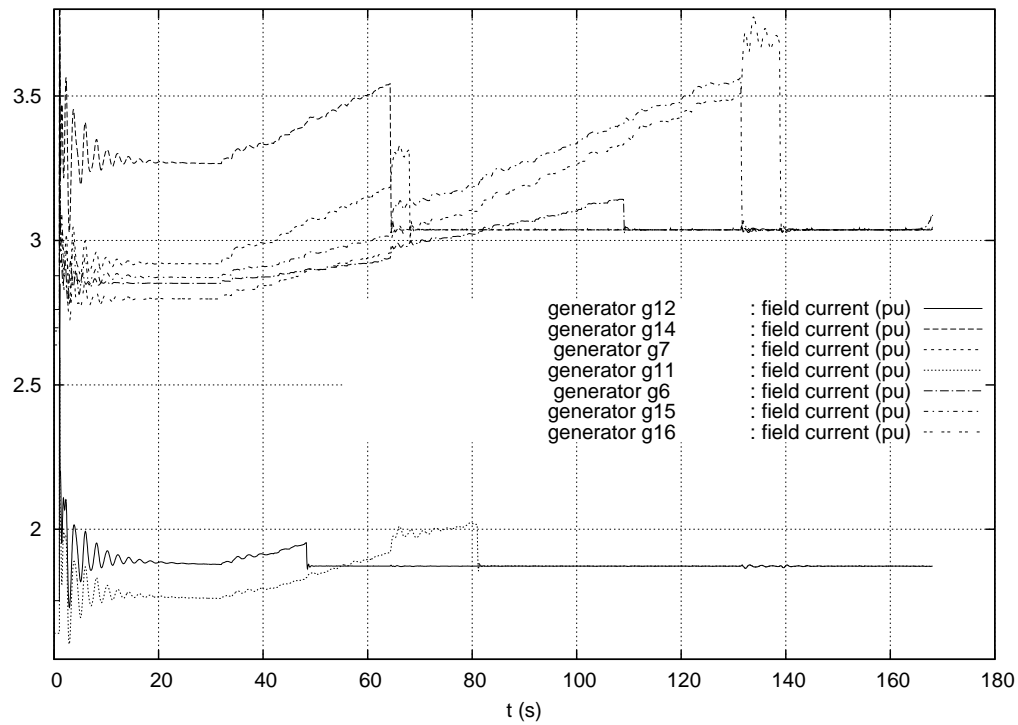


Figure 3.2: Operating point A, fault on line 4032-4044 cleared by opening line: field currents of the seven limited generators

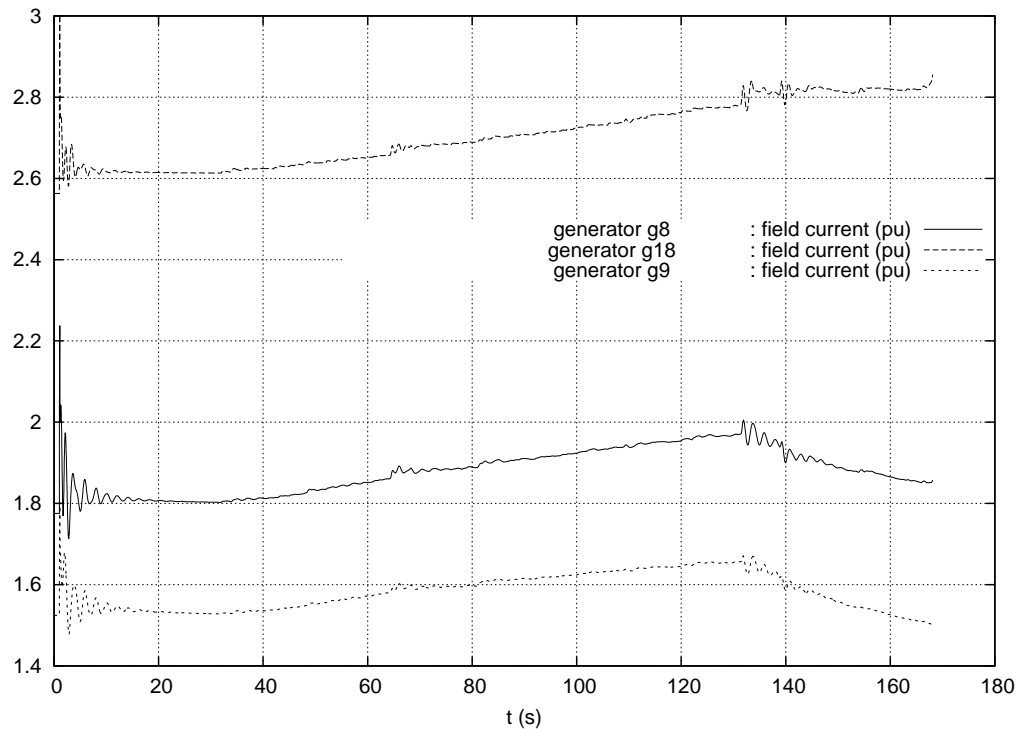


Figure 3.3: operating point A, fault on line 4032-4044 cleared by opening line: field currents of three non limited generators

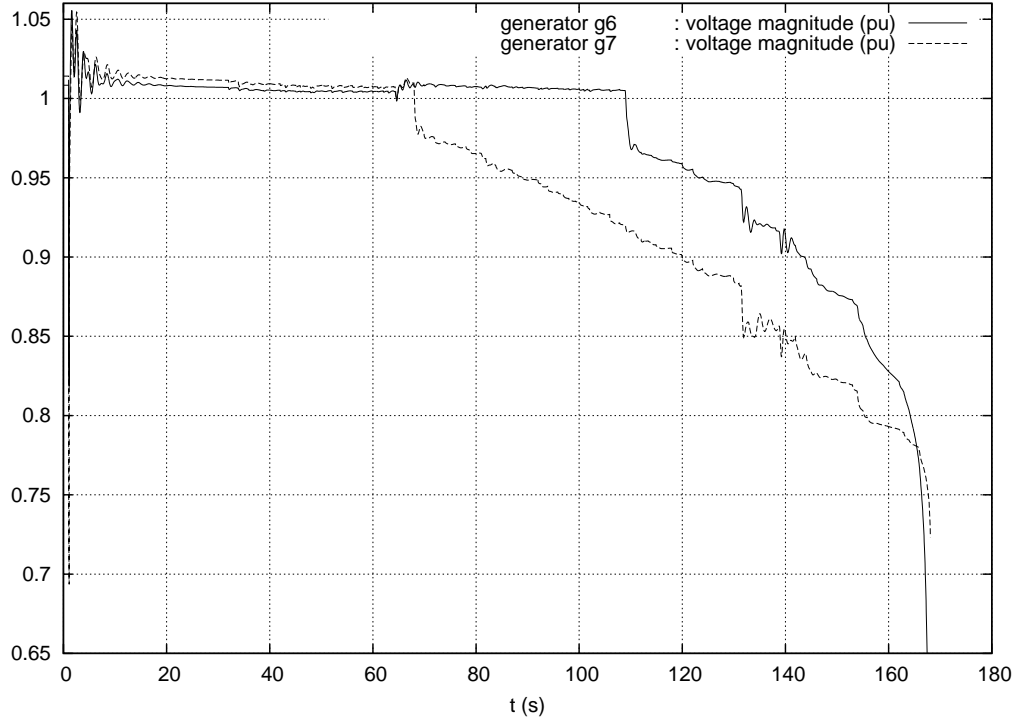


Figure 3.4: operating point A, fault on line 4032-4044 cleared by opening line: terminal voltages of two generators that get limited

### Transformer ratios

Figure 3.5 shows a sample of distribution transformer ratios evolving with various delays to control distribution voltages.

A more detailed view is given in Fig. 3.6, which refers to the transformer connected at bus 1041 and feeding the distribution bus 1. The plot shows the unsuccessful attempt to bring the distribution voltage of bus 1 back within the [0.99 1.01] pu deadband.

The figure also illustrates the multi-dimensional aspect of the problem, i.e. interactions between the various LTCs. Indeed, it is seen that each tap change makes the corresponding distribution voltage move towards the target deadband but in between tap changes, the same voltage drops under the effect of the other LTCs acting to restore their own voltages [11]. All in all, the distribution voltages, and hence the load powers cannot be restored, which is typical of long-term voltage instability.

### Rotor speeds and angles

Fig. 3.7 shows the rotor speed deviations of respectively g6, g7 (both located in Central area), g17 (located in the South) and g20 (large equivalent generator in the North). The machines swing with respect to each other

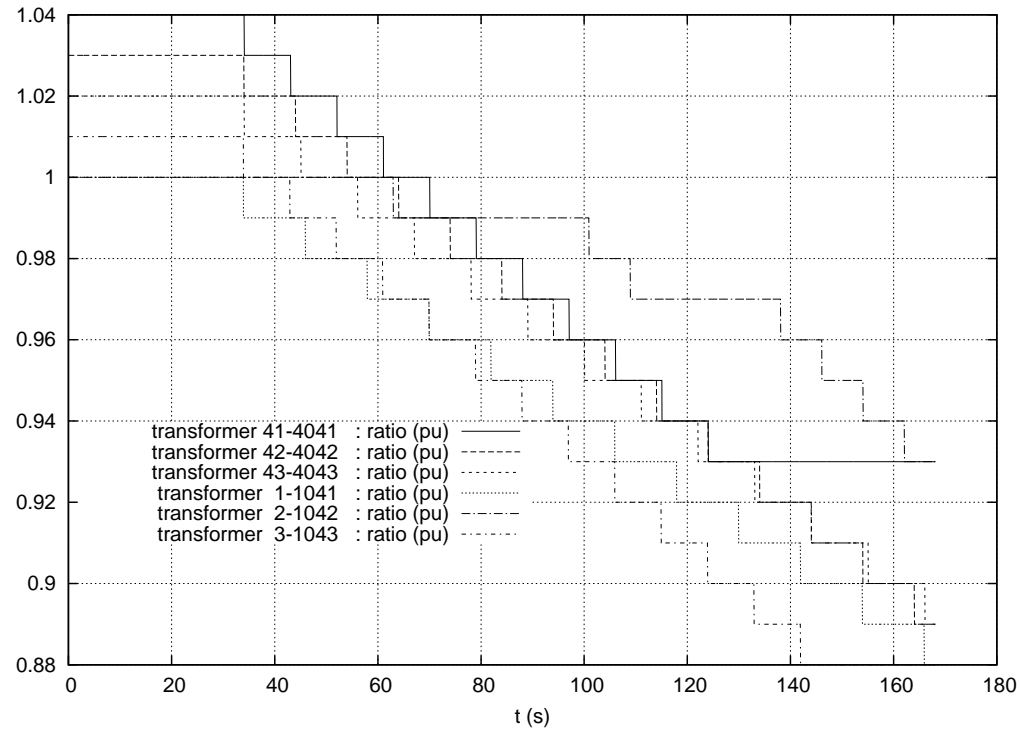


Figure 3.5: operating point A, fault on line 4032-4044 cleared by opening line: distribution transformer ratios

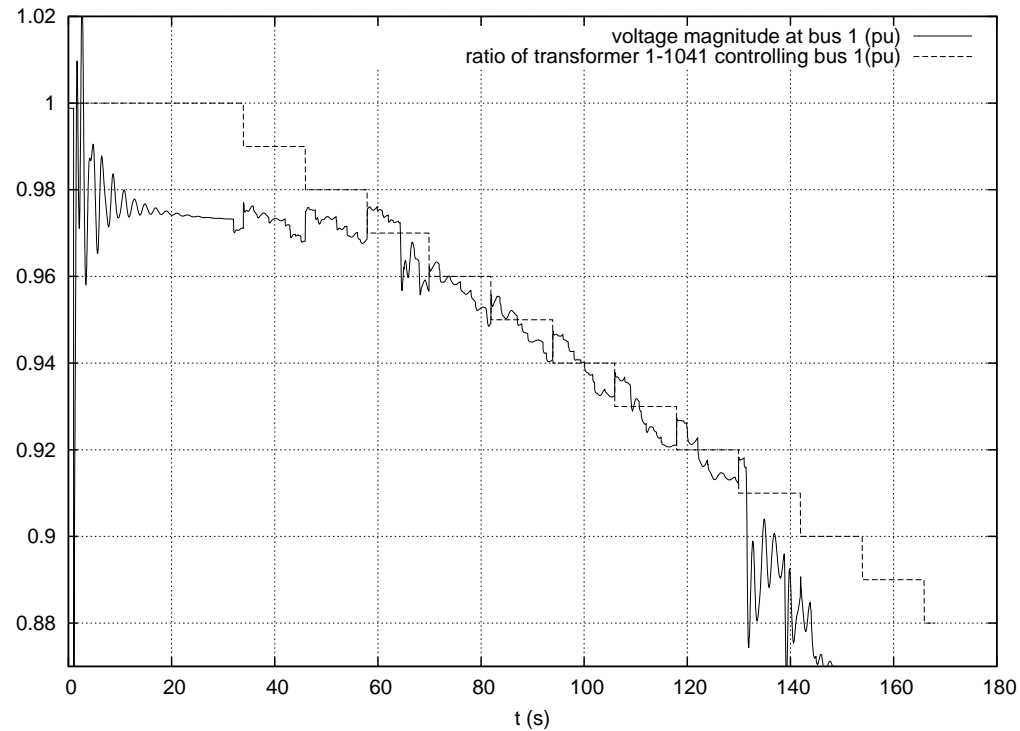


Figure 3.6: operating point A, fault on line 4032-4044 cleared by opening line: unsuccessful restoration of a distribution voltage by LTC

in a stable way until  $t \simeq 170$  s. The curves also show the frequency deviations in response to the variations of load active power with voltages. The jumps at  $t \simeq 65$  and 132 s correspond to machines switching under field current limit, which causes voltages, and hence load powers, to drop.

The final system collapse corresponds to the loss of synchronism of generator g6 with respect to the other machines, as confirmed by Fig. 3.8 showing the deviations of rotor angles with respect to the Center Of Inertia (COI) of the system.

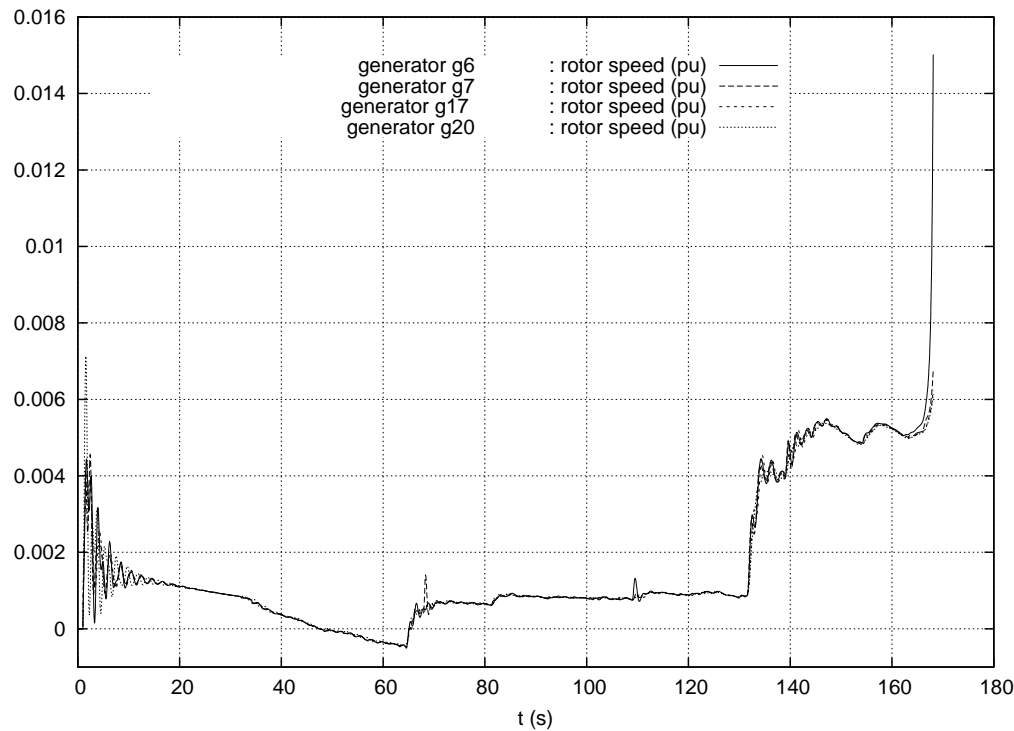


Figure 3.7: operating point A, fault on line 4032-4044 cleared by opening line: speed deviations of synchronous machines

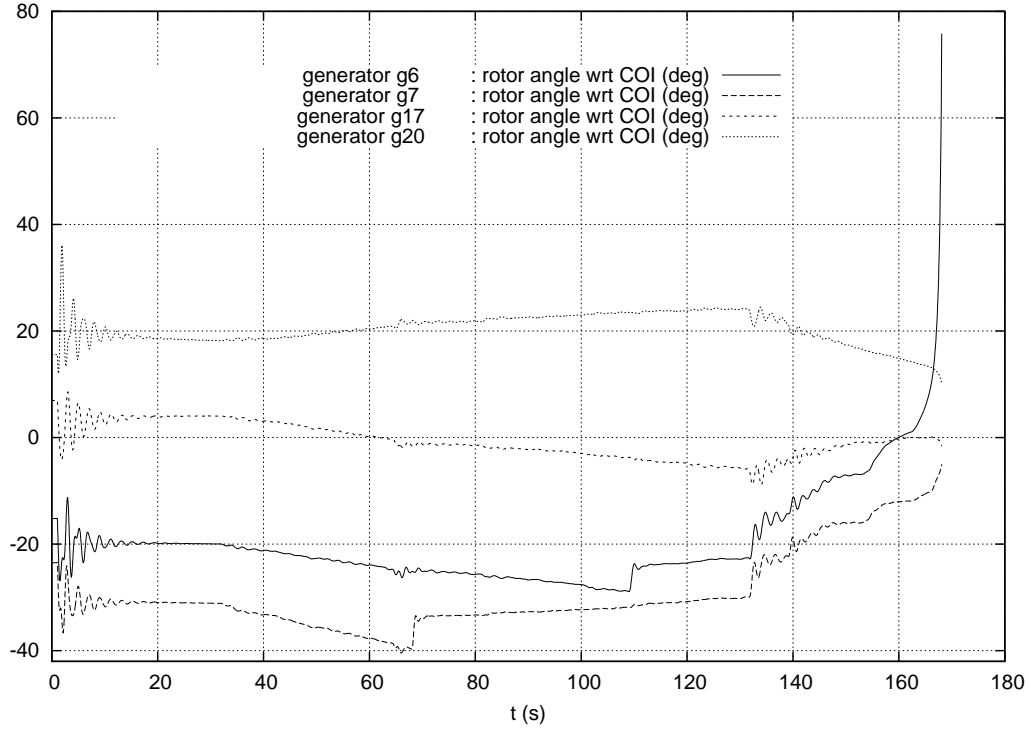


Figure 3.8: operating point A, fault on line 4032-4044 cleared by opening line: deviations of rotor angles of synchronous machines with respect to the Center Of Inertia (COI)

### 3.2 Operating point B

At this operating point, an exhaustive contingency analysis has been performed using time simulation.

The following contingencies have been considered:

- a 5-cycle (0.1 s) fault on any line, cleared by tripping the line;
- the outage of any single generator, except g19 and g20, which are equivalent generators. This includes the outage of one among the generators: g15, g15b, g16, g16b, g18 and g18b<sup>1</sup>.

The post-contingency evolution has been considered acceptable if, over a simulation interval of 600 seconds:

- all distribution bus voltages are restored in their [0.99, 1.01] pu deadbands;
- no generator has its terminal voltage falling below 0.85 pu, except possibly for the fault-on period;
- no loss of synchronism takes place.

<sup>1</sup>Let us recall that the nominal powers of g15, g15b, g18 and g18b have been halved compared to operating point A.

By way of illustration, Fig. 3.9 shows the stable evolution of the voltage at bus 1041 for the previously considered disturbance, namely a fault on line 4032-4044, cleared by opening the line. Fig. 3.10, relative to the same disturbance, shows five distribution voltages that are successfully restored in their deadbands by LTCs.

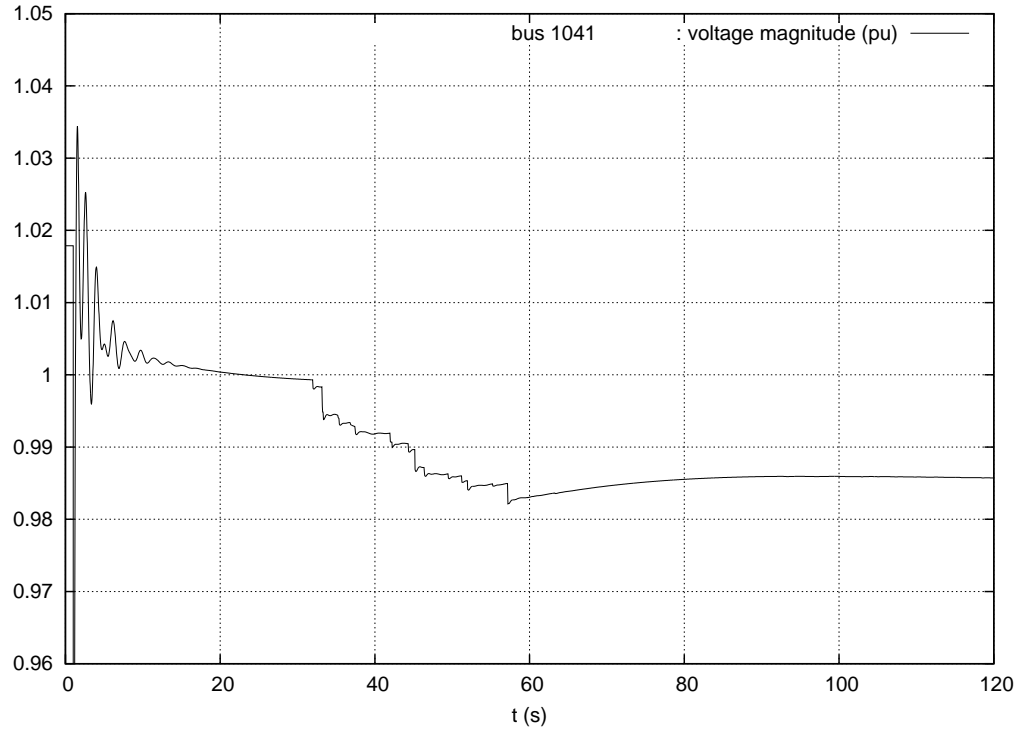


Figure 3.9: Operating point B, fault on line 4032-4044 cleared by opening line: transmission voltages

With the exception of one disturbance, all system responses satisfy the above criteria.

The exception is the outage of generator g6. The evolutions of voltages at the 130-kV buses of the Central region are shown in Fig. 3.11. It is clear that the impact is limited to bus 1042. The corresponding distribution voltages are shown in Fig. 3.12. It can be seen that the LTCs succeed restoring the distribution voltages in their deadbands, except the one controlling bus 2. After a number of unsuccessful steps, the ratio of transformer 1042-2 hits its lower limit, which explains the return of the system to an equilibrium condition, though with unacceptably low voltages at buses 1042 and 2.

This very localized problem could be easily solved by providing bus 1042 with shunt compensation switched upon detection of a low voltage<sup>2</sup>. For instance, Fig. 3.13 shows the voltages at the above two buses when two shunt capacitors, each of 80 Mvar nominal power, are connected. This takes place 10 and 20 seconds after the disturbance occurrence, respectively. The transmission voltage recovers to an acceptable value, while the LTC succeeds restoring the distribution voltage.

In view of the very localized nature of the problem, and the ability to solve it through corrective, post-disturbance control, it is reasonable to consider operating point B as secure.

---

<sup>2</sup>Bus 1042 is the only 130-kV bus not provided with shunt compensation.

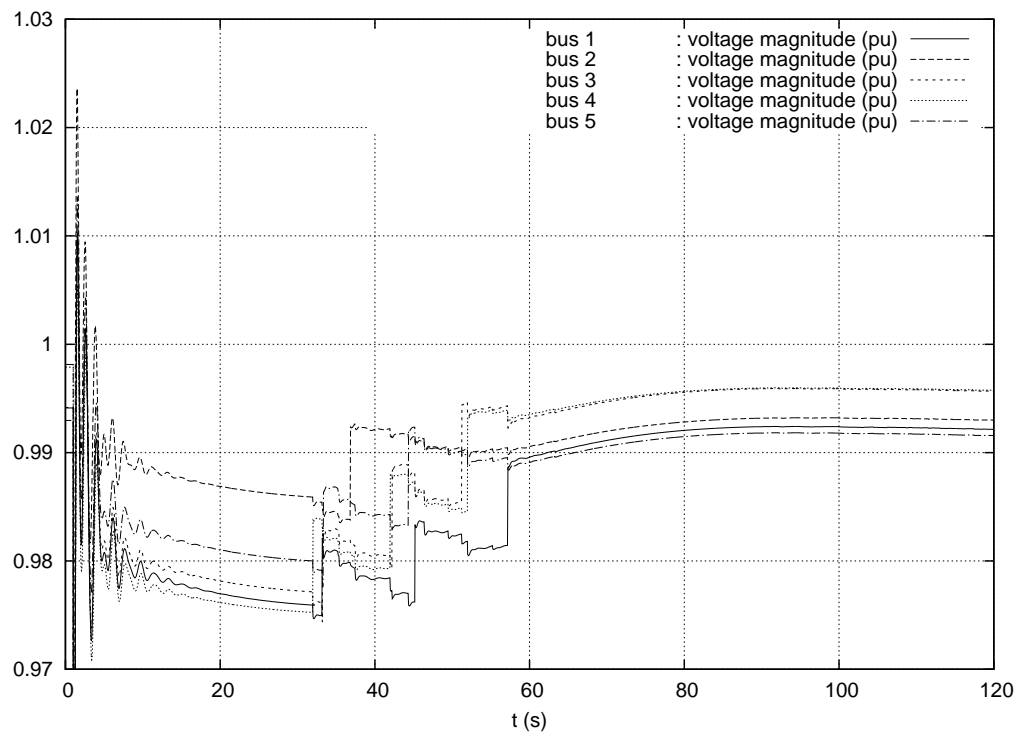


Figure 3.10: Operating point B, fault on line 4032-4044 cleared by opening line: distribution voltages

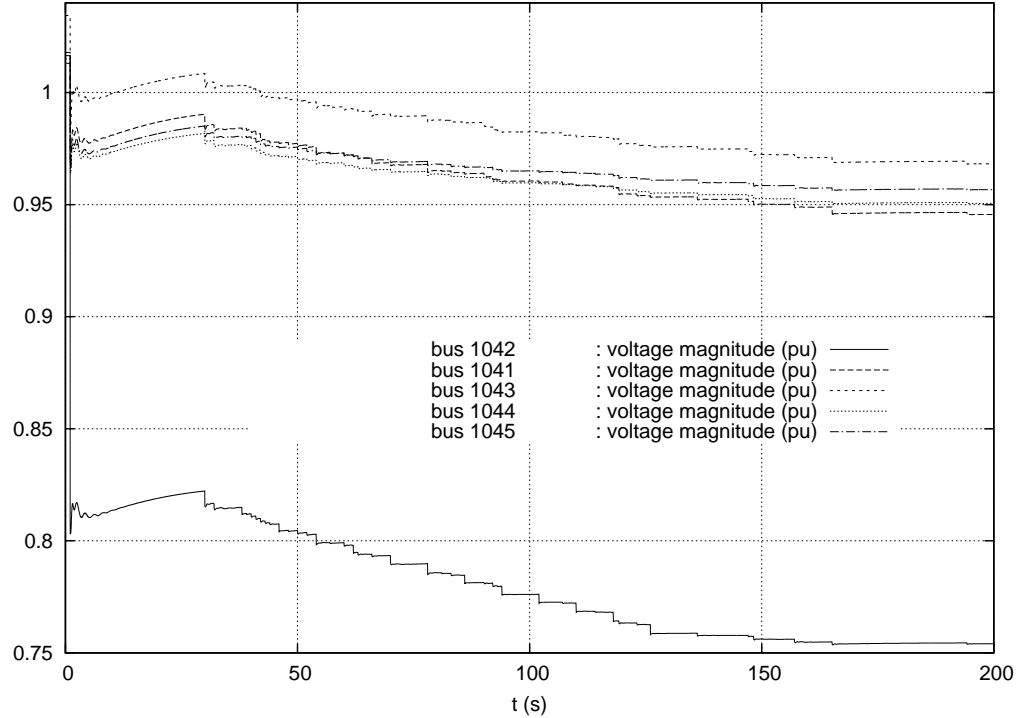


Figure 3.11: operating point B, outage of generator g6: transmission voltages

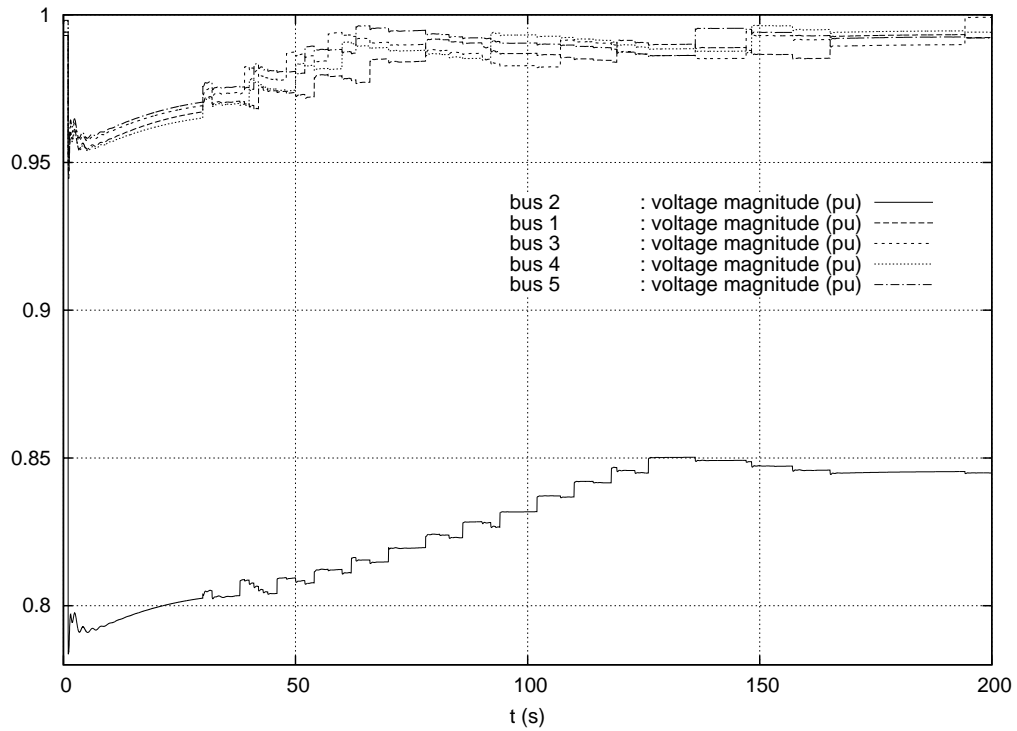


Figure 3.12: operating point B, outage of generator g6: distribution voltages

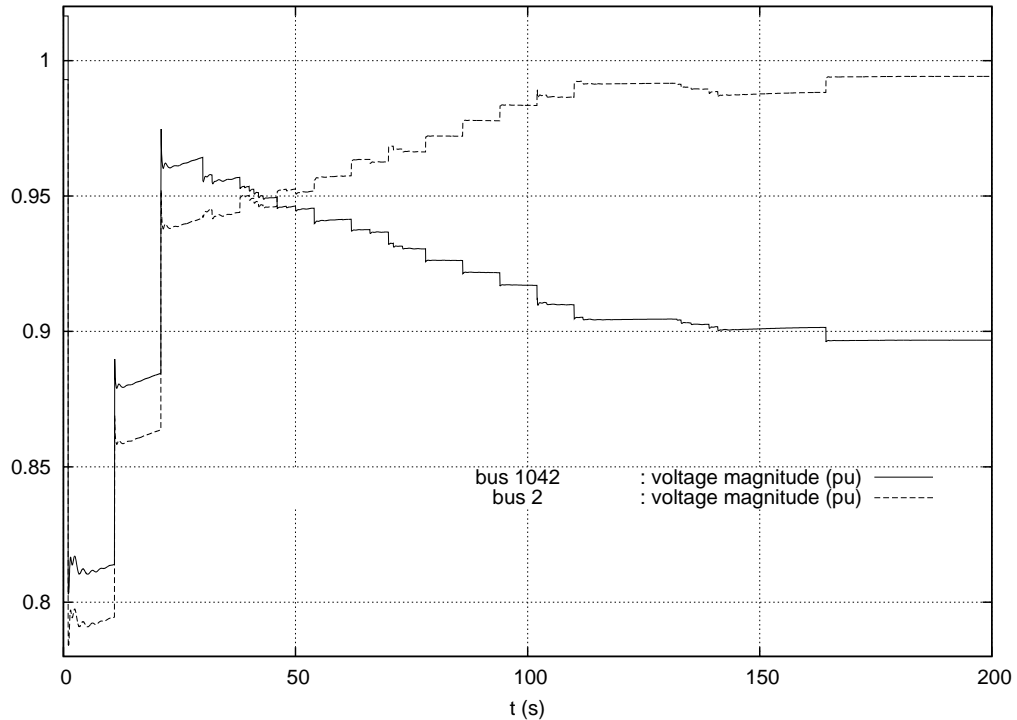


Figure 3.13: operating point B, outage of generator g6 followed by shunt compensation switching: transmission and distribution voltages

# **Chapter 4**

## **Nordic test system: preventive voltage security assessment**

This chapter is devoted to the determination of secure operation limits and power margins for the system operating at point B.

### **4.1 Determination of secure operation limits**

#### **Definition**

A Secure Operation Limit (SOL) involves stressing the system in its pre-contingency configuration. The stress considered here is an increase of loads in the Central area.

The SOL corresponds to the maximum load power that can be accepted in the pre-contingency configuration such that the system responds in a stable way to each of the specified contingencies [4].

To this purpose, power flow computations are performed for increasing values of the Central active and reactive loads. For each so determined operating point, the disturbance is simulated and the system response is analyzed.

In all cases, the criteria that lead to accepting the system response are those detailed in Section 3.2.

#### **Pre-contingency stress**

For illustration purposes, the following system stress has been considered. The Central area load is increased by steps of 25 MW. The total active power variation is shared by the 11 loads present in this area, in

proportion to their base case value. The power factor of each load is kept constant. The active power variations are compensated by generator g20, taken as slack-bus.

In the pre-contingency power flow calculations, transformer ratios are adjusted in response to load changes as follows:

1. the 22 distribution transformers are adjusted in order to maintain the distribution voltages in the deadbands as previously described;
2. the 400/130-kV transformers 1044-4044, 1044-4044b, 1045-4045 and 1045-4045b are assumed to be controlled by operators, adjusting their ratio to maintain the voltages at buses 1044 and 1045 in deadbands. Note that these transformers do not have their tap changed in the post-disturbance simulation, whose duration is considered too short for operators to react.

In both cases, ratios are modified when the controlled voltages leave their deadbands, and vary in discrete steps. The ratios of transformers in parallel are varied together.

The data of the distribution transformers have been given in Section 2.11, while Table 4.1 gives the data relative to the 400/130 kV transformers.

Table 4.1: Data for pre-contingency adjustment of the 400/130-kV transformers

transformer	controlled bus	minimum ratio	maximum ratio	number of tap positions	voltage deadband (pu)
1044-4044	1044	0.87	1.11	25	[1.0006 , 1.0206]
1044-4044b	1044	0.87	1.11	25	[1.0006 , 1.0206]
1045-4045	1045	0.87	1.11	25	[1.0046 , 1.0246]
1045-4045b	1045	0.87	1.11	25	[1.0046 , 1.0246]

Table 4.2 provides the values of the transformer ratios for various pre-contingency load levels mentioned in this section. The ones that are not given in this table can be calculated based on the aforementioned explanation.

Table 4.2: Pre-contingency transformer ratios

transformer	base case ratio	ratio after a load increase (in MW) of								
		25	50	100	250	275	350	375	400	500
1044-4044	1.08	1.08	1.08	1.08	1.06	1.06	1.05	1.05	1.05	1.03
1044-4044-2	1.08	1.08	1.08	1.08	1.06	1.06	1.05	1.05	1.05	1.03
1045-4045	1.09	1.09	1.09	1.08	1.07	1.07	1.06	1.06	1.05	1.04
1045-4045-2	1.09	1.09	1.09	1.08	1.07	1.07	1.06	1.06	1.05	1.04
11-1011	1.06	1.06	1.06	1.06	1.06	1.06	1.06	1.06	1.06	1.05
12-1012	1.06	1.06	1.06	1.06	1.06	1.06	1.06	1.06	1.06	1.06
13-1013	1.04	1.04	1.04	1.04	1.04	1.04	1.04	1.04	1.04	1.04
22-1022	1.08	1.08	1.08	1.08	1.07	1.07	1.07	1.06	1.06	1.05
1-1041	1.01	1.01	1.00	1.00	0.99	0.99	0.98	0.98	0.98	0.98
2-1042	1.01	1.01	1.01	1.00	1.00	1.00	1.00	0.99	0.99	0.99
3-1043	1.02	1.02	1.01	1.01	1.00	1.00	1.00	0.99	0.99	0.99
4-1044	1.00	1.00	1.00	0.99	0.99	0.99	0.99	0.98	0.98	0.98
5-1045	1.00	1.00	1.00	1.00	0.99	0.99	0.99	0.99	0.99	0.99
31-2031	1.07	1.07	1.07	1.07	1.06	1.05	1.05	1.04	1.04	1.03
32-2032	1.07	1.07	1.07	1.07	1.07	1.07	1.07	1.07	1.07	1.06
41-4041	1.09	1.09	1.09	1.09	1.08	1.07	1.07	1.06	1.06	1.05
42-4042	1.08	1.08	1.08	1.08	1.06	1.06	1.05	1.05	1.04	1.03
43-4043	1.07	1.07	1.07	1.07	1.05	1.05	1.04	1.04	1.04	1.02
46-4046	1.06	1.06	1.06	1.06	1.05	1.04	1.04	1.03	1.03	1.02
47-4047	1.06	1.06	1.06	1.06	1.05	1.05	1.05	1.04	1.04	1.03
51-4051	1.08	1.08	1.08	1.08	1.08	1.07	1.07	1.07	1.07	1.06
61-4061	1.05	1.05	1.05	1.05	1.05	1.05	1.04	1.04	1.04	1.03
62-4062	1.05	1.05	1.05	1.05	1.05	1.05	1.05	1.05	1.05	1.05
63-4063	1.03	1.03	1.03	1.03	1.03	1.03	1.03	1.03	1.03	1.03
71-4071	1.03	1.03	1.03	1.03	1.03	1.03	1.03	1.03	1.03	1.03
72-4072	1.05	1.05	1.05	1.05	1.05	1.05	1.05	1.05	1.05	1.05

## SOL with respect to the contingency of Section 3.1

First, the contingency of Section 3.1 is considered.

Figure 4.1 shows the post-disturbance evolution of the voltage at transmission bus 1041, for various pre-contingency load levels. The case with 375 MW loading seems stable but instability is revealed at  $t \simeq 800$  s. Thus, for that contingency, the power margin with respect to the SOL is 350 MW.

Incidentally, the figure illustrates a well-known fact about saddle-node bifurcations: the smaller the amplitude of the (positive or negative) margin, the more time it takes for the system to show its stability or instability.

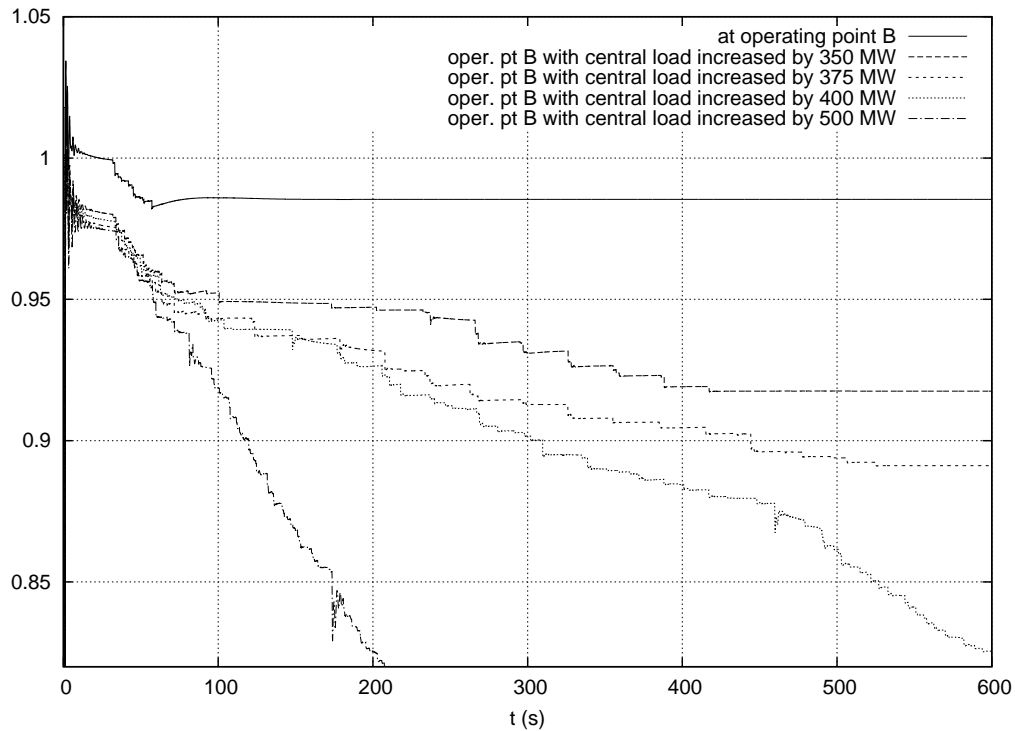


Figure 4.1: fault on line 4032-4044 cleared by opening line: evolution of voltage at bus 1041 for various pre-contingency stress levels

The SOL can be expressed in terms of the North-Central interface flow, which is the total power transfer across the North-Central border, shown with dotted line in Fig. 2.1, with the individual line flows measured at the Northern ends.

## SOL with respect to generator outages

The contingencies of concern here are the outage (without fault) of any single generator, except g19 and g20, which are equivalents.

The outage of g14 is found to be the most severe one with a power margin with respect to the SOL of only 25 MW !

Figure 4.2 shows the post-disturbance evolution of the voltage at bus 1041, for various pre-contingency load levels.

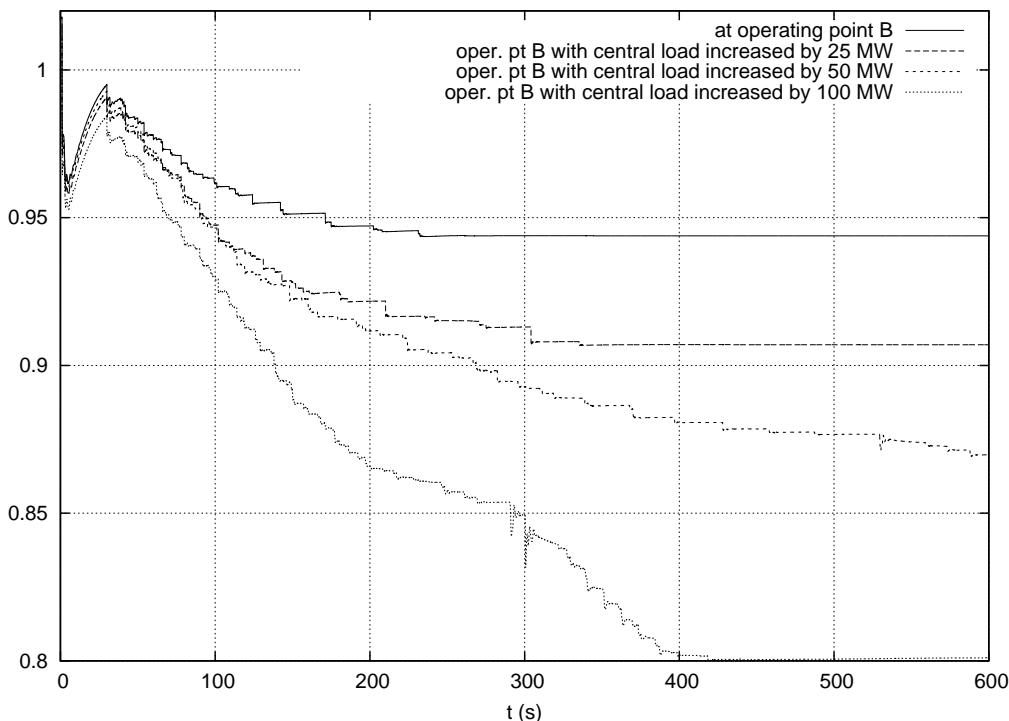


Figure 4.2: outage of generator g14: evolution of voltage at bus 1041 for various pre-contingency stress levels

The outage of g14 is a severe contingency because : (i) voltage control and reactive reserve are lost at bus g14, and (ii) the 630-MW power produced by g14 is compensated by the Northern and equivalent generators, which increases the North-Central power transfer.

## SOL with respect to line outages

The contingencies of concern here are the tripping, after a 5-cycle fault, of any single transmission line<sup>1</sup>.

The outage of line 4011-4021 is found to be the most severe one with a power margin with respect to the SOL of 250 MW.

Figure 4.3 shows the post-disturbance evolution of the voltage at bus 4022, for various pre-contingency load levels.

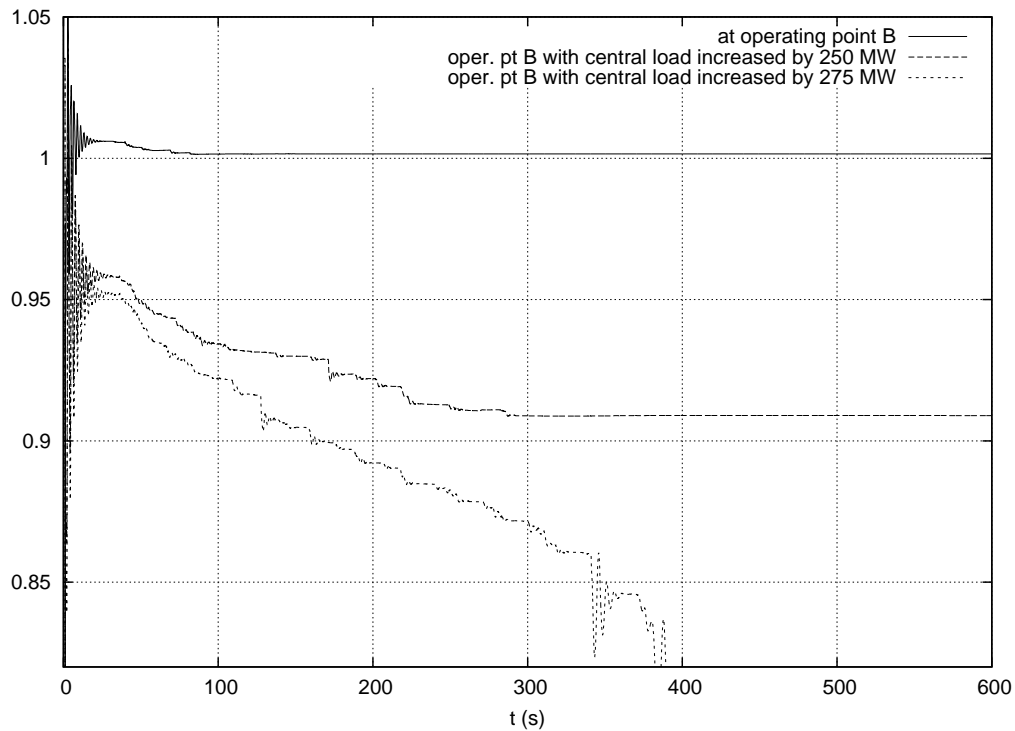


Figure 4.3: fault on line 4011-4021 cleared by opening line: evolution of voltage at bus 4022 for various pre-contingency stress levels

Note that this contingency involves a line located in the North area. The sequence of events is as follows. The outage of line 4011-4021 causes the active power to be redirected to the “corridor” between buses 4011, 4012, 4022 and 4031. This requires more reactive power support from generator g12. For a pre-contingency stress of 250 MW, g12 switches under field current limit at  $t = 89$  s, while for a stress of 275 MW, this limitation takes place at  $t = 67$  s. The earlier limitation confirms the higher reactive support by g12. As regards generator g8, for a stress of 250 MW, it remains under voltage control, while for a stress of 275 MW, it gets limited at  $t = 340$  s. The switching of g8 under field current limit restarts some LTC actions, and the voltages keep on decreasing, until both generators, operating under constant excitation, lose synchronism by lack of synchronizing torque.

---

<sup>1</sup>Each fault was applied at the “from” bus of the line: see Tables 2.2 and 2.3. Transformers were not considered.

## 4.2 Determination of loadability limits

The following results show PV curves computed to determine the loadability limit of the system in its pre-disturbance configuration. They were obtained with the N-1 secure operating point B (see Section 2.3).

Unlike classical PV curves obtained from (continuation) power flow computations, the ones shown here were obtained from dynamic simulations of the *same* model as considered before. Namely, a slow ramp increase in demand was simulated, quite close to what could be observed on the real system. With reference to Eq. (2.1), it consists of increasing linearly over time the  $P_0$  and  $Q_0$  coefficients. The response is computed with all dynamic components active, in particular LTCs and OELs. The simulation stops whenever a bus voltage reaches an unacceptably low value, or it is ascertained that maximum load power has been crossed. PV curves are obtained by recording the evolutions of voltages and load power with time, and plotting the former as a function of the latter.

The following choices have been made:

- for simplicity, the load change is compensated by primary frequency control (thus, the generator power set points have been left unchanged);
- as the smooth load increase is supposed to take place over a long time interval, the reaction of operators is considered. The four transmission transformers, i.e. 1044-4044, 1044-4044-2, 1045-4045, and 1045-4045-2 (see Fig. 2.1) are assumed to be under operator control, and adjusted to keep the voltages at buses 1044 and 1045 in pre-specified intervals. To this purpose, this particular dynamic simulation has been performed with LTC acting on the above transformers (20 s delay on the first tap change, and 5 s on the subsequent changes);
- the LTCs on distribution transformers continue to react as considered before, keeping the distribution voltages in the pre-specified voltage dead-bands.

Figure 4.4 shows three PV curves obtained in this way. In this simulation, all loads in the Central area have been increased at a rate of 0.15 MW/s for the whole area. Constant power factors have been assumed, by keeping the ratios  $Q_0/P_0$  constant. The underlying dynamic simulation has been performed with time steps of 0.05 s. The base load level is 6190 MW while the maximum load power is around 6830 MW. The load power margin is thus 640 MW. It can be seen that the voltage at bus 1044 is kept almost constant, and corrected by successive tap changes (by operators) on transformers 1044-4044 and 1044-4044-2. The voltage at bus 1041 is not controlled by an LTC but is electrically close to 1044; hence, it drops a little during the load increase. On the other hand, at the transmission bus 4044, the decline is much more pronounced.

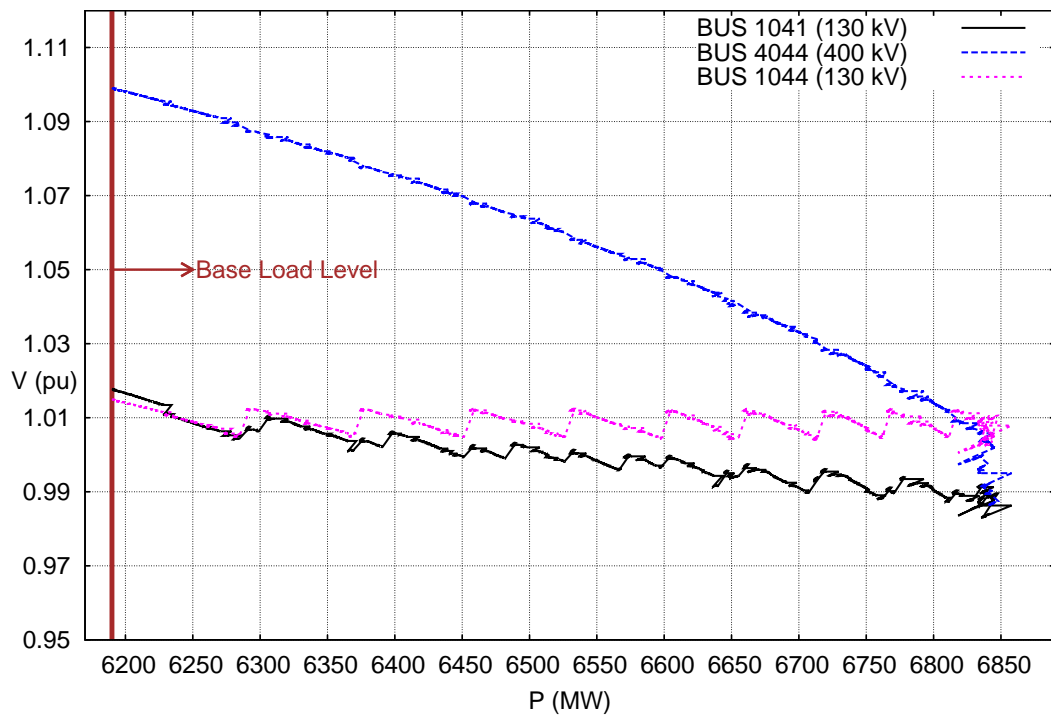


Figure 4.4: PV curve

# Chapter 5

## Nordic test system: corrective (post-disturbance) control

### 5.1 Modified tap changer control

This section and the next one illustrate emergency control actions, typical of System Integrity Protection Scheme (SIPS). Note that the material does not intend to be an exhaustive investigation of emergency controls; neither have these controls been “optimized” (for instance to minimize customer inconvenience).

The emergency control example consists of decreasing by 0.05 pu the voltage setpoint of LTCs controlling loads. This exploits the sensitivity of load power to voltage. For active power, with a constant current characteristic, one can expect a 5 % reduction, while for reactive power, with a constant impedance characteristic, one can expect a reduction of approximately 10 %.

Although many variants can be thought of, in the considered scenario the action is applied at  $t = 100$  s, a little after the lowest transmission voltage (at bus 1041) has reached 0.90 pu. Two sets of LTCs have been considered:

- the five LTCs controlling loads at buses 1, 2, 3, 4 and 5;
- the same together with the six LTCs controlling loads at buses 41, 42, 43, 46, 47 and 51.

Figure 5.1 shows the evolution of the voltage magnitude at bus 1041 when reducing the setpoints of respectively the 5 LTCs and the 11 LTCs. For comparison purposes, it also shows the evolution without action on LTCs. It can be seen that acting on 5 LTCs is not sufficient: the system collapses a little later. On the other hand, acting on 11 LTCs is effective and even succeeds bringing the transmission voltage above its pre-disturbance value, although after a long time due to LTC delays.

Note that all generators that were switched under field current limit in the case without emergency control

(see Fig. 3.2) now reset under voltage control after some time. Without their regaining voltage control, some severe overvoltages would be experienced in the transmission system.

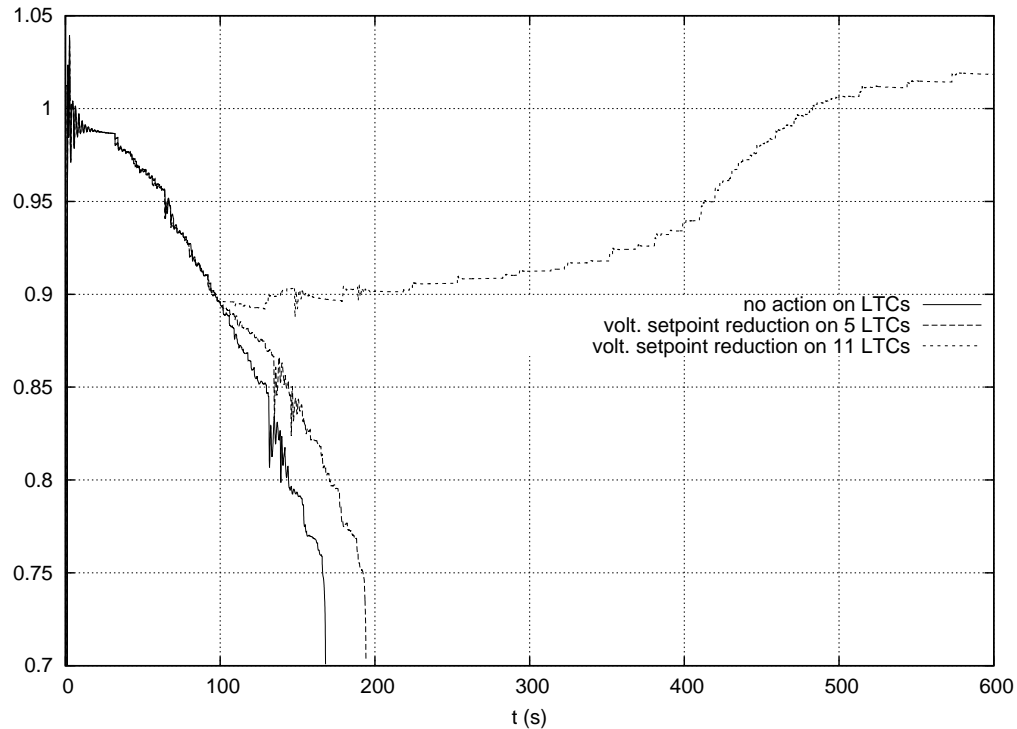


Figure 5.1: Evolution of voltage magnitude at bus 1041, without and with emergency control of LTCs

## 5.2 Undervoltage load shedding

The second example of emergency control deals with undervoltage load shedding. Distributed controllers have been considered as detailed in [13]. Each controller monitors the voltage at a transmission bus and acts on the load at the nearest distribution bus, according to the following simple logic:

shed  $\Delta P$  of load when the monitored voltage  $V$  goes below a threshold  $V^{th}$  for more than  $\tau$  seconds.

Important features are the ability of each controller to act several times (a closed-loop behaviour that yields a robust and adaptive protection) and the absence of communication between controllers.

The example given hereafter has been obtained with  $V^{th} = 0.90$  pu,  $\Delta P = 50$  MW, and  $\tau = 3$  seconds. Each time a block is shed, the value of  $P_o$  in (2.1) is decreased by  $\Delta P$  and  $Q_o$  by  $\Delta Q$ .  $\Delta Q$  has been chosen so that the load power factor at 1 pu voltage is preserved.

Figure 5.2 shows the performance of the so adjusted load shedding controllers. Six blocks of load are shed, two by the controller monitoring bus 1041 and acting on bus 1 (at  $t = 100$  and  $144.95$  s) and four by the controller of monitoring bus 1044 and acting on bus 4 (at  $t = 112.10, 123.10, 180.40$  and  $290.45$  s), for a total of 300 MW.

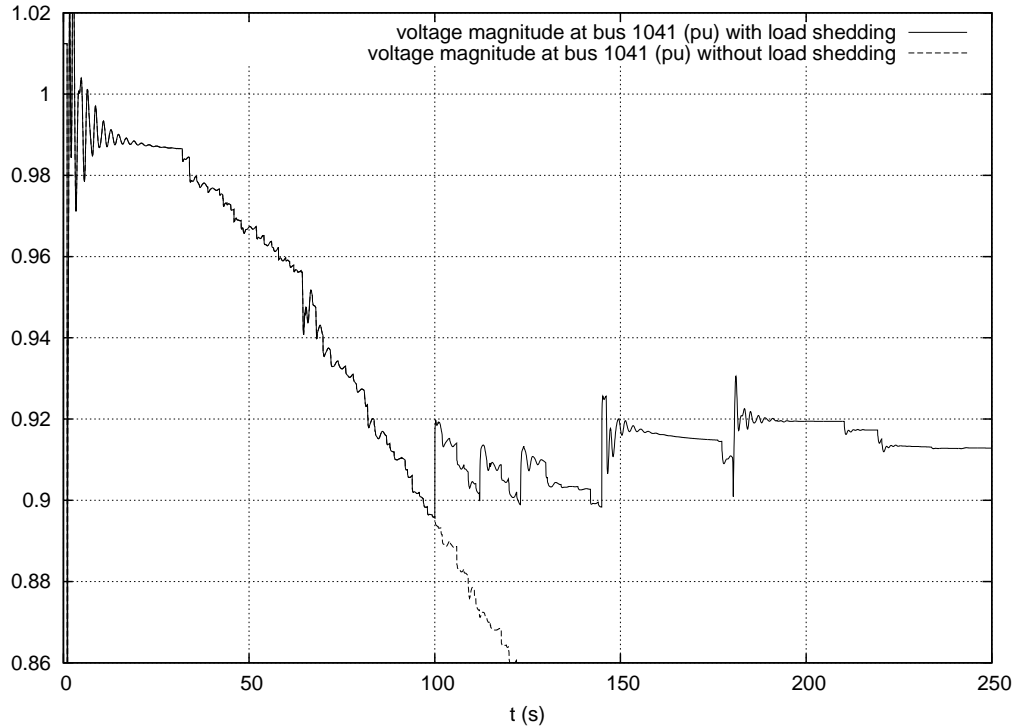


Figure 5.2: Evolution of voltage magnitude at bus 1041, without and with load shedding

Figure 5.3 shows the active powers of the loads at buses 1 and 4, respectively. The power evolves under the effect of LTCs and curtailments. The latter are easily identified from the curves. When one load is curtailed, its own power decreases while the other load power (slightly) increases, under the effect of the increasing voltage.

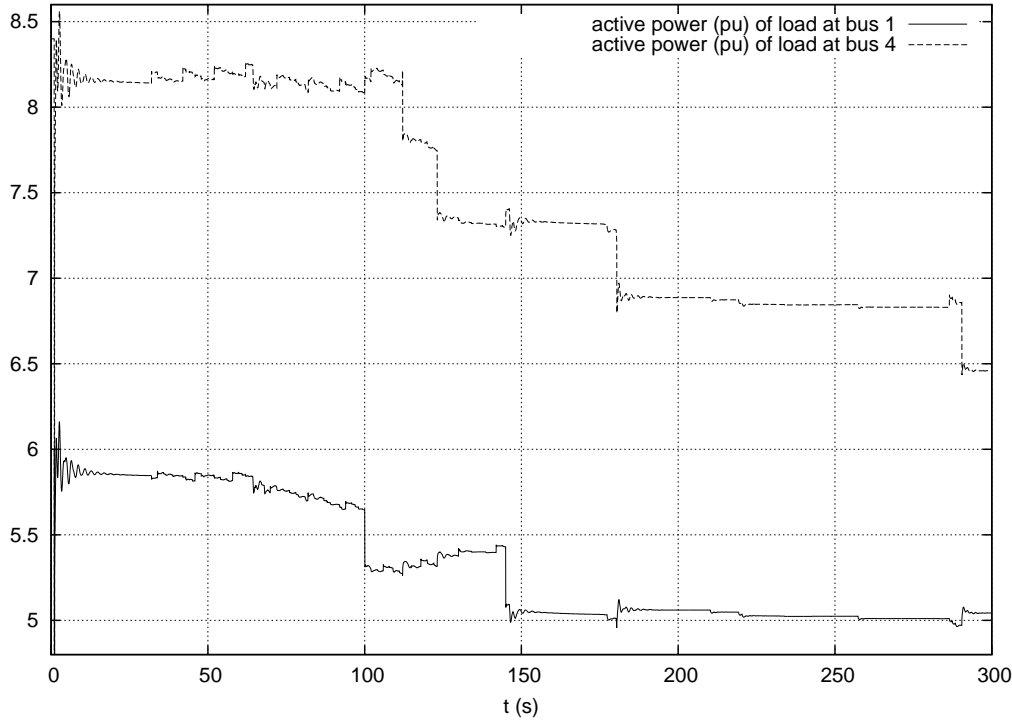


Figure 5.3: Evolution of active power of loads at buses 1 and 4, with load shedding

### 5.3 Long-term voltage instability analysis through sensitivities

Long-term voltage instability results from the attempt of loads to restore their powers at a level that the combined transmission and generation systems cannot provide [4]. In this test system, as in many real-life systems, load power restoration comes from the LTCs which try to restore load voltages. At the same time, the system weakening caused by the line outage reduces the maximum power that can be delivered to loads, while the reactive power limits of generators contribute to further reducing this power.

In their attempt to restore load power, the LTCs make the system pass through a maximum load power point. This is easily shown on the well-known 2-bus example: the system passes through the “nose” of the PV curve (determined with appropriate assumption on load reactive power). In a real-life system, it is a combination of load active and reactive powers that passes through a maximum. This can be detected with sensitivity analysis carried out along the system trajectory. We consider the sensitivity of the total reactive power generation to individual load reactive powers. When approaching the maximum power point, those sensitivities take larger and larger values while when crossing it, they suddenly change sign. More details can be found in [12], together with considerations on how synchronized phasor measurements could be used

in the future to determine those sensitivities in a wide-area monitoring scheme.

The dashed line in Fig. 5.4 shows the sensitivity relative to bus 1041. The above mentioned sign change takes place at  $t \simeq 87$  s. Plotting a PV curve with suitable load increase pattern would show that the corresponding point lies on the nose of this curve. Figure 3.1 shows that voltages are still rather high at that point. The solid line in Fig. 5.4 is the same sensitivity computed with anticipation of generator limitation, i.e. as soon as a generator field current stays above the  $i_{fd}^{lim}$  limit for more than three seconds, the OEL equation is anticipatively substituted to the AVR equation in the sensitivity calculation [12]. The figure shows that the resulting alarm takes place at  $t \simeq 72$  s.

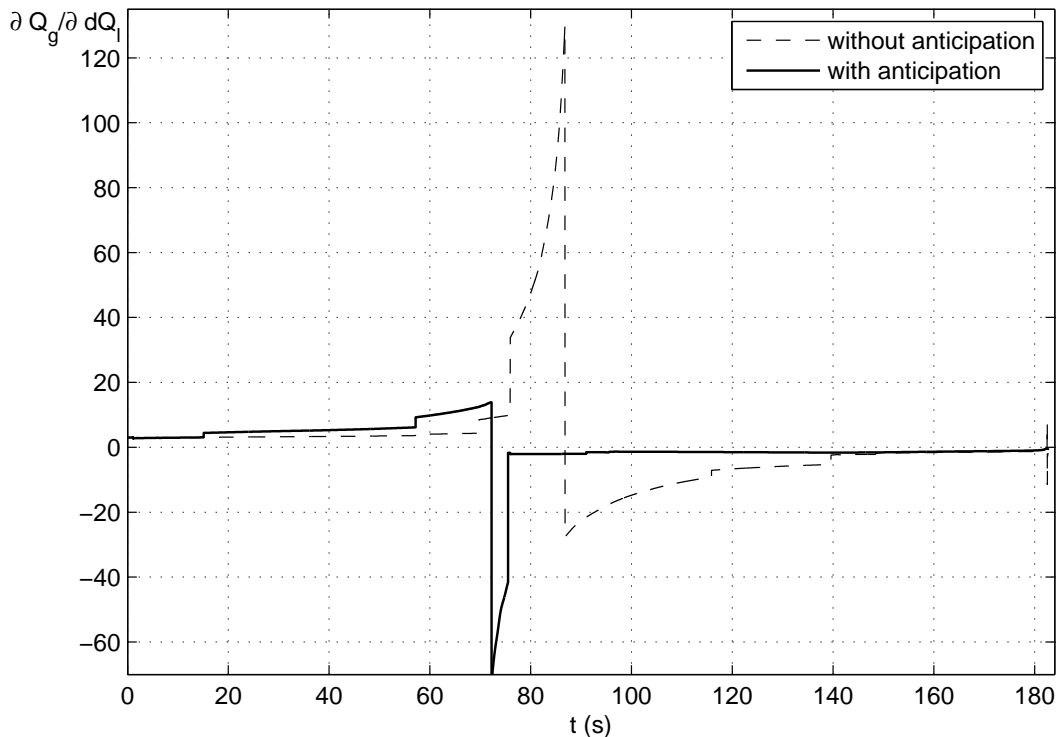


Figure 5.4:  $\partial Q_g / \partial Q_l$  at bus 1041

## **Part II**

# **The Reliability and Voltage Stability (RVS) test system**

# Chapter 6

## RVS test system: models and data

### 6.1 System overview

This benchmark system corresponds, to a large extent, to the 1979 IEEE Reliability Test System [24]. It was extended to represent multi-area systems in the 1996 version of the IEEE Reliability Test System [25].

The data presented in this report is related to the so-called "one area RTS-96" system, which is equivalent to the 1979 Reliability Test System. The data for the IEEE Reliability Test Systems are available for download [33].

This benchmark system is a 60 Hz system. Several modifications were introduced in the power flow data of the original 1979 Reliability Test System. These changes were done to make the resulting test system more suitable for voltage stability/voltage collapse analysis.

The modifications include:

- The synchronous condenser at bus 10114 was replaced by an SVC with the same nominal range (-50/+200 Mvar). In practice, the reactive power output of this device becomes voltage dependent and its reactive power output is severely reduced under low voltage conditions.
- The shunt at bus 10106 was replaced by an SVC with a range of (-50/+100 Mvar). This change introduces an additional control capability that is quite important to the voltage control. This SVC is a key component in the proposed system data and is usually required to avoid voltage collapse during dynamic simulations.
- The step-up transformers of generators and SVCs are explicitly represented in the case, assuming 5 tap positions and without LTC. The generators are connected to the low voltage bus, assumed to be 18 kV. The SVCs control local (terminal) voltage. The power flow solution considers all generators remotely controlling the voltage at the high voltage side of their step-up transformers. In the dynamic simulation, all excitation systems are controlling the generator terminal voltage (18 kV bus voltage).

- All other transformers in the RVS Test System are represented with an LTC varying the ratio between -10 and +10%, over 33 steps (thus, with a change of 0.625% per step). Tap changers are located at the high voltage side of the transformer. Each LTC controls the voltage at the low voltage side of the transformer.
- Loads are no longer connected to the 138 kV or 230 kV buses. Step-down transformers to 13.8 kV (again, the base kV is arbitrary) with LTC controlling the low voltage side are introduced with an estimated 15% reactance on the MVA base calculated by rounding up (multiple of 50 MVA) 110% of the load MVA.

Figure 6.1 presents the single line diagram of the system. Table 6.1 contains the dimensions of the resulting base-case power flow while Table 6.2 shows the total generation and load in the case.

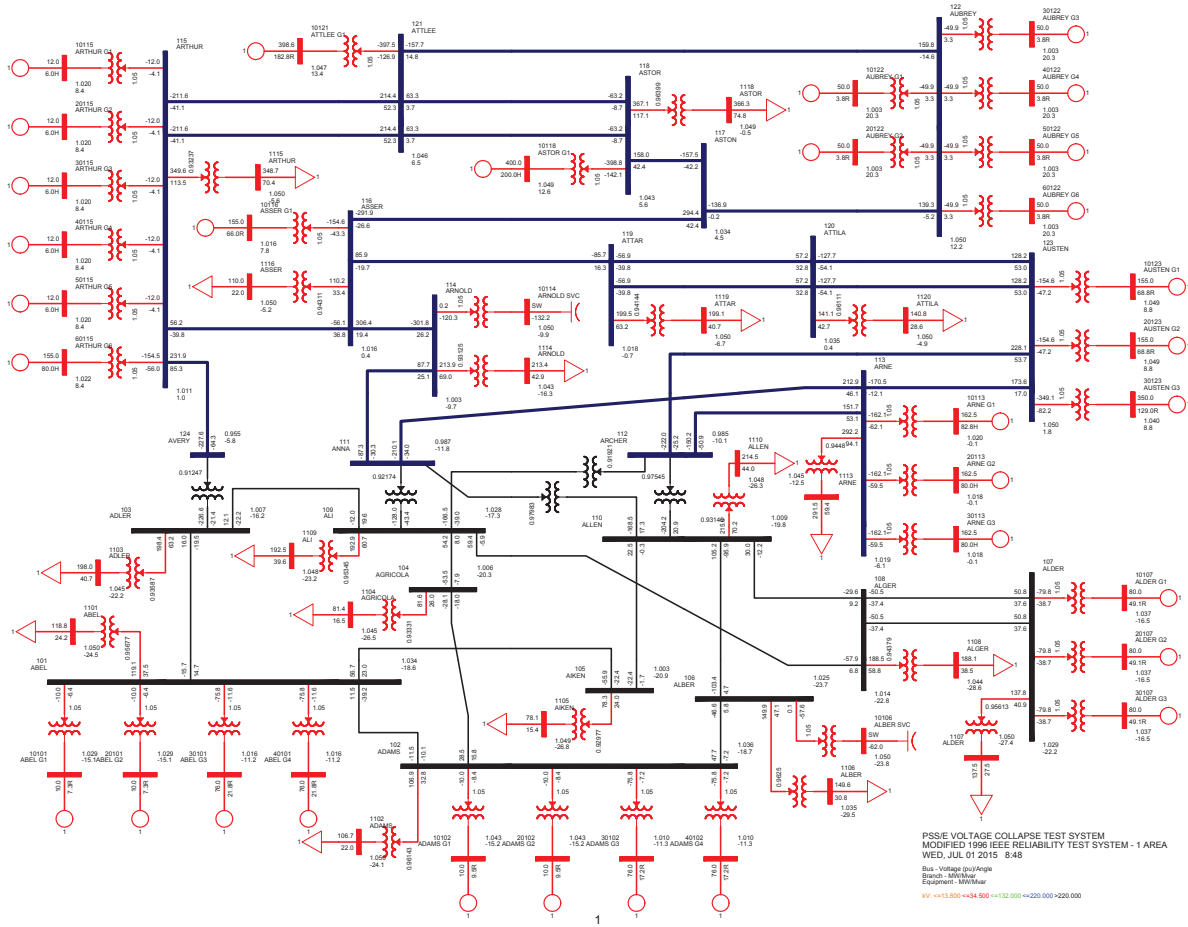


Table 6.1: Benchmark test system summary

component	quantity
buses	75
generators	32
switched shunts	2
loads	17
transmission lines	89
transformers	56

Table 6.2: Total generation and load

	active power (MW)	reactive power (Mvar)
generation	3200.1	1349.8
load	3135.0	638.0

## 6.2 Operating point data

Table 6.3 shows the power flow data for the original buses (138 kV and 230 kV buses) plus the new 13.8 kV buses corresponding to the loads. The generators are moved to lower voltage (18 kV) buses, as shown in Table 6.4 <sup>1</sup>.

The generator data for the power flow solution is presented in Table 6.5. All synchronous machines, in the power flow solution, are represented with remote voltage control, controlling the high voltage side of respective step-up transformer. The scheduled voltages for the generators are shown in Table 6.6.

The remote voltage control was used to maintain a degree of compatibility with the original 1979 IEEE Reliability Test System, where the generators were represented directly connected to the HV buses.

The loads data are given in Table 6.7.

## 6.3 Network data

The transmission lines are represented by equivalent  $\pi$ -sections, with the data shown in Table 6.8 for the 138 kV and in Table 6.10 for the 230 kV circuits.  $B$  is the total shunt susceptance of the line. Tables 6.9 and 6.11 present the ratings and lengths of these lines, as considered in the RVS test system.

---

<sup>1</sup>The swing bus was moved from the HV bus 121 to the LV bus 10121, the terminal of generator ATTLEE G1, once the step-up transformer was explicitly modeled. In order to maintain the voltage angle of the HV bus equal to the power flow solution of the original Reliability Test System, a nonzero voltage phase angle was specified at the new swing bus. This explains why no bus has zero voltage phase angle.

Table 6.3: Bus data

Bus no	Bus name	Base Voltage (kV)	Bus Type	Voltage Magnitude (pu)	Voltage Angle (degrees)
101	ABEL	138.00	PQ	1.0342	-18.6
102	ADAMS	138.00	PQ	1.0358	-18.7
103	ADLER	138.00	PQ	1.0072	-16.2
104	AGRICOLA	138.00	PQ	1.0055	-20.3
105	AIKEN	138.00	PQ	1.0030	-20.9
106	ALBER	138.00	PQ	1.0250	-23.7
107	ALDER	138.00	PQ	1.0286	-22.2
108	ALGER	138.00	PQ	1.0136	-22.8
109	ALI	138.00	PQ	1.0280	-17.3
110	ALLEN	138.00	PQ	1.0088	-19.8
111	ANNA	230.00	PQ	0.9872	-11.8
112	ARCHER	230.00	PQ	0.9851	-10.1
113	ARNE	230.00	PQ	1.0191	-6.1
114	ARNOLD	230.00	PQ	1.0033	-9.7
115	ARTHUR	230.00	PQ	1.0111	1.0
116	ASSER	230.00	PQ	1.0164	0.4
117	ASTON	230.00	PQ	1.0338	4.5
118	ASTOR	230.00	PQ	1.0425	5.6
119	ATTAR	230.00	PQ	1.0180	-0.7
120	ATTILA	230.00	PQ	1.0349	0.4
121	ATTLEE	230.00	PQ	1.0459	6.5
122	AUBREY	230.00	PQ	1.0500	12.2
123	AUSTEN	230.00	PQ	1.0499	1.8
124	AVERY	230.00	PQ	0.9550	-5.8
1101	ABEL	13.800	PQ	1.0497	-24.5
1102	ADAMS	13.800	PQ	1.0496	-24.1
1103	ADLER	13.800	PQ	1.0446	-22.2
1104	AGRICOLA	13.800	PQ	1.0450	-26.5
1105	AIKEN	13.800	PQ	1.0488	-26.8
1106	ALBER	13.800	PQ	1.0350	-29.5
1107	ALDER	13.800	PQ	1.0497	-27.4
1108	ALGER	13.800	PQ	1.0442	-28.6
1109	ALI	13.800	PQ	1.0477	-23.2
1110	ALLEN	13.800	PQ	1.0484	-26.3
1113	ARNE	13.800	PQ	1.0453	-12.5
1114	ARNOLD	13.800	PQ	1.0433	-16.3
1115	ARTHUR	13.800	PQ	1.0497	-5.6
1116	ASSER	13.800	PQ	1.0496	-5.2
1118	ASTOR	13.800	PQ	1.0492	-0.5
1119	ATTAR	13.800	PQ	1.0498	-6.7
1120	ATTILA	13.800	PQ	1.0497	-4.9

Table 6.4: Bus data (continued)

Bus no	Bus name	Base Voltage (kV)	Bus Type	Voltage Magnitude (pu)	Voltage Angle (degrees)
10101	ABEL G1	18.000	PV	1.0290	-15.1
10102	ADAMS G1	18.000	PV	1.0430	-15.2
10106	ALBER SVC	18.000	PQ	1.0500	-23.8
10107	ALDER G1	18.000	PV	1.0370	-16.5
10113	ARNE G1	18.000	PV	1.0198	-0.1
10114	ARNOLD SVC	18.000	PQ	1.0500	-9.9
10115	ARTHUR G1	18.000	PV	1.0204	8.4
10116	ASSER G1	18.000	PV	1.0159	7.8
10118	ASTOR G1	18.000	PV	1.0487	12.6
10121	ATTLEE G1	18.000	slack	1.0468	13.4
10122	AUBREY G1	18.000	PV	1.0034	20.3
10123	AUSTEN G1	18.000	PV	1.0491	8.8
20101	ABEL G2	18.000	PV	1.0290	-15.1
20102	ADAMS G2	18.000	PV	1.0430	-15.2
20107	ALDER G2	18.000	PV	1.0370	-16.5
20113	ARNE G2	18.000	PV	1.0181	-0.1
20115	ARTHUR G2	18.000	PV	1.0204	8.4
20122	AUBREY G2	18.000	PV	1.0034	20.3
20123	AUSTEN G2	18.000	PV	1.0491	8.8
30101	ABEL G3	18.000	PV	1.0155	-11.2
30102	ADAMS G3	18.000	PV	1.0096	-11.3
30107	ALDER G3	18.000	PV	1.0370	-16.5
30113	ARNE G3	18.000	PV	1.0181	-0.1
30115	ARTHUR G3	18.000	PV	1.0204	8.4
30122	AUBREY G3	18.000	PV	1.0034	20.3
30123	AUSTEN G3	18.000	PV	1.0401	8.8
40101	ABEL G4	18.000	PV	1.0155	-11.2
40102	ADAMS G4	18.000	PV	1.0096	-11.3
40115	ARTHUR G4	18.000	PV	1.0204	8.4
40122	AUBREY G4	18.000	PV	1.0034	20.3
50115	ARTHUR G5	18.000	PV	1.0204	8.4
50122	AUBREY G5	18.000	PV	1.0034	20.3
60115	ARTHUR G6	18.000	PV	1.0220	8.4
60122	AUBREY G6	18.000	PV	1.0034	20.3

Table 6.5: Generator data

Bus no	Bus name	<i>S</i> MVA	<i>P</i> MW	<i>Q</i> Mvar	<i>Q<sub>max</sub></i> Mvar	<i>Q<sub>min</sub></i> Mvar
10115	ARTHUR G1	14	12	6	6	0
20115	ARTHUR G2					
30115	ARTHUR G3					
40115	ARTHUR G4					
50115	ARTHUR G5					
10101	ABEL G1	24	10	7.3689	10	0
20101	ABEL G2					
10102	ADAMS G1	24	10	9.5355	10	0
20102	ADAMS G2					
10122	AUBREY G1	53	50	3.7514	16	-10
20122	AUBREY G2					
30122	AUBREY G3					
40122	AUBREY G4					
50122	AUBREY G5					
60122	AUBREY G6					
30101	ABEL G3	89	76	21.7756	30	-25
40101	ABEL G4					
30102	ADAMS G3					
40102	ADAMS G4					
10107	ALDER G1	118	80	49.1462	60	0
20107	ALDER G2					
30107	ALDER G3					
60115	ARTHUR G6	182	155	80	80	-50
10116	ASSER G1	182	155	65.9791	80	-50
10123	AUSTEN G1	182	155	68.8361	80	-50
20123	AUSTEN G2					
10113	ARNE G1	232	162.5	82.7791	82.7791	0
20113	ARNE G2	232	162.5	80	80	0
30113	ARNE G3					
30123	AUSTEN G3	412	350	128.9053	150	-25
10118	ASTOR G1	471	400	200	200	-50
10121	ATTLEE G1	471	398.6392	182.7737	200	-50

Table 6.6: Generator controlled voltages data

generator				controlled bus		
Bus no	Bus name	Base Voltage (kV)	Scheduled Voltage (pu)	Bus no	Bus name	Base Voltage (kV)
10101	ABEL G1	18.000	1.0342	101	ABEL	138.00
20101	ABEL G2	18.000	1.0342	101	ABEL	138.00
30101	ABEL G3	18.000	1.0342	101	ABEL	138.00
40101	ABEL G4	18.000	1.0342	101	ABEL	138.00
10102	ADAMS G1	18.000	1.0358	102	ADAMS	138.00
20102	ADAMS G2	18.000	1.0358	102	ADAMS	138.00
30102	ADAMS G3	18.000	1.0358	102	ADAMS	138.00
40102	ADAMS G4	18.000	1.0358	102	ADAMS	138.00
10107	ALDER G1	18.000	1.0286	107	ALDER	138.00
20107	ALDER G2	18.000	1.0286	107	ALDER	138.00
30107	ALDER G3	18.000	1.0286	107	ALDER	138.00
10113	ARNE G1	18.000	1.0200	113	ARNE	230.00
20113	ARNE G2	18.000	1.0200	113	ARNE	230.00
30113	ARNE G3	18.000	1.0200	113	ARNE	230.00
10115	ARTHUR G1	18.000	1.0113	115	ARTHUR	230.00
20115	ARTHUR G2	18.000	1.0113	115	ARTHUR	230.00
30115	ARTHUR G3	18.000	1.0113	115	ARTHUR	230.00
40115	ARTHUR G4	18.000	1.0113	115	ARTHUR	230.00
50115	ARTHUR G5	18.000	1.0113	115	ARTHUR	230.00
60115	ARTHUR G6	18.000	1.0113	115	ARTHUR	230.00
10116	ASSER G1	18.000	1.0164	116	ASSER	230.00
10118	ASTOR G1	18.000	1.0432	118	ASTOR	230.00
10121	ATTLEE G1	18.000	1.0468	121	ATTLEE	230.00
10122	AUBREY G1	18.000	1.0500	122	AUBREY	230.00
20122	AUBREY G2	18.000	1.0500	122	AUBREY	230.00
30122	AUBREY G3	18.000	1.0500	122	AUBREY	230.00
40122	AUBREY G4	18.000	1.0500	122	AUBREY	230.00
50122	AUBREY G5	18.000	1.0500	122	AUBREY	230.00
60122	AUBREY G6	18.000	1.0500	122	AUBREY	230.00
10123	AUSTEN G1	18.000	1.0499	123	AUSTEN	230.00
20123	AUSTEN G2	18.000	1.0499	123	AUSTEN	230.00
30123	AUSTEN G3	18.000	1.0499	123	AUSTEN	230.00

Table 6.7: Load data

Bus no	Bus name	Base Voltage (kV)	Active Power (MW)	Reactive Power (Mvar)
1101	ABEL	13.8	118.8	24.2
1102	ADAMS	13.8	106.7	22.0
1103	ADLER	13.8	198.0	40.7
1104	AGRICOLA	13.8	81.4	16.5
1105	AIKEN	13.8	78.1	15.4
1106	ALBER	13.8	149.6	30.8
1107	ALDER	13.8	137.5	27.5
1108	ALGER	13.8	188.1	38.5
1109	ALI	13.8	192.5	39.6
1110	ALLEN	13.8	214.5	44.0
1113	ARNE	13.8	291.5	59.4
1114	ARNOLD	13.8	213.4	42.9
1115	ARTHUR	13.8	348.7	70.4
1116	ASSER	13.8	110.0	22.0
1118	ASTOR	13.8	366.3	74.8
1119	ATTAR	13.8	199.1	40.7
1120	ATTILA	13.8	140.8	28.6

Table 6.8: 138-kV Transmission line data

Bus no	from bus		to bus		circuit no	<i>R</i> (pu)	<i>X</i> (pu)	<i>B</i> (pu)
	Bus no	Bus name	Bus no	Bus name				
101	ABEL	102	ADAMS		1	0.0030	0.0140	0.4610
101	ABEL	103	ADLER		1	0.0550	0.2110	0.0570
101	ABEL	105	AIKEN		1	0.0220	0.0850	0.0230
102	ADAMS	104	AGRICOLA		1	0.0330	0.1270	0.0340
102	ADAMS	106	ALBER		1	0.0500	0.1920	0.0520
103	ADLER	109	ALI		1	0.0310	0.1190	0.0320
104	AGRICOLA	109	ALI		1	0.0270	0.1040	0.0280
105	AIKEN	110	ALLEN		1	0.0230	0.0880	0.0240
106	ALBER	110	ALLEN		1	0.0140	0.0610	2.4590
107	ALDER	108	ALGER		1	0.0080	0.0300	0.0085
107	ALDER	108	ALGER		2	0.0080	0.0300	0.0085
108	ALGER	109	ALI		1	0.0430	0.1650	0.0450
108	ALGER	110	ALLEN		2	0.0430	0.1650	0.0450

all values expressed in (pu) of system MVA (100 MVA)

Table 6.9: 138-kV Transmission line data (continued)

Bus no	from bus Bus name	Bus no	to bus Bus name	circuit no	Rate A (MVA)	Rate B (MVA)	Rate C (MVA)	Line Length (km)
101	ABEL	102	ADAMS	1	175.0	193.0	200.0	3.0
101	ABEL	103	ADLER	1	175.0	208.0	220.0	55.0
101	ABEL	105	AIKEN	1	175.0	208.0	220.0	22.0
102	ADAMS	104	AGRICOLA	1	175.0	208.0	220.0	33.0
102	ADAMS	106	ALBER	1	175.0	208.0	220.0	50.0
103	ADLER	109	ALI	1	175.0	208.0	220.0	31.0
104	AGRICOLA	109	ALI	1	175.0	208.0	220.0	27.0
105	AIKEN	110	ALLEN	1	175.0	208.0	220.0	23.0
106	ALBER	110	ALLEN	1	175.0	193.0	200.0	16.0
107	ALDER	108	ALGER	1	87.5	104.0	110.0	16.0
107	ALDER	108	ALGER	2	87.5	104.0	110.0	16.0
108	ALGER	109	ALI	1	175.0	208.0	220.0	43.0
108	ALGER	110	ALLEN	2	175.0	208.0	220.0	43.0

Table 6.10: 230-kV Transmission line data

Bus no	from bus Bus name	Bus no	to bus Bus name	circuit no	R (pu)	X (pu)	B (pu)
111	ANNA	113	ARNE	1	0.0060	0.0480	0.1000
111	ANNA	114	ARNOLD	1	0.0050	0.0420	0.0880
112	ARCHER	113	ARNE	1	0.0060	0.0480	0.1000
112	ARCHER	123	AUSTEN	1	0.0120	0.0970	0.2030
113	ARNE	123	AUSTEN	1	0.0110	0.0870	0.1820
114	ARNOLD	116	ASSER	1	0.0050	0.0590	0.0820
115	ARTHUR	116	ASSER	1	0.0020	0.0170	0.0360
115	ARTHUR	121	ATTLEE	1	0.0060	0.0490	0.1030
115	ARTHUR	121	ATTLEE	2	0.0060	0.0490	0.1030
115	ARTHUR	124	AVERY	1	0.0070	0.0520	0.1090
116	ASSER	117	ASTON	1	0.0030	0.0260	0.0550
116	ASSER	119	ATTAR	1	0.0030	0.0230	0.0490
117	ASTON	118	ASTOR	1	0.0020	0.0140	0.0300
117	ASTON	122	AUBREY	1	0.0140	0.1050	0.2210
118	ASTOR	121	ATTLEE	1	0.0030	0.0260	0.0550
118	ASTOR	121	ATTLEE	2	0.0030	0.0260	0.0550
119	ATTAR	120	ATTILA	1	0.0050	0.0400	0.0830
119	ATTAR	120	ATTILA	2	0.0050	0.0400	0.0830
120	ATTILA	123	AUSTEN	1	0.0030	0.0220	0.0460
120	ATTILA	123	AUSTEN	2	0.0030	0.0220	0.0460
121	ATTLEE	122	AUBREY	1	0.0090	0.0680	0.1420

all values expressed in (pu) of system MVA (100 MVA)

Table 6.11: 230-kV Transmission line data (continued)

Bus no	from bus Bus name	Bus no	to bus Bus name	circuit no	Rate A (MVA)	Rate B (MVA)	Rate C (MVA)	Line Length (km)
111	ANNA	113	ARNE	1	500.0	600.0	625.0	33.0
111	ANNA	114	ARNOLD	1	500.0	600.0	625.0	29.0
112	ARCHER	113	ARNE	1	500.0	600.0	625.0	33.0
112	ARCHER	123	AUSTEN	1	500.0	600.0	625.0	67.0
113	ARNE	123	AUSTEN	1	500.0	600.0	625.0	60.0
114	ARNOLD	116	ASSER	1	500.0	600.0	625.0	27.0
115	ARTHUR	116	ASSER	1	500.0	600.0	625.0	12.0
115	ARTHUR	121	ATTLEE	1	500.0	600.0	625.0	34.0
115	ARTHUR	121	ATTLEE	2	500.0	600.0	625.0	34.0
115	ARTHUR	124	AVERY	1	500.0	600.0	625.0	36.0
116	ASSER	117	ASTON	1	500.0	600.0	625.0	18.0
116	ASSER	119	ATTAR	1	500.0	600.0	625.0	16.0
117	ASTON	118	ASTOR	1	500.0	600.0	625.0	10.0
117	ASTON	122	AUBREY	1	500.0	600.0	625.0	73.0
118	ASTOR	121	ATTLEE	1	500.0	600.0	625.0	18.0
118	ASTOR	121	ATTLEE	2	500.0	600.0	625.0	18.0
119	ATTAR	120	ATTILA	1	500.0	600.0	625.0	27.5
119	ATTAR	120	ATTILA	2	500.0	600.0	625.0	27.5
120	ATTILA	123	AUSTEN	1	500.0	600.0	625.0	15.0
120	ATTILA	123	AUSTEN	2	500.0	600.0	625.0	15.0
121	ATTLEE	122	AUBREY	1	500.0	600.0	625.0	47.0

Table 6.12: 138 kV Generator step-up transformers data

Bus no	from bus Bus name	Bus no	to bus Bus name	R (pu)	X (pu)	Rating (MVA)	HV tap (pu)
101	ABEL	10101	ABEL G1	0.003	0.15	24	1.05
101	ABEL	20101	ABEL G2	0.003	0.15	24	1.05
101	ABEL	30101	ABEL G3	0.003	0.15	89	1.05
101	ABEL	40101	ABEL G4	0.003	0.15	89	1.05
102	ADAMS	10102	ADAMS G1	0.003	0.15	24	1.05
102	ADAMS	20102	ADAMS G2	0.003	0.15	24	1.05
102	ADAMS	30102	ADAMS G3	0.003	0.15	89	1.05
102	ADAMS	40102	ADAMS G4	0.003	0.15	89	1.05
107	ALDER	10107	ALDER G1	0.003	0.15	118	1.05
107	ALDER	20107	ALDER G2	0.003	0.15	118	1.05
107	ALDER	30107	ALDER G3	0.003	0.15	118	1.05
106	ALBER	10106	ALBER SVC	0.003	0.15	100	1.05

all impedances expressed in (pu) of transformer MVA  
all transformers represented with 5 tap positions (2.5%), no LTC

Table 6.13: 230 kV Generator step-up transformers data

Bus no	from bus Bus name	Bus no	to bus Bus name	R (pu)	X (pu)	Rating (MVA)	HV tap (pu)
113	ARNE	10113	ARNE G1	0.003	0.15	232	1.05
113	ARNE	20113	ARNE G2	0.003	0.15	232	1.05
113	ARNE	30113	ARNE G3	0.003	0.15	232	1.05
115	ARTHUR	10115	ARTHUR G1	0.003	0.15	14	1.05
115	ARTHUR	20115	ARTHUR G2	0.003	0.15	14	1.05
115	ARTHUR	30115	ARTHUR G3	0.003	0.15	14	1.05
115	ARTHUR	40115	ARTHUR G4	0.003	0.15	14	1.05
115	ARTHUR	50115	ARTHUR G5	0.003	0.15	14	1.05
115	ARTHUR	60115	ARTHUR G6	0.003	0.15	182	1.05
116	ASSER	10116	ASSER G1	0.003	0.15	182	1.05
118	ASTOR	10118	ASTOR G1	0.003	0.15	471	1.05
121	ATTLEE	10121	ATTLEE G1	0.003	0.15	471	1.05
122	AUBREY	10122	AUBREY G1	0.003	0.15	53	1.05
122	AUBREY	20122	AUBREY G2	0.003	0.15	53	1.05
122	AUBREY	30122	AUBREY G3	0.003	0.15	53	1.05
122	AUBREY	40122	AUBREY G4	0.003	0.15	53	1.05
122	AUBREY	50122	AUBREY G5	0.003	0.15	53	1.05
122	AUBREY	60122	AUBREY G6	0.003	0.15	53	1.05
123	AUSTEN	10123	AUSTEN G1	0.003	0.15	182	1.05
123	AUSTEN	20123	AUSTEN G2	0.003	0.15	182	1.05
123	AUSTEN	30123	AUSTEN G3	0.003	0.15	412	1.05
114	ARNOLD	10114	ARNOLD SVC	0.003	0.15	200	1.05
all impedances expressed in (pu) of transformer MVA							
all transformers represented with 5 tap positions (2.5%), no LTC							

Table 6.14: 230/138 kV Transformers data

138 kV bus Bus no	230 kV bus Bus no	R (pu)	X (pu)	Rating (MVA)	HV tap (pu)
103	ADLER	124	AVERY	0.002	0.084
109	ALI	111	ANNA	0.002	0.084
109	ALI	112	ARCHER	0.002	0.084
110	ALLEN	111	ANNA	0.002	0.084
110	ALLEN	112	ARCHER	0.002	0.084
all impedances expressed in (pu) of transformer MVA					

In the RVS test system, the generators were moved to 18 kV buses and therefore generator step-up transformers had been introduced. All generator step-up transformers are represented with 15% reactance on the transformer MVA base, with 5 tap positions (+5%, +2.5%, 0, -2.5% and -5%) on the high-voltage side of the generator step-up transformer, and no LTCs. Table 6.12 presents the data for the 138/18 kV generator step-up transformers, while Table 6.13 corresponds to the 230/18 kV generator step-up transformers.

The 230/138 kV transformers are represented with 33 tap positions between 90% and 110%, with automatic LTC. The tap changer is on the HV side of the transformers (230 kV) but it is controlling the voltages of the 138 kV network. The voltages are controlled (part of the power flow solution) to stay within the voltage range shown in Table 6.15.

The loads in the RVS test system were moved to 13.8 kV buses and thus step-down transformers (either 230/13.8 kV or 138/13.8 kV transformers) were introduced. These load step-down transformers are represented with 15% reactance on the transformer MVA base, with 33 tap positions (+/- 10% range, with steps of 0.625%, plus the central position) and on-load tap changers. The tap changer is located at the HV side of the transformers, but it controls the voltage at the load side (13.8 kV bus). Table 6.16 presents the data associated with the load step-down transformers.

The LTC is automatically adjusted to maintain the voltages at the load buses (13.8 kV buses) within the voltage ranges presented in Table 6.17. These voltage ranges define the deadband of the dynamic model of the on-load tap changers. It was decided to use quite small ranges, in order for the taps to be adjusted more often (thus leading to a higher total number of tap changes).

Table 6.15: LTC 230/138 kV transformers data

138 kV bus		230 kV bus		voltage range	
Bus no	Bus name	Bus no	Bus name	max (pu)	min (pu)
103	ADLER	124	AVERY	1.01458	0.99573
109	ALI	111	ANNA	1.03278	1.01359
109	ALI	112	ARCHER	1.03278	1.01359
110	ALLEN	111	ANNA	1.01951	1.00057
110	ALLEN	112	ARCHER	1.01951	1.00057
voltage range at 138 kV buses					

## 6.4 Shunts and SVC data

The original 1979 IEEE Reliability Test System had a synchronous condenser at bus 114. This was replaced by an SVC with the same nominal range (-50 / + 200 Mvar), but it should be noted that the actual reactive power output of this device is now voltage dependent and its reactive power output is severely reduced under low voltage conditions. The original system also had a shunt at bus 106, but that fixed shunt has been replaced by an SVC with a range of (-50/+100 Mvar). The results will show that this SVC is a key component in the proposed system and is usually required to avoid voltage collapse during dynamic simulations. In power flow (steady state), these SVCs are represented as variable shunts, as shown in Table 6.18.

Table 6.16: Load step-down transformers data

Bus no	HV bus Bus name	Bus no	LV bus Bus name	R (pu)	X (pu)	Rating (MVA)	HV tap (pu)
101	ABEL	1101	ABEL	0.003	0.15	150	0.9568
102	ADAMS	1102	ADAMS	0.003	0.15	150	0.9614
103	ADLER	1103	ADLER	0.003	0.15	250	0.9359
104	AGRICOLA	1104	AGRICOLA	0.003	0.15	100	0.9333
105	AIKEN	1105	AIKEN	0.003	0.15	100	0.9298
106	ALBER	1106	ALBER	0.003	0.15	200	0.9625
107	ALDER	1107	ALDER	0.003	0.15	200	0.9561
108	ALGER	1108	ALGER	0.003	0.15	250	0.9438
109	ALI	1109	ALI	0.003	0.15	250	0.9534
110	ALLEN	1110	ALLEN	0.003	0.15	250	0.9315
113	ARNE	1113	ARNE	0.003	0.15	350	0.9448
114	ARNOLD	1114	ARNOLD	0.003	0.15	250	0.9313
115	ARTHUR	1115	ARTHUR	0.003	0.15	400	0.9324
116	ASSER	1116	ASSER	0.003	0.15	150	0.9431
118	ASTOR	1118	ASTOR	0.003	0.15	450	0.9640
119	ATTAR	1119	ATTAR	0.003	0.15	250	0.9414
120	ATTILA	1120	ATTILA	0.003	0.15	200	0.9611

all impedances expressed in (pu) of transformer MVA

Table 6.17: LTC step-down transformers data

Bus name	HV Bus no	LV Bus no	voltage range (at load LV bus)	
			max (pu)	min (pu)
ABEL	101	1101	1.05	1.03982
ADAMS	102	1102	1.05	1.03974
ADLER	103	1103	1.05	1.04
AGRICOLA	104	1104	1.05	1.03974
AIKEN	105	1105	1.05	1.03967
ALBER	106	1106	1.045	1.025
ALDER	107	1107	1.05	1.03983
ALGER	108	1108	1.05	1.03996
ALI	109	1109	1.05	1.03998
ALLEN	110	1110	1.05	1.03999
ARNE	113	1113	1.05	1.04003
ARNOLD	114	1114	1.05	1.04
ARTHUR	115	1115	1.05	1.04006
ASSER	116	1116	1.05	1.03979
ASTOR	118	1118	1.05	1.04005
ATTAR	119	1119	1.05	1.03997
ATTILA	120	1120	1.05	1.03984

One key element in this test system is the underground 138 kV cable between buses 106 and 110 (Alber - Allen), which is a critical contingency in the test system. The underground cable is characterized by a large charging (see Table 6.8) and line-connected reactors were added to partially compensate the cable charging. Table 6.19 presents the nominal Mvar of the reactors connected at both terminals of the cable. It is fundamental to understand that these are line-connected reactors, and therefore they are tripped with the cable, when the terminal breakers are opened. Therefore, the critical contingency in the RVS Test System corresponds to disconnecting the cable (branch) between buses 106 and 110 and, simultaneously, disconnecting the shunt reactors described in Table 6.19.

Table 6.18: Static VAR Compensator (SVC) data

Bus no	Bus name	Base Voltage (kV)	Scheduled Voltage (pu)	Inductive Range (Mvar)	Capacitive Range (Mvar)
10106	ALBER SVC	18.000	1.0500	-50.00	100.00
10114	ARNOLD SVC	18.000	1.0500	-50.00	200.00

Table 6.19: Line shunt data

Bus no	Bus name	Base Voltage (kV)	Line Reactor (Mvar)
106	ALBER	138.00	75.00
110	ALLEN	138.00	75.00

## 6.5 Load tap changer model and data

The representation of the effect of LTC transformers is particularly important for the analysis of slow voltage collapse phenomena. This model is usually associated with longer term dynamic simulations, of up to several minutes after fault clearing. All transformers modeled with on-load tap changers in power flow are represented in dynamic simulations by a model that does not contain any differential equations (state variables). The dynamic model only considers an initial delay for the first tap change of 30 seconds, with 1 second delay in the switching action and 5 seconds delay before consecutive tap changes are allowed.

It should be recognized that this is quite fast and probably faster than most practical settings, with the effect of the LTC becoming evident with simulations lasting just one to two minutes after fault clearing.

The dynamic model for the on-load tap changers will try to maintain the controlled voltages within the ranges indicated in Table 6.17. These ranges specify the deadband for the operation of the tap changers. Thus, the controlled voltage has to remain outside the specified range for longer than 30 seconds before the first change in tap position is allowed (initial delay). Once the tap changer has started changing positions, there is a fixed time delay of 5 seconds for any subsequent change in tap position.

## 6.6 Load models and data

The representation of the changes in demand (loads) as a function of changes in voltages is obviously a very important aspect of dynamic simulations, particularly for voltage stability assessment. At least as an initial approach, loads are usually represented as constant power (constant MW and constant Mvar) in power flow (steady state) solutions, and as voltage-dependent loads in dynamic simulations, particularly short-term simulations.

This report includes dynamic simulation results for the RVS test system considering different representations of the load. Fast voltage collapse events are associated with the dynamic response of induction motors and, in particular, to higher inductive currents drawn by induction motors during re-acceleration (following a fault and low voltage conditions) or during stalling conditions. Thus, it is fundamental to represent a fraction of the total demand as induction motors, with proper dynamic models. One approach is the use of the complex load model [35] shown in Fig. 6.2. A similar approach is also being proposed in [36]. The advantage of this approach is to provide a relatively straightforward model that would allow sensitivity studies, comparing the dynamic response (and voltage recovery or voltage collapse) with different levels of penetration of induction motors as a fraction of the total load. The complex load model shown in Fig. 6.2 represents the impedance of a step-down transformer, and splits the demand ( $P$  and  $Q$ ) into different components, including a large induction motor component (such as industrial motors), small induction motor component (such as air conditioning and residential appliances), and discharge lighting (fluorescent lamps and similar equipment that will turn off for low voltages).

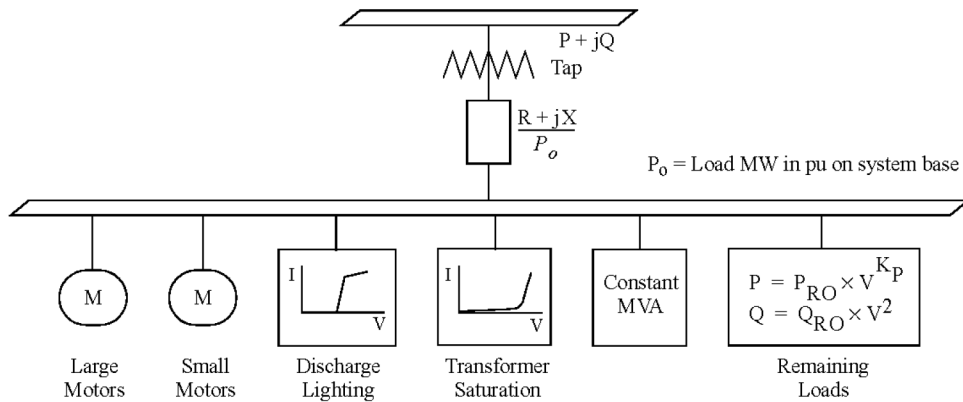


Figure 6.2: Load model

The following load composition is proposed [35, 36]:

- 15% of large induction motors (industrial motors);
- 35% of small induction motors (air conditioning);
- 2% of transformer excitation current;
- 15% of discharge lighting;

- 5% of constant MVA load.

Remaining part of the load (28%) represented as 100% constant current for the real part and 100% constant admittance for the reactive part with 5% reactance (on load MW base) in the step-down transformer. The parameter  $P_0$  shown in Figure 6.2 simply indicates the conversion of the transformer impedance from the load MW base to the system MVA base.

To compare the results of a long-term dynamic simulation with the results from a power flow analysis, it is necessary to reconcile the representation of the loads and, in particular, their dependency with voltage. It is well established that aggregate loads, representing the combined demand from a large number of consumers or individual equipment, tend to restore their constant power (MW and Mvar) over a period of time, following system disturbances. Thus, it is quite justifiable to represent the loads as constant power in power flow analyses. Then, it might be necessary to represent the loads in a long-term dynamic simulation with some mechanism to represent this recovery of the demand from their short-term voltage-dependent representation to the long-term constant power (voltage independent) model.

Load recovery (or load reset) characteristic is represented by the model shown in Fig. 6.3. This model represents a simple load recovery mechanism controlled by a single parameter, the gain  $K_P$ . The output of the integrator  $P_{MLT}$  is initialized as 1.0 pu, and thus the load (output of the model,  $P_{load}$ ) is equal to the initial load  $P_{initial}$ . When a disturbance is applied, and the voltage changes, the voltage dependent part of the model will modify the load, depending on the exponent  $\alpha$ . A change in the load  $P_{load}$  will result in a nonzero error signal  $P_{err}$  that will drive the integrator in the load reset model, increasing or decreasing the multiplying factor  $P_{MLT}$  until the load is restored to its initial value. A similar implementation (parameter  $K_Q$ ) is applied to the reactive power demand of the load.

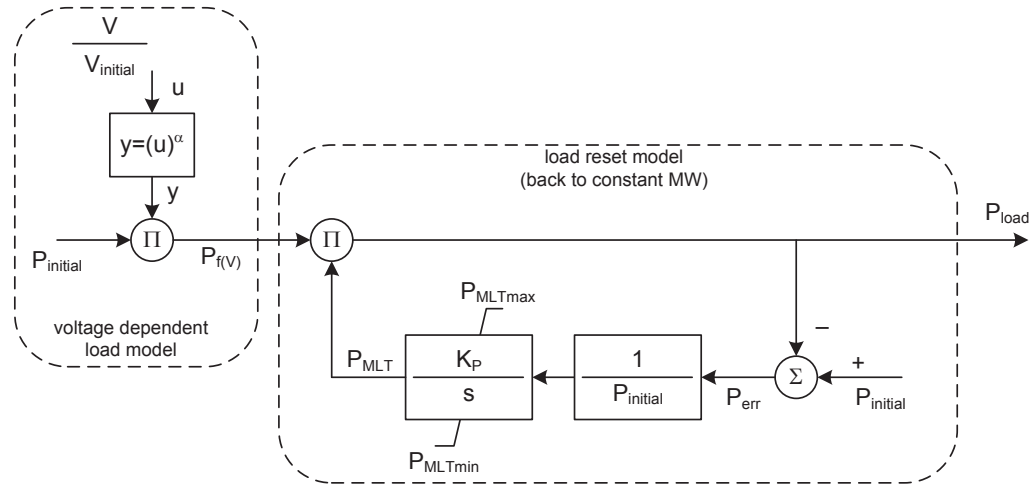


Figure 6.3: Load recovery model

## 6.7 Synchronous machine models and data

The data presented in Tables 6.20, 6.21, 6.22, and 6.23 are related to the machine MVA of power flow data for the generators shown in Table 6.5. The units identified as hydro turbines in the original Reliability Test System are represented by a salient pole machine model. All other units are thermal units and are represented by a round-rotor machine model.

The inertias were set to the values originally proposed, even though they are probably on the lower end of the typical range for similar units. This lower inertia might imply that the system will be more susceptible to angular instability (loss of synchronism) and poorly damped oscillations than would be expected if more realistic inertias are considered. Thus, this test system is not documented and perhaps it is not ideal as a test system for angular stability or small-signal stability phenomena. All other parameters are representative of generation units of comparable MVA ratings.

Table 6.20: Round rotor synchronous generator data

Description	Symbol	471 MVA	412 MVA	232 MVA	Units
d-axis OC transient time const.	$T'_{do}$	6.5	9.5	9.5	s
d-axis OC subtransient time const.	$T''_{do}$	0.025	0.023	0.023	s
q-axis OC transient time const.	$T'_{qo}$	0.34	0.99	0.99	s
q-axis OC subtransient time const.	$T''_{qo}$	0.25	0.035	0.035	s
inertia	$H$	5	3	2.8	s
damping	$D$	0	0	0	pu
d-axis synchronous reactance	$X_d$	2	2.46	2.46	pu
q-axis synchronous reactance	$X_q$	1.6	2.32	2.32	pu
d-axis transient reactance	$X'_d$	0.329	0.25	0.25	pu
q-axis transient reactance	$X'_q$	0.5	0.41	0.41	pu
subtransient reactance ( $X''_d = X''_q$ )	$X''$	0.252	0.25	0.19	pu
leakage reactance	$X_\ell$	0.2	0.16	0.17	pu
saturation factor at 1.0 pu	S(1.0)	0.158	0.1	0.0625	
saturation factor at 1.2 pu	S(1.2)	0.46	0.4	0.229	
rated field current	$I_{FD_{rated}}$	2.933	3.297	3.149	pu

Values in per unit given in Tables 6.20, 6.21, 6.22, and 6.23 are on the generator MVA base. All reactances are unsaturated values, while the damping factor for all units is set to zero.

## 6.8 Exciter and power system stabilizer model and data

Three different excitation system models were adopted. The IEEE type 1 (IEEET1) and IEEE type AC1A (EXAC1) models correspond to AC rotating exciters [37, 38, 39, 40, 41], while the SCRX model represents a bus-fed static exciter. The block diagrams for models IEEET1, EXAC1 and SCRX are shown in Figs 6.4 to 6.6, respectively. The parameters for these excitation systems provide a reasonable, representative response for these equipment (Tables 6.24, 6.25, and 6.26).

Table 6.21: Round rotor synchronous generator data (continued)

Description	Symbol	118 MVA	89 MVA	24 MVA	14 MVA	Units
d-axis OC transient time const.	$T'_{do}$	5.642	5.108	5.115	5.1	s
d-axis OC subtransient time const.	$T''_{do}$	0.022	0.023	0.023	0.023	s
q-axis OC transient time const.	$T'_{qo}$	0.469	0.421	0.415	0.41	s
q-axis OC subtransient time const.	$T''_{qo}$	0.044	0.059	0.055	0.05	s
inertia	$H$	2.8	3	2.8	2.8	$\frac{MWs}{MVA}$
damping	$D$	0	0	0	0	pu
d-axis synchronous reactance	$X_d$	2.201	1.676	1.867	1.65	pu
q-axis synchronous reactance	$X_q$	2.098	1.586	1.76	1.52	pu
d-axis transient reactance	$X'_d$	0.314	0.212	0.256	0.24	pu
q-axis transient reactance	$X'_q$	0.468	0.377	0.453	0.41	pu
subtransient reactance ( $X''_d = X''_q$ )	$X''$	0.218	0.144	0.174	0.115	pu
leakage reactance	$X_\ell$	0.185	0.119	0.143	0.095	pu
saturation factor at 1.0 pu	S(1.0)	0.11	0.118	0.08	0.06	
saturation factor at 1.2 pu	S(1.2)	0.45	0.377	0.35	0.19	
rated field current	$I_{FD_{rated}}$	3.046	2.473	2.636	2.35	pu

Table 6.22: Round rotor synchronous generator data for the 182 MVA machines

Description	Symbol	ARTHUR G6	ASSER G1	AUSTEN G1/G2	Units
d-axis OC transient time const.	$T'_{do}$	9.5	9.5	8.533	s
d-axis OC subtransient time const.	$T''_{do}$	0.023	0.023	0.043	s
q-axis OC transient time const.	$T'_{qo}$	0.99	0.99	0.948	s
q-axis OC subtransient time const.	$T''_{qo}$	0.035	0.035	0.084	s
inertia	$H$	3	3.2	3	s
damping	$D$	0	0	0	pu
d-axis synchronous reactance	$X_d$	2.46	2.46	1.891	pu
q-axis synchronous reactance	$X_q$	2.32	2.32	1.829	pu
d-axis transient reactance	$X'_d$	0.25	0.25	0.1964	pu
q-axis transient reactance	$X'_q$	0.41	0.41	0.3821	pu
subtransient reactance ( $X''_d = X''_q$ )	$X''$	0.19	0.19	0.153	pu
leakage reactance	$X_\ell$	0.17	0.17	0.1203	pu
saturation factor at 1.0 pu	S(1.0)	0.0625	0.0625	0.077	
saturation factor at 1.2 pu	S(1.2)	0.229	0.229	0.29	
rated field current	$I_{FD_{rated}}$	3.149	3.149	2.624	pu

Table 6.23: Salient pole synchronous generator data (53 MVA units)

Description	Symbol	Value	Units
d-axis OC transient time const.	$T'_{do}(> 0)$	5.5	s
d-axis OC subtransient time const.	$T''_{do}(> 0)$	0.05	s
q-axis OC subtransient time const.	$T'_{qo}(> 0)$	0.12	s
inertia	$H$	3.5	s
damping	$D$	0	pu
d-axis synchronous reactance	$X_d$	0.959	pu
q-axis synchronous reactance	$X_q$	0.87	pu
d-axis transient reactance	$X'_d$	0.35	pu
subtransient reactance ( $X''_d = X''_q$ )	$X''_d = X''_q$	0.338	pu
leakage reactance	$X_1$	0.3	pu
saturation factor at 1.0 pu	$S(1.0)$	0.21	
saturation factor at 1.2 pu	$S(1.2)$	0.75	
rated field current	$I_{FD_{rated}}$	2.374	pu

The model parameters are in per unit considering the IEEE non-reciprocal base values for generator field voltage and current (see IEEE Std. 1110 and IEEE Std. 421.5). Namely, the base value for the generator field current is the field current required to sustain rated terminal voltage on the air-gap line of the generator operating at full speed and no load. The base value for the field voltage is the product of the base field current and the field winding resistance.

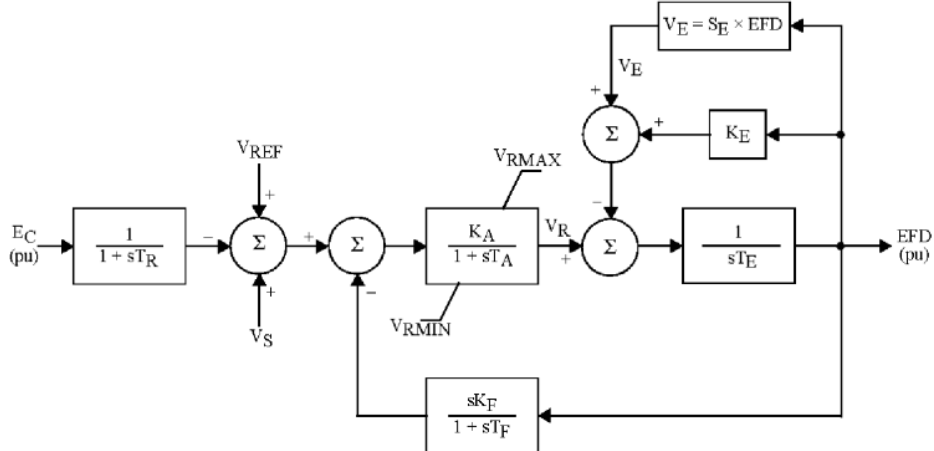


Figure 6.4: Block diagram of the model IEEET1

The limits are set in such way as to limit the ceiling (maximum field voltage) at around twice the rated (full load) field voltage. The resulting response ratios are above 1.0, with the exception of the generator at bus 30123, providing a quite responsive voltage control, consistent with modern excitation systems.

Values given in Table 6.24 apply for the units at buses ABEL and ADAMS, in Table 6.25 to the units at buses ASTOR and ATTLEE, and those in Table 6.26 to the units at buses: ALDER, ARNE, ARTHUR, ASSER, AUBREY, and AUSTEN.

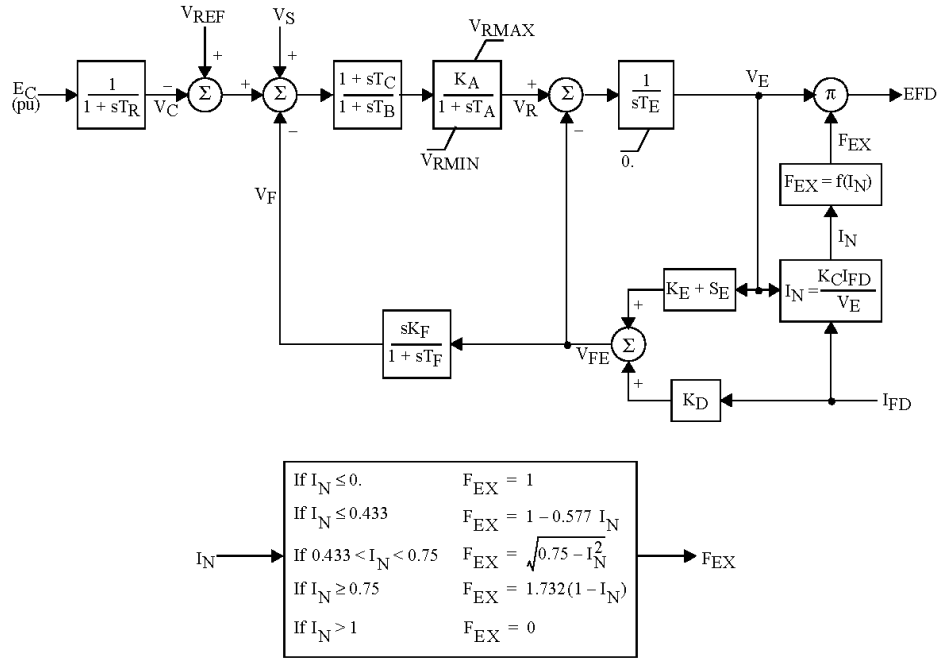
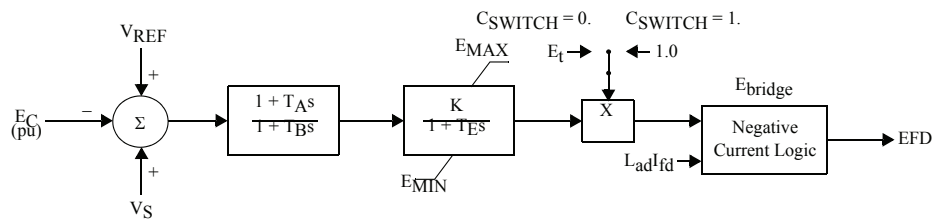


Figure 6.5: Block diagram of the model EXAC1



$$V_S = VOTHSG + VUEL + VOEL$$

Figure 6.6: Block diagram of the static exciter model SCRX

Table 6.24: AC rotating exciter data (EXAC1)

Description	Symbol	Value	Unit
voltage input time const.	$T_R$	0	s
AVR lead-lag time const.	$T_B$	0	s
AVR lead-lag time const.	$T_C$	0	s
AVR gain	$K_A$	400	
AVR time const.	$T_A$	0.02	s
max. AVR output	$V_{Rmax}$	9	pu
min. AVR output	$V_{Rmin}$	-5.43	pu
exciter time const.	$T_E$	0.8	s
rate feedback gain	$K_F$	0.03	
rate feedback time const.	$T_F$	1	s
rectifier load factor	$K_C$	0.2	
exciter demagnetizing factor	$K_D$	0.48	
exciter field gain	$K_E$	1	
exciter sat. point 1	$E_1$	5.25	pu
saturation at $E_1$	$S_E(E_1)$	0.03	
exciter sat. point 2	$E_2$	7	pu
saturation at $E_2$	$S_E(E_2)$	0.1	

Table 6.25: DC rotating exciter data (IEEEET1)

Description	Symbol	Value	Unit
voltage input time const.	$T_R$	0	s
AVR gain	$K_A$	400	
AVR time const.	$T_A$	0.04	s
max. AVR output	$V_{Rmax}$	7.3	pu
min. AVR output	$V_{Rmin}$	-7.3	pu
exciter field gain	$K_E$	1	
exciter time const.	$T_E$	0.8	s
rate feedback gain	$K_F$	0.03	
rate feedback time const.	$T_F$	1	s
exciter sat. point 1	$E_1$	3.375	pu
saturation at $E_1$	$S_E(E_1)$	0.035	
exciter sat. point 2	$E_2$	4.5	pu
saturation at $E_2$	$S_E(E_2)$	0.47	

Table 6.26: Static excitation system data (SCRX)

Description	Symbol	Value	Unit
transient gain reduction	$T_A/T_B$	0.1	
gain reduction time const.	$T_B$	10	s
AVR gain	K	200	
AVR time const.	$T_E$	0.2	s
min. AVR output	$E_{min}$	-3.2	pu
max. AVR output	$E_{max}$	4	pu

Poorly damped electromechanical oscillations were observed when the simulations were performed without power system stabilizers. The main focus of this test system is on voltage stability, so these oscillations are not an impediment to the overall use of the test data and the analysis of voltage stability issues. Nonetheless, power system stabilizers were added to the larger units in the system, so additional damping of these electromechanical oscillations is provided. Figure 6.7 presents the block diagram for power system stabilizer model (IEEE type PSS2B-Dual-Input PSS, [38, 39]).

The PSS2B model represents the integral of accelerating power PSS structure that is a de facto standard in North America. The following rules should always be followed when setting up data for the PSS2B model [42]:  $T_{w1} = T_{w2} = T_{w3} = T_7, K_{S3} = 1, T_6 = 0, K_{S2} = \frac{T_w}{2H}$ , the first input is rotor speed deviation (compensated frequency) and the second input is electrical power output of the generator in per unit of the generator MVA base. Table 6.27 shows the values for the parameters that are the same in all PSSs in this dynamic setup. Table 6.28 lists the machines that have an active PSS and the calculated values for the gain  $K_{S2}$  for each of these PSSs.

The phase compensation part of the PSS transfer function (lead-lag blocks), in theory, should be individually adjusted to each machine, as the proper phase compensation depends on the generator and excitation system models. On the other hand, as the units with the same MVA rating are represented by the same generator and exciter models, only two phase compensation settings were required and they are identified as Group 1 and Group 2 in Table 6.29. The machines using each set of parameters (Group 1 or Group 2) are identified in Table 6.28.

Table 6.27: PSS2B parameters common to all PSSs in the system

Description	Symbol	Value
washout time constant	$T_{w1} = T_{w2} = T_{w3} = T_7$	10 s
gain	$K_{S3}$	1
washout time constant	$T_{w4}$	0 s
time constant	$T_6$	0 s
maximum output limit	$V_{STmax}$	0.05 pu
minimum output limit	$V_{STmin}$	-0.05 pu
maximum input limit	$V_{SI1max} = V_{SI2max}$	2.0 pu
minimum input limit	$V_{SI1min} = V_{SI2min}$	-2.0 pu
ramp-track filter numerator time constant	$T_8$	0.5 s
ramp track filter denominator time constant	$T_9$	0.1 s
ramp-track filter denominator order	$M$	5
ramp-track filter order	$N$	1

## 6.9 Overexcitation limiter model and data

Each OEL acts on the main summation point of the AVR (where the output of the PSS also acts). It has an inverse time characteristic. The latter is shown in Fig. 6.8 with the corresponding block diagram, while the parameters are given in Table 6.30.

Table 6.28: Machines with a PSS and gain  $K_{S2}$  for the PSS models

Bus no	Bus Name	Gain	Group
		$K_{S2}$	number
10113	ARNE G1	1.7857	1
20113	ARNE G2	1.7857	1
30113	ARNE G3	1.7857	1
10123	AUSTEN G1	1.667	1
20123	AUSTEN G2	1.667	1
30123	AUSTEN G3	1.667	1
10116	ASSER G1	1.667	1
60115	ARTHUR G6	1.667	1
10118	ASTOR G1	1	2
10121	ATTLEE G1	1	2

Table 6.29: PSS phase compensation parameters

Description	Symbol	Group 1		Units
		Value	Value	
PSS main gain	$K_{S1}$	10	10	
1st lead-lag numerator time constant	$T_1$	0.2	0.25	s
1st lead-lag denominator time constant	$T_2$	0.025	0.06	s
2nd lead-lag numerator time constant	$T_3$	0.2	0.1	s
2nd lead-lag denominator time constant	$T_4$	0.025	0.02	s
3rd lead-lag numerator time constant	$T_{10}$	0.5	0.1	s
3rd lead-lag denominator time constant	$T_{11}$	0.1	0.02	s

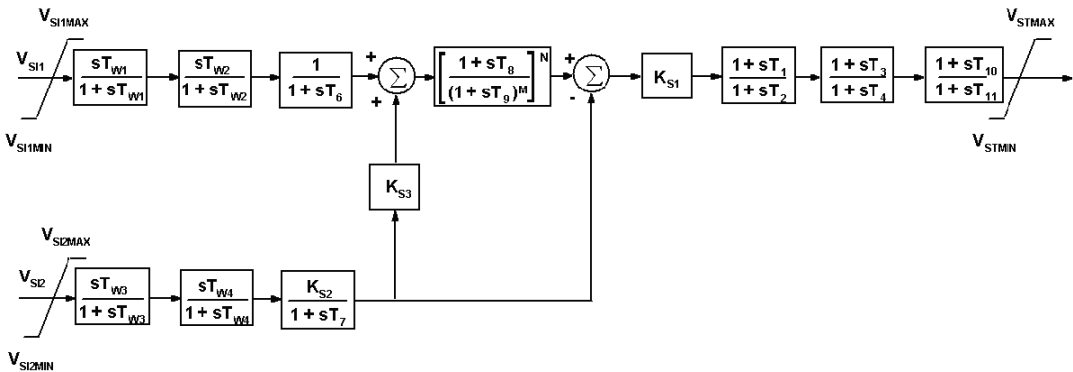


Figure 6.7: Block diagram of the PSS model

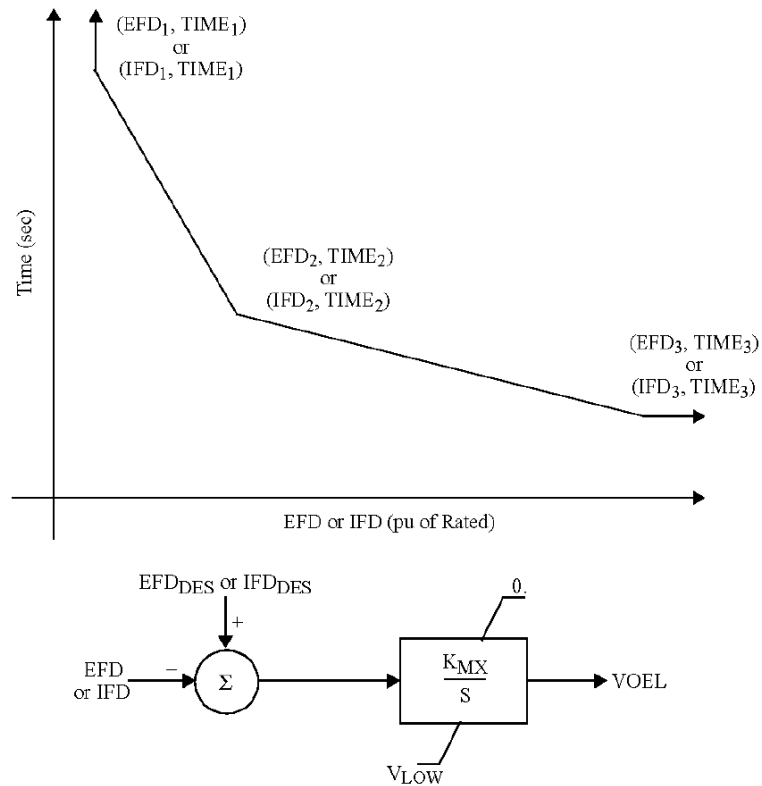


Figure 6.8: Time characteristic and block diagram of OEL model. The output  $VOEL$  is one term of the supplementary signal  $V_S$  in Figs. 6.4 to 6.6

Table 6.30: OEL data

Description	Symbol	Value	Unit
low OEL limit	$I_{FD_1}$	1.1	pu
timing for low OEL	$TIME_1$	60	s
medium OEL limit	$I_{FD_2}$	1.2	pu
timing for medium OEL	$TIME_2$	30	s
high OEL limit	$I_{FD_3}$	1.5	pu
timing for high OEL	$TIME_3$	15	s
$I_{FD}$ setpoint	$I_{FDDES}$	1	pu
minimum OEL output	$V_{LOW}$	-0.05	pu

Values given in Table 6.30 are applicable to all units with specific values for  $I_{FD_{rated}}$  given in Tables 6.20, 6.21, 6.22, and 6.23. Field current values in pu are with respect to the rated  $I_{FD}$  and OEL output limits in pu are with respect to voltage reference.

## 6.10 Generator capability curves

The capability curves, together with open circuit saturation characteristics, of generation units are shown in Figures 6.9 to 6.17.

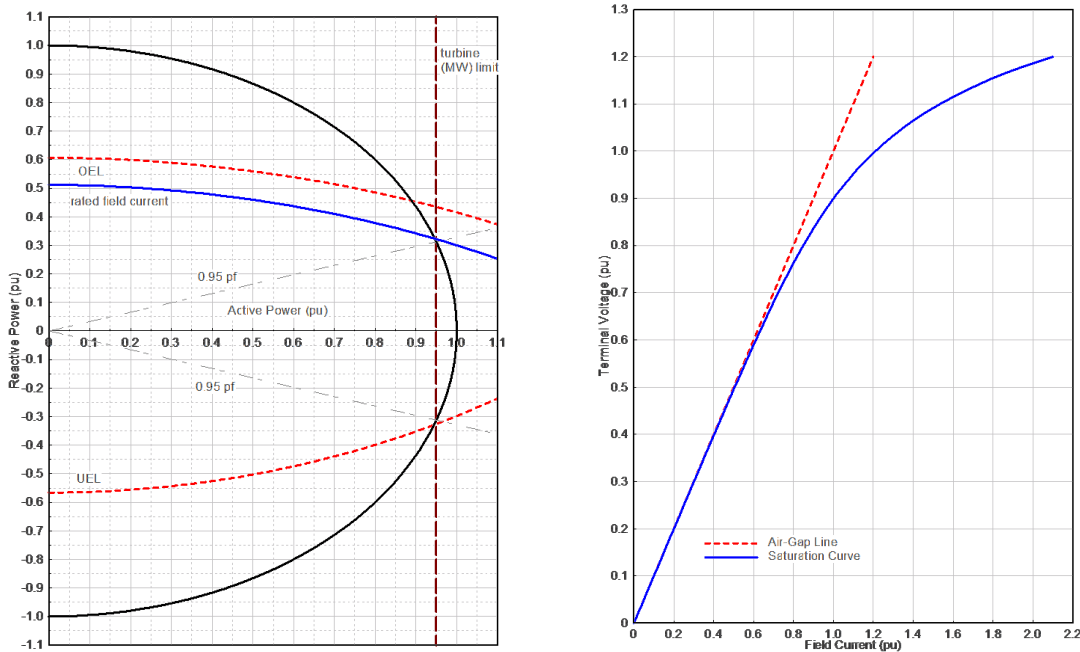


Figure 6.9: Capability curve and open circuit saturation curve for the salient pole machines

## 6.11 Turbine and speed governor models and data

Only a few generators in this test system have a turbine/speed governor model [43, 44]. Those machines without such model are simulated with constant mechanical power. There is only a limited amount of spinning reserves in the RVS test system, as most generation units are dispatched close to their maximum power output. Therefore, the simulation of large imbalances between generation and load should be avoided, since there is a significant risk of large frequency excursions and even the inability of the simulation model to control frequency.

The hydro turbines are represented by the HYGOV model shown in Fig. 6.18 [44], while the steam units are modeled by the IEEEG1 model shown in Fig. 6.19 [43]. The parameters for these models are given in

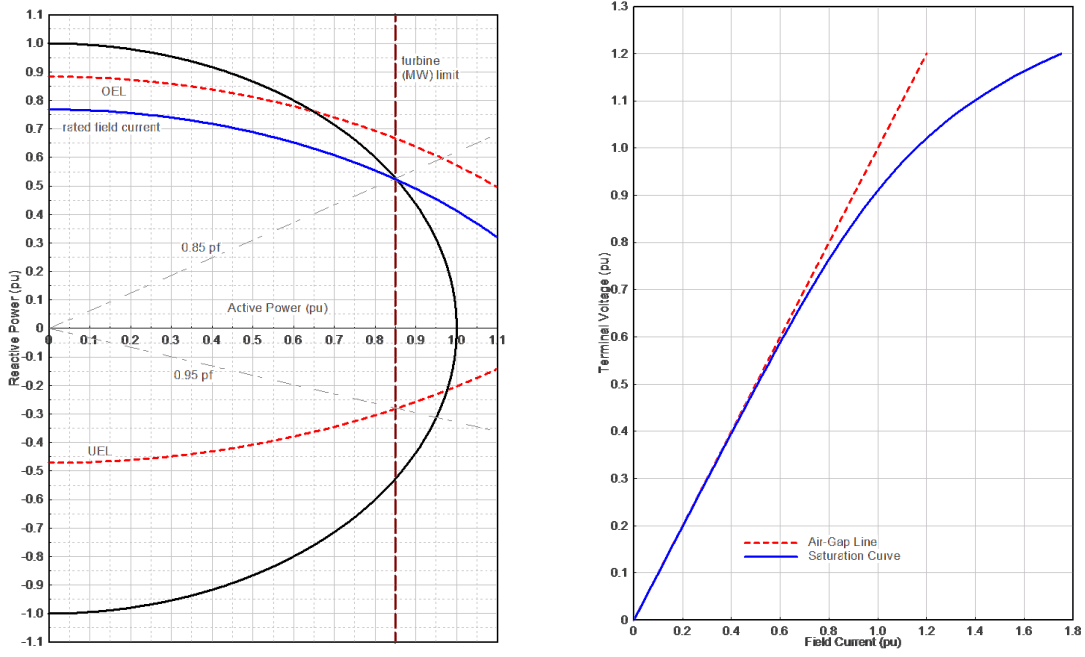


Figure 6.10: Capability curve and open circuit saturation curve for the 400 MW round rotor units

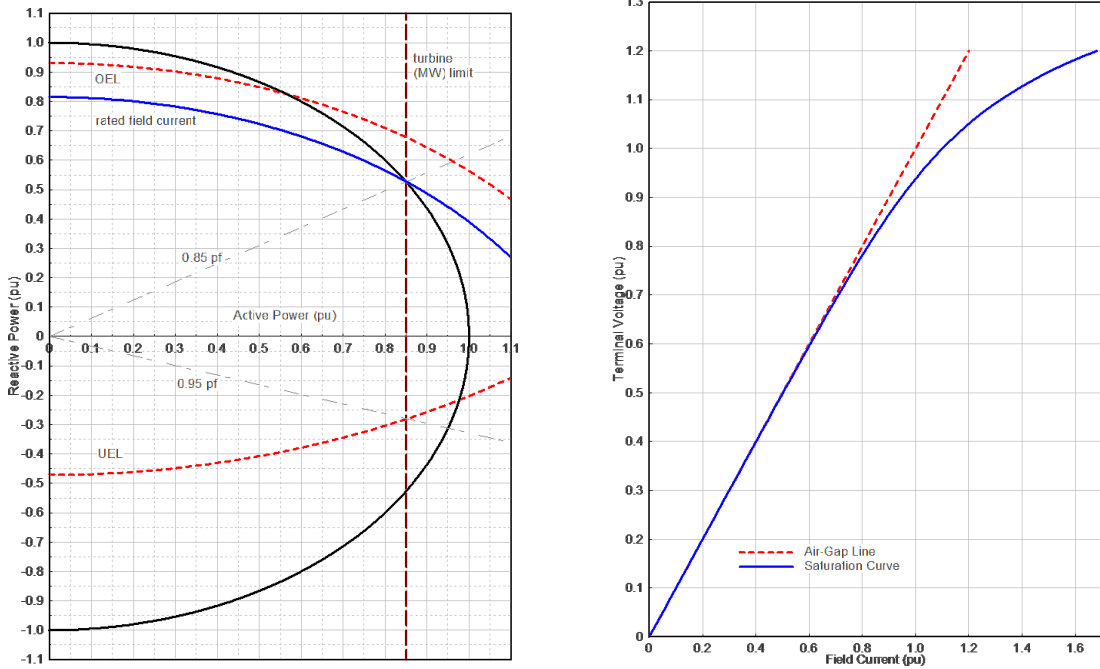


Figure 6.11: Capability curve and open circuit saturation curve for the 350 MW round rotor units

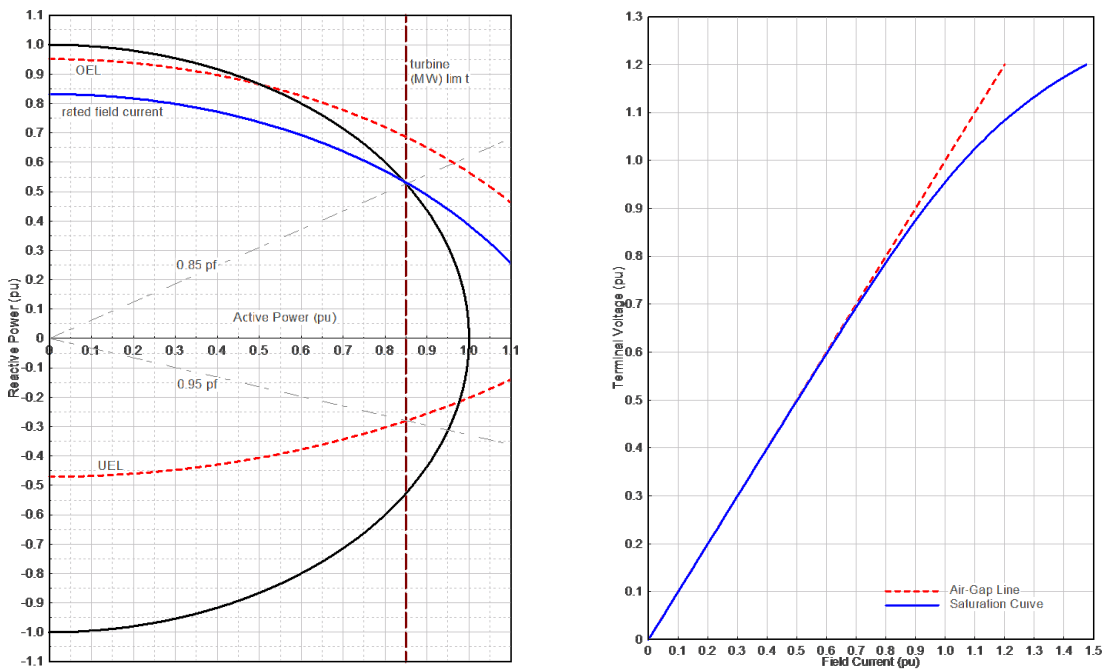


Figure 6.12: Capability curve and open circuit saturation curve for the 197 MW round rotor units

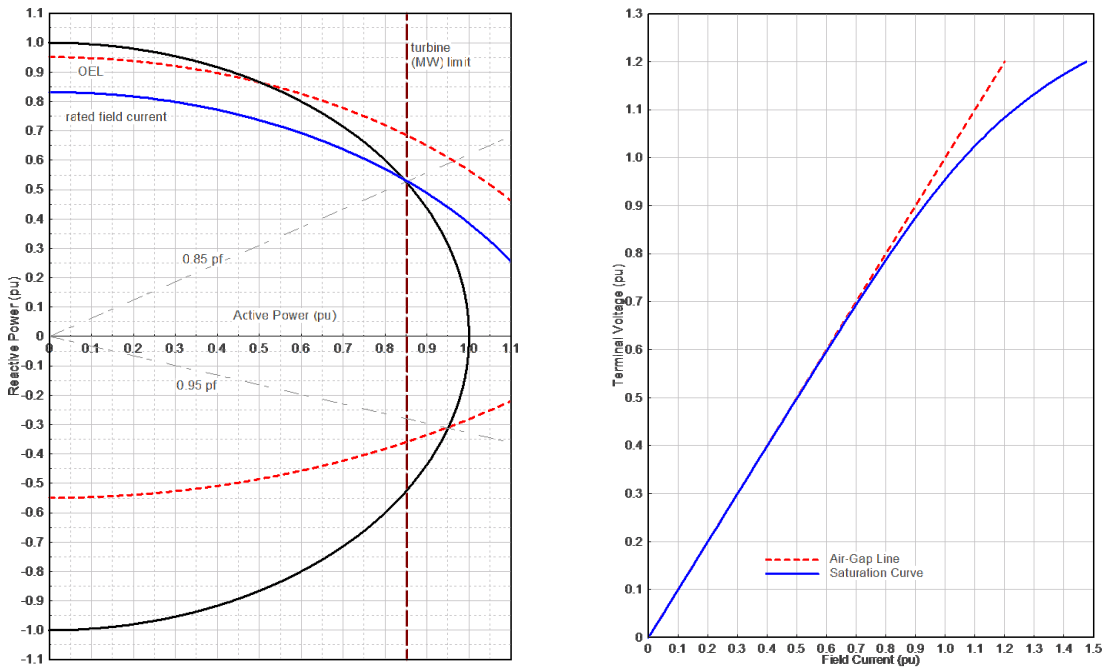


Figure 6.13: Capability curve and open circuit saturation curve for the 155 MW round rotor units

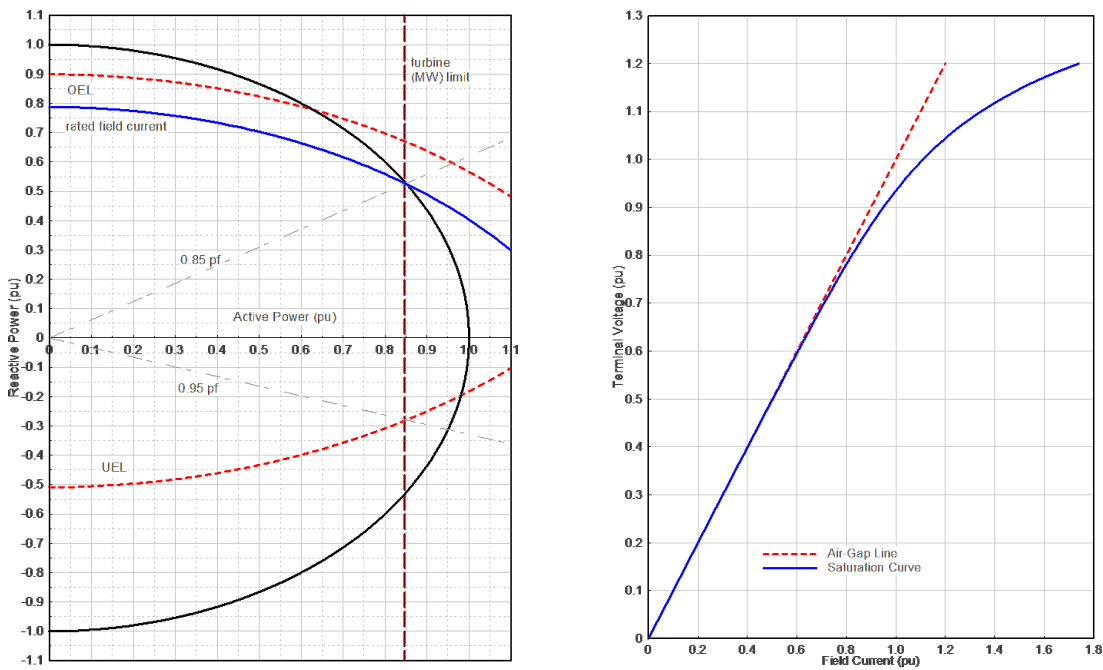


Figure 6.14: Capability curve and open circuit saturation curve for the 100 MW round rotor units

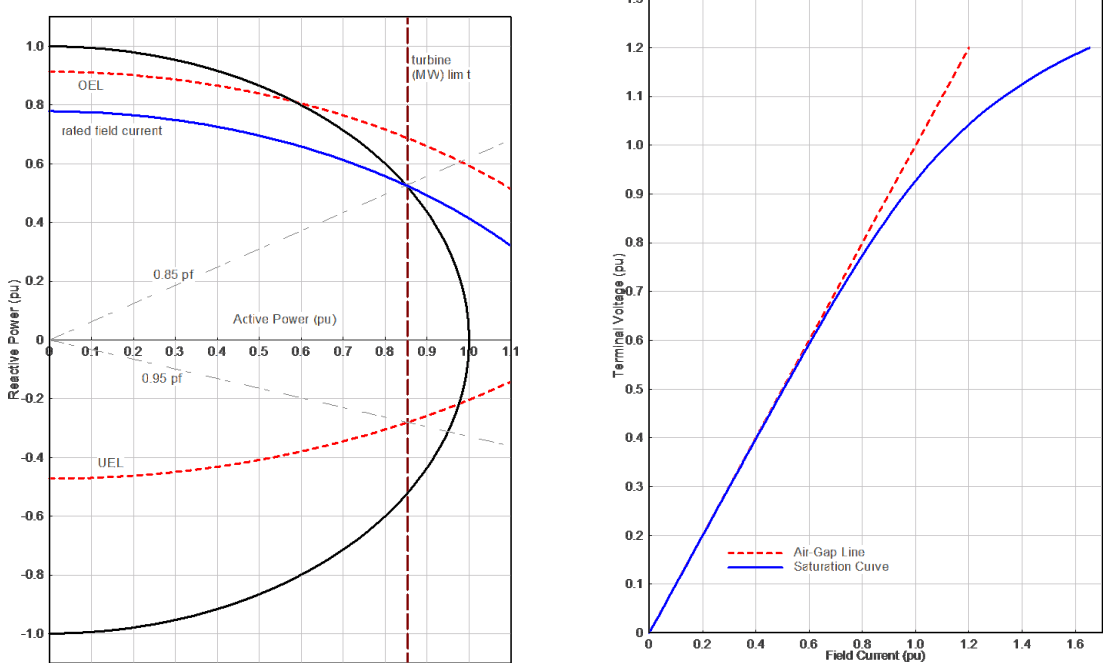


Figure 6.15: Capability curve and open circuit saturation curve for the 76 MW round rotor units

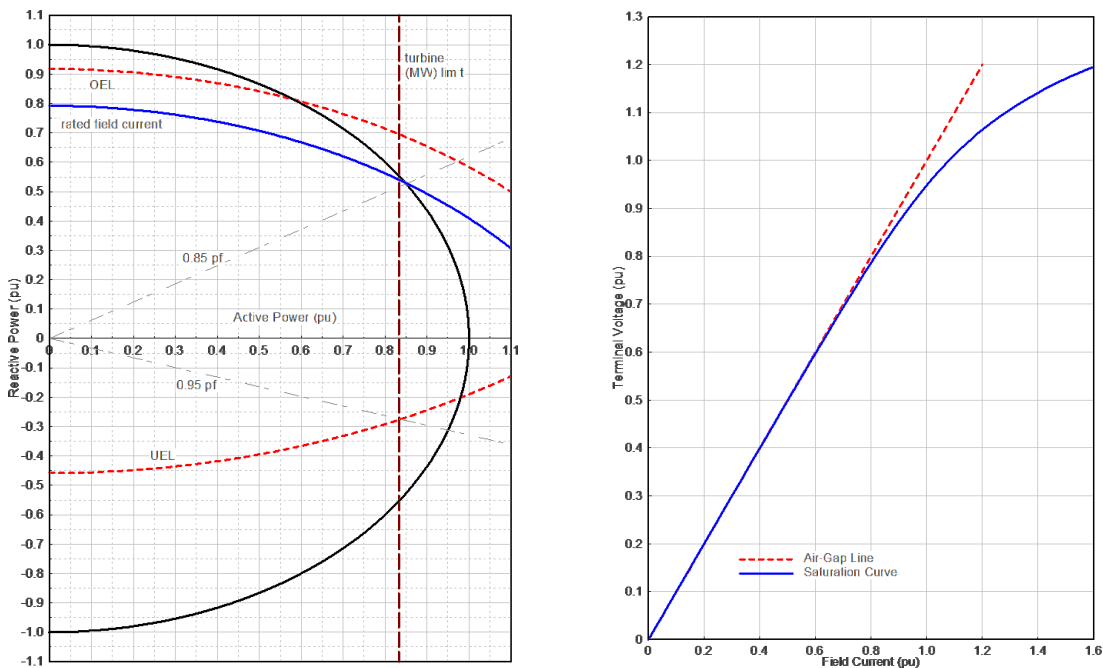


Figure 6.16: Capability curve and open circuit saturation curve for the 20 MW round rotor units

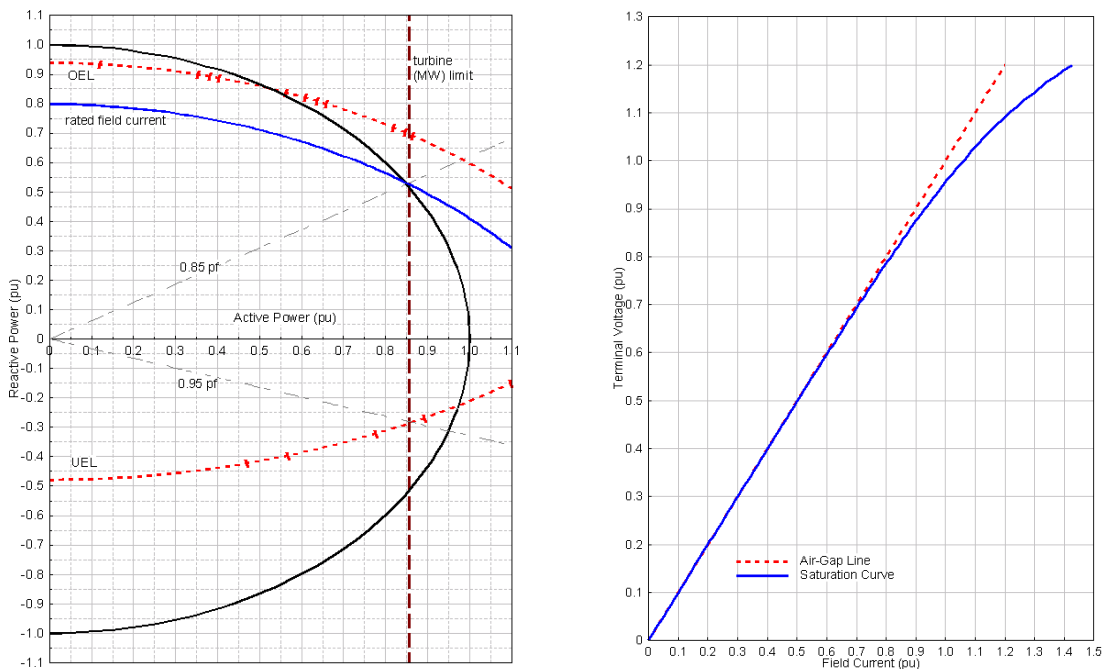


Figure 6.17: Capability curve and open circuit saturation curve for the 12 MW round rotor units

Tables 6.31 and 6.32.

The parameter  $V_{ELM}$  in the HYGOV model relates to the rate of change of the gate position, the lower (resp. upper) limit on the latter being  $-V_{ELM}$  (resp.  $+V_{ELM}$ ). Similarly, the parameter  $G_{min}$  (resp.  $G_{max}$ ) is minimum (resp. maximum) gate opening. All these parameters refer to the transfer function between variables  $e$  and  $c$  in Fig. 6.18.

As regards the steam turbines, they are assumed to be tandem-compound with a single reheat. The lower part of the IEEEG1 model (gains  $K2$ ,  $K4$ ,  $K6$ ,  $K8$ ) are used to represent cross-compound steam turbines, which is not the case here. Therefore, these gains are set to zero.

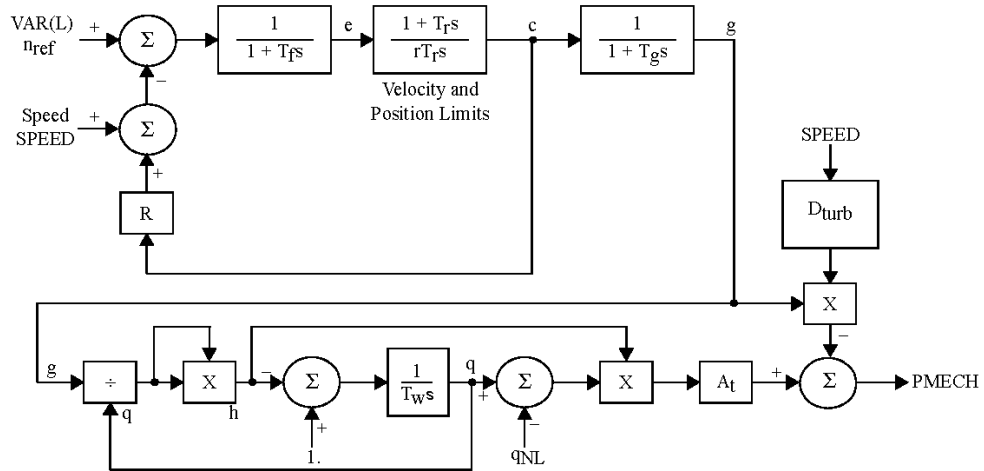


Figure 6.18: Block diagram of the hydro turbine/governor model

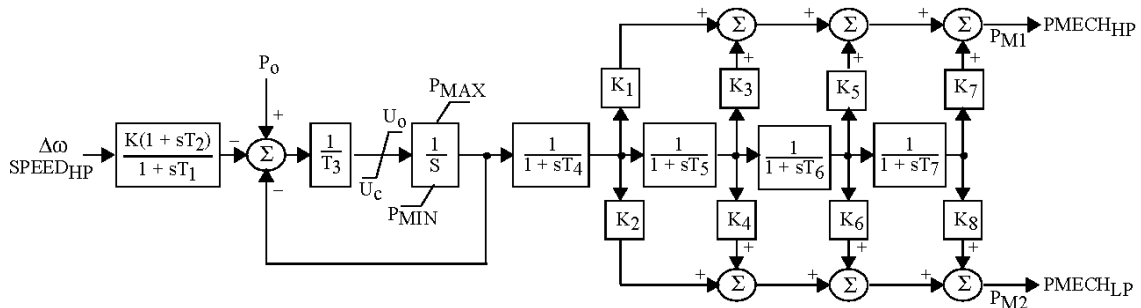


Figure 6.19: Block diagram of the thermal turbine/governor model

Values in pu given in Tables 6.31 and 6.32 are at generator MVA base. Values given in Table 6.31 apply to the generators at AUBREY, buses: 10122, 20122, 30122, 40122, 50122, and 60122 while those given in Table 6.32 apply to all other generators (parameters not given in this table are set to zero).

Table 6.31: Hydro turbine/speed governor data (HYGOV)

Description	Symbol	Value	Unit
permanent droop	R	0.05	
temporary droop	r	0.3	
governor time constant	$T_r$	5	s
filter time constant	$T_f$	0.05	s
servo time constant	$T_g$	0.5	s
gate open/close velocity limit	$V_{ELM}$	0.2	
maximum gate limit	$G_{max}$	0.9	
minimum gate limit	$G_{min}$	0	
water time constant	$T_w$	1.25	s
turbine gain	$A_t$	1.2	
turbine damping	$D_{turb}$	0.2	
water flow at no load	$q_{nl}$	0.08	

Table 6.32: Steam turbine/speed governor data (IEEEG1)

Description	Symbol	Value	Unit
governor gain (1/R)	K	20	
control time constant	$T_1$	0	s
control time constant	$T_2$	0	s
control valve time constant	$T_3$	0.1	s
max. rate of valve opening	$U_0$	0.1	
max. rate of valve closing	$U_C$	-0.1	
max. valve position	$P_{max}$	0.903	pu
min. valve position	$P_{min}$	0	pu
HP section time constant	$T_3$	0.4	s
fraction of power from HP	$K_1$	0.3	
reheat+IP time constant	$T_3$	9	s
fraction of power from IP	$K_3$	0.4	
LP section time constant	$T_3$	0.5	s
fraction of power from LP	$K_5$	0.3	

## 6.12 Static VAR Compensator (SVC) model and data

The case contains two SVCs. The first one is connected to bus 10114 and is rated -50/+200 MVar. The other one is rated -50/+100 MVar and is connected to bus 10106. Figure 6.20 presents the block diagram for the SVC model. The steady state gain  $K$  is set to 150 pu/pu, but since the control path in the model in Fig. 6.20 is expressed in physical units (Mvar), the gain  $K$  has to be set to 150 times the Mvar range of the device. This results in the values 37,500 ( $150 \times 250$  Mvar) and 22,500 ( $150 \times 150$  Mvar). The thyristor bridge is represented by a first order lag, with a time constant  $T_5=30$  ms. The time constant  $T_3$  was calculated for each SVC to provide a reasonable closed-loop response (adequate phase margin), resulting in  $T_3=3.45$  s for the SVC at bus 10106 and  $T_3 = 3.55$  s for the one at bus 10114. All other time constants  $T_1$ ,  $T_2$  and  $T_4$  are set to zero (or any necessary values to eliminate them from the SVC transfer function). The limits  $V_{max}$  and  $V_{min}$  are the maximum capacitive and the inductive ranges for the SVC, respectively, as given in the power flow data in Table 6.18.

The SVC model shown in Fig 6.20 includes a voltage override capability, which is represented in the bottom part of the associated block diagram. The voltage override capability provides a discontinuous control for large voltage deviations, forcing the SVC output to the limits when the voltage error is larger than  $V_{ov} = 0.5$  pu. If the voltage error is positive and greater than 0.50 pu (i.e., low voltage, as compared to the reference set point), the SVC goes to the maximum capacitive output. For a negative voltage error it goes to the maximum inductive output.

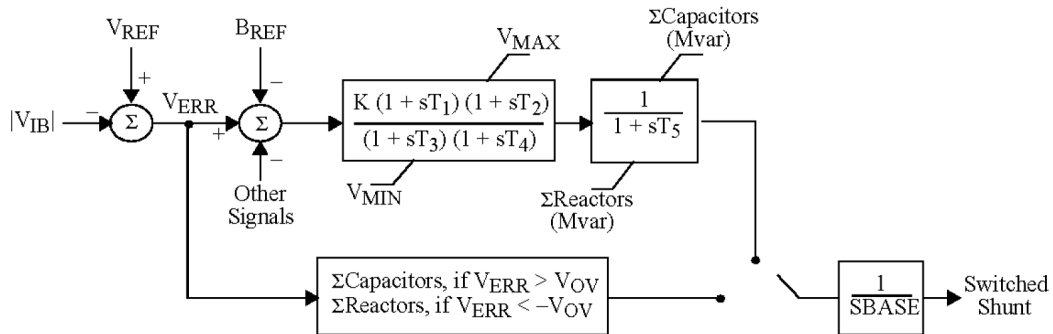


Figure 6.20: Block diagram of the SVC model

# Chapter 7

## RVS test system: simulation results

### 7.1 Steady-state analysis

The steady state analysis starts with the N-1 contingency analysis of all 230 kV and 138 kV circuits. Three contingencies led to non-convergent power flow conditions, as shown in Table 7.1:

- Outage of the 230 kV circuit between buses 115 and 124;
- Outage of the 138 kV circuit between buses 106 and 110 (with the associated outage of the line-connected shunt reactors, see Table 6.19);
- Outage of the 138 kV circuit between buses 107 and 108. The outage of this line results in the islanding of 5 buses; to avoid this difficulty, the branch was converted to a double circuit.

The outage of the cable between buses 106 and 110 was identified as the worst contingency. This cable has a large charging (about 250 Mvar) and no line reactors are connected to it in the original data. Line reactors were added at each terminal of the cable (75 Mvar in each end). This change results in a more realistic system, taking into consideration the usual requirement for such line reactors due to overvoltages during energization and load rejection of such cables. It should be noted that these reactors have to be disconnected when the cable is switched off.

The power flow solution was adjusted using Optimal Power Flow to bring all voltages within normal range (1.05 to 0.95 pu). This OPF solution modified tap positions and generator scheduled voltages as compared to the original data for the IEEE Reliability Test System.

Figure 7.1 presents the VQ plots calculated for bus 110 for the base case and some of the critical contingencies. The reactive power margin in the base case is 116 Mvar, dropping to just 10 Mvar for contingency number 4 (230 kV circuit between buses 112 and 123). Voltage collapse conditions are identified for contingency number 10 (230 kV circuit between buses 115 and 124) and contingency number 30 (138 kV circuit between buses 106 and 110).

Table 7.1: Non-convergent power flow solution of N-1 contingencies

contingency No	from bus	to bus
10	115	124
30	106	110
31	107	108

It should be noted that the reactive power deficiency for contingency number 10 is greater than 150 Mvar and the minimum of the associated VQ curve is associated with bus voltage greater than 1.0 pu. The VQ curve associated with contingency number 30 is incomplete, since the power flow solution did not converge for voltages below 0.97 pu. These VQ results were obtained using a full Newton power flow solution and the non-divergent power flow solution in PSS/E. The transformer taps are locked during the contingency calculation, but the switched shunts (SVCs) are allowed to respond.

The PV analysis considered generation to load transfers from the 230 kV to the 138 kV networks. In other words, the generation connected to buses 113, 114, 115, 116, 118, 121, 122 and 123 is increased, with the additional power being transferred to the loads connected to buses 101, 102, 103, 104, 105, 106, 107, 108, 109 and 110.

The additional generation available in the 230 kV system ( $P_{max} - P_{gen}$ ) is about 100 MW. Transfers greater than 100 MW imply in ignoring the data associated with maximum power output of the generation units. Furthermore, since the ratings for the generator step-up transformers match the generator MVA capability, the overload of the generators also imply in overloading the step-up transformers.

Figure 7.2 presents some of the calculated PV plots. These plots correspond to the voltages at the 138 kV buses 106 and 110, as well as the voltages at the load buses (13.8 kV) 1106 and 1110. The maximum transfer calculated for the base case is slightly under 100 MW. No incremental transfer is possible for contingency number 30 (see the VQ results), as well as for contingency number 6 (outage of the 138 kV circuit between buses 114 and 116) and contingency number 10 (outage of the 230 kV circuit between buses 115 and 124). Contingency number 4 resulted in a maximum incremental transfer of just 10 MW.

## 7.2 Dynamic responses to contingencies

The following disturbances were considered in the dynamic simulations:

- Test A: Connecting a 250 Mvar reactor at bus 101 at time = 0.1 s;
- Test B: Outage of the cable between buses 106 and 110 (with the associated outage of the line-connected shunt reactors), without faults;
- Test C: Outage of the cable between buses 106 and 110 to clear a three-phase fault at bus 106 after 6 cycles (total clearing time).

Study bus: 110

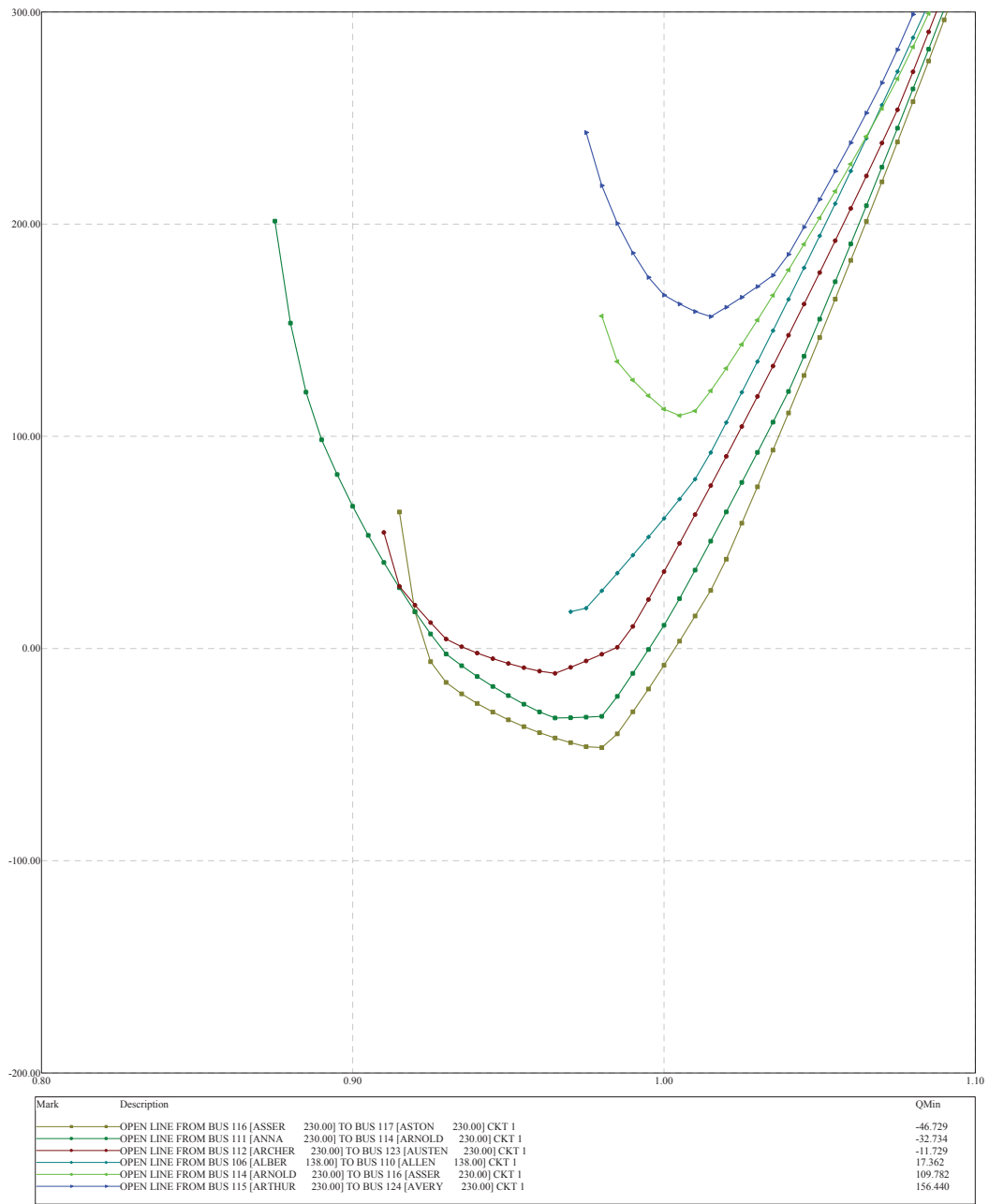


Figure 7.1: VQ plot for bus 110

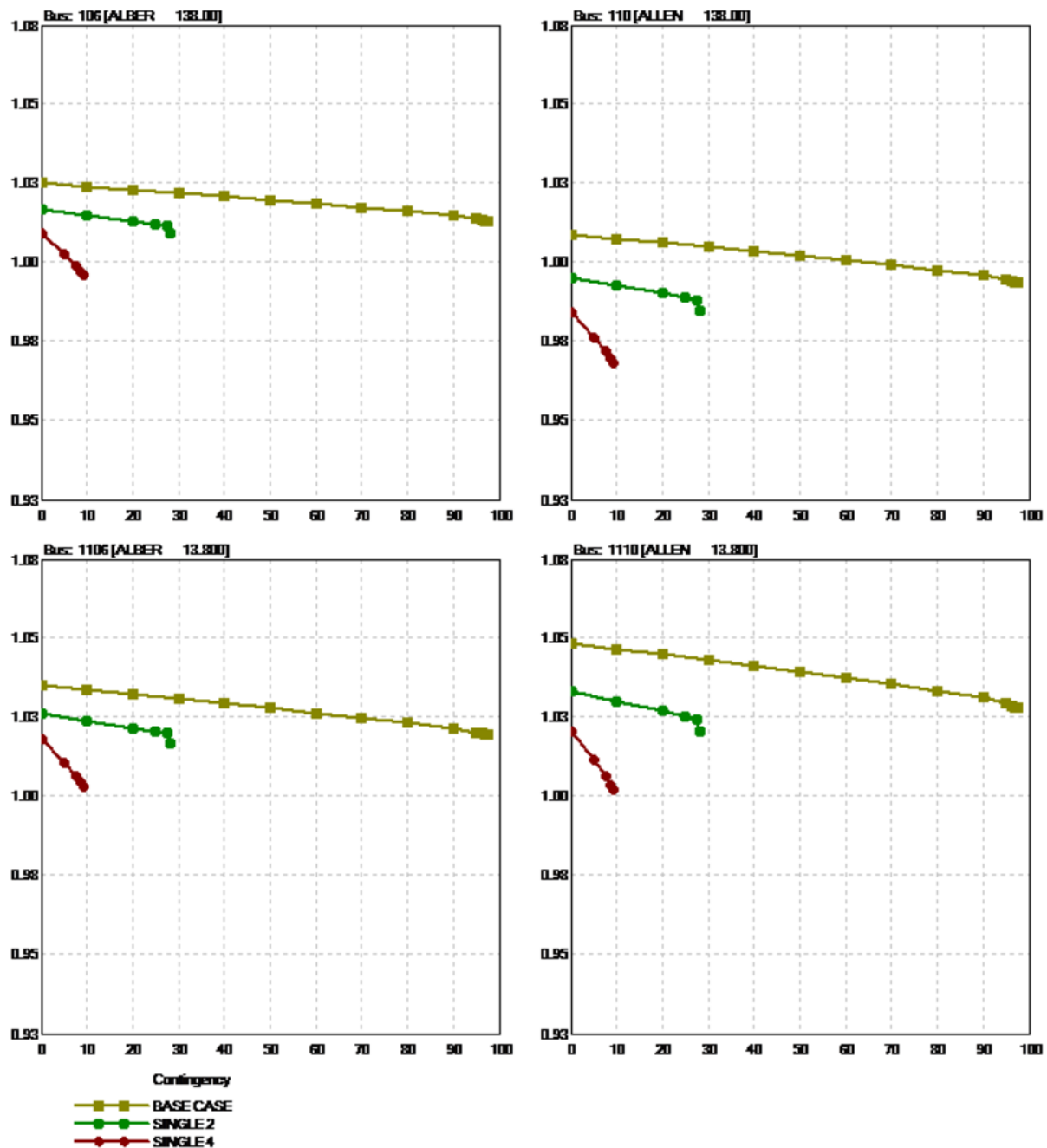


Figure 7.2: PV plots for transfers from the 230 kV to the 138 kV networks

These simulations are performed, initially, with all loads represented as 100% constant current for the active power and 100% constant impedance for the reactive power components. PSS/E activities ESTR/ERUN and GSTR/GRUN were applied to make sure that the excitation systems and speed governors are properly tuned [34]. The key test regarding the control tuning of excitation systems is the open circuit step test. Figure 7.3 presents the response of the EXAC1 model to 2% step change in voltage reference. It can be seen that the voltage regulator provides a fast response with minimal overshoot. Similarly, Fig. 7.4 and Fig. 7.5 present the responses obtained with IEEET1 and SCR1 models, respectively.

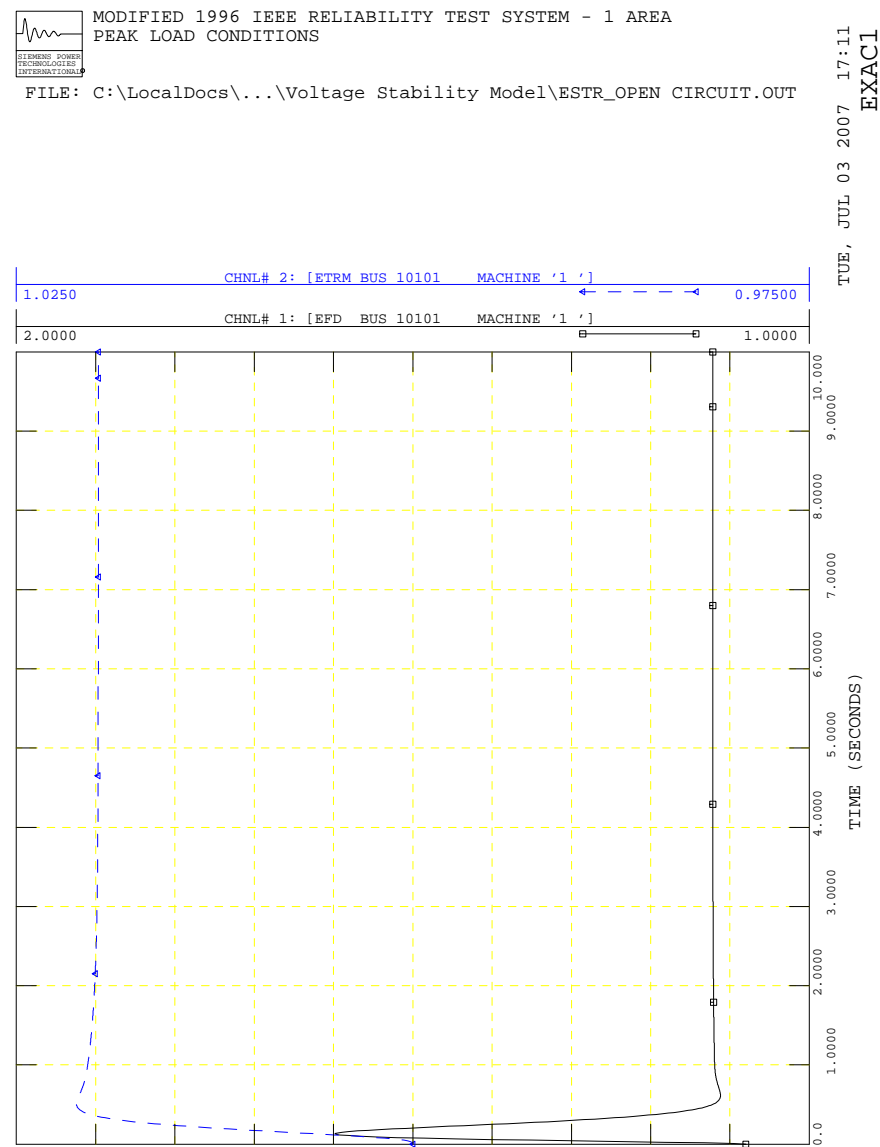


Figure 7.3: Open circuit step response (2% step in voltage reference) for EXAC1 exciter model

The test for the speed governor response consists of the generator feeding a constant MW load in isolated mode. A sudden change in the load demand is applied and the speed governor reacts to modify the mechanical power output. Typically, the simulation is initialized with the generator power output at around 60% of

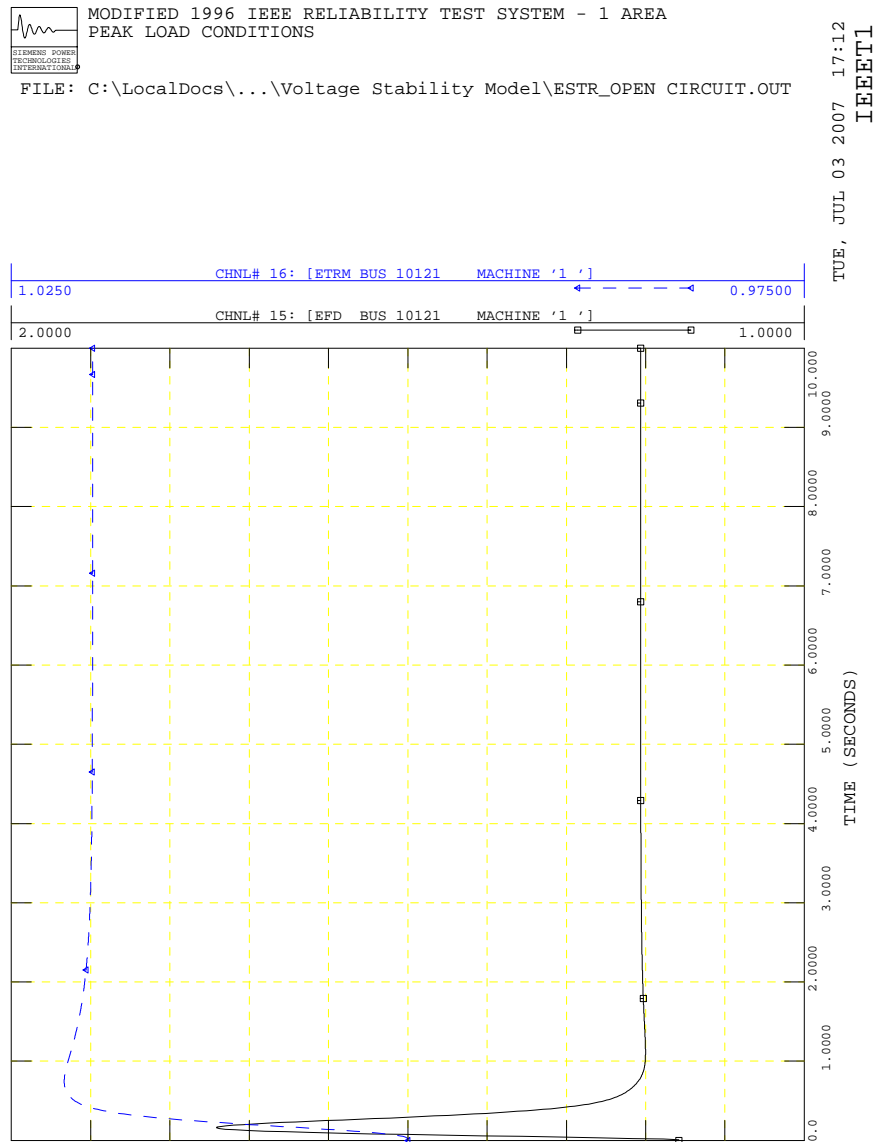


Figure 7.4: Open circuit step response (2% step in voltage reference) for IEEEET1 exciter model

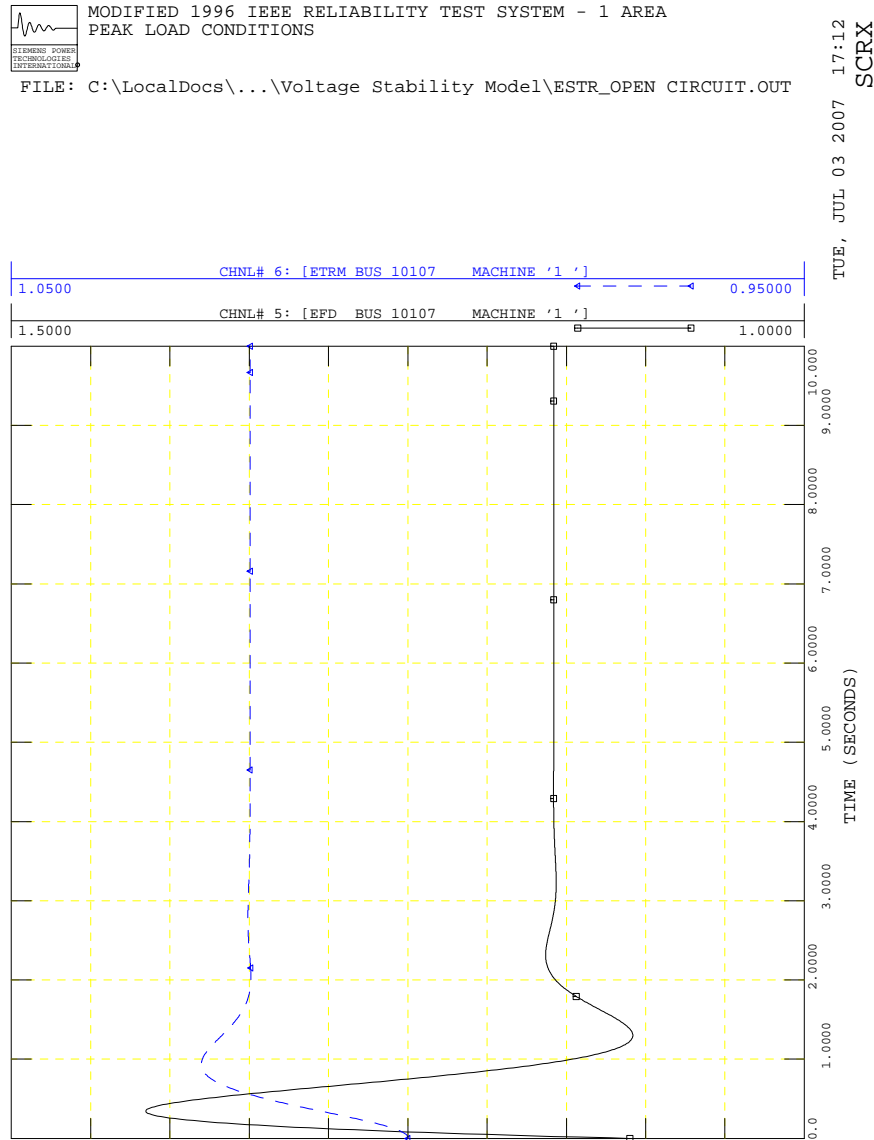


Figure 7.5: Open circuit step response (2% step in voltage reference) for SCRX exciter model

the generator MVA rating and the load demand is increased to 70% (10% step).

Figure 7.6 shows the response of one of the generators with the IEEEG1 governor model. It can be seen that frequency (speed) reaches a new steady state in about 15 seconds, without restoring frequency to its nominal value. The steady state frequency deviation in this simulation is proportional to the steady state droop in the model and the magnitude of the step change in load.

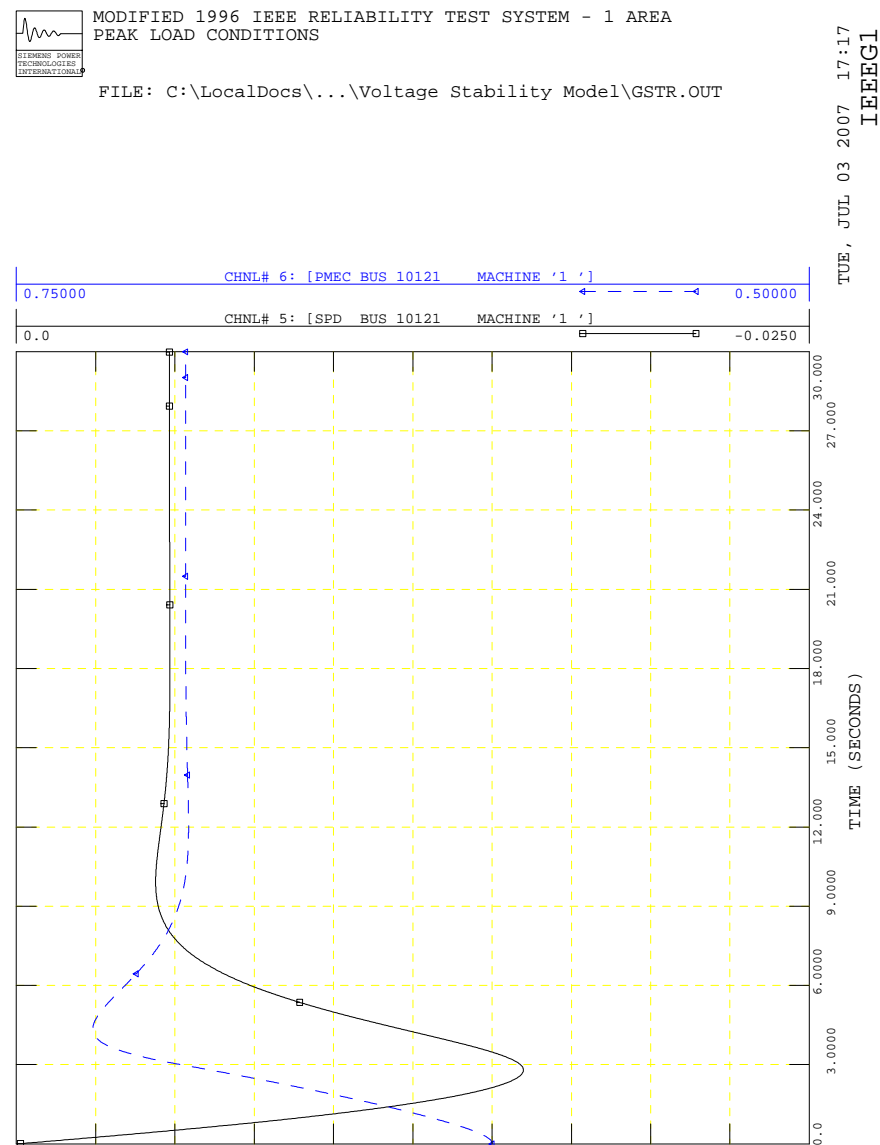


Figure 7.6: Speed governor response test for IEEEG1 model

Figure 7.7 depicts the response of the hydro units (HYGOV model), which is characteristically slower and depends on the settings for the transient droop.



MODIFIED 1996 IEEE RELIABILITY TEST SYSTEM - 1 AREA  
PEAK LOAD CONDITIONS

FILE: C:\LocalDocs\...\Voltage Stability Model\GSTR.OUT

TUE, JUL 03 2007 17:17  
HYGOV

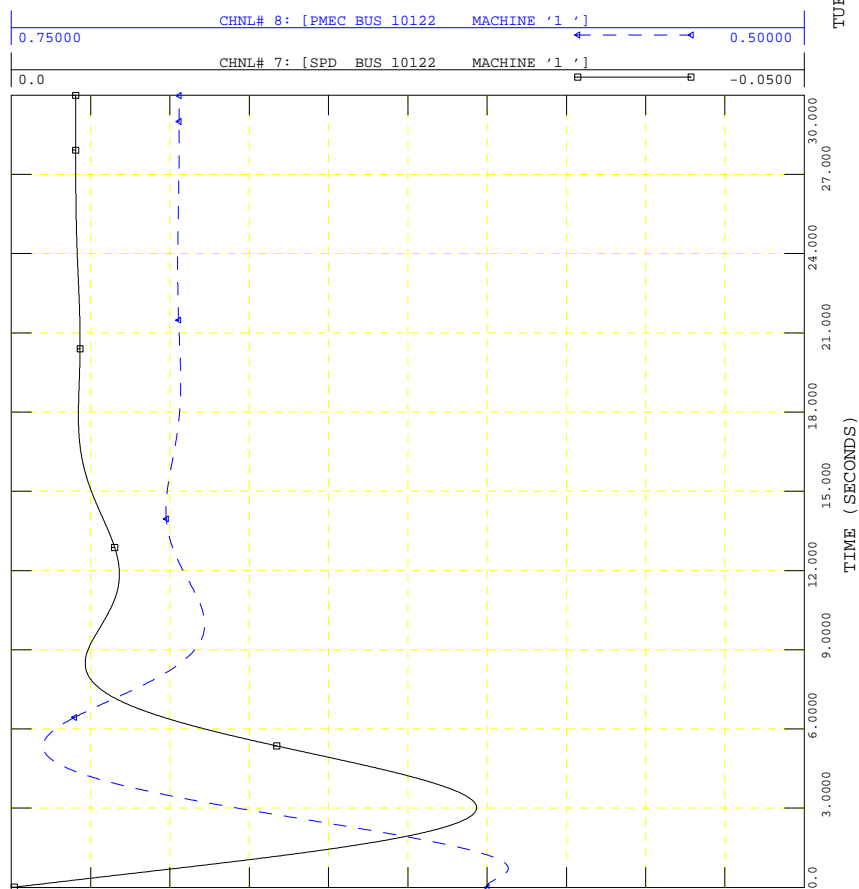


Figure 7.7: Speed governor response test for HYGOV model

## Test A

The first simulated disturbance, Test A, corresponds to a 250 Mvar shunt reactor being connected to bus 101 at time = 0.1 s. The loads are represented as 100% constant current and 100% constant admittance for the active and reactive power components, respectively. Since this is a relatively small disturbance, the voltage at bus 101 drops from the initial value (1.034 pu) to approximately 0.906 pu once the reactor is switched on. On the other hand, this is sufficient to push 2 generators connected to bus 101 (generators 3 and 4, at buses 30101 and 40101) to hit their over-excitation limits.

Figure 7.8 presents the response of the generator 3 (bus 30101). It shows the active and reactive power outputs of the machine (in pu of the system base, 100 MVA), terminal voltage, generator field voltage and the output of the OEL. Following the initial disturbance, the generator field current reaches 2.82 pu, higher than the rated field current for this machine, 2.473 pu, entering the inverse time characteristic of the OEL model. The OEL model becomes active at approximately t=50 s. Since the OEL model represents a summation point OEL action, the OEL starts to lower the voltage reference setpoint for the generator, so terminal voltage and reactive power output are ramped down until a new steady state is reached, at lower voltages.

Figure 7.9 shows the response of the load connected to bus 101 (13.8 kV bus 1101), where the effect of the on-load tap changers is clearly observed. The initial voltage at bus 1101 is 1.049 pu and, after several steps in the OLTC response, it recovers to 1.036 pu. Since voltage recovers to almost the initial value, the load demand recovers to almost a constant power characteristic, at the end of the simulation.

## Test B

The second simulated disturbance corresponds to Figures 7.10 to 7.13 which present the voltages at buses 106 and 1106, as well as the active and reactive demand of the load at bus 1106.

The load reset characteristic is simulated in PSS/E using the model EXTLAL, shown in Figure 6.3. Table 7.2 presents the parameters adopted for the EXTLAL model and Table 7.3 contains the DYRE file record that should be used in PSS/E to add this model to the dynamic simulation setup.

Table 7.2: Parameters for the load reset characteristic model EXTLAL

KP	PMLTMX	PMLTMN	KQ	QMLTMX	QMLTMN
0.05000	2.0000	0.9000	0.05000	2.0000	0.9000

Table 7.3: Dynamic input record (DYRE) for model EXTLAL

```
0 'EXTLAL' * 0.50000E-01 2.0000 0.90000 0.50000E-01 2.0000 0.90000 /
```

It should be noted that the selected values for the gains KP and KQ (5%) are quite high, resulting in an artificially fast load recover to constant power characteristics (few minutes). Actual recordings of load characteristics indicate that this is a much slower phenomenon, spanning many minutes.

It can be seen that the dynamic response of the SVC is critical to avoid a voltage collapse condition around

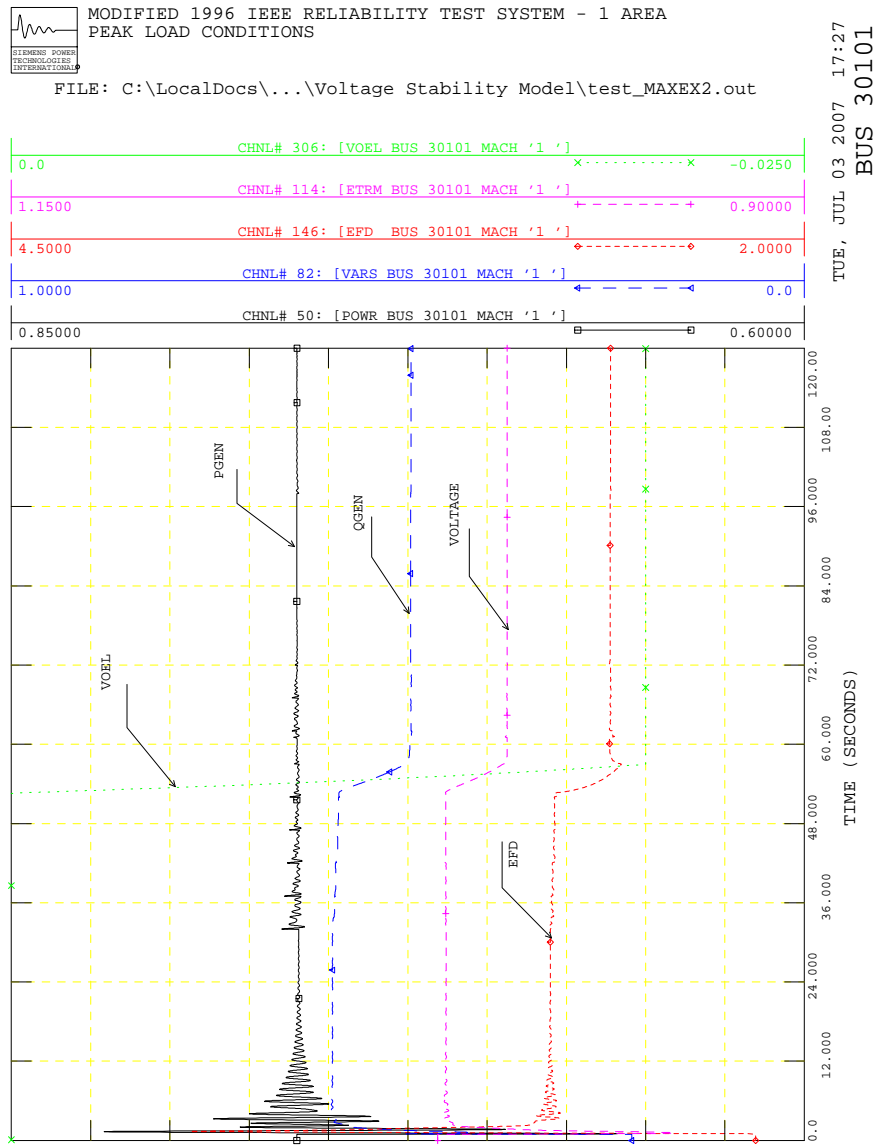


Figure 7.8: Response of generator at bus 30101

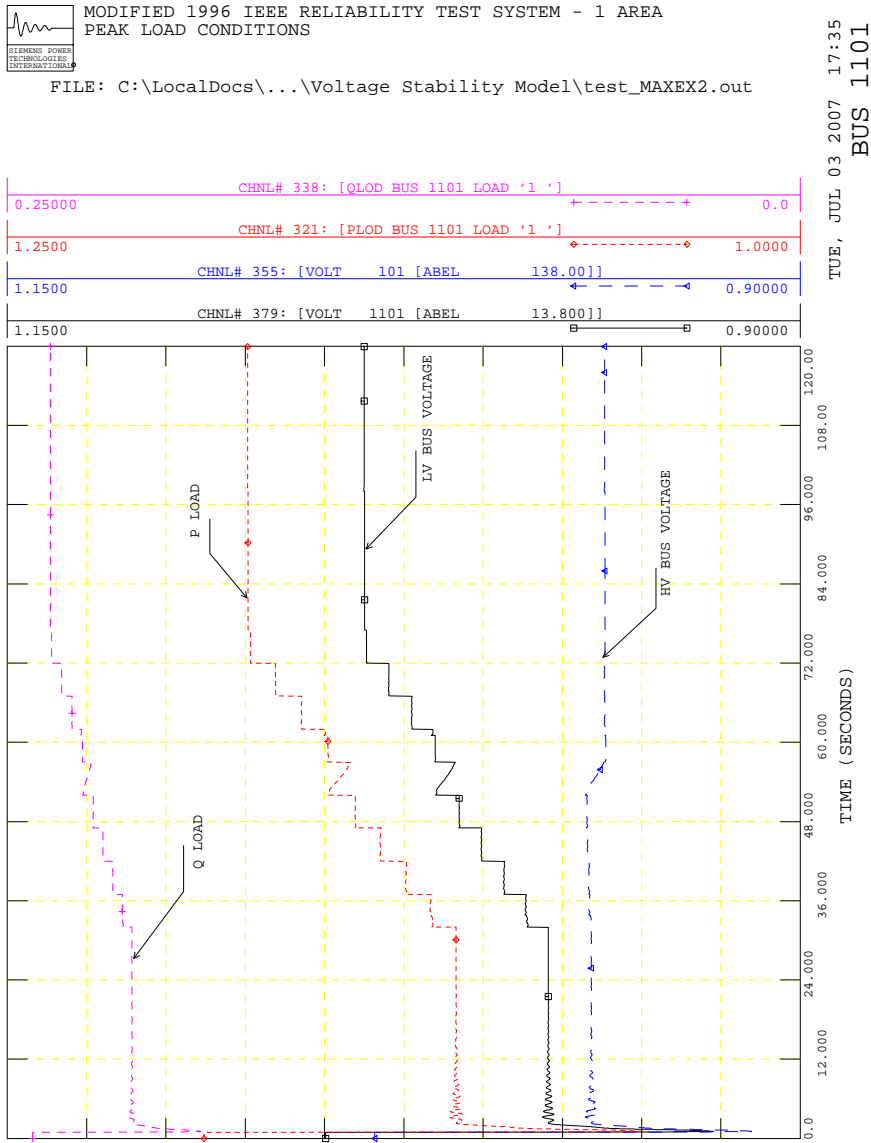


Figure 7.9: Response of load at bus 1101

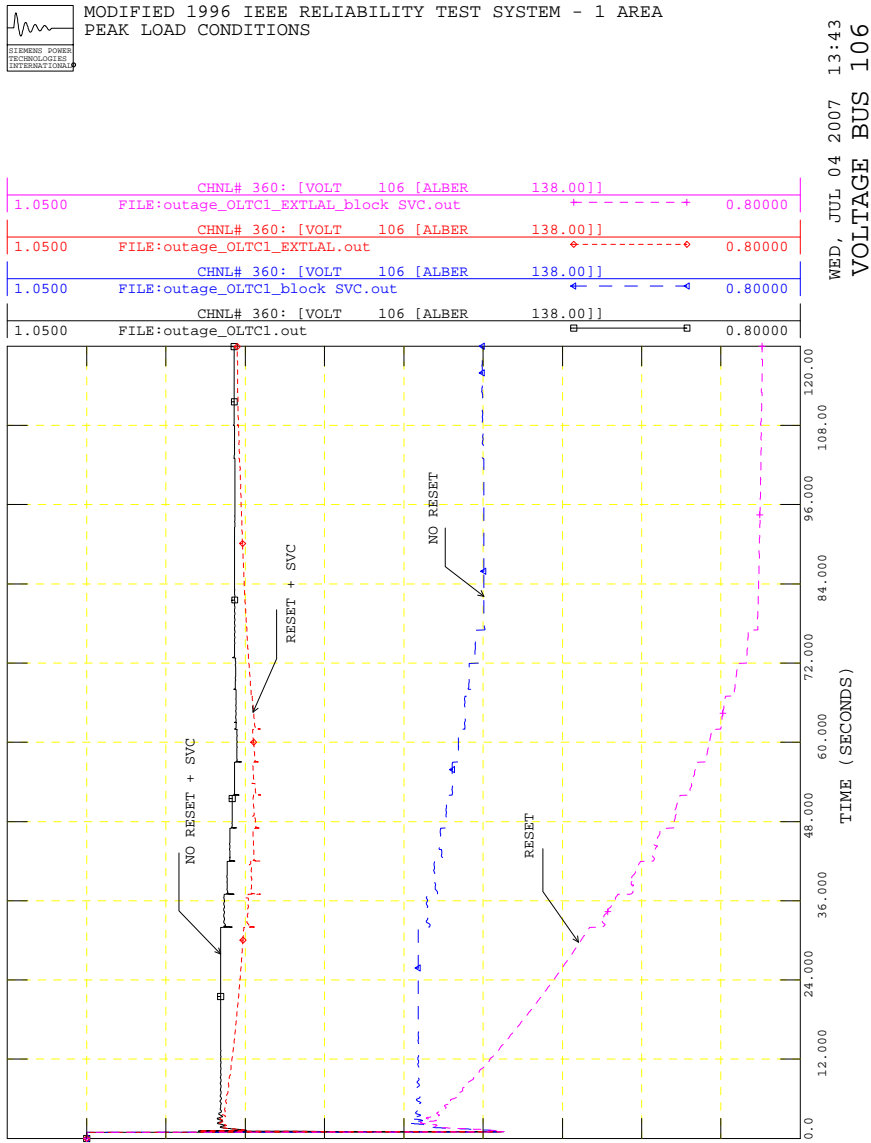


Figure 7.10: Voltage at 138 kV bus 106

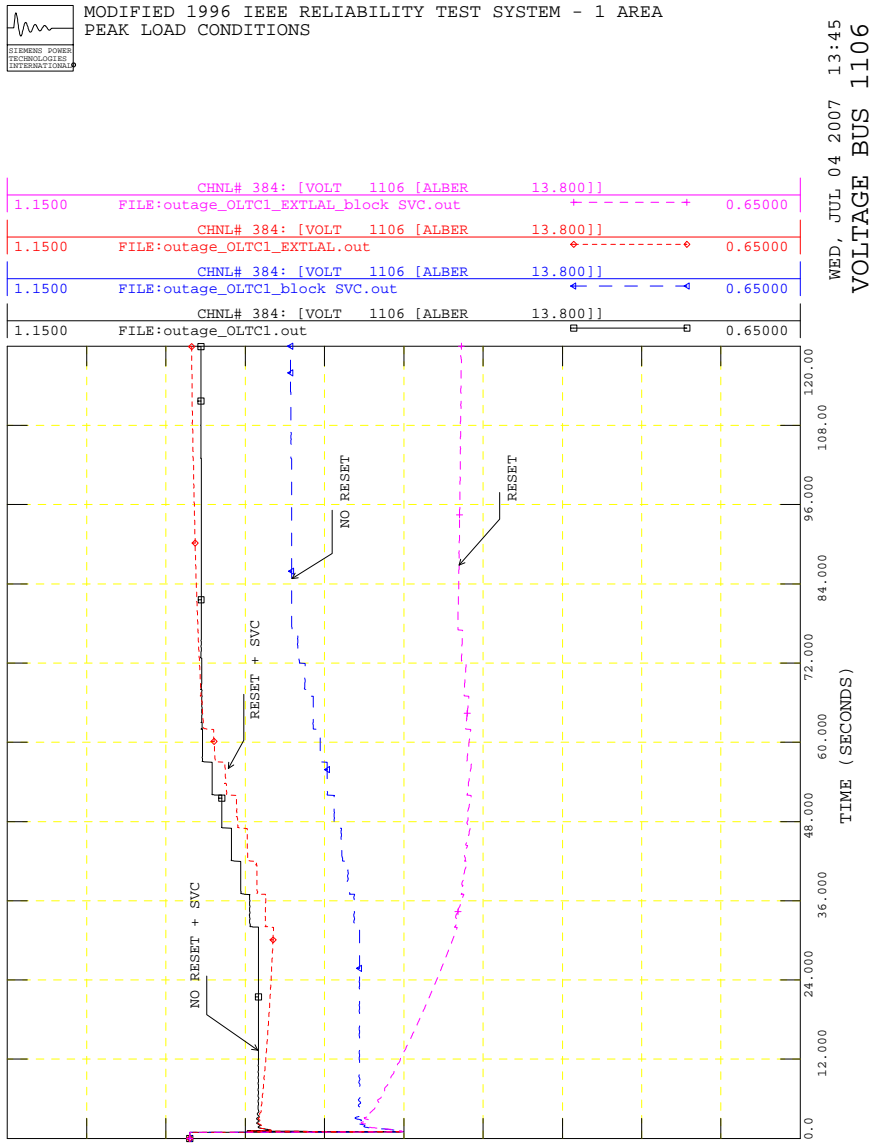


Figure 7.11: Voltage at 13.8 kV load bus 1106

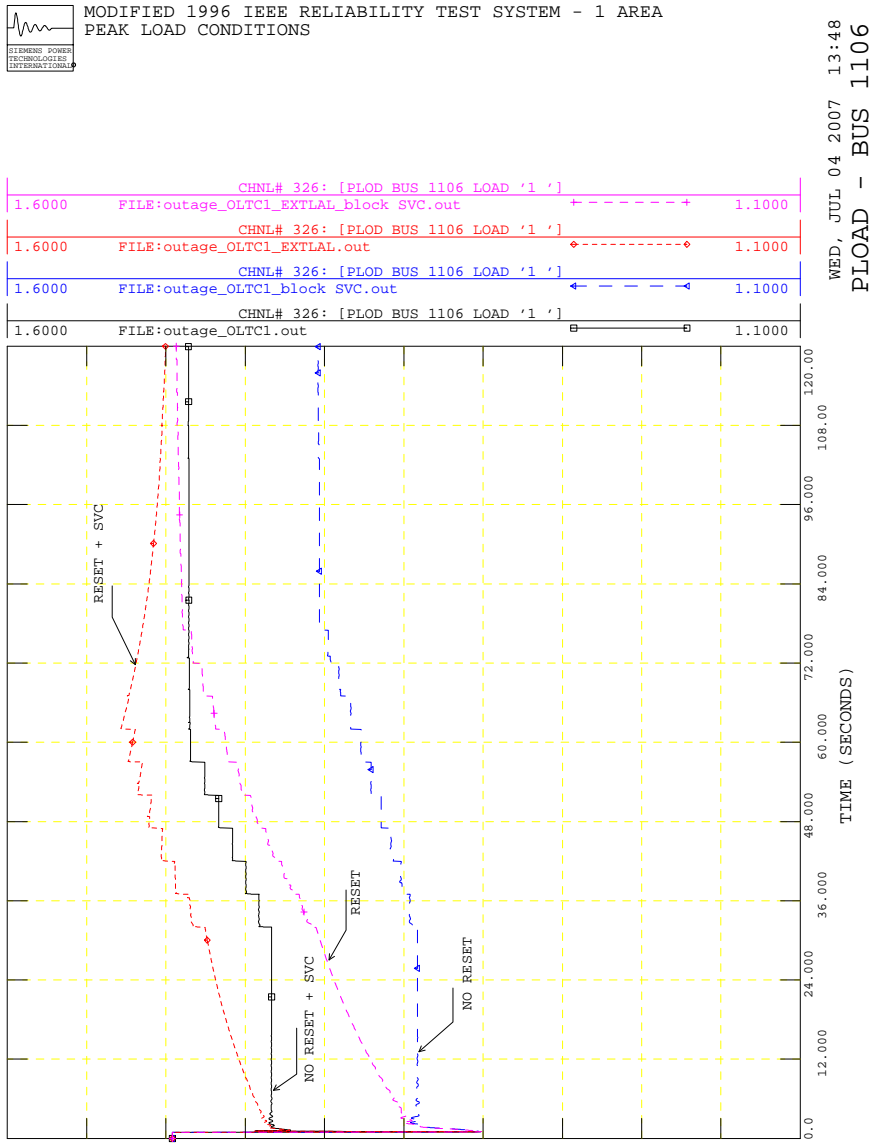


Figure 7.12: Active power demand of load at bus 1106

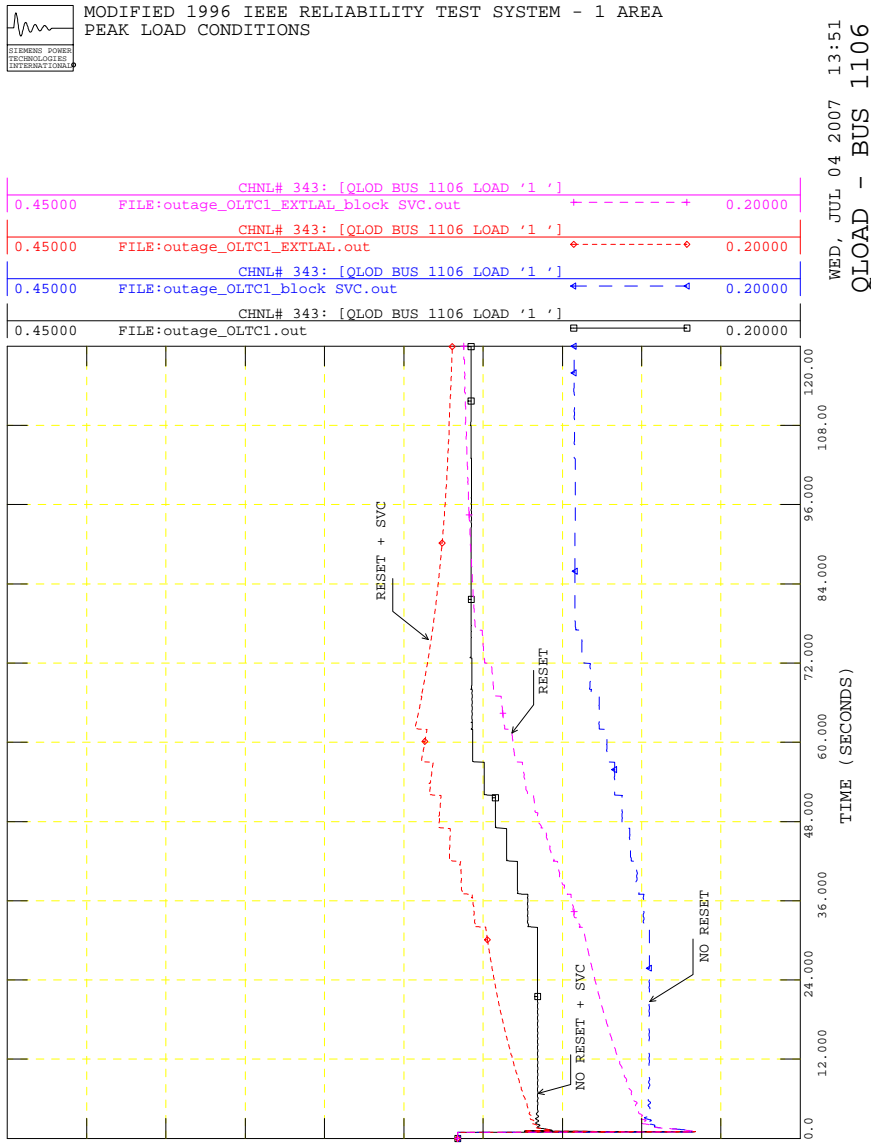


Figure 7.13: Reactive power demand of load at bus 1106

bus 106. In fact, the SVC response combines with the LTC response to bring the voltage at the load bus 1106 to a higher value than the initial (pre-disturbance) condition. Since the load is modeled with a voltage dependence characteristic, the load demand becomes greater than the initial (steady-state) value and the load reset model ends up reducing the load demand.

On the other hand, when the SVC is blocked (shunt is held constant at its initial value given by the power flow solution), the voltages at buses 106 and 1106 do not recover. Without the load reset characteristic, these voltages stabilize at around 0.9 pu due to the associated reduction in active and reactive power load demand. When the load is reset to its pre-disturbance power demand, voltages decrease even further and stabilize just above 0.8 pu.

Since this is a slow voltage collapse condition, it is conceivable that mechanically-switched capacitor banks could be applied instead of a much more expensive SVC. The SVC will also play a fundamental role in the fast voltage collapse condition.

## Test C

The third simulated disturbance corresponds to Figures 7.14 to 7.17 which present the voltages at buses 106 and 1106, as well as the active and reactive demand of the load at bus 1106.

Once again, the dynamic response of the SVC is critical to avoid a voltage collapse condition around bus 106, caused by the increase in reactive power demand due to stalling induction motors. This is a fast dynamic phenomena and, in this case, the control capability of the SVC is required to avoid sluggish voltage recovery and the potential of load disconnection due to sustained low voltages.

Figure 7.18 presents the SVC output admittance for the cases with and without the complex load model (induction motors). It can be seen that the SVC stays almost 2 seconds at its maximum limit when the induction motors are represented. This reactive power support is fundamental to allow the re-acceleration of the motors. When the SVC is blocked and the induction motors are present, the voltages at buses 106 and 1106 do not recover, staying below 0.6 pu.

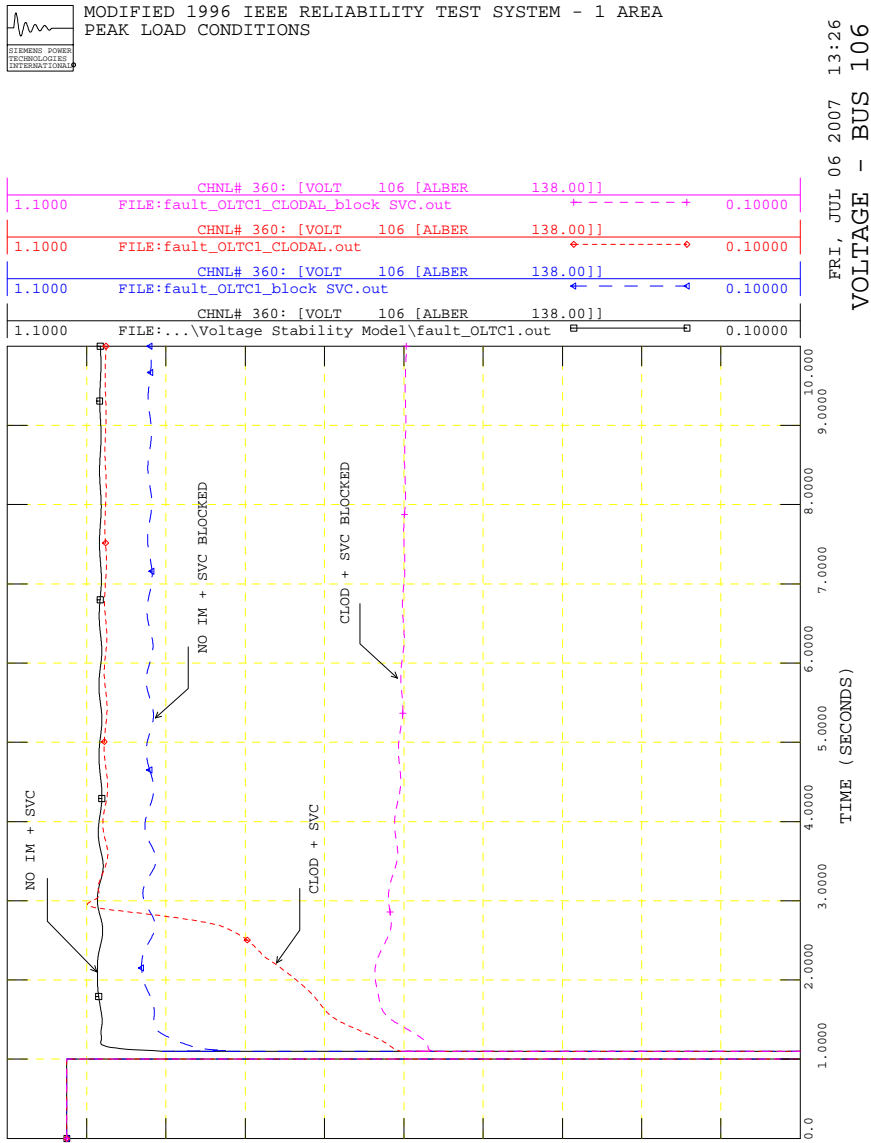


Figure 7.14: Voltage at 138 kV bus 106

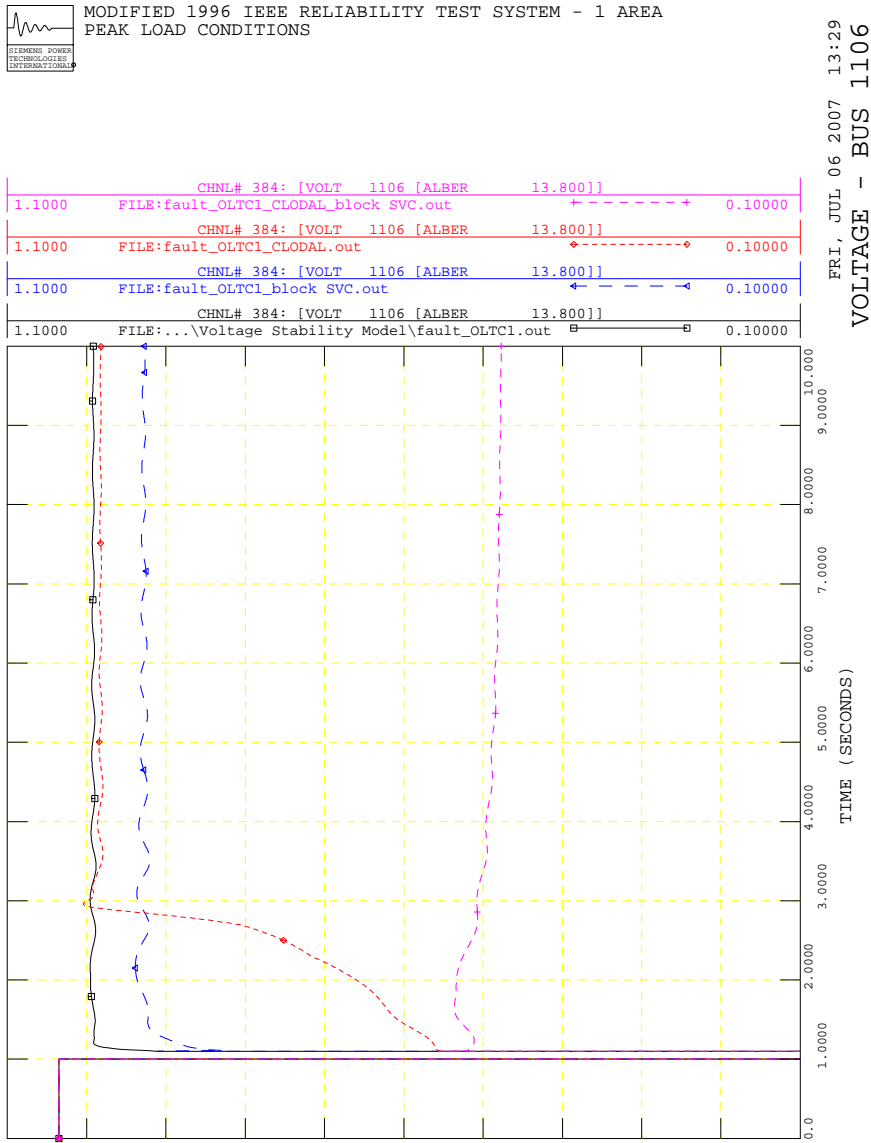


Figure 7.15: Voltage at 13.8 kV load bus 1106

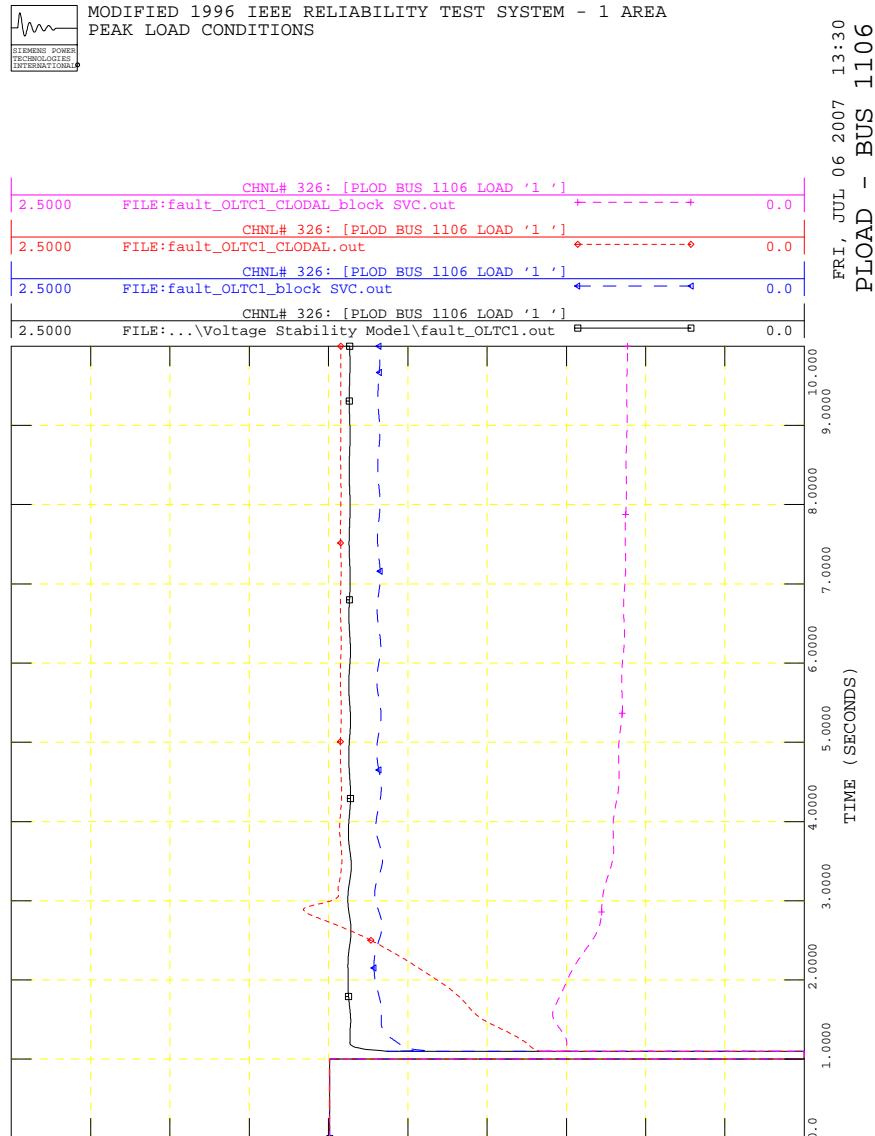


Figure 7.16: Active power demand of load at bus 1106

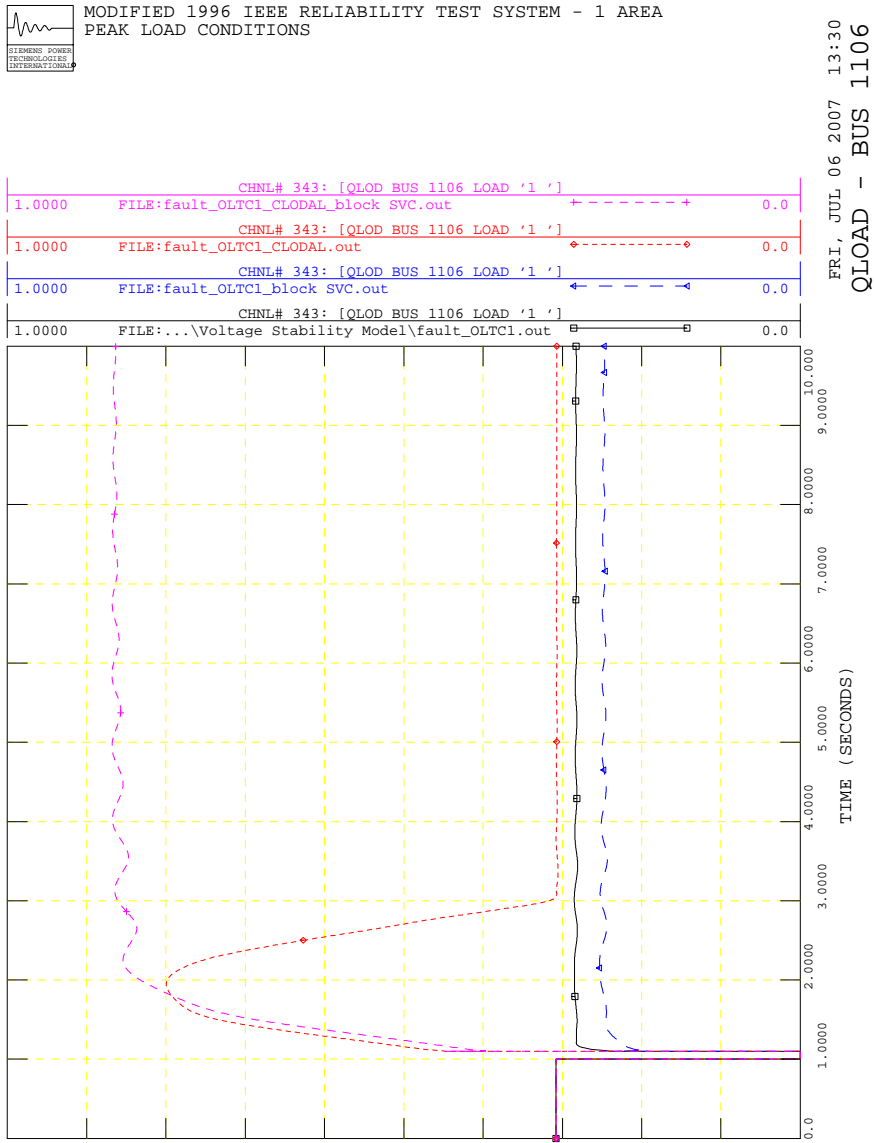


Figure 7.17: Reactive power demand of load at bus 1106

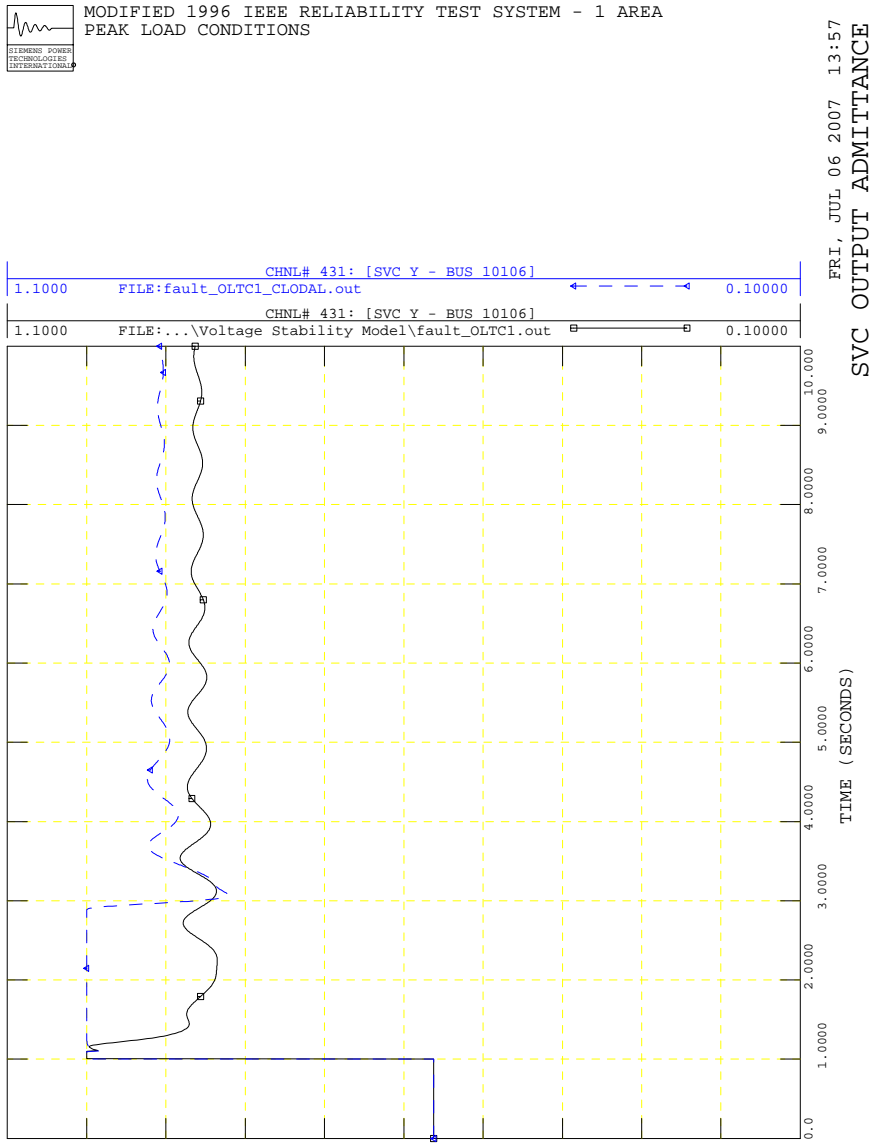


Figure 7.18: SVC output admittance

## **Part III**

## **Appendices**

# **Chapter 8**

## **Nordic test system: simulation results using DSATools**

### **8.1 General remarks on the use of DSATools**

Remarks on the use of the DSATools [45] are summarized below:

1. Generally, DSATools recognized most of the PSS/E models and was able to internally convert them to its native format from the provided PSS/E data format. However, there were some models and components which DSATools did not recognize and needed to be defined manually.
2. DSATools did not recognize OEL (MAXEX2 in PSS/E), although this model is very important in voltage stability studies. However, some components can be introduced into DSAT as User Defined Models (UDMs); thus, an equivalent MAXEX2 model was defined and added to the system. DSATools version 10 is equipped with a graphical model editor that allows for creating and editing certain user defined models, which was used to model the inverse time characteristic of the OEL.
3. Some of the studies required the EXTLAL and CLODAL models. However, UDMs could not be used to represent these models in DSATools, since the program does not allow using these to represent loads; therefore, the results obtained in those cases were different. LTCs are represented as simple switching delays in both programs.

### **8.2 Simulation conditions**

Standard or user-defined DSATools models are used for system components described in section 2. It is assumed that there are 31 steps in the turn ratios of the LTCs, each of them 0.01 pu with an operation range within 0.85 pu to 1.15 pu. All the OELs are modeled with DSATools User Defined Models (UDM), since there is no standard OEL in DSATools to duplicate the suggested OEL model of section 2.

OELs for all generators, except g6, g7, g11, and g12, are modeled as illustrated in Fig. 8.1 left, while for these four generators the model of Fig. 8.1 right is adopted.

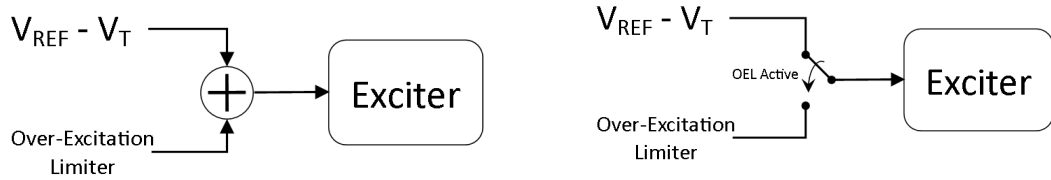


Figure 8.1: Over-excitation limiter and exciter connection: summation (left) and switch (right)

### 8.3 Dynamic simulations

A three-phase fault is simulated on the line 4032-4044, at 10% of the distance from bus 4032, and at  $t = 2.0$  s; the fault is then cleared after 5 cycles by removing the line. Figures 8.2 to 8.6 show the voltage magnitudes for certain buses, as well as field currents for some generators, obtained from the DSATools simulations. The changes in speeds (Hz) of selected generators up to the system collapse are depicted in Fig. 8.7. These graphs are similar to the ones in Chapter 3, although not identical due to the differences in the component models, specially the connection of OELs and exciters.

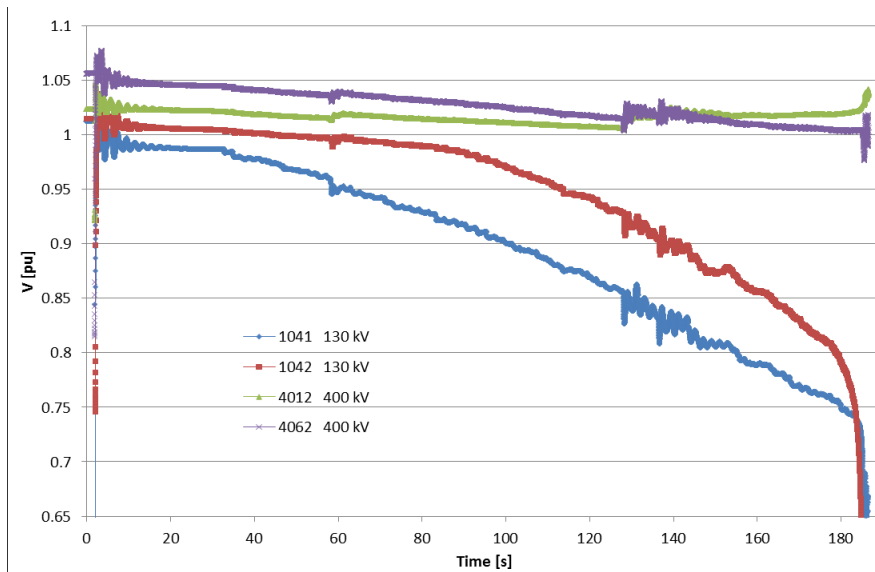


Figure 8.2: Bus voltage magnitudes

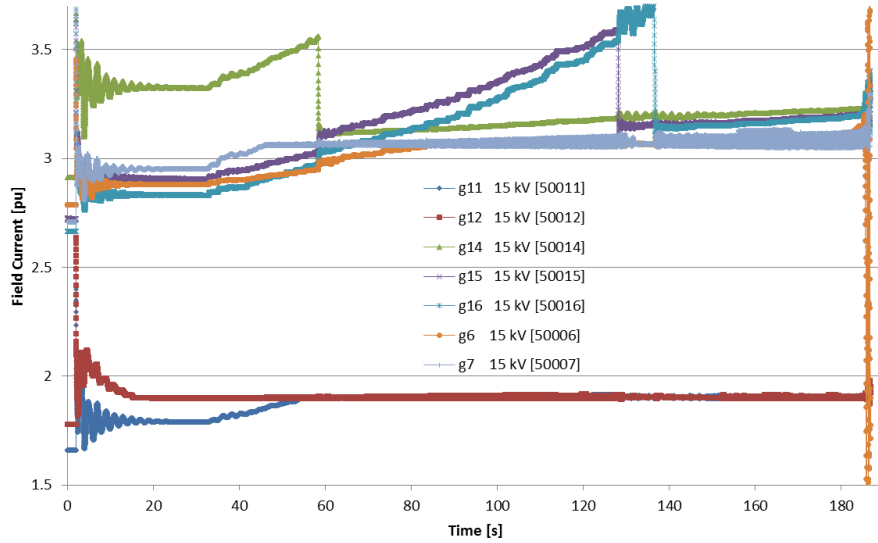


Figure 8.3: Field currents of limited generators

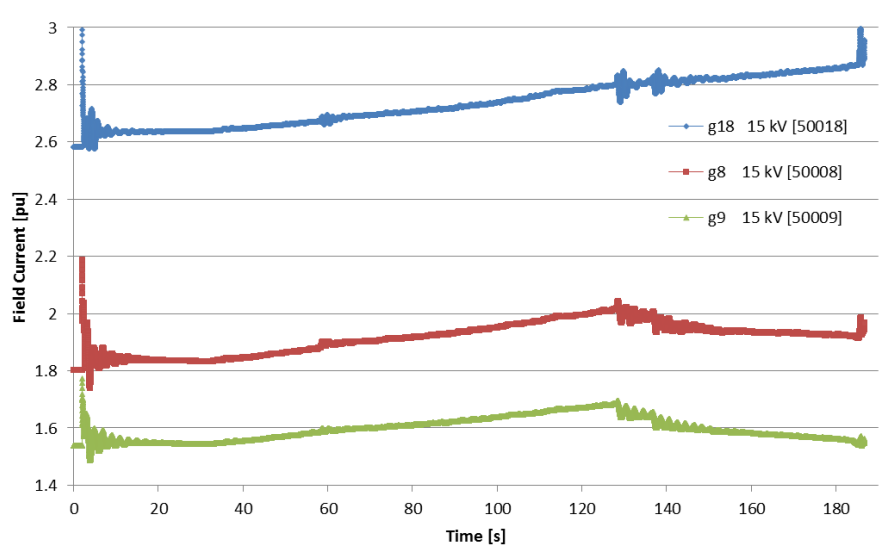
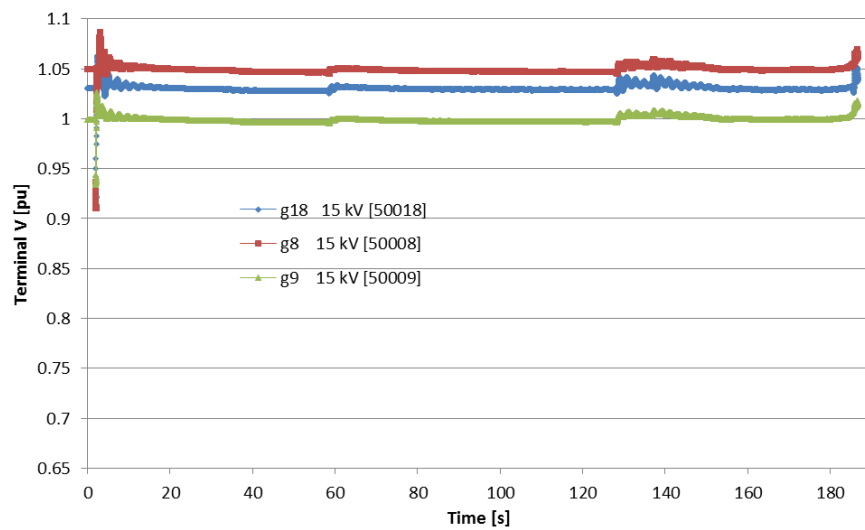
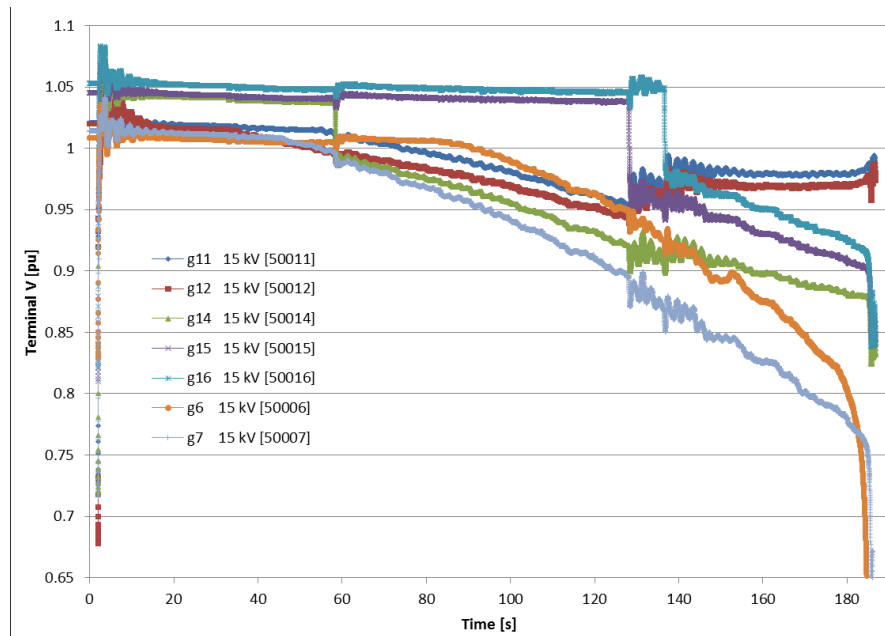


Figure 8.4: Field currents of non-limited generators



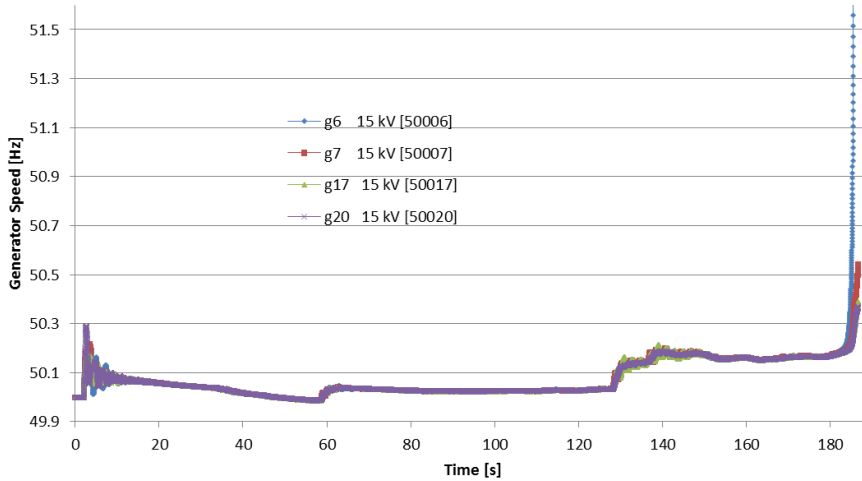


Figure 8.7: Generator speed during the system transient

## 8.4 PV curves from power flow computations

It was observed in Section 3.1 that the system is not secure against the given contingency on the North-Central corridor. Two solutions are suggested: to reduce the load in the Central area to bring the system within a safe operating region or adding a generator in the Central area to accomplish the same goal.

### Load reduction

The load reduction scenario is studied in this section. Accordingly, PV curves yield load power margins of the pre-contingency and contingency systems with regard to load increases in the Central area. Modal analysis of the system close to the point of collapse for the contingency system is also carried out to obtain the participation factors for different system nodes, and thus determine the main contributors to the voltage collapse problem. For the PV curves studies, the load in the Central area is assumed initially to decrease by 5%, i.e. from 6190 MW in the original case to 5880.5 MW, assuming constant power factor for the loads. This load change is assumed to be supplied by generators in the Equivalent area, i.e. g19 and g20 (the slack bus), and is enough to guarantee a stable contingency system. The load in the Central area is then increased in small steps until the power flow fails to converge, for both contingency and pre-contingency cases, thus, obtaining relevant load power margins and PV curves. The distribution transformer tap changers are fixed in the study, as PQ models are assumed for the loads. Four transmission transformers, i.e. 1044-4044 A, 1044-4044 B, 1045-4045 A, and 1045-4045 B, are assumed to be controlled by operators, regulating the voltages at buses 1044 and 1045 in pre-specified voltage dead-bands. However, the ratios of these transformers are assumed to remain fixed in the contingency simulations, since the time is considered to not be long enough for the operators' reaction. The reactive power upper limits  $Q_{gmax}$  of generators used in these simulations were obtained from the capability curves at base-loading conditions, and are shown in Table 8.1.

The PV curves for certain buses are shown in Fig. 8.8, as the demand in the Central area changes. The PV curves for the limited generators, g7, g12, and g14, which loose voltage regulation capabilities, are shown in

Table 8.1: Generators reactive power upper limits

generator	$Q_{gmax}$ (Mvar)
g1	340.
g2	318.
g3	297.5
g4	300.
g5	110.
g6	208.
g7	104.
g8	318.8
g9	520.
g10	380.
g11	127.5
g12	140.
g13	300.
g14	350.
g15	600.
g16	367.5
g17	315.
g18	624.
g19	262.5
g20	2587.5

Fig. 8.9 for pre-contingency and contingency cases. Observe that as the load increases, it pushes the system to its loadability limits until it collapses due to lack of adequate voltage support. From these figures, it can be observed that the given contingency at the base load is beyond the maximum loadability of the contingency system, thus yielding a voltage collapse. Table 8.2 shows the system loadability limits for contingency and pre-contingency cases, obtained from PV curve studies. Therefore, a minimum load reduction of 220 MW (= 6190 - 5970) is required to secure the system against the given contingency.

The voltage stability status of a system can be studied by examining the power flow Jacobian matrix and its modes and submatrices. The eigenvalue of the V-Q submatrix with the smallest absolute value can be used as an indicator in this regard [3]. This eigenvalue (or critical mode) goes through a sign change roughly at the point of collapse. The critical nodes in the network for a specific scenario can be identified by calculating the participation factors of different buses in that critical mode. Thus, the participation factors for the contingency system near the collapse point (a "step" before the maximum Central load of 5970 MW), i.e. at the Central load of 5956 MW, are shown in Table 8.3. The factors are sorted in a descending order to highlight their contribution to the critical mode. From this table, any reactive power compensation at certain buses (e.g. 1, 1041, 3, and 1043) or an improvement in the reactive power capability of certain generators (g7 and g14) would be beneficial. Note that these generators are among those which lost their voltage regulation capabilities for the contingency system in Fig. 8.9.

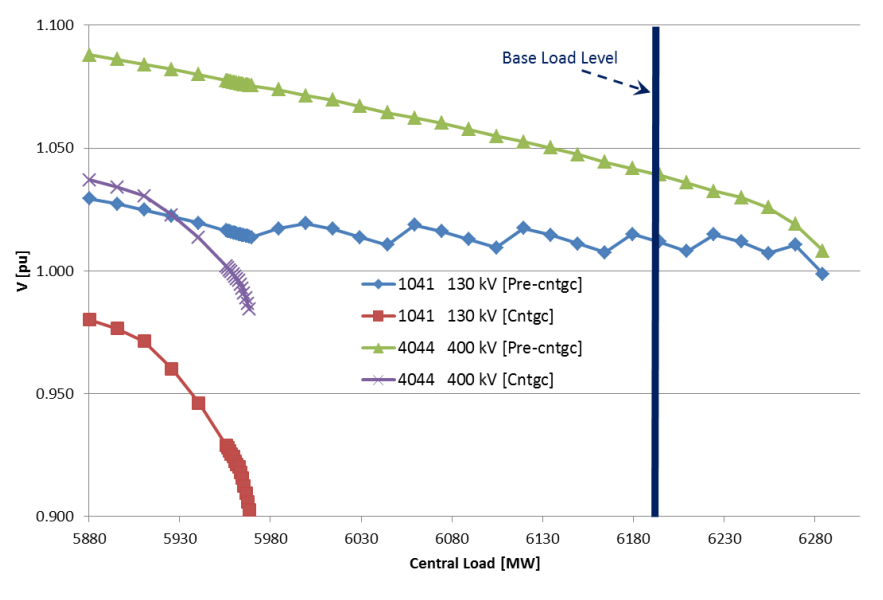


Figure 8.8: PV curves for transmission buses

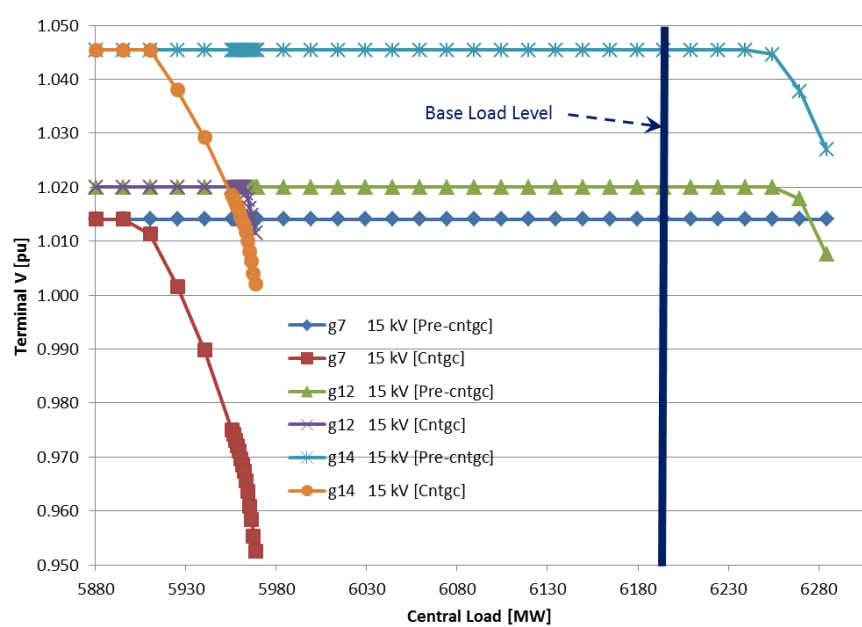


Figure 8.9: PV curves for critical generators

Table 8.2: System maximum loading in Central area

system	load (MW)	margin (MW)
contingency	5970.	-220.
pre-contingency	6300.	110

Table 8.3: Participation factors of different nodes for the critical mode of the contingency system

no.	bus	description	area	part. factor
1	1	load 20 kV	CENTRAL	1.0
2	1041	130 kV	CENTRAL	0.91717
3	3	load 20 kV	CENTRAL	0.89947
4	1043	130 kV	CENTRAL	0.78117
5	50007	g7 15 kV	CENTRAL	0.69634
6	4	load 20 kV	CENTRAL	0.35723
7	1044	130 kV	CENTRAL	0.32397
8	5	load 20 kV	CENTRAL	0.31951
9	1045	130 kV	CENTRAL	0.25987
10	42	load 20 kV	CENTRAL	0.29254
11	4044	400 kV	CENTRAL	0.25707
12	4042	400 kV	CENTRAL	0.23516
13	4045	400 kV	CENTRAL	0.23389
14	43	load 20 kV	CENTRAL	0.20747
15	50014	g14 15 kV	CENTRAL	0.19563
16	4043	400 kV	CENTRAL	0.19168
17	46	load 20 kV	CENTRAL	0.15679
18	4046	400 kV	CENTRAL	0.14413
19	41	load 20 kV	CENTRAL	0.10845
20	4032	400 kV	NORTH	0.10539

## Addition of generator

The addition of a generator at bus 16 is studied in this section using PV curves. The modifications of the system with regard to the original system studied so far are according to the Section 2 and some additional assumptions, as follows:

- The reactive power upper limits  $Q_{gmax}$  of generators from Table 8.1 are used in these simulations.
- The Central load is increased in small steps from 6190 MW, the base load level, until the power flow fails to converge, assuming constant power factor for the demand.
- The load change is assumed to be supplied by generators in the Equivalent area, i.e. g19 and g20.
- The distribution transformers turn ratios are assumed to remain fixed to have a valid constant power load model during the load evolution.
- The four transmission transformers, i.e. 1044-4044 A, 1044-4044 B, 1045-4045 A, and 1045-4045 B, are assumed to be controlled by operators, regulating the voltages at buses 1044 and 1045 in pre-specified voltage dead-bands. However, the ratios of these transformers are assumed to remain fixed in the contingency simulations.

The contingency results pertaining to the outage of line 4032-4044 are presented next. Figure 8.10 shows the PV curves for certain transmission buses. The effect of transmission transformers is noticeable in the Bus 1041 voltage changes in the pre-contingency state. The PV curves for generators g6, g7, and g14

are shown in Fig. 8.11, as the demand in the Central area changes for both pre- and contingency cases. Comparison of Figs. 8.10 and 8.11 highlights the limited reactive power capability of g14 and its impact on the system response to load changes in the Central area with and without contingency. Two other critical contingencies are also considered here, namely, the outage of line 4011-4021 and the outage of generator g14. Table 8.4 shows the maximum loading levels for the Central area for the three contingencies, as well as the pre-contingency case. The margins for all the cases are positive confirming a secure operating point against the considered contingencies.

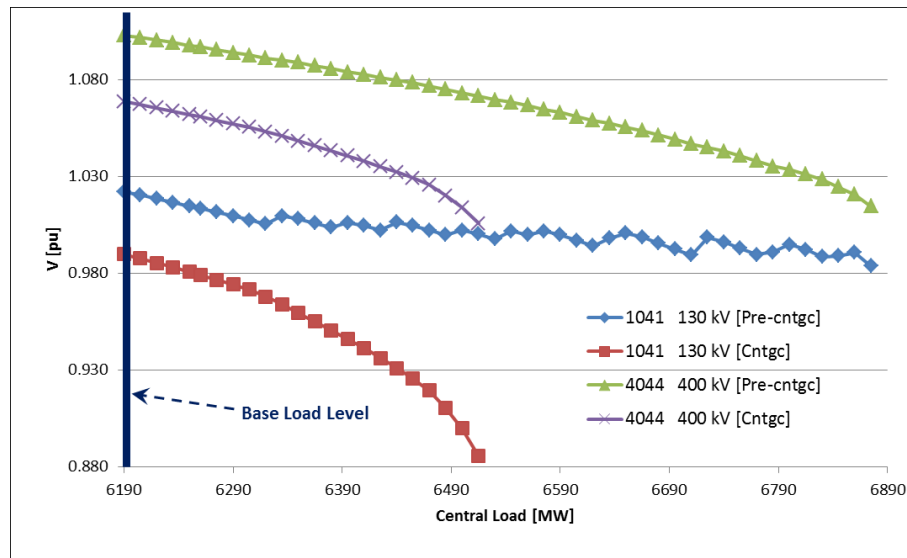


Figure 8.10: PV curves for transmission buses

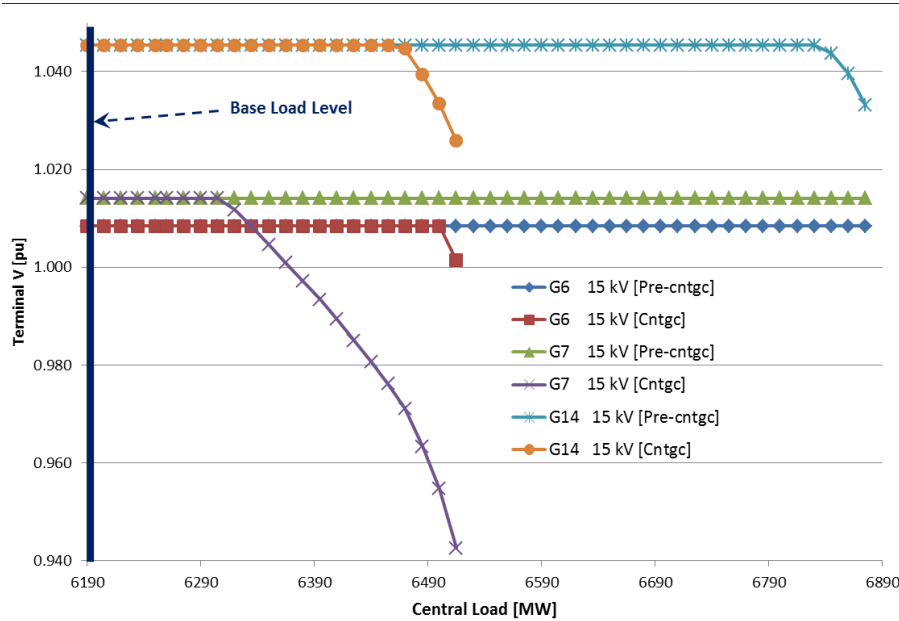


Figure 8.11: PV curves for critical generators

Table 8.4: System maximum loading in Central area

contingency	Load (MW)	Margin (MW)
no contingency	6885.	695.
outage of line 4032-4044	6520.	330.
outage of line 4011-4021	6420.	230.
outage of g14	6255.	65

# **Chapter 9**

## **RVS test system: simulation results using PSAT**

### **9.1 General remarks on the use of PSAT**

The remarks on the use of the PSAT [46, 47, 48] are summarized below:

1. A six order model of synchronous machines was chosen in PSAT to represent them in detail.
2. LTC and OEL in PSAT react almost immediately, while in PSS/E and DSATools, there is a delay before any response from these components.
3. SVC model in the PSAT is simply modeled as a lag.
4. Static system components (i.e. power flow components) can be imported to PSAT directly. However, the dynamic components should be added and modified manually.
5. An induction motor of order III with proper rating is used in PSAT simulations. This motor is connected to the load bus 1106 while the rest of the loads are modeled as constant current for active power and constant impedance for reactive power.
6. In PSAT, new components can be coded in MATLAB format to add to the library, or existing components can be modified to meet specific requirements. In presented simulations an intentional effort has been made to use the standard and already existing PSAT library components to build the system.

### **9.2 Steady-state analysis**

The same contingencies as in section 7.1 are considered with PSAT.

The PSAT results presented and discussed here were obtained using Power Flow (PF) and Continuation Power Flow (CPF) routines included in the package [46, 47, 48].

PV curves were obtained here using CPF with respect to load level increases, based on power flow models [6, 49]. Therefore, only static models of the system components are considered in this analysis.

The loads (for both active and reactive powers) connected to buses 1101, 1102, 1103, 1104, 1105, 1106, 1107, 1108, 1109 and 1110 were increased, while the required additional power is provided by generating units connected to buses 113, 115, 116, 118, 122, 123 and the swing bus 121. Bus 114 is not included in the generator set, as there is no generation at this particular bus. The additional generation available to supply the load increase is almost 100 MW; thus, the power transfer is limited by this amount.

The PV curves (referring to load power increase) obtained using PSAT for the two contingencies and the base case are shown in Fig. 9.1 with SVCs operational and LTCs blocked.

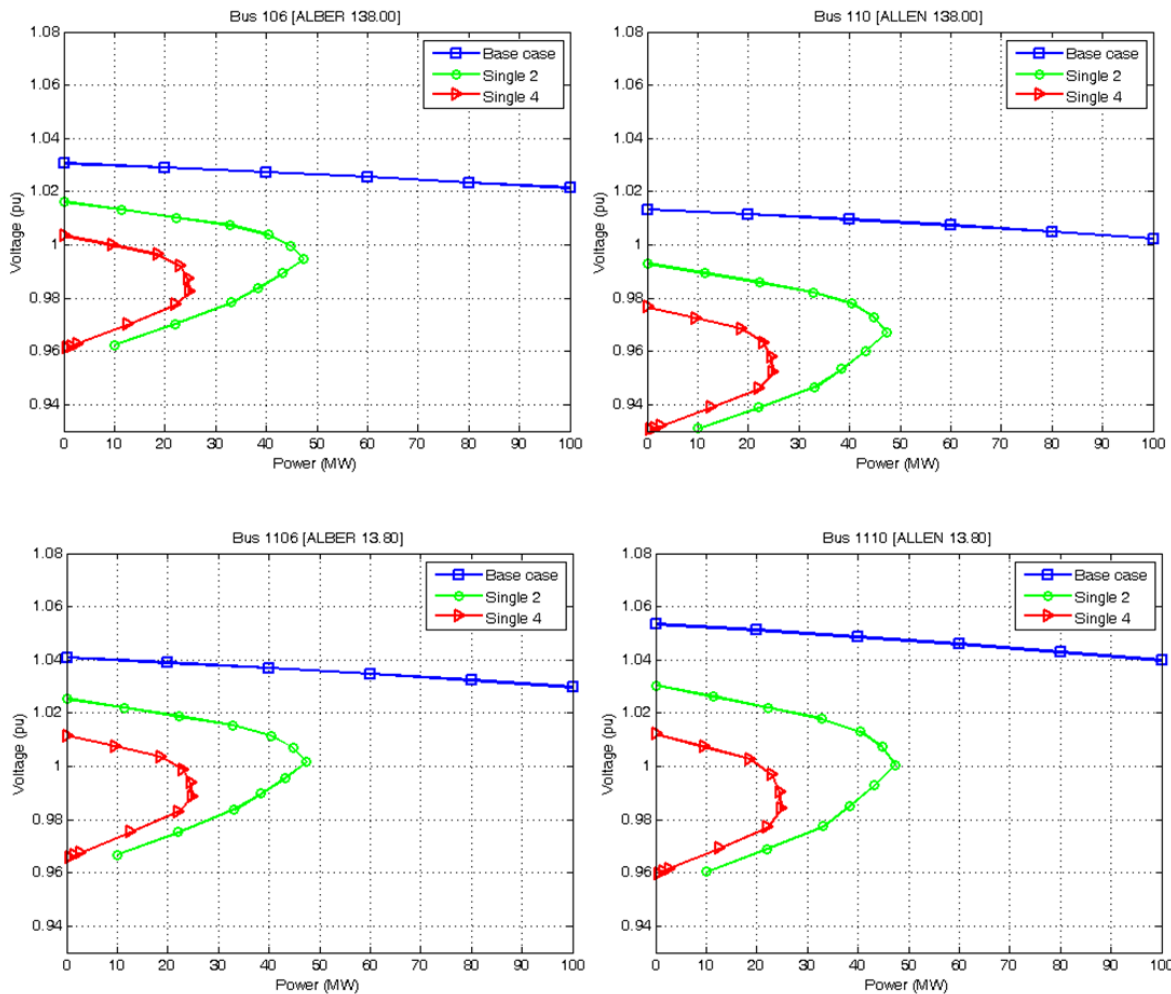


Figure 9.1: PV curves for the base case and two contingencies with SVCs operational

In the next step, SVCs are removed and two equivalent shunts are added to the system at the same buses to

emulate SVC's role. Their values for different system conditions are shown in Table 9.1. The PV curves obtained using PSAT with these shunts instead of SVCs are shown in Fig. 9.2.

Table 9.1: Fixed shunts values replacing the SVCs for different system conditions

bus	Base case (pu)	Single 2 (pu)	Single 4 (pu)
10106	0.48	0.58	0.72
10114	1.08	1.28	1.54

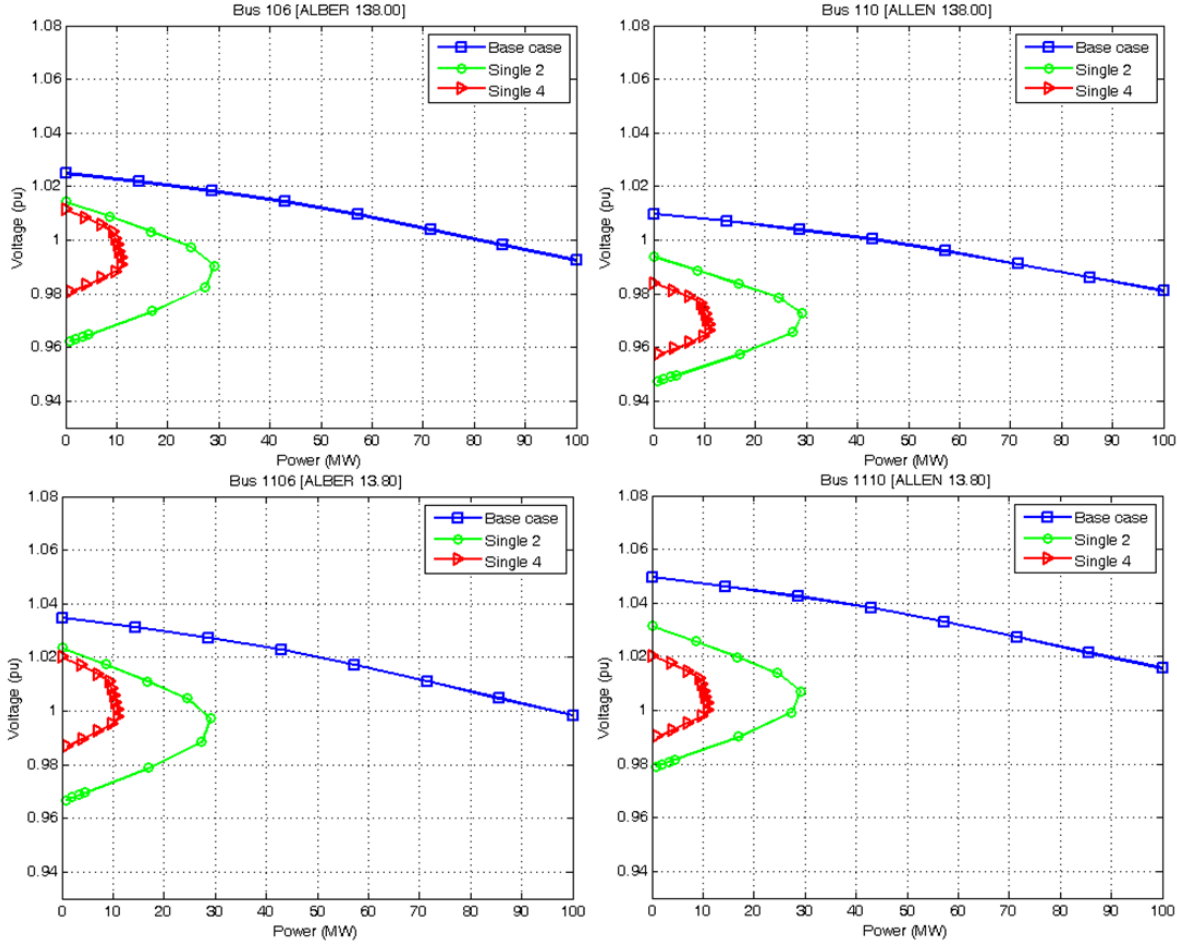


Figure 9.2: PV curves for the base case and two contingencies with SVCs removed

Notice that with PSAT the complete PV curve can be obtained, including the part beyond the maximum point for which the power flow no longer converges.

### 9.3 Dynamic simulations

Some dynamic models available in PSAT are different than those presented earlier (compliant with PSS/E tool). In PSAT, LTC and OEL react almost immediately (there is no noticeable delay before any response from these components).

Figure 9.3 depicts the LTC control block diagram in PSAT. Notice that there are no time delays; however, increasing the time constant of the first block can lead to a slower operation of the component. Moreover, the component can operate with discrete step and continuous changes; however, this may lead to convergence problems [48]. Figure 9.4 shows the models for the SVC modeled in PSAT as simple lag.

Table 9.2 shows the PSS/E models and their equivalent PSAT models. These models are similar but not identical to the PSS/E ones.

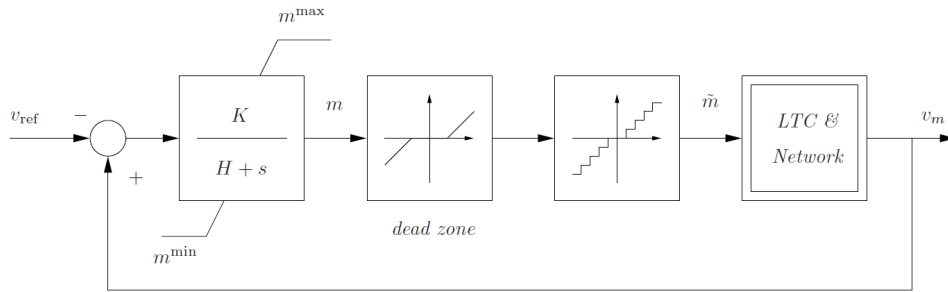


Figure 9.3: LTC control diagram in PSAT

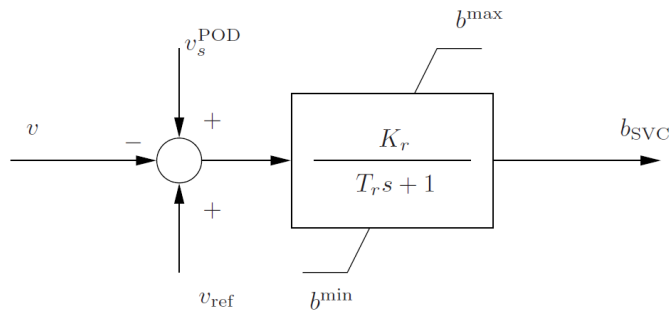


Figure 9.4: SVC model in PSAT

Table 9.2: Component models in PSS/E and PSAT environments

Component	PSS/E model	PSAT model
Generator	GENSAL	Syn order VI
Generator	GENROU	Syn order VI
Excitation system	IEEEET1	Exc type II
Excitation system	EXAC1	Exc type II
Excitation system	SCRX	Exc type III
Maximum excitation limiter	MAXEX2	Oxl
Turbine/Speed governor	HYGOV	Tg type II
Turbine/Speed governor	IEEEEG1	Tg type I
Static VAR Compensator	CSSCS1	Svc type I
Tap changer	OLTC1	Ltc
Load recovery	EXTLAL	Exload
Complex load model	CLODAL	Ind order III

## Test A

Figure 9.5 shows active and reactive powers, terminal voltage and the internal voltage for the generating unit at bus 30101 as produced by PSAT. The per-unit values are with respect to a 100 MW base. Observe that the maximum excitation limiter responds quickly and all voltage magnitudes and reactive power output change accordingly. There is no considerable change in the active power output of the unit; however, some oscillations can be observed which highlights the risk of the instability in the system.

Figure 9.6 shows active and reactive powers and the voltage magnitude at the load bus 1101, as well as the voltage magnitude at HV bus 101 in PSAT; thus, this figure mainly highlights the tap changer response, which is continuous and without time delays in this case. The tap changer reacts instantaneously in PSAT, with the load voltage recovering almost to its initial value at the end.

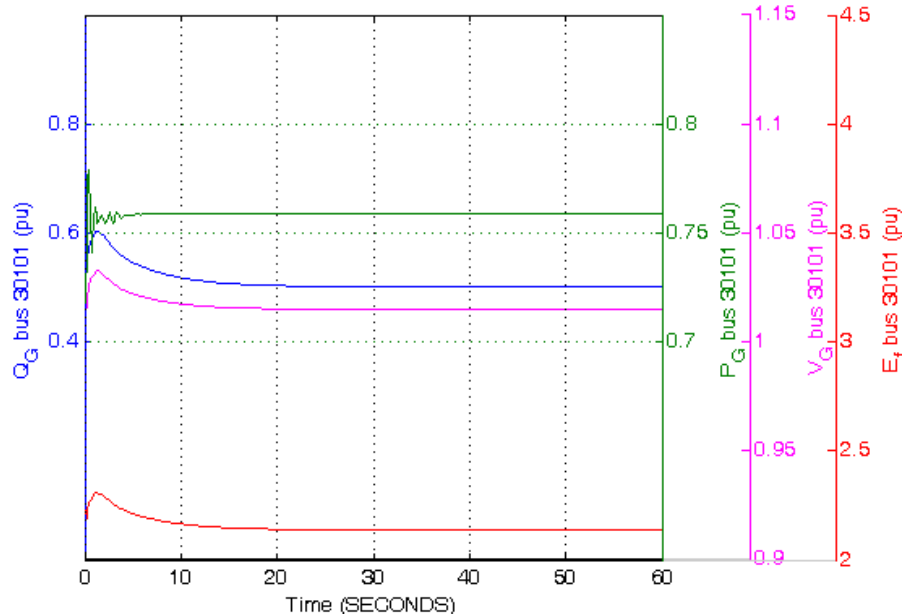


Figure 9.5: Active and reactive power, terminal voltage, and internal voltage for the generating unit at bus 30101

## Test B

Figures 9.7 to 9.10 show the voltages at buses 106 (HV) and 1106 (load bus), together with active and reactive powers at bus 1106.

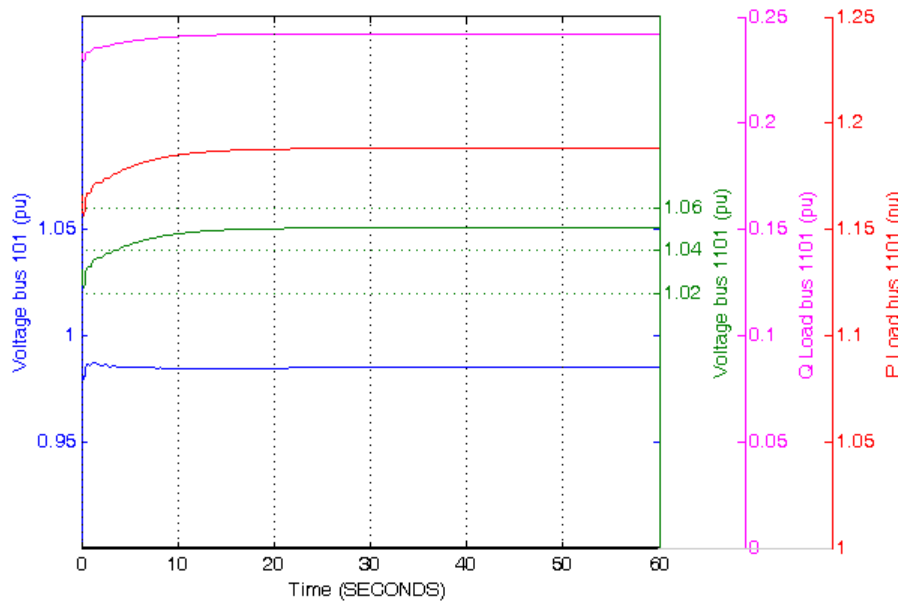


Figure 9.6: Active, reactive powers, voltage magnitude at the load bus 1101 and the voltage magnitude at HV bus 101

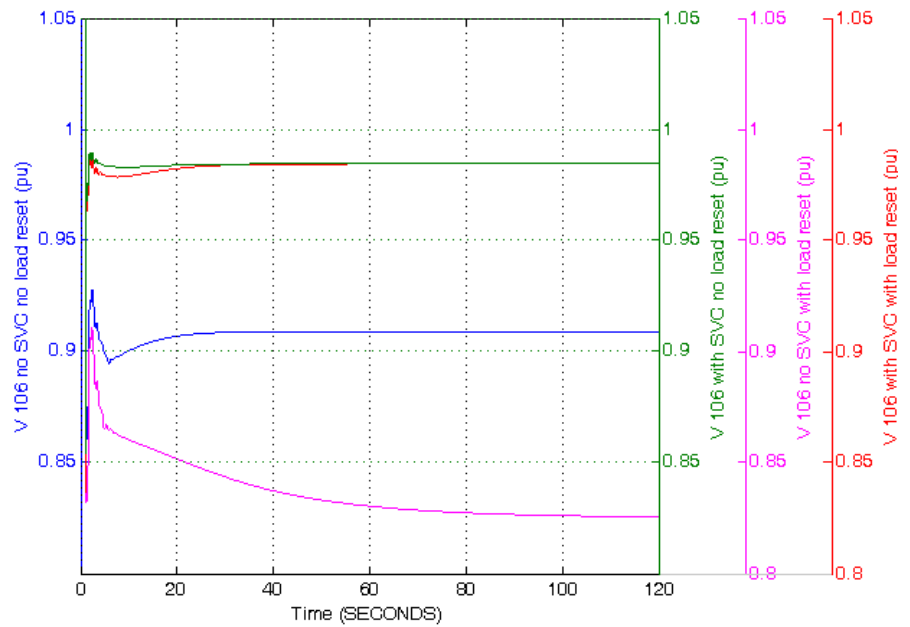


Figure 9.7: Voltage at bus 106

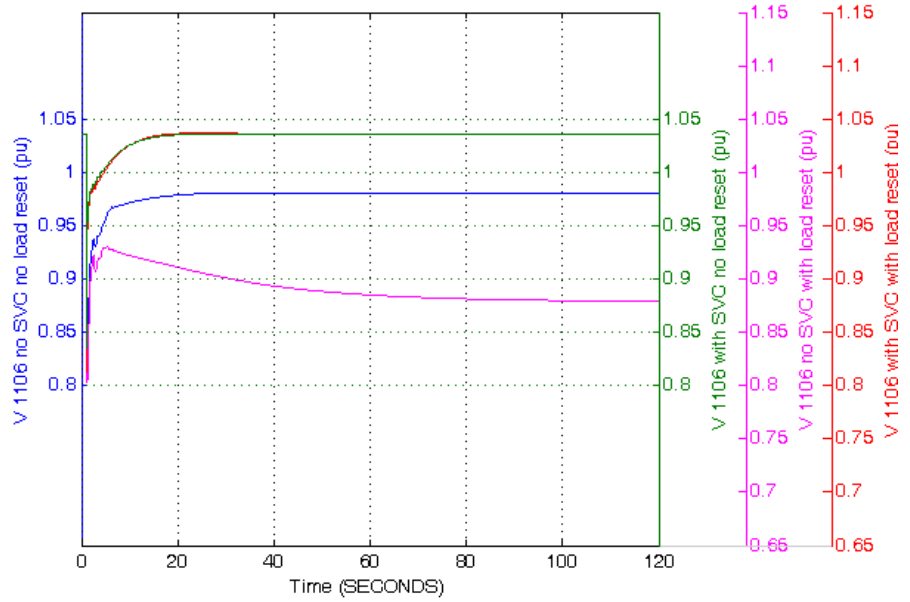


Figure 9.8: Voltage at bus 1106

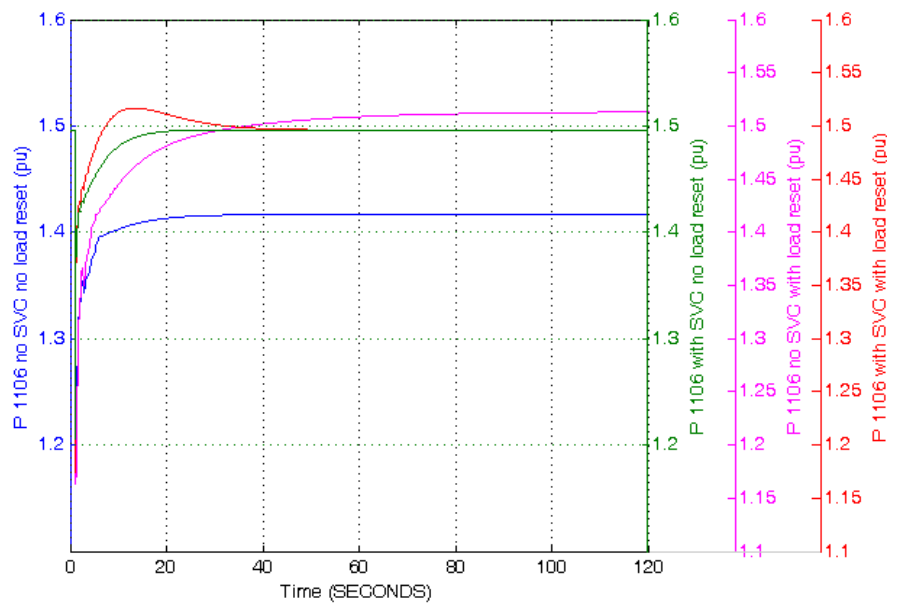


Figure 9.9: Active power consumption at bus 1106

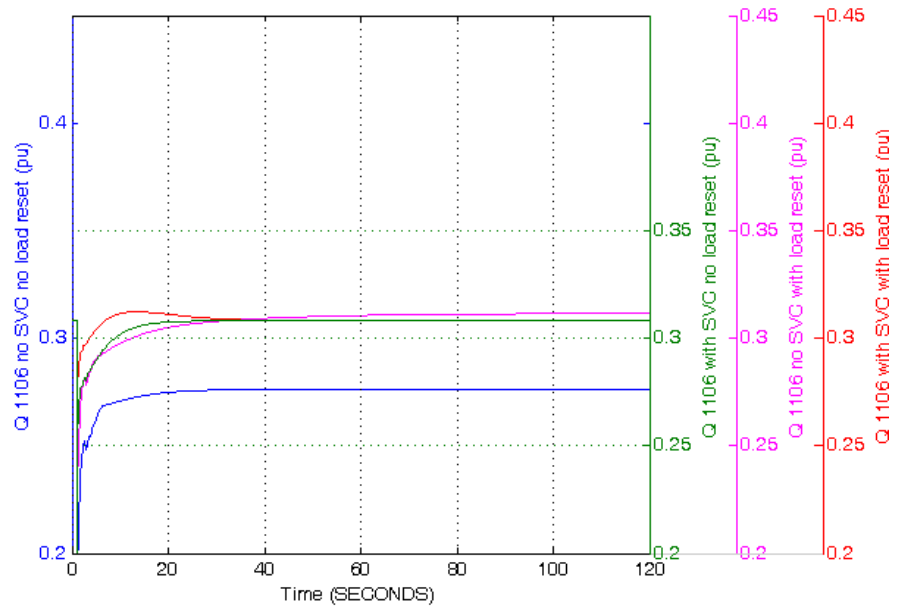


Figure 9.10: Reactive power consumption at bus 1106

### Test C

Figures 9.11 to 9.14 display the voltages at buses 106 and 1106 as well as active and reactive demands at the load bus 1106 obtained with PSAT for different SVC and load models.

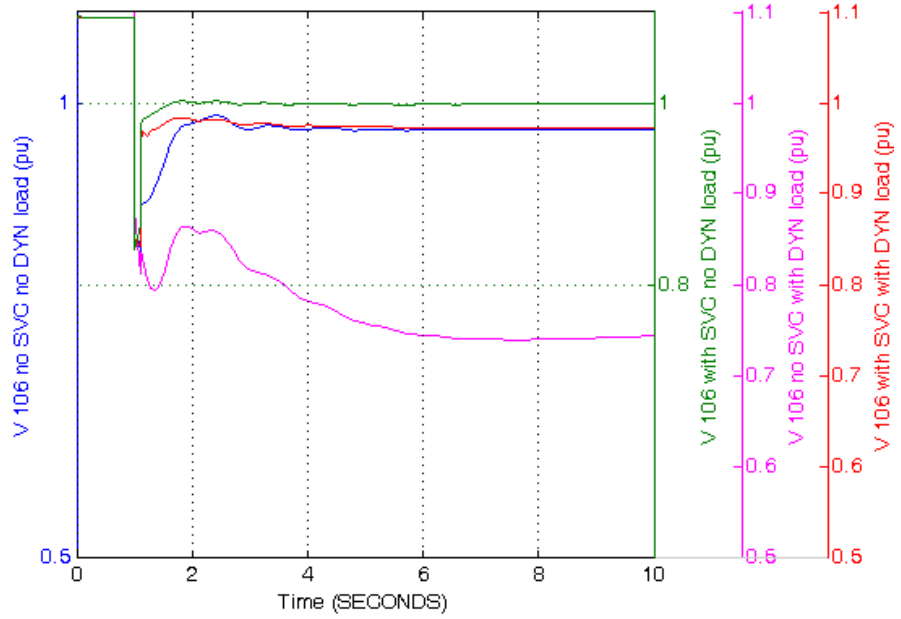


Figure 9.11: Voltage at bus 106

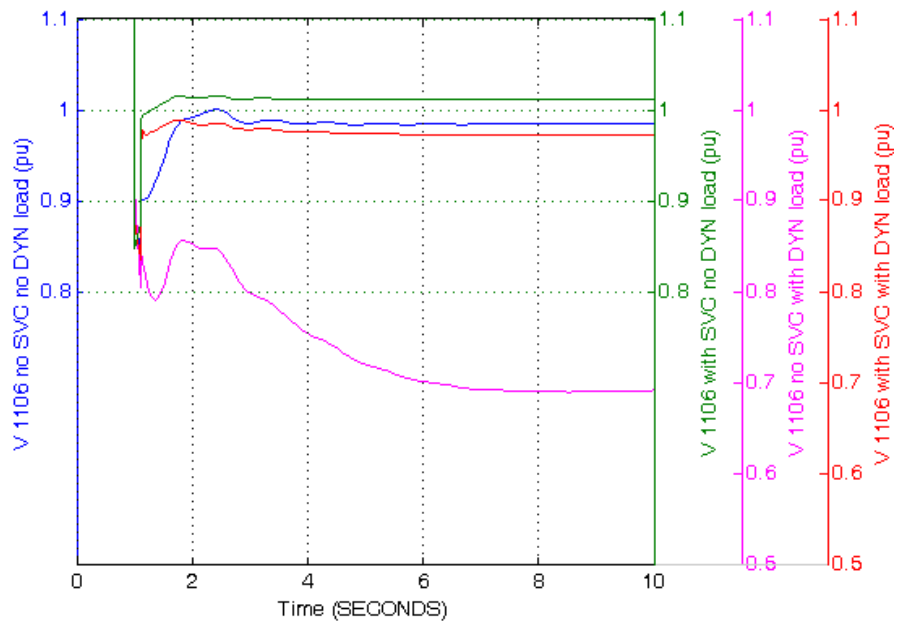


Figure 9.12: Voltage at bus 1106

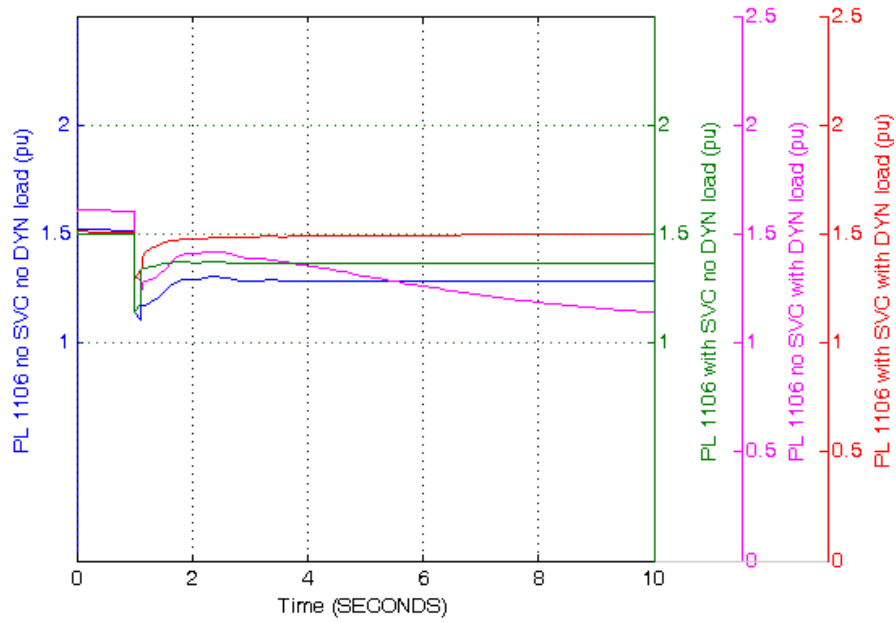


Figure 9.13: Active power consumption at bus 1106

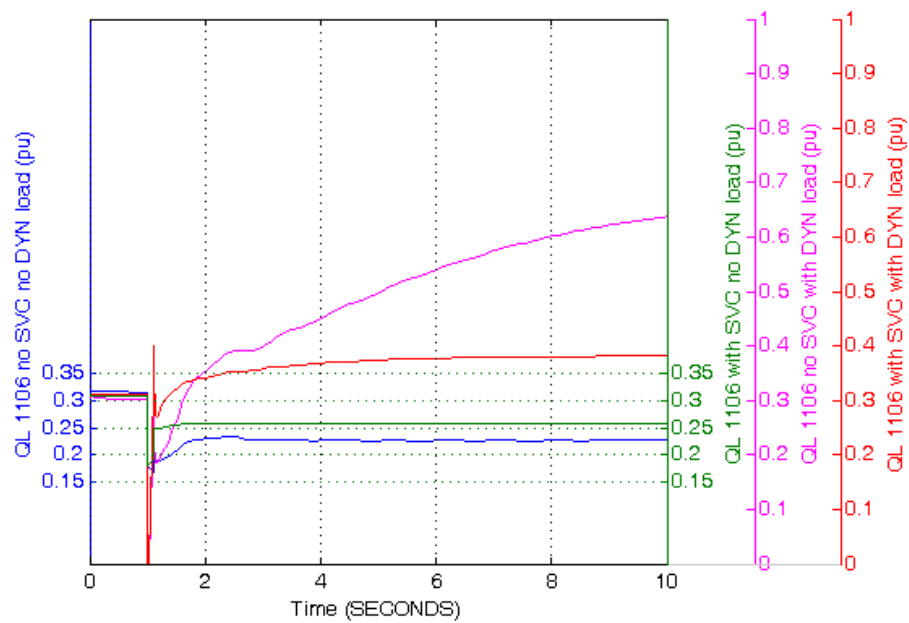


Figure 9.14: Reactive power consumption at bus 1106

# **Chapter 10**

## **RVS test system: simulation results using DSATools**

### **10.1 Steady-state analysis**

The same contingencies as in 7.1 are considered with DSATools.

DSATools version 10 comprises different parts including VSAT and TSAT components which are capable of performing voltage security and transient security analyses, respectively [45]. The PV curves were obtained using VSAT. The loads (for both active and reactive powers) connected to buses 1101, 1102, 1103, 1104, 1105, 1106, 1107, 1108, 1109 and 1110 were increased, while the power is provided by generating units connected to buses 113, 115, 116, 118, 122 and 123. The buses 114 and 121 were not included in the generator set, as the first bus is not a generator bus and the second one is the swing bus.

The additional generation available at the generator buses to supply the load increase is close to 100 MW; thus, the power transfer is limited by this amount.

The PV curves (referring to load power increase) obtained using VSAT for the two contingencies and the base case are shown in Fig. 10.1.

### **10.2 Dynamic simulations**

These simulations were conducted using TSAT component. Table 10.1 shows the components and their associated modeling in both DSATools and PSS/E. This version is equipped with a graphical model editor that allows for creating and editing certain user defined models, which was used to model the inverse time characteristic of the OEL along with its three knots via a stepwise graph (this device is not directly recognized if modeled as given in an earlier section) as shown in Fig. 10.2.

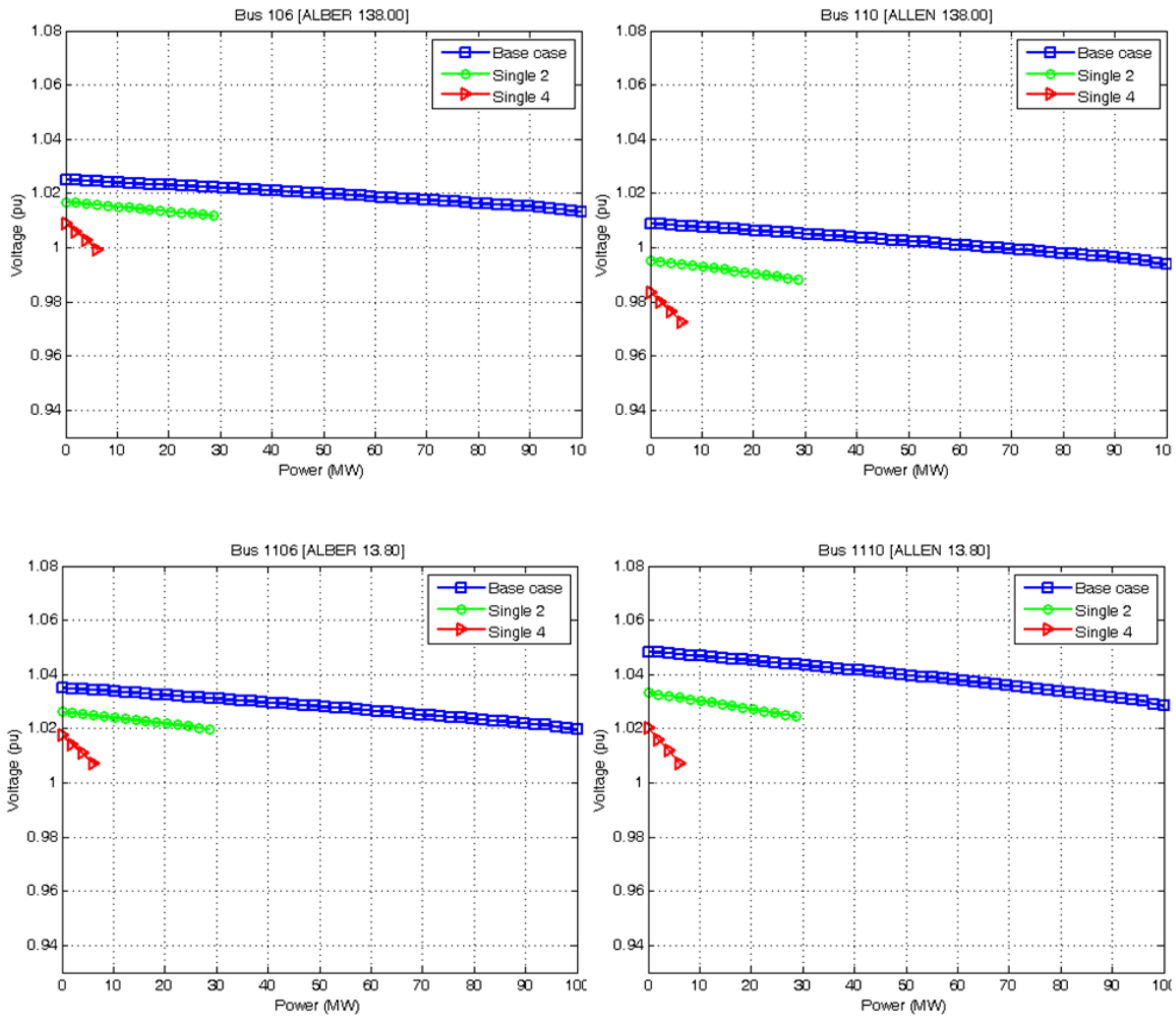


Figure 10.1: PV curves obtained with VSAT for the base case and two contingencies

Table 10.1: Component models in PSS/E and DSATools environments

Component	PSS/E model	DSATools model	Number of components
Generator	GENSAL	Automatically imported	6
Generator	GENROU	Automatically imported	26
Excitation system	IEEET1	Automatically imported	8
Excitation system	EXAC1	Automatically imported	2
Excitation system	SCRX	Automatically imported	22
Maximum excitation limiter	MAXEX2	Not available	32
Turbine/Speed governor	HYGOV	Automatically imported	6
Turbine/Speed governor	IEEEG1	Automatically imported	7
Static VAR Compensator	CSSCS1	Automatically imported	2
Tap changer	OLTC1	Special	22
Load recovery	EXTLAL	Not available	17
Complex load model	CLODAL	Automatically imported	17

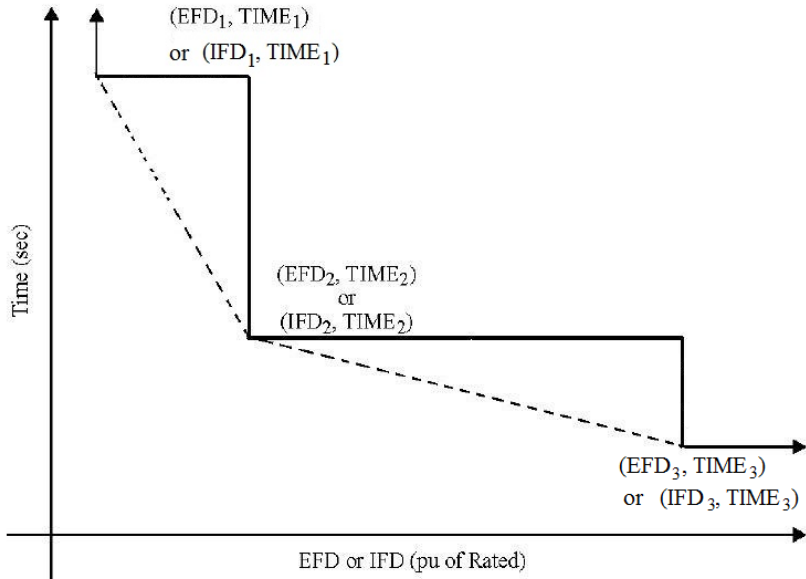


Figure 10.2: Approximated inverse time characteristic of the OEL introduced in DSATools

Table 10.2 shows the parameter values used; the first column shows the nominal  $EFD_N$  and columns 2, 4 and 6 show the normalized parameters based on the nominal value.

Table 10.2: OEL parameters

$EFD_N$	$EFD_1$	$TIME_1$	$EFD_2$	$TIME_2$	$EFD_3$	$TIME_3$	$K_{MX}$	$V_{LOW}$
2.154 (pu)	1.1	60 (s)	1.2	45 (s)	1.5	15 (s)	0.02	-0.05

### Test A

Figures 10.3 and 10.4 show reactive and active powers, terminal voltage, internal voltage and OEL output for the generating unit at bus 30101 and the voltage magnitude at bus 101 as produced by DSATools. The per unit values were obtained assuming a 100 MW base value. As it can be seen, the OEL gets activated around  $t = 50$  sec and all voltage magnitudes and reactive power output change accordingly. There is no considerable change in the active power output of the unit; however, some oscillations can be observed which highlights the risk of the instability in the system. Figure 10.5 shows active and reactive powers as well as the voltage magnitude at the load bus 1101 in DSATools. This figure mainly depicts the LTC response. At the beginning, the 30 sec delay for the first step is noticeable, while the delay for the next steps is only 5 sec. Moreover, around  $t = 50$  sec there is an interaction between the LTC and OEL. Observe that the load voltage almost recovers to its initial value due to the tap changer.

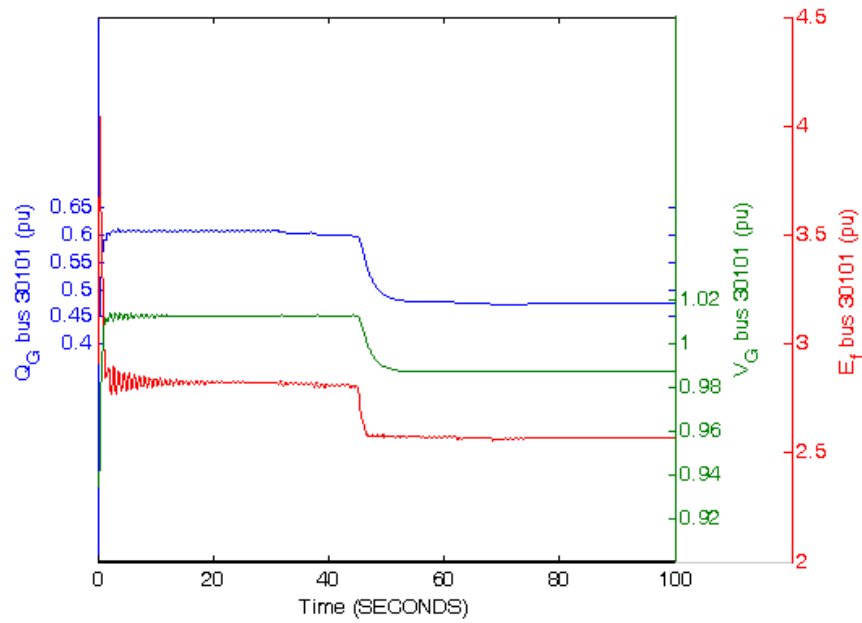


Figure 10.3: Reactive power, terminal voltage, and internal voltage for the generating unit at bus 30101

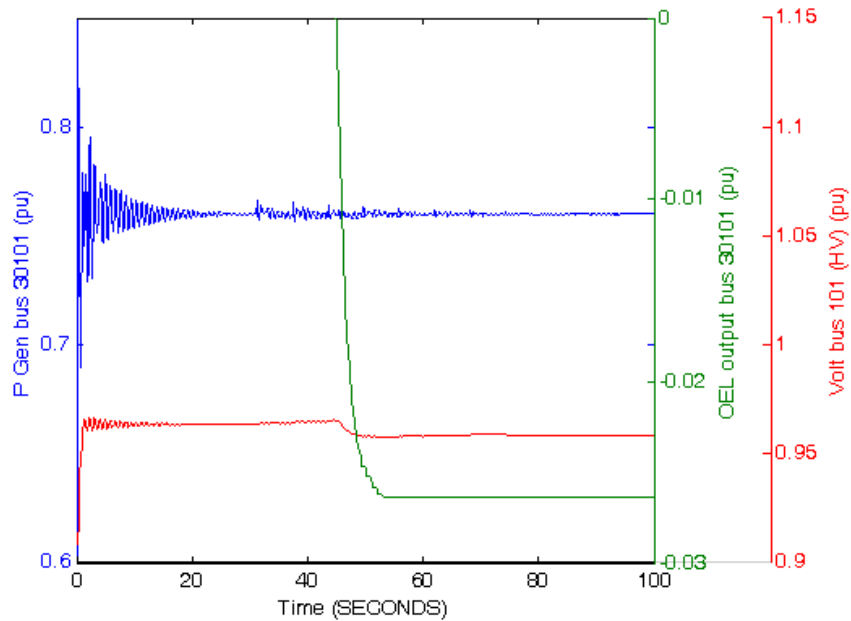


Figure 10.4: Active power and OEL output for the generating unit at bus 30101 and the voltage magnitude at bus 101

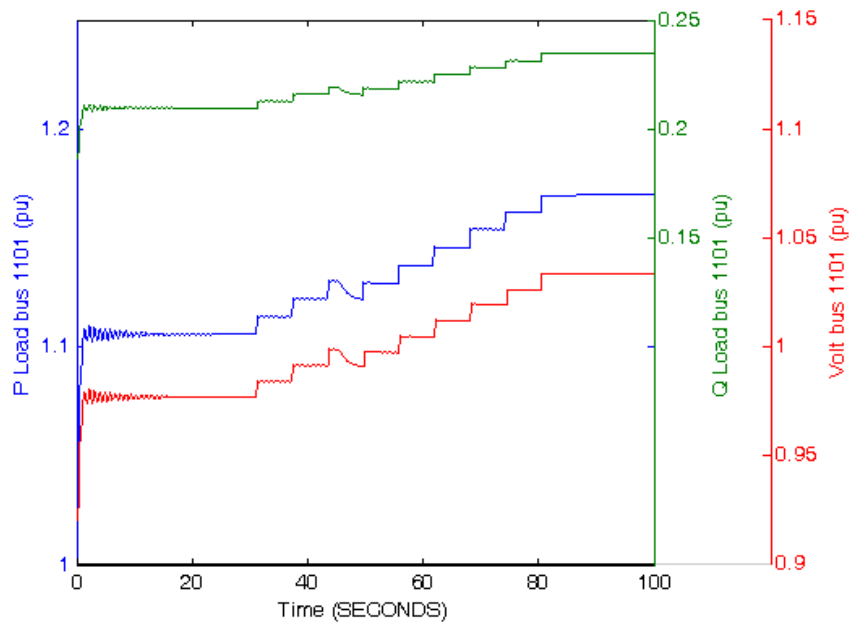


Figure 10.5: Active, reactive powers and voltage magnitude at the load bus 1101

### Test B

Figures 10.6 to 10.9 show the voltages at buses 106 (HV) and 1106 (load bus), together with active and reactive powers at bus 1106 for two different cases, namely, with an SVC at bus 10106 and with the SVC replaced by an equivalent fixed shunt.

Similar to Test A, the tap changer action and its delays are clearly seen. Note that, the SVC and the tap changer recover the voltage and the active and reactive demand at the load bus; however, this is not the case when a fixed shunt is used. Notice that given the slow time constants the SVC is not necessarily the best choice to recover the voltage and mechanically switched capacitor banks would basically yield the same recovery.

### Test C

Figures 10.10 to 10.13 display the voltages at buses 106 and 1106 as well as active and reactive demands at the load bus 1106 obtained with DSATools for different SVC and load modeling conditions. Observe that the fast response of the SVC recovers the voltages and the demand after a short period; which is not the case with a fixed capacitor. Moreover, no tap changer action is seen in this case as the considered time frame is shorter than the designated LTC delay.

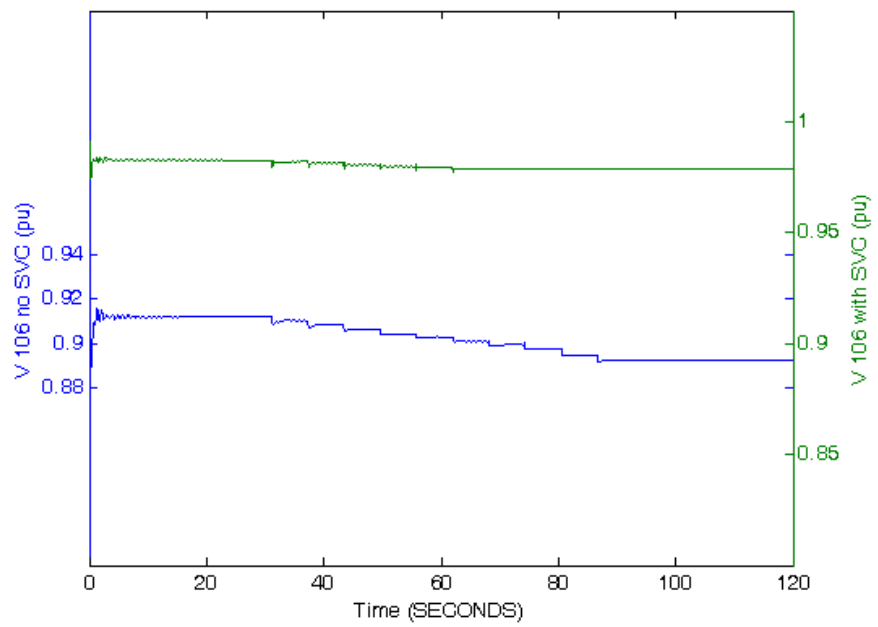


Figure 10.6: Voltage at bus 106

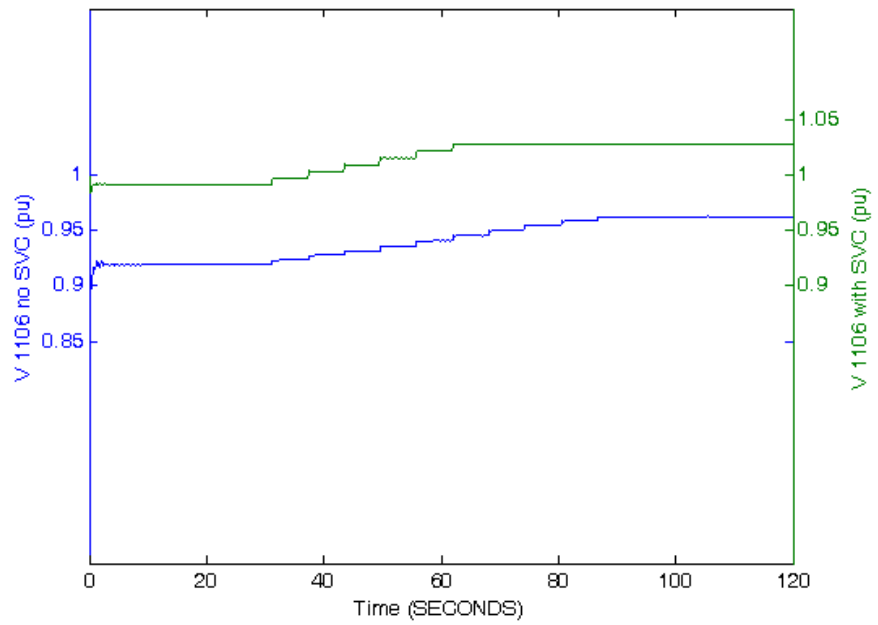


Figure 10.7: Voltage at bus 1106

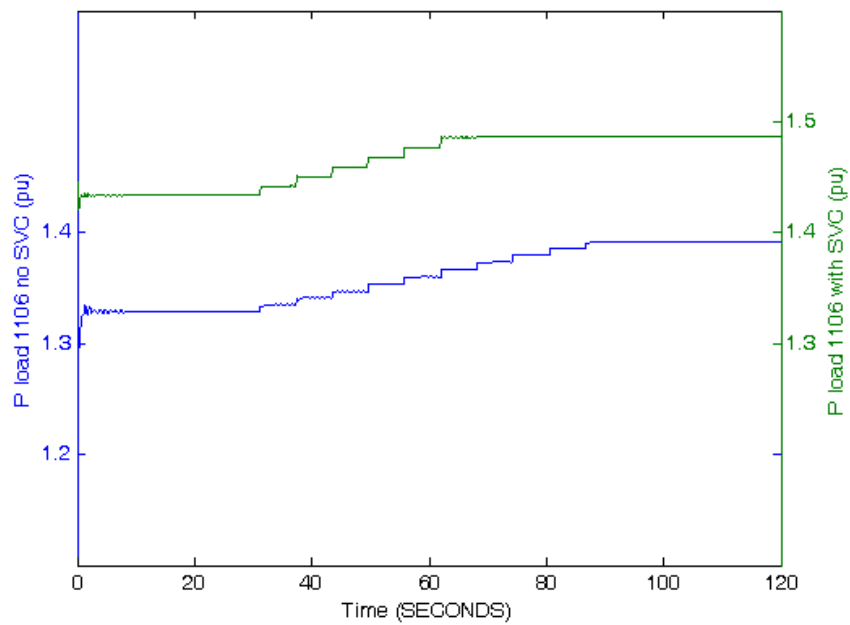


Figure 10.8: Active power consumption at bus 1106

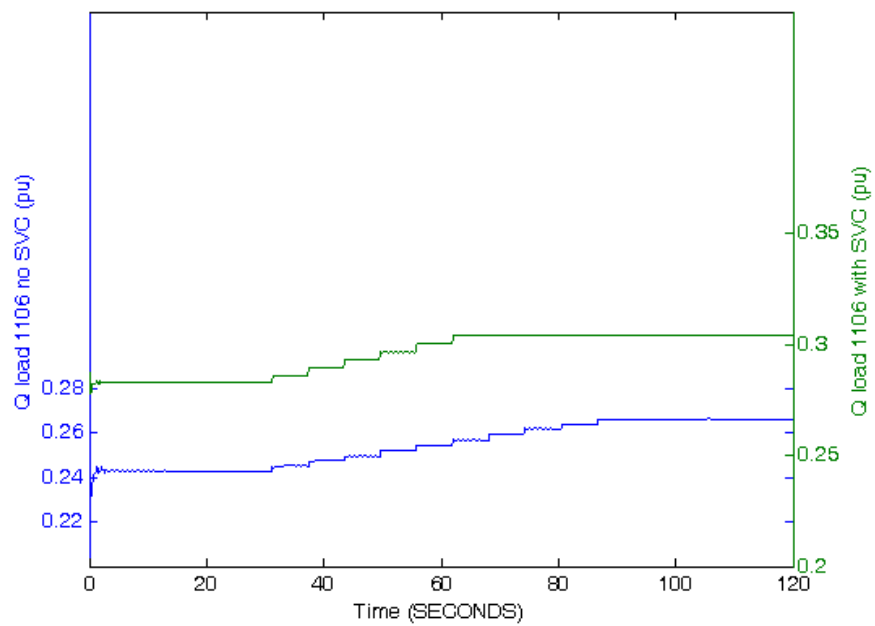


Figure 10.9: Reactive power consumption at bus 1106

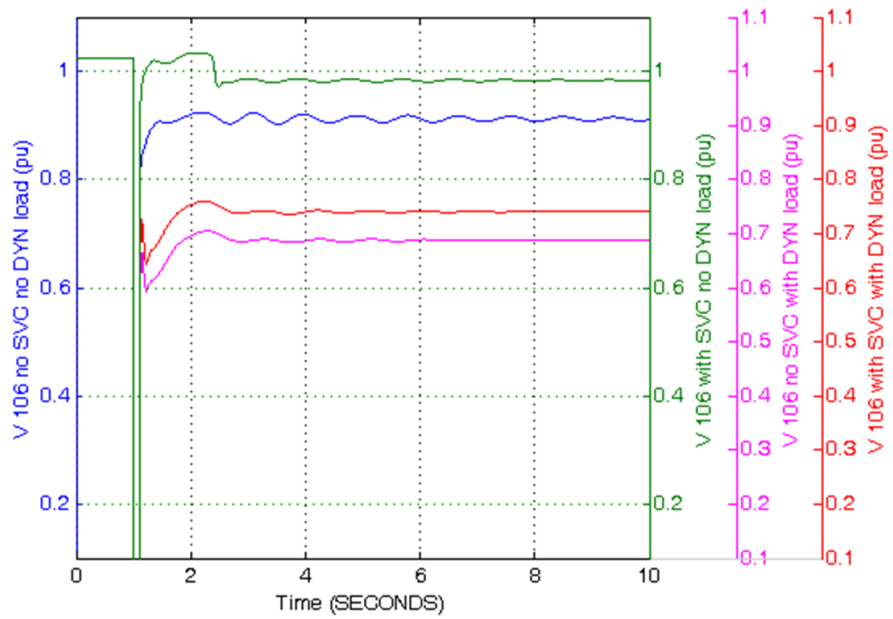


Figure 10.10: Voltage at bus 106

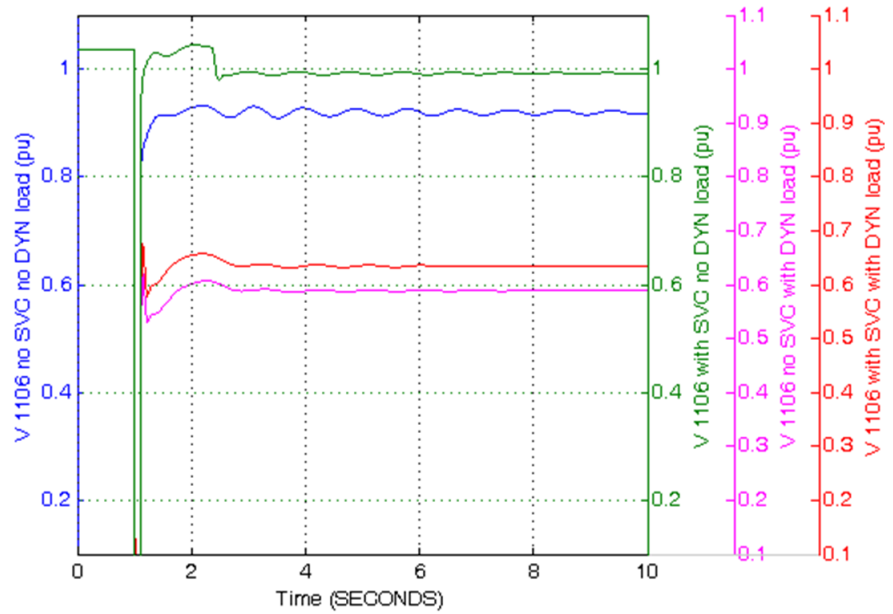


Figure 10.11: Voltage at bus 1106

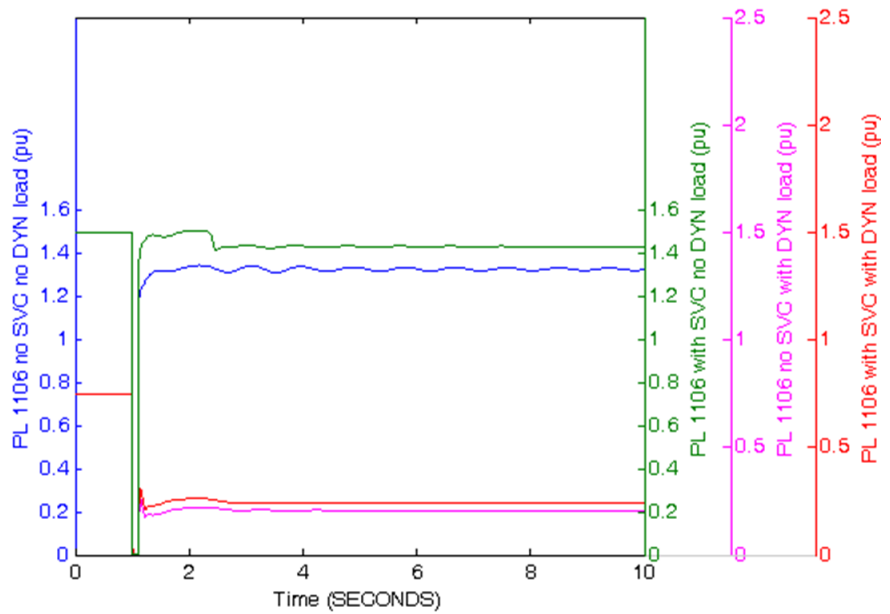


Figure 10.12: Active power consumption at bus 1106

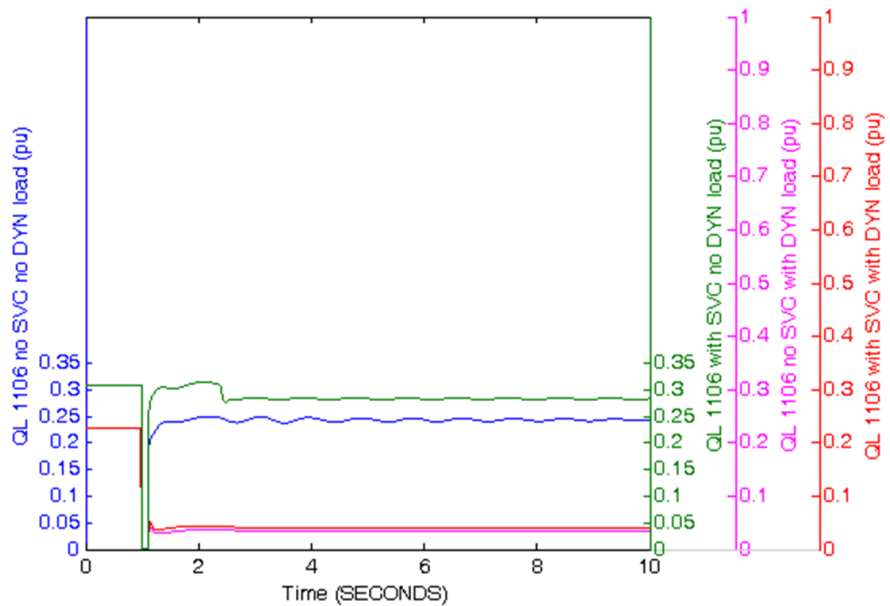


Figure 10.13: Reactive power consumption at bus 1106

## Chapter 11

# Nordic test system: simulation results using QSS simulation tool WpSTAB

This appendix contains a comparison of Quasi-Steady-State (QSS) simulation of the Nordic System using the software WpSTAB [50] to the benchmark full-time simulation of this report. The contingency is the same as in Section 3 and the loading is for operating point A. One key detail in obtaining comparable results of QSS and full-time-scale simulation is the representation of OELs. The model used is the proportional takeover, with error-signal substitution shown in Fig. 11.1 with the data given in the report.

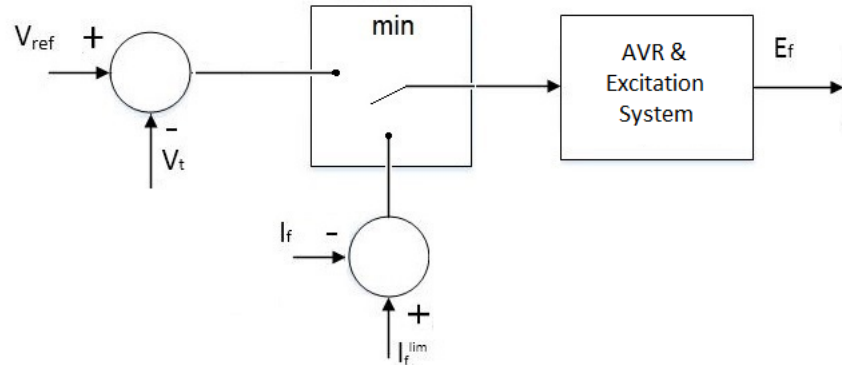


Figure 11.1: Takeover OEL with error-signal substitution

The equation of the proportional AVR when the OEL takes over is,

$$E_f = G(I_f^l im - I_f) \quad (11.1)$$

In the steady state (QSS approach)  $E_f = I_f$  and the previous equation becomes,

$$E_f = G((I_f^l im)/(G + 1)) \quad (11.2)$$

Several responses follow showing the comparison between the QSS and full simulations. In Fig. 11.2 the internal  $E_f$  of generator g6 is depicted. As can be observed, the two responses are the same until  $t=50$  s when the disturbance occurs. After the disturbance,  $E_f$  increases steadily and crosses the limit  $I_{f,g6}^l im = 3.0618pu$ . The OEL constant timer of the QSS simulation is set so that the timing of the limitation is closer than 3 seconds from that of the full simulation. This is necessary, as the time-dependent timer will be different in the QSS simulation due to the different (stair-case) responses. At  $t=200$ s both simulations show the loss of synchronism which is the result of voltage instability.

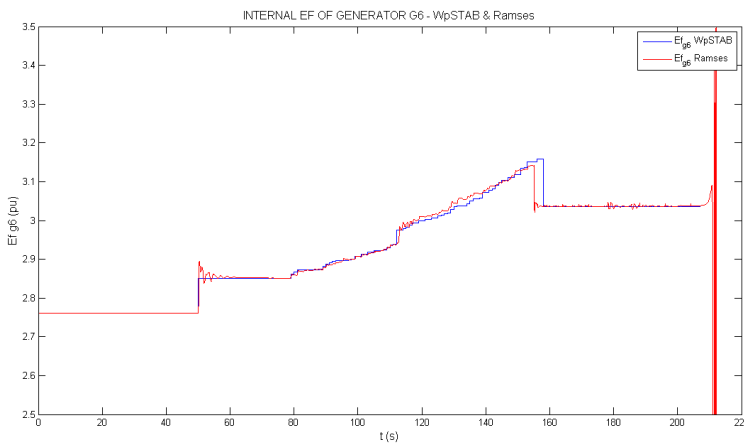


Figure 11.2:  $E_f$  of generator g6 in WpSTAB and RAMSES

In Fig 11.3 the response of generator g12 is shown. When  $E_f$  violates the limit, which for this generator is  $I_{f,g6}^l im = 1.8991pu$ , the OEL brings back the excitation within the desired limits.

In Fig. 11.4 the response of  $E_f$  of generator g5 is shown. As seen in the full simulation, after limitation the generator cannot achieve a steady state. On the other hand QSS simulation anticipates an equilibrium and thus the QSS simulation departs from the full simulation response leading to a slightly earlier collapse as seen at the end of the simulation.

Figure 11.5 shows the voltage of HV bus 4042. The response is identical for both simulations until the disturbance. Then the responses are similar as the voltage declines continuously until the final stage of the voltage collapse. The only difference is again the time of loss of synchronism that occurs some seconds later in full-time simulation.

Finally, Fig 11.6 shows the voltage of an MV bus, as well as the ratios of the corresponding LTC. After the disturbance, in both simulations, the voltage remains inside the deadband for some time. The time that the voltage exits the deadband cannot be identical in the QSS simulation. For the QSS simulation the voltage enters again the deadband and as a result the timer switches to the long delay. Although the responses are

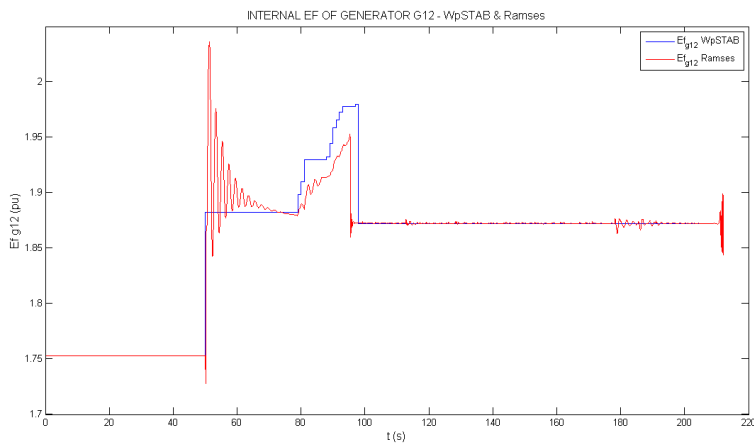


Figure 11.3:  $E_f$  of generator g12 in WpSTAB and RAMSES

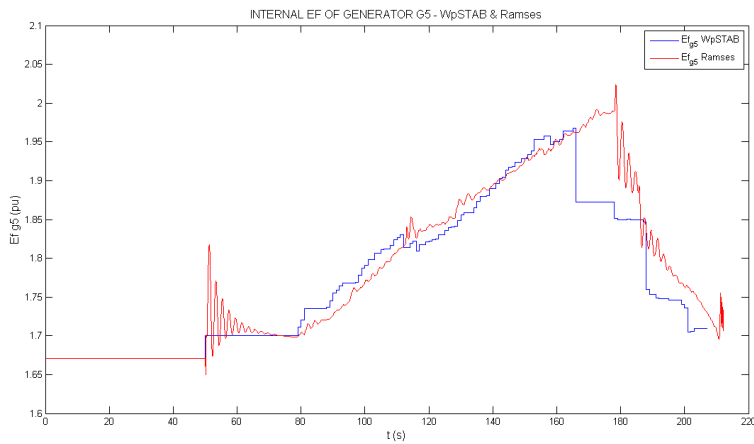


Figure 11.4:  $E_f$  of generator g5 in WpSTAB and RAMSES

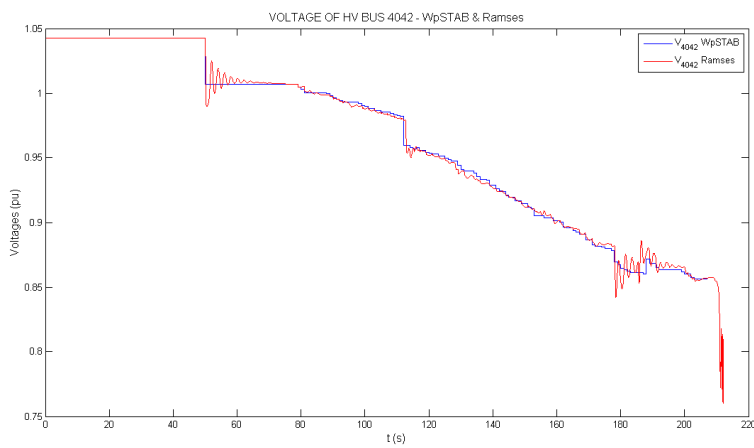


Figure 11.5: Voltage of HV bus 4042

different, the general trend is maintained, with again the QSS simulation anticipating by few seconds the final collapse.

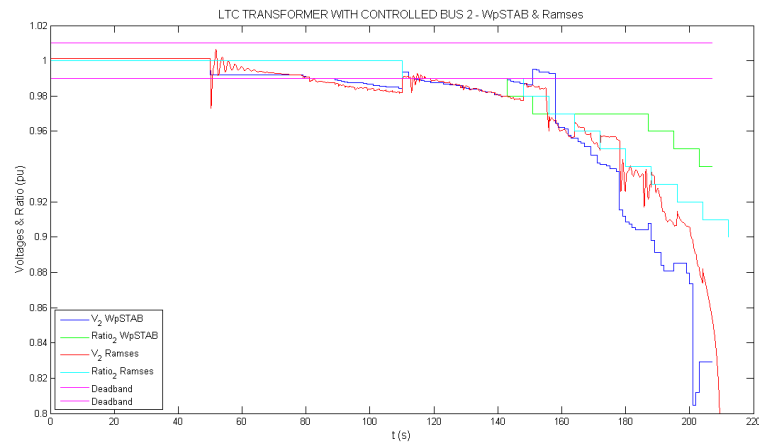


Figure 11.6: LTC Transformer of MV bus 2

# **Chapter 12**

## **Nordic test system: simulation results using ANATEM**

This text contains a set of results on the use of the ANATEM software [51] for reproducing the Nordic system under some of the conditions described in this Technical Report. Before presenting these results, however, a set of remarks on the use of ANATEM is given.

### **12.1 General remarks on the use of ANATEM**

The previously mentioned remarks on the use of ANATEM are summarized below:

1. A fifth-order model was used for salient pole synchronous machines. This corresponds to the *MD2* ANATEM built-in model for this type of machine [51];
2. A sixth-order model was used for round synchronous machines. This corresponds to the *MD3* ANATEM built-in model for this type of machine [51];
3. In both models, exponential saturation characteristics were used, with the following values defined by the DCST execution code [51]:  $Y_1 = 0.005$ ,  $Y_2 = 5.49306$  and  $X_1 = 0.45463$ . The comparison between the saturation curves used in ANATEM and the ones provided in this Technical Report is shown in Figure 12.1;
4. All controller and other dynamic equipment models (exciter, automatic voltage regulator, power system stabilizer, overexcitation limiter, turbine, speed governor and load tap changer), with the exception of the generators and the loads, were implemented as user-defined blocks. This was necessary because ANATEM does not provide built-in models similar to the ones used in this Technical Report;
5. The model of the overexcitation limiter in ANATEM is associated to a normalization of the field current used to check the machine limitation. For this reason, in ANATEM the base value of the field

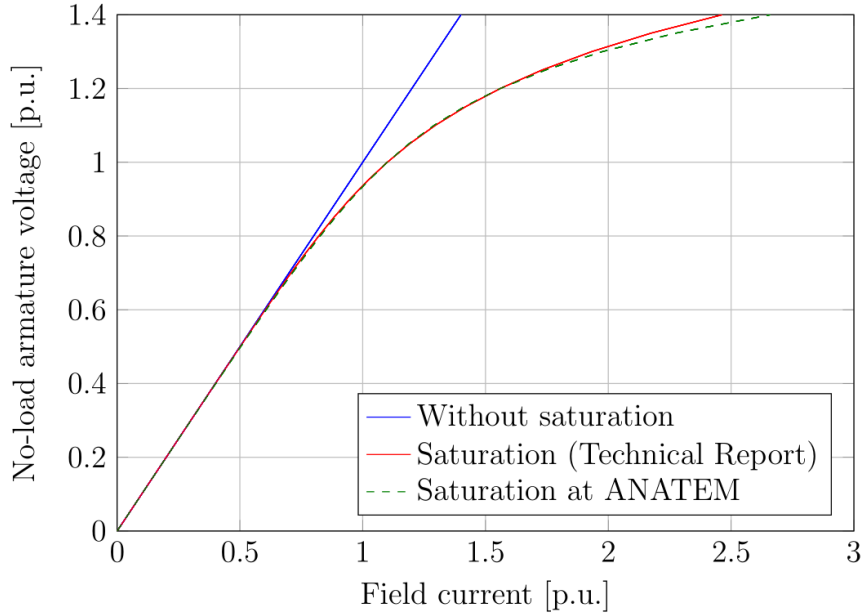


Figure 12.1: Comparison between the saturation curves used in ANATEM and the ones given in this Technical Report

current is such that, when the generator operates at no load with a terminal voltage of 1.0 p.u. and without saturation, the per unit value of the field current is also unitary. This can be expressed as follows:

The rated and the limit values of the field current are related to this base value in the model.

$$i_{fd}^{TechnicalReport} = (X_d - X_l) i_{fd}^{ANATEM}$$

This definition of the field current base is a source of discrepancy between the results provided by ANATEM and the ones given in this Technical Report. However, as the reader will notice in the figures shown in the next section, the discrepancies are small and the qualitative behavior of the system exhibits a very good match between the two sets of results.

6. The use of ANATEM for the determination of loadability limits with the same approach employed in this Technical Report requires a huge number of events (and consequently a very large computational effort as well), because the smooth increase of the power demand by the loads is handled by ANATEM as a series of discrete events. Furthermore, the maximum number of events supported by ANATEM is 6600. The combination of these two features creates a limitation in the feasibility of the use of ANATEM for reproducing the results of this Technical Report, which had to be overcome with an adjustment in the rate of change in the power demand increase.

Therefore, instead of increasing 1 MW of the active component of the loads each second, increments of 10 MW can be applied with an interval of 10 seconds among them, for example. For point B, the application of this approach resulted in a number of events that could be handled by ANATEM while still preserving satisfactorily matching results from both the qualitative and quantitative viewpoints, as will be better explained in Section 12.3.

## 12.2 Dynamic simulations

The system operating at point A was subject to a three-phase solid fault on line 4032-4044, near bus 4032. For simplicity, this fault was assumed to happen close enough to bus 4032, in such a way that, for simulation purposes, the fault was actually applied to bus itself. The disturbance was cleared out in five cycles (0.1s) by opening the line, which remains opened until the end of the simulation. During the simulation, the disturbance was applied at  $t = 2.0$  s.

Figure 12.2 shows de voltage magnitude of selected buses and Figure 12.3 shows the behavior of the field currents of seven generators that reach their limits, while in Figure 12.4 the behaviors of the field currents of three generators that do not reach their limits is shown. Figure 12.5 shows the terminal voltage behavior of two generators that reach their limits. The voltage drops at the moments when the field currents reach their corresponding limits can be clearly seen in Figure 12.5.

Figure 12.6 shows selected ratios of transformers in the Central Area, for which the tap changers are activated with different initial delays. Also regarding with transformer ratios, Figure 12.7 illustrates the unsuccessful attempt to bring the distribution voltage of bus 1 back to its dead-band (i.e., the range between 0.99 and 1.01 p.u.) by LTC 1-1041.

Figures 12.8 and 12.9 show the rotor speed deviations and rotor angles related to the Center Of Inertia (COI) of the system, respectively. It is evident from these two figures that the problem under study is indeed of a voltage instability nature, since the machines oscillate in a coherent manner until the instant when the maximum loadability of the system is reached, inducing a voltage collapse.

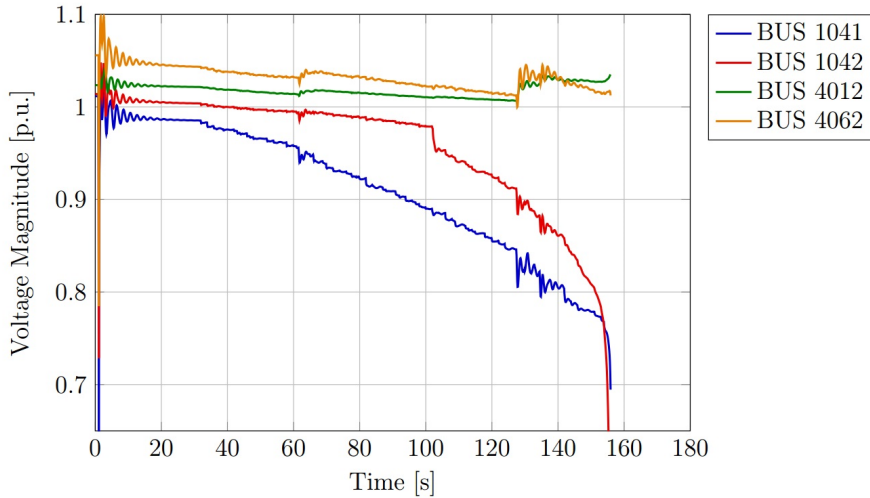


Figure 12.2: Selected transmission voltages after a fault in line 4032-4044 cleared by opening the line (operating point A)

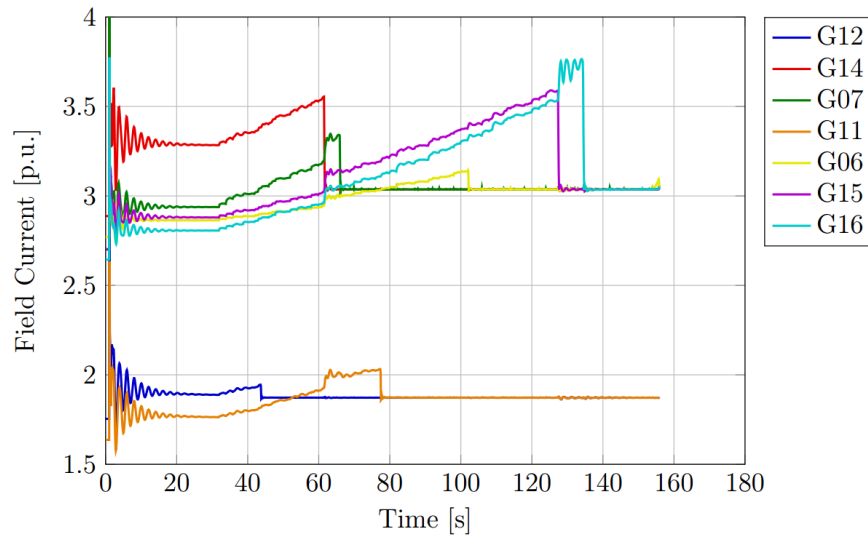


Figure 12.3: Field voltages of seven generators with limits reached, after a fault in line 4032-4044 cleared by opening the line (operating point A)

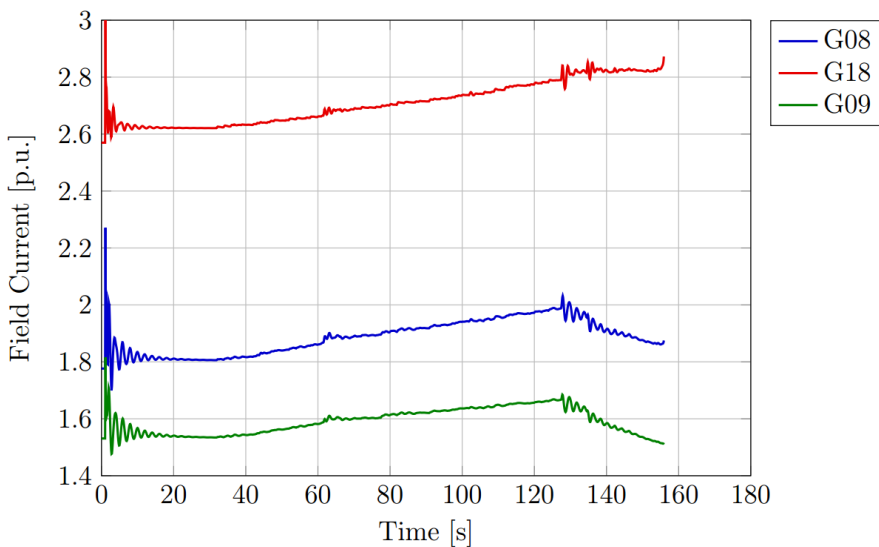


Figure 12.4: Field voltages of three generators with limits not reached, after a fault in line 4032-4044 cleared by opening the line (operating point A)

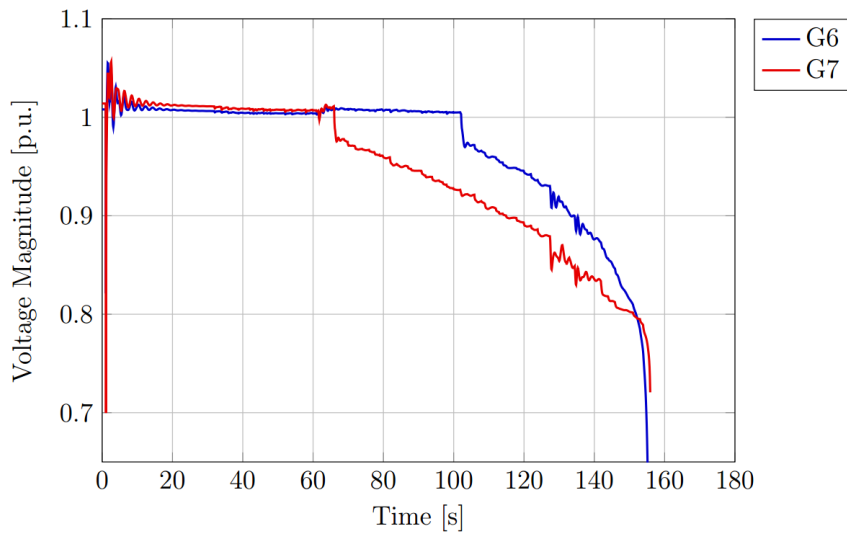


Figure 12.5: Terminal voltages of two generators with limits reached, after a fault in line 4032-4044 cleared by opening the line (operating point A)

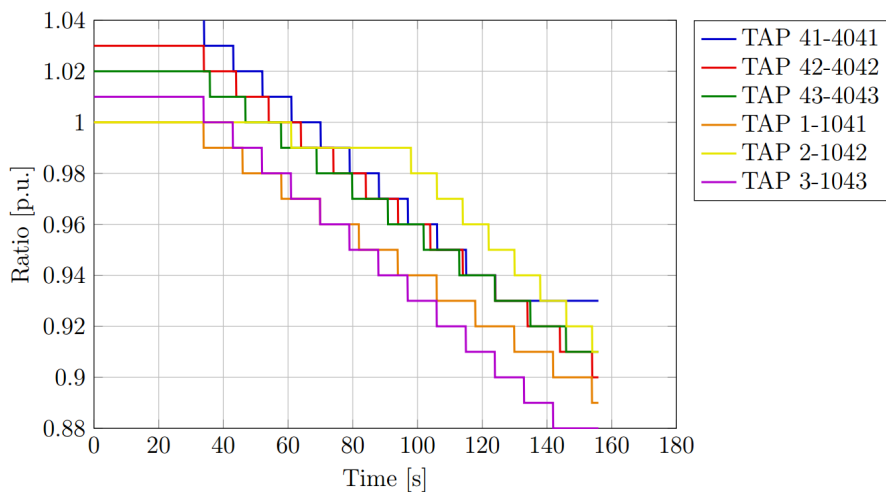


Figure 12.6: Selected distribution transformer ratios, after a fault in line 4032-4044 cleared by opening the line (operating point A)

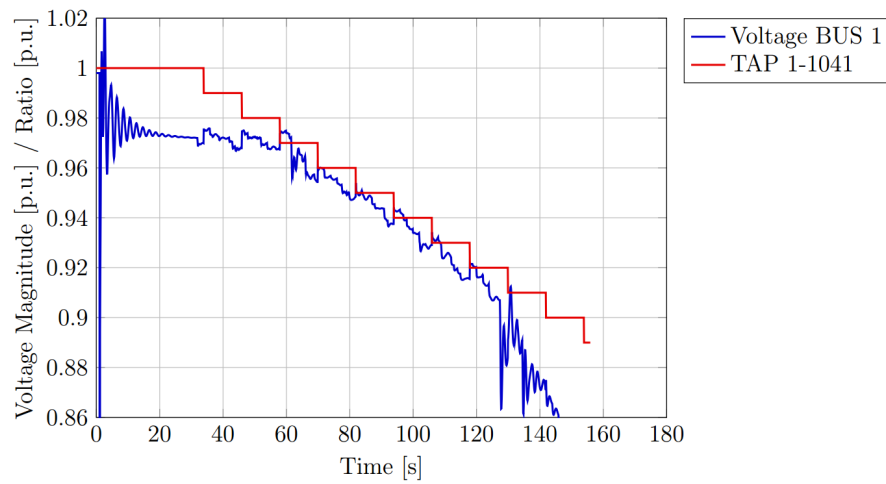


Figure 12.7: Unsuccessful restoration of the distribution voltage of bus 1 by LTC 1-1041, after a fault in line 4032-4044 cleared by opening the line (operating point A)

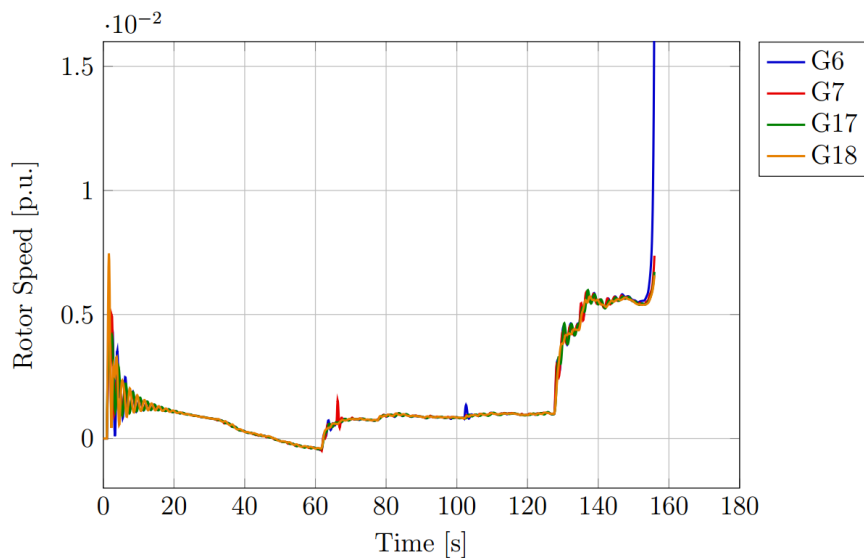


Figure 12.8: Rotor speed deviations of selected synchronous machines, after a fault in line 4032-4044 cleared by opening the line (operating point A)

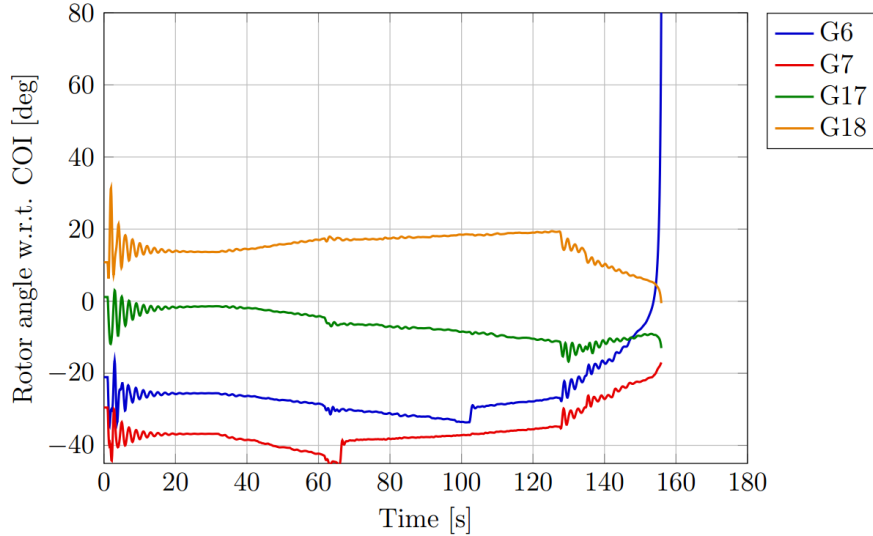


Figure 12.9: Rotor angle deviations (w.r.t. the COI) of selected synchronous machines, after a fault in line 4032-4044 cleared by opening the line (operating point A).

### 12.3 Determination of loadability limits

The results presented in this section show PV curves computed to determine the loadability limit of the system operating at point B. The PV curves are obtained by a ramp increase the load demand, as previously defined in Section 12.1. The same considerations used to generate the PV curves shown in this Technical Report are also used in ANATEM, except for the manner in which the loads of the Central Area have been increased.

In the results given in this Technical Report, the increment occurs at a rate of 0.15 MW/s in the Central Area. In ANATEM analysis, 1.5 MW are added each 10 seconds, in such a way that the rate of load increase is the same. Figure 12.10 shows three PV curves obtained with this approach. The base load level is 6190 MW, while the maximum load power is around 6830 MW. Therefore, the load power margin is 640 MW, which is the same margin given in this Technical Report.

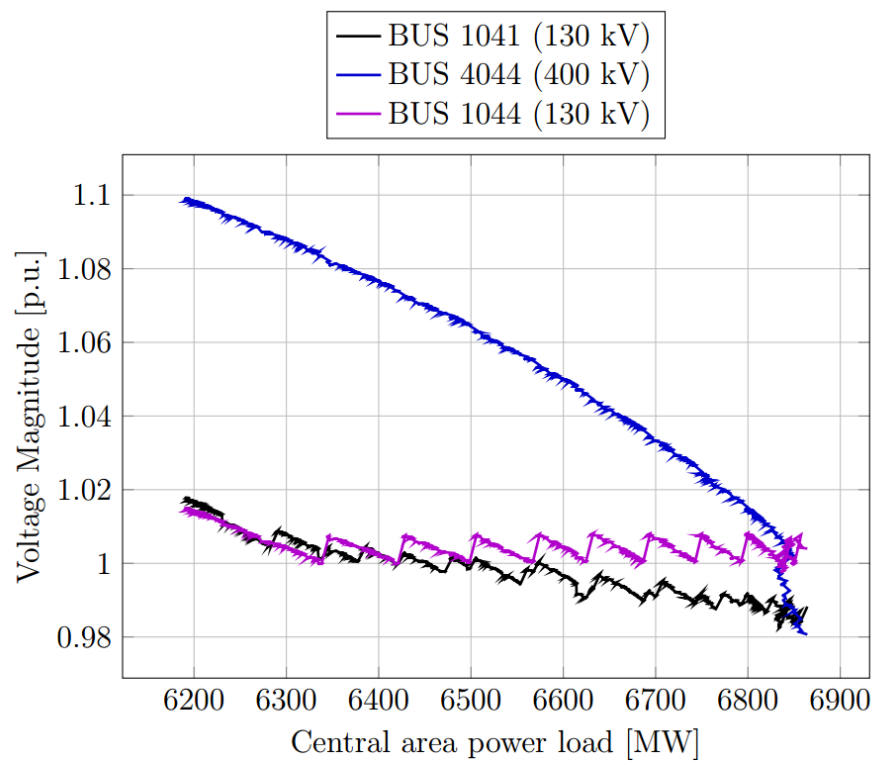


Figure 12.10: PV curve simulation for calculation of the loadability limit (operating point B)

# Bibliography

- [1] F. Alvarado and Y. Mansour (Editors/Coordinators), *Suggested Techniques for Voltage Stability Analysis*, IEEE PES Publication, Power System Engineering Committee, ISBN 9780780399839, 1993.
- [2] C. W. Taylor, *Power System Voltage Stability*, EPRI Power System Engineering Series, McGraw Hill, 1994.
- [3] P. Kundur, *Power System Stability and Control*, Mc Graw Hill, EPRI Power System Engineering Series, 1994.
- [4] T. Van Cutsem, C. Vournas, *Voltage stability of electric power systems*, Springer (previously Kluwer Academic Publishers), Boston (USA), 1998.
- [5] C. Cañizares (Editor/Coordinator), *Voltage Stability Assessment: Concepts, Practices and Tools*, IEEE PES Publication, Power System Stability Subcommittee, ISBN 0780379695, 2002.
- [6] V. Ajjarapu, *Computational Techniques for Voltage Stability Assessment and Control*, Springer, Boston (USA), 2006.
- [7] P. Kundur, J. Paserba. V. Ajjarapu, G. Andersson, A. Bose, C. Cañizares, N. Hatzargyriou, D. Hill. A. Stankovic, C. Taylor, T. Van Cutsem. V. Vittal, “Definition and Classification of Power Systems Stability,” IEEE Trans. on Power Systems, vol. 19, no. 2, pp. 1387-1401, May 2004.
- [8] P. Aristidou, D. Fabozzi, and T. Van Cutsem, Dynamic Simulation of Large-Scale Power Systems Using a Parallel Schur-Complement-Based Decomposition Method, IEEE Trans. on Parallel and Distributed Systems, vol. 25, no. 10, pp. 2561-2570, Oct. 2013.
- [9] M. Glavic and T. Van Cutsem, “A short Survey of Methods for Voltage Instability Detection,” In Proceedings of IEEE PES General Meeting, 2011.
- [10] M. Stubbe (Convener), *Long-Term Dynamics - Phase II*, Report of CIGRE Task Force 38.02.08, Jan. 1995.
- [11] C. Vournas, T. Van Cutsem, “Local Identification of Voltage Emergency Situations,” IEEE Trans. on Power Systems, vol. 23, no 3, pp. 1239-248, Aug. 2008.
- [12] M. Glavic, T. Van Cutsem, “Wide-area Detection of Voltage Instability from Synchronized Phasor Measurements. Part I: Principle. Part II: Simulation Results,” IEEE Trans. on Power Systems, vol. 24, no. 3, pp. 1408-1425, Aug. 2009.

- [13] B. Otomega, T. Van Cutsem, "Undervoltage load shedding using distributed controllers," IEEE Trans. on Power Systems, vol. 22, no 4, pp. 1898-1907, Nov. 2007.
- [14] M. Hajian, W. Rosehart, M. Glavic, H. Zareipour, and T. Van Cutsem, "Linearized Power Flow Equations Based Predictive Control of Transmission Voltages," In Proceedings of the 46th Hawaii International Conference on System Sciences (HICSS-46), 2013.
- [15] B. Otomega, M. Glavic, and T. Van Cutsem, "Wide-Area Adaptive Load Shedding Control to Counteract Voltage Instability," In Proceedings of the Power Plant and Power System Control Conference (PPPSC 2012), 2012.
- [16] M. Glavic and T. Van Cutsem, "State Reconstruction from a Limited Number of Synchronized Phasor Measurements: Application to Voltage Instability Detection," In Proceedings of the IEEE PES General Meeting. 2012.
- [17] M. Glavic, M. Hajian, W. Rosehart, and T. Van Cutsem, "Receding-horizon multi-step optimization to correct nonviable or unstable transmission voltages," IEEE Trans. on Power Systems, vol. 26, no. 3, pp. 1641-1650, Aug. 2011.
- [18] B. Otomega and T. Van Cutsem, "A load shedding scheme against both short- and long-term voltage instabilities in the presence of induction motors," In Proceedings of the IEEE Trondheim Power Tech 2011 conference, 2011.
- [19] M. Glavic and T. Van Cutsem, "Adaptive Wide-Area Closed-Loop Undervoltage Load Shedding Using Synchronized Measurements," In Proceedings of IEEE PES General Meeting, 2010.
- [20] F. Capitanescu, T. Van Cutsem, and L. Wehenkel, "Coupling optimization and dynamic simulation for preventive-corRECTive control of voltage instability," IEEE Trans. on Power Systems, vol. 24, no. 2, pp. 796-805, May 2009.
- [21] M. Hajian, M. Glavic, W. D. Rosehart, and H. Zareipour, "A chance-constrained optimization approach for control of transmission voltages," IEEE Trans. on Power Systems, vol. 27, no. 3, pp. 1568-1576, Aug. 2012.
- [22] F. Capitanescu and T. Van Cutsem, "Preventive control of voltage security margins: A multicontingency sensitivity-based approach," IEEE Transactions on Power Systems, vol. 17, no. 2, pp. 358-364, May 2002.
- [23] C. Moors and T. Van Cutsem, "Determination of optimal load shedding against voltage instability," In Proc. 13th Power System Computation Conference (PSCC), 1999.
- [24] Reliability Test System Task Force of the Application of Probability Methods Subcommittee, "IEEE Reliability Test System," IEEE Trans. on PAS, vol. 98, no. 6, pp. 2047-2054, Nov./Dec. 1979.
- [25] Reliability Test System Task Force of the Application of Probability Methods Subcommittee, "The IEEE Reliability Test System-1996," IEEE Trans. on Power Systems, vol. 14, no. 3, pp. 1010-1020, Aug. 1999.
- [26] R. Billinton, S. Aboreshaid, "Voltage stability considerations in composite power system reliability evaluation," IEEE Trans. on Power Systems, vol. 13, no. 2, pp. 655-660, May 1998.

- [27] J. A. Momoh, Y. V. Makarov, W. Mittelstadt, "A framework of voltage stability assessment in power system reliability analysis," *IEEE Trans. on Power Systems*, vol. 14, no. 2, pp. 484-491, May 1999.
- [28] H. Wan, J. D. McCalley, V. Vittal, "Risk Based Voltage Security Assessment," *IEEE Trans. on Power Systems*, vol. 15, no. 4, pp. 1247-1254, Nov. 2000.
- [29] F. Milano, C. A. Cañizares, A. J. Conejo, "Sensitivity-based Security-constrained OPF Market Clearing Model," *IEEE Trans. on Power Systems*, vol. 20, no. 4, pp. 2051-2060, Nov. 2005.
- [30] A. Conejo, F. Milano, R. Garcia-Bertrand, "Congestion Management Ensuring Voltage Stability," *IEEE Trans. on Power Systems*, vol. 21, no. 1, pp. 357-364, Feb. 2006.
- [31] A. B. Rodrigues, R. B. Prada, M. D. G. da Silva, "Voltage Stability Probabilistic Assessment in Composite Systems: Modeling Unsolvability and Controllability Loss," *IEEE Trans. on Power Systems*, vol. 25, no. 3, pp. 1575-1588, Aug. 2010.
- [32] V. Storvann, E. Hillberg, and K. Uhlen, "Indicating and mitigating voltage collapse comparing voltage stability indicators," In Proceedings of IEEE PES ISGT Europe, 2012.
- [33] University of Washington Power System Test Case Archive. Available at <http://www.ee.washington.edu/research/pstca/>
- [34] Siemens PTI, "PSS/E online documentation," available online at: <http://www.energy.siemens.com/hq/en/services/power-transmission-distribution/power-technologies-international/software-solutions/pss-e.htm>.
- [35] P. Pourbeik, R. J. Koessler, W. Quaintance, and W. Wong, "Performing Comprehensive Voltage Stability Studies for the Determination of Optimal Location, Size and Type of Reactive Compensation," in Proceedings of IEEE PES Power Systems Conference and Exposition, 2006.
- [36] T. J. Koessler, Q. Wenzheng, M. Patel, and H. Clark, "Voltage Stability Study of the PJM System Following Extreme Disturbances," in Proceedings of IEEE PES General Meeting, 2007.
- [37] IEEE Task Force on Excitation Limiters, "Recommended Models for Over Excitation Limiting Devices," *IEEE Trans. on Energy Conversion*, vol. 10, no. 4, pp. 706-713, Dec. 1995.
- [38] IEEE Std. 421.4-2005, *IEEE Recommended Practice for Excitation System Models for Power System Stability Studies*, IEEE, New York, USA, Apr. 2006.
- [39] J. W. Feltes, L. T. G. Lima, and J. Senthil, "IEEE 421.5 standard - perspective of a user and supplier of simulation software," in Proceedings of IEEE PES General Meeting, 2005.
- [40] IEEE Committee Report, "Excitation System Models for Power System Stability Studies," *IEEE Trans. on PAS*, vol. PAS-100, pp. 494-509, Feb. 1981.
- [41] IEEE Committee Report, "Computer Representation of Excitation Systems," *IEEE Trans. on PAS*, vol. PAS-87, pp. 1460-1464, Jun. 1968.
- [42] G. R. Berube and L. M. Hajagos, "Accelerating-Power Based Power System Stabilizers," Kestrel Power Engineering Ltd., available online: <http://www.kestrelpower.com>

- [43] IEEE Committee Report, “Dynamic Models for Steam and Hydro Turbines in Power System Studies,” IEEE Trans. on PAS, vol. PAS-92, pp. 1904-1915, Jan. 1973.
- [44] IEEE Working Group on Prime Mover and Energy Supply Models for System Dynamic Performance Studies, “Hydraulic Turbine and Turbine Control Models for System Dynamic Studies,” IEEE Trans. on Power Systems, vol. 7, no 1, pp. 167-179, Feb. 1992.
- [45] Documentation of DSAtools suite, Powertech Labs (Canada), available online at <http://www.powertechlabs.com/software-modeling/dynamic-security-assessment-software/dsatoools/>
- [46] PSAT software, available online at <http://faraday1.ucd.ie/software.html>
- [47] F. Milano, “An Open Source Power System Analysis Toolbox,” IEEE Trans. on Power Systems, vol. 20, no. 3, pp. 1199-1206, Aug. 2005.
- [48] F. Milano, *Power System Modeling and Scripting*, Springer-Verlag, London (UK), 2010.
- [49] C. A. Cañizares and F. L. Alvarado, “Point of Collapse and Continuation Methods for Large AC/DC Systems,” IEEE Trans. on Power Systems, vol. 8, no. 1, pp. 1-8, Feb. 1993.
- [50] C. Vournas (Scientific Co-ordinator), “Software Development for Voltage Stability Analysis,” Project 96 SYN 1995, Final Report, NTUA, Greece, 1995.
- [51] CEPEL (Brazil), Programa Anatem Analise de Transitorios Eletromecanicos V.10.04.06, March 2012, available online: <http://www.anatem.cepel.br>.